MASSACHUSETTS INSTITUTE OF TECHNOLOGY
DEPARTMENT OF NUCLEAR ENGINEERING
Cambridge 39, Massachusetts

MIT-2344-5 MITNE-67

A STUDY OF THE SPATIAL DISTRIBUTIONS OF FAST NEUTRONS IN LATTICES OF SLIGHTLY ENRICHED URANIUM RODS MODERATED BY HEAVY WATER

by
Gene L. Woodruff, I. Kaplan, T. J. Thompson

November 1965

Contract AT (30-1) 2344
U.S. Atomic Energy Commission

MASSACHUSETTS INSTITUTE OF TECHNOLOGY

DEPARTMENT OF NUCLEAR ENGINEERING

Cambridge 39, Massachusetts

A STUDY OF THE SPATIAL DISTRIBUTIONS OF FAST NEUTRONS IN LATTICES OF SLIGHTLY ENRICHED URANIUM RODS MODERATED BY HEAVY WATER

by

Gene L. Woodruff, I. Kaplan, T. J. Thompson

November 1965

MITNE - 67

MIT - 2344 - 5

AEC Research and Development Report

UC - 34 Physics

(TID - 4500, 46th Edition)

Contract AT(30-1)2344

U. S. Atomic Energy Commission

ABSTRACT

Intracellular distributions of the activation of threshold foil detectors were measured in seven heavy water-moderated lattices of uranium metal rods: 0.25-inch-diameter, 1.027% U-235 rods on triangular spacings of 1.25 inches, 1.75 inches, and 2.50 inches; 0.25-inch-diameter, 1.143% U-235 rods on triangular spacings of 1.25 inches, 1.75 inches, and 2.50 inches; and 0.75-inch-diameter, 0.947% U-235 rods on a triangular spacing of 2.50 inches. The reactions used in the measurements included $In^{115}(n, n')In^{115m}$, $U^{238}(n, f)$, $Ni^{58}(n, p)Co^{58}$, and $Zn^{64}(n, p)Cu^{64}$. The distributions were found to be the same for the different reactions with the possible exception of the zinc reaction in the more widely spaced lattices. The distributions were found to be strongly dependent on rod diameter and rod spacing, but independent of U-235 concentration, at least for the small differences in concentrations existing in the lattices studied. Methods were developed for correcting the experimental data for the activity resulting from competing capture reactions which accompany the threshold reactions.

A kernel method was developed, the UNCOL code, for computing the spatial distribution of the uncollided fast flux in assemblies with cylindrical fuel elements. Good agreement was obtained between experimental results and the results of UNCOL calculations using values of 0.093 cm^{-1} and 0.100 cm^{-1} for the removal cross sections for heavy water and uranium, respectively. These values, which can be considered experimental values of the removal cross sections, are close to the calculated values found in the literature for one energy group above 1.35 Mev, 0.0899 cm^{-1} for heavy water and 0.1039 cm^{-1} for uranium.

The results of UNCOL calculations also gave good agreement with distributions of the $Ni^{58}(n, p)Co^{58}$ reaction measured in the experimental facilities in and around the MITR core.

A relationship between δ_{28} and the UNCOL results was derived. This relationship was applied to previous measurements of δ_{28} and was found to correlate the experimental results very well for values of δ_{28} less than about 0.055. The systematic discrepancies for higher values was attributed to spectral shifts occurring in the more tightly spaced lattices of 0.75-inch and larger rods.

The HEETR code was used to calculate the intracellular distributions of the threshold reactions used in the experiments as well as values of $\delta 28$ for the lattices in which experimental results had been obtained. The calculated intracellular distributions agreed well with both the experimental results and those of UNCOL calculations. The calculated values of δ_{28} were consistently lower than corresponding experimental values.

DISTRIBUTION

MIT-2344-5 MITNE-67

AEC Research and Development Report

UC-34 Physics

(TID-4500, 46th Edition)

1. USAEC, New York Operations Office (D. Richtmann)
2. USAEC, Division of Reactor Development (P. Hemmig)
3-5. USAEC, Division of Reactor Development (I. Zartman)
6. USAEC, Division of Reactor Development (S. Strauch)
7. USAEC, Division of Reactor Development (H. Honeck)
8. USAEC, New York Patents Office (H. Potter)
9. USAEC, New York Operations Office (H. Fish)
10. USAEC, New York Operations Office
Research and Development Division
11. USAEC, Maritime Reactors Branch
12. USAEC, Civilian Reactors Branch
13. USAEC, Army Reactors Branch
14. USAEC, Naval Reactor Branch
15. Advisory Committee on Reactor Physics (E. R. Cohen)
16. ACRP (G. Dessauer)
17. ACRP (D. de Bloisblanc)
18. ACRP (M. Edlund)
19. ACRP (R. Ehrlich)
20. ACRP (I. Kaplan)
21. ACRP (J. Chernick)
22. ACRP (F. C. Maienschein)
23. ACRP (R. Avery)
24. ACRP (P. F. Zweifel)
25. ACRP (P. Gast)
26. ACRP (G. Hansen)
27. ACRP (S. Krasik)
28. ACRP (L. W. Nordheim)
29. ACRP (T. M. Snyder)
30. ACRP (J. J. Taylor)
31-33. O.T.I.E., Oak Ridge, for Standard Distribution
34-100. Internal Distribution

TABLE OF CONTENTS

LIST OF TABLES

LIST OF FIGURES

ACKNOWLEDGMENTS

The success of the M.I.T. Lattice Project has been due to the contributions of a number of individuals. The results of this particular report are primarily due to the work of its principal author, Gene Woodruff, who has submitted substantially the same report in partial fulfillment for the Ph.D. degree at M.I.T. He has been assisted by other graduate students as well as those mentioned below.

Overall direction of the project and its research is shared by Prof. I. Kaplan, Prof. T. J. Thompson, and M. J. Driscoll. Messrs. Joseph Barch, Albert Supple, and Norman Berube have been of valuable assistance in the setup of experiments and in the operation and maintenance of the facility. Miss Barbara Kelley has helped in the procurement of materials and in the reduction of data.

Staffs of the M.I.T. Reactor, Machine Shop, Electronics Shop, and Radiation Protection Office have provided much assistance and advice during the experimental portion of this work. Miss Rae Visminas and Mrs. Mary Bosco have given valuable aid in the typing of this report.

Dr. H. K. Clark, of the Savannah River Laboratory, has provided a copy of the HEETR Code, a set of nuclear data for use with the code, and assistance in early attempts to use the code. The computer calculations were performed at the M.I.T. Computation Center.

All these individuals and groups were essential to the completion of this work.

Chapter I

INTRODUCTION

1.1 The MIT Heavy Water Lattice Project

The Department of Nuclear Engineering of MIT, with the support of the United States Atomic Energy Commission, has undertaken a program of experimental and theoretical studies of the physics of D_2O-moderated lattices of slightly enriched uranium rods.

The main purpose of this program is to add to the understanding of fundamental reactor physics. The emphasis, therefore, has been on the development of methods for determination of basic lattice parameters, comparison of the experimental results with existing theory, and, where possible, extension of the theory.

The results of this program are given in annual progress reports as well as in individual reports. A summary of reports and papers on the work of the Lattice Project as of August 1965 is given in Appendix E.

1.2 Significance of Fast Neutron Distributions

Although intracellular thermal flux distributions have been studied experimentally in great detail in lattices, little attention has been given to the fast neutron flux distribution. A knowledge of fast neutron distributions is important for the following reasons:

(1) it can lead to a better understanding of δ_{28} (the ratio of fissions in U^{238} to fissions in U^{235}) and the fast fission effect;
(2) it is needed in order to predict certain radiation damage effects;
(3) it can make possible improvements in the calculation of resonance absorption;
(4) it may improve or simplify the treatment of fast neutrons in multigroup methods;
(5) techniques used to study fast neutron distributions in thermal assemblies may be useful in fast assemblies where fast neutrons constitute a major part of the neutron energy spectrum.

Some of these factors are considered in more detail below.

The contribution of fast fission to the multiplication process in thermal reactors is frequently expressed through the fast fission factor, ϵ, one of the terms of the four-factor formula. In low enrichment assemblies, the combination of a relatively high value of ϵ and a relatively low over-all multiplication factor makes fast fission important because it contributes a substantial portion of the excess reactivity. The fast fission factor is not a uniquely defined quantity, and several definitions have been used (S1, C2, C3, D1). Furthermore, ϵ cannot be measured experimentally; instead, a related parameter δ_{28}, defined as the ratio of the U^{238} fission rate to the U^{235} fission rate, has been extensively measured (B1, B2, C4, C5, C6, C7, C8, E1, F1, F2, G1, H1, H2, K1, K2, K3, K4, K5, K6, M2, N1, O1, P1, P2, P3, S2, U1, W1, W3, W4).

Wolberg, Kaplan, and Thompson (W4) have reviewed the experimental δ_{28} data and discussed some of the various techniques that have been used.

Theoretical methods of calculating ϵ and/or δ_{28} include those based on collision probabilities (C2, M3), escape and transmission probabilities (C9, C10), those using Monte Carlo results (D1, A2) and a semi-empirical one-group method proposed by Hellens and Honeck (H2). The methods based on collision probabilities are of limited applicability and accuracy. One difficulty is the limited accuracy of much of the high energy cross-section data, and another difficulty is the complexity involved when more than a single rod is treated. The Monte Carlo results from the MOCA-II code (D1) appear to agree quite well with experiment, though many high energy cross-section data are needed. One example of the use of escape and transmission probabilities is the HEETR code written by Dr. H. K. Clark (C9, C10). This code has been used in the present work and is discussed in greater detail in sections 3.3 and A.2. The semi-empirical one-group theory of Hellens and Honeck is discussed in sections 4.2.

The importance of fast neutron distributions for the calculation of radiation damage is exemplified by organic coolant or moderator materials such as santowax. Radiation damage is important in the use of santowax, and more than one-half of the dose rate is due to fast neutrons in a typical reactor environment. Furthermore, there is experimental evidence that

fast neutrons produce a much greater effect per unit dose (i. e., a higher "G value") than gamma rays in the degradation of santowax (T1).

The spatial distribution of the fast neutrons can affect resonance absorption because the fast neutrons constitute the sources for the resonance energy region. In any homogenized treatment, therefore, the resonance absorption, particularly at the higher energies, is influenced by the spatial distribution of the fast neutrons. Thus, D'Ardenne (D2) has improved resonance absorption calculations by reading into the GAM-II code (J1) weighting coefficients based on fast neutron advantage factors measured in the present work.

1.3 Contents of the Report

In the present work, the spatial distributions of fast neutrons were studied both experimentally and theoretically. The experimental work was based on measurements of the spatial distributions of the activation of several threshold reactions in a number of lattice configurations as well as in the MIT Reactor. The theoretical study included the development of a kernel method, the UNCOL code, for computing the spatial distribution of the fast flux. The theoretical study also included calculations of both spatial and energy distributions of fast neutrons using the HEETR code.

A description of the physical facilities used for the experimental work is given in Chapter II; the experimental procedures, including counting and data analysis methods, are described in that chapter. In Chapter III, the theoretical foundation of the kernel method used in the development of the UNCOL code is discussed. The assumptions implied in the use of the HEETR code and some of the features of this code are given in Chapter III. The RATIO code, which was written to compute certain energy-dependent parameters by using the results of HEETR calculations, is also briefly described in Chapter III. In Chapter IV, the experimental fast neutron distributions, as determined by threshold foil activation, and the corresponding fast neutron advantage factors are compared with those predicted by UNCOL and HEETR. Experimentally determined δ_{28} values are compared with the predictions of HEETR; and fast neutron advantage factors are compared with the results of the one-group theory. Results of UNCOL calculations for the MIT Reactor

are also given in this chapter; they are compared with the results of foil measurements made in experimental facilities of the MITR and with data obtained by the MIT Organic Loop Project. In Chapter V, recommendations for future work are proposed.

In Appendix A, a description of the input, the Fortran listing, and the output, along with sample problems, are given for the UNCOL, HEETR, and RATIO codes. Appendix B contains some remarks about the single collision transport kernel. These remarks are a result of the experience of developing the UNCOL code and may be useful in other work in which integrals of a similar type are used. Appendix C describes a method of analysis for complex gamma-ray spectra that was developed for use with the results of the indium reaction. Appendix D contains results of additional UNCOL calculations which illustrate the effects of variations in the values of the cross sections used in the UNCOL code. A summary of the publications of the MIT Heavy Water Lattice Project is given in Appendix E. Nomenclature and references are given in Appendices E and F, respectively.

Chapter II

EXPERIMENTAL METHODS

2.1 The MIT Lattice Facility

Cross-sectional drawings of the MIT exponential facility are shown in Figs. 2.1 and 2.2. The facility consists of an exponential tank which is supported above a graphite-lined cavity or "hohlraum." The 5 ft. × 5 ft. thermal column of the MITR is used as a source of thermal neutrons which enter the cavity and are reflected upward through a graphite pedestal into the bottom of the exponential tank. The tank, which contains the lattices and the heavy water, is 67-1/4 inches high and either 36 inches or 48 inches in diameter, depending on the particular lattice being studied.

Studies were made with seven lattices in the present work. The first three consisted of 0.25-inch-diameter uranium metal rods enriched to 1.027% U^{235}.* The rods were clad with Type 1100 aluminum, 0.028 inches thick, and arranged on triangular spacings of 1.25 inches, 1.75 inches, and 2.50 inches. The next three lattices were identical to the first three except that the U^{235} concentration was 1.143%. The seventh lattice was composed of 0.75-inch-diameter uranium metal rods, clad with 0.0325-inch-thick, Type 1100 aluminum and arranged on a triangular spacing of 2.50 inches. In all cases, the length of the fuel rods was 48 inches. The fuel rods were supported by aluminum upper adapters positioned in girders at the top of the tank. Aluminum adapters were also used at the bottom of the rods and were positioned in holes drilled for the purpose in an aluminum grid plate.

Lattices studied earlier with the MIT Lattice Facility included 1.00-inch-diameter, natural uranium metal, aluminum-clad rods on

---

*The exact U-235 concentration of these rods is somewhat uncertain at the present time. It is likely that the correct value is closer to 1.016% U-235 (P5). In view of the uncertainty, and to be consistent with earlier reports, the value of 1.027% will be used throughout this report.

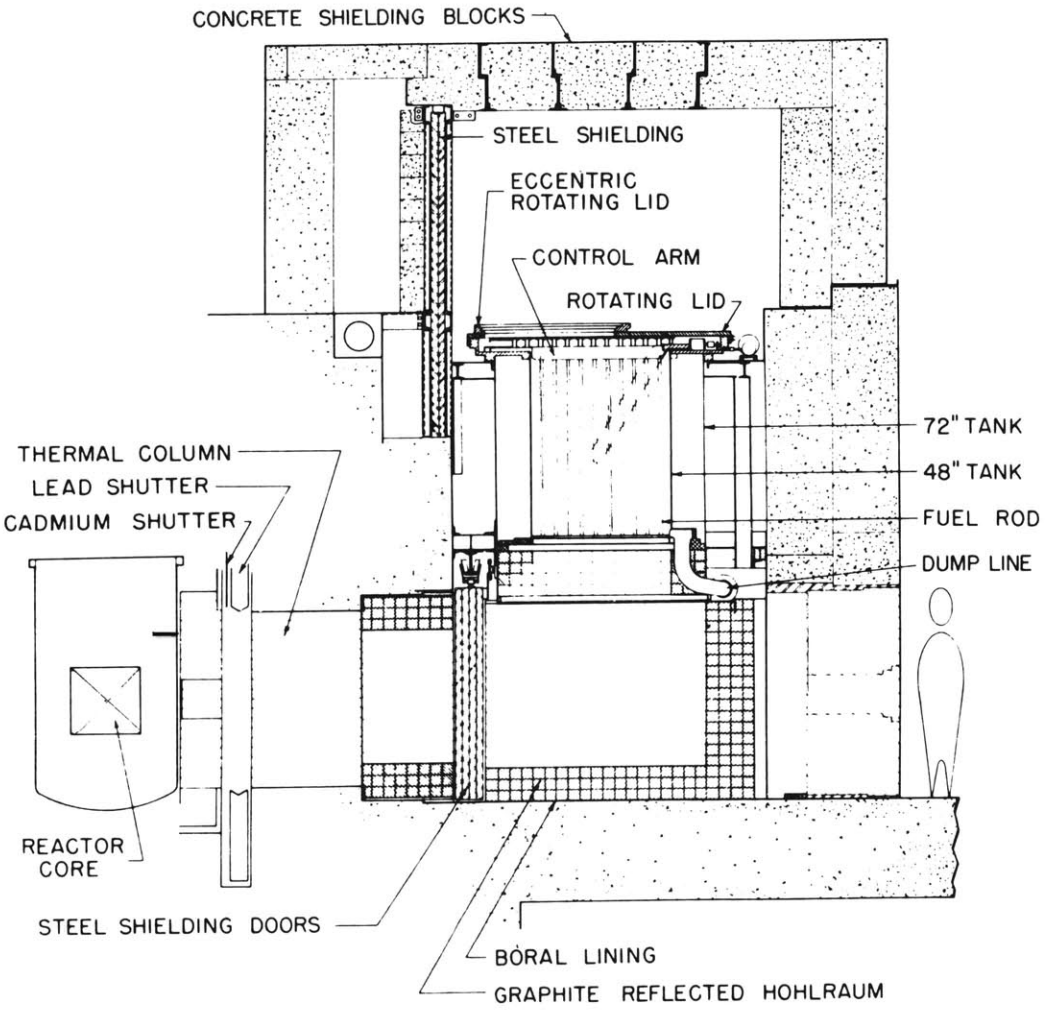

FIG. 2.1 VERTICAL SECTION OF THE SUBCRITICAL ASSEMBLY

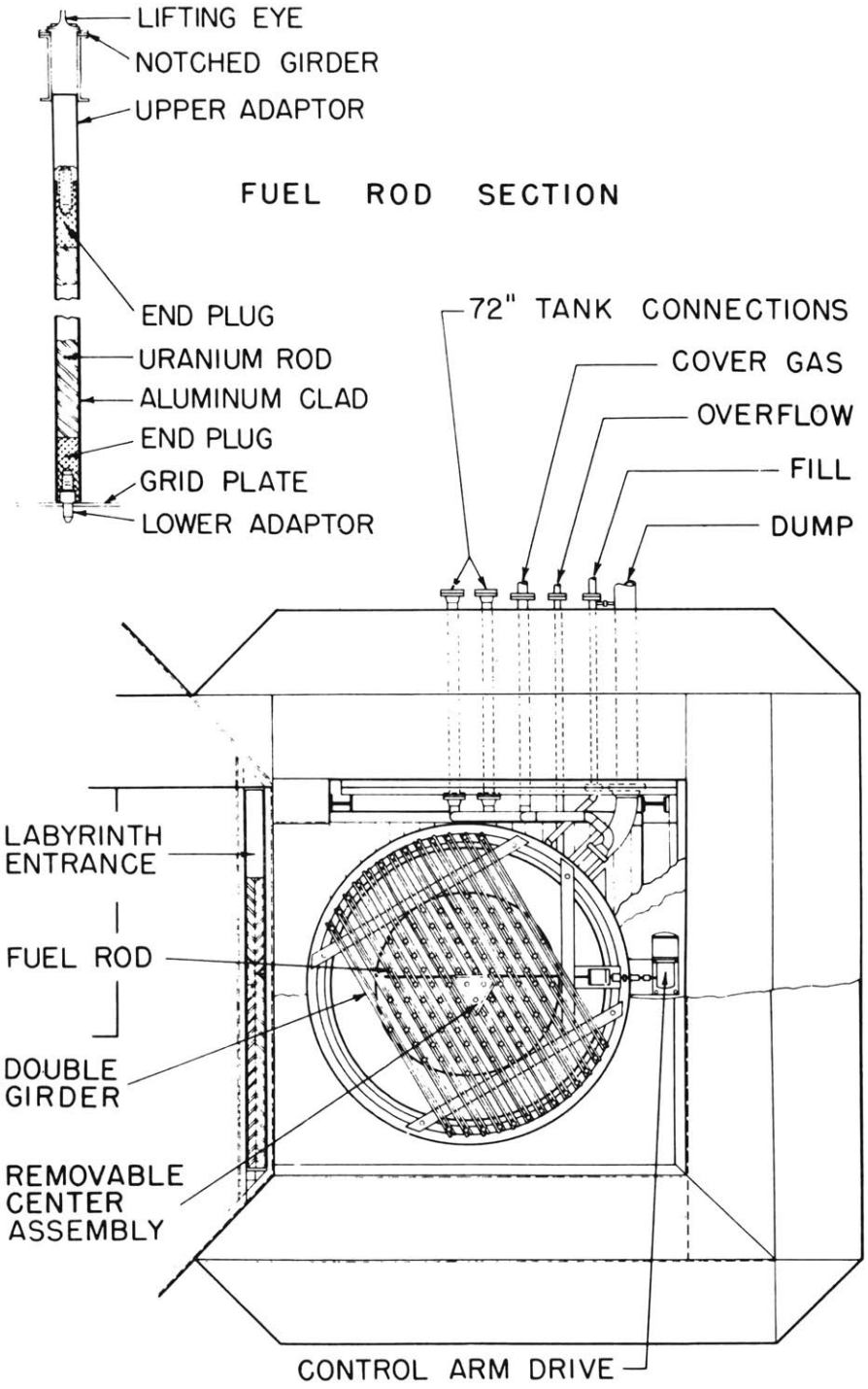

FIG. 2.2 PLAN VIEW OF THE SUBCRITICAL ASSEMBLY

triangular spacings of 4.5 inches, 5.0 inches, and 5.75 inches (see Appendix E). The MIT Lattice Facility, together with its ancillary equipment, has been described in detail in an earlier report (H3). Other MITR irradiation facilities used for foil irradiation include the vertical sample assembly in Fuel Position #1, the sample assembly in Position #23, the Graphite Vertical Sample Positions #2, #5, and #6, and the pneumatic tube facility 1PH2. The MITR facilities are discussed in more detail in section 2.10.

2.2 Methods of Measuring Fast Neutron Distributions

The two principal methods used for the detection of fast neutrons are foil activation and ionization chambers. Other methods, such as the use of calorimeters, have also been used but are of interest mainly for special applications.

Foil activation methods (A3, B3, B4, D3, D4, D5, G2, G3, H4, H5, K7, L1, L2, M4, M5, R1, R2, R3, S2, S3, S4, S5, T2, T3, T4, T5, U2, W4) are based on threshold reactions, i. e., reactions that are energetically possible only for neutrons of a minimum, or threshold, energy. These reactions include (n, p) reactions, (n, f) reactions and inelastic scattering (n, n′) reactions which form isomers with a sufficiently long half-life. The greatest advantage to be gained from the use of foils over competing methods is that foils can be made very small. Foil activation can therefore be used to measure the fine structure of the flux without significantly perturbing the details of the flux being studied. Foils also offer the advantage of providing information relative to energy-dependent parameters. This is accomplished by the use of several different reactions with different cross-section energy dependence. Some nuclear reactions occurring in foils permit the direct measurement of a parameter of interest, an obvious example being the fast fission of U^{238}.

The use of threshold reaction foils has the disadvantage of providing integral results from which the determination of differential parameters such as the differential energy spectrum is difficult. Furthermore, cross sections for fast neutrons are generally small compared with thermal cross sections. This fact, coupled with the generally smaller magnitude of the fast flux, means that reaction rates can ordinarily be expected to be

small, producing low counting rates, with consequent loss of accuracy. Foil activation generally requires a large number of corrections, such as, for differences in foil weight, irradiation and decay times. Foil data analysis must also take into account any neutron flux depression by the foil, radiation, absorption within the foil, and errors that may be introduced by competing reactions. Table 2.1 lists some of the threshold reactions most often used.

Ionization chambers sometimes utilize one of the threshold reactions such as fast fission. These have some of the advantages of foils and are usually more convenient to use than foils. In other types of ionization chambers, the particles detected are the secondaries resulting from elastic collisions. With suitable data analysis, these devices can be used to measure neutron energy spectra. The chief disadvantage of the use of ionization chambers is their size. Even small ones produce perturbations that can be difficult to account for, and fine-structure measurements such as intracellular distributions are not possible. It is primarily for the latter reason that foil activation was chosen as the method to be used in the present work.

2.3 Fast Neutron Threshold Reactions Used in This Work

The choices of reactions for use in the present work were limited by several considerations. The magnitude of the fast flux above about 1 Mev in the lattices studied was comparatively low (as opposed to typical values for reactors, for example). Furthermore, in the high energy range, the neutron flux is certain to decrease with increasing energy. These two factors combined to eliminate all but the reactions having thresholds less than about 3 Mev and with comparatively large cross sections. That this criterion is essential is evident when one considers that the results of the reactions finally chosen had statistical uncertainties as high as 20%. Although low count rates can often be increased simply by increasing the foil size, this was not possible in the present case because of the small dimensions available for intracellular traverses. Similarly, only those reactions which permitted the use of metallic foils were attempted because the density of foil material in powdered foils was too low. Only reactions resulting in gamma-ray

TABLE 2.1

A Listing of Fast Neutron Threshold Reactions

Reaction	Half-Life of Product	Approx. Threshold Energy (Mev)
$Rh^{103}(n, n')Rh^{103m}$	54 min.	0.2
$Np^{237}(n, f)$	--	0.4
$Hg^{199}(n, n')Hg^{199m}$	43 min.	0.5
$In^{115}(n, n')In^{115m}$	4.5 hr.	0.5
$U^{238}(n, f)$	--	1.0
$Th^{232}(n, f)$	--	1.2
$Ni^{58}(n, p)Co^{58}$	71 days	2.0
$Fe^{54}(n, p)Mn^{54}$	291 days	2.0
$Nb^{93}(n, n')Nb^{93m}$	3.7 years	2.0
$P^{31}(n, p)Si^{31}$	2.62 hr.	2.3
$S^{32}(n, p)P^{32}$	14.5 days	2.3
$Zn^{64}(n, p)Cu^{64}$	12.8 hr.	3.0
$Pb^{204}(n, n')Pb^{204m}$	67 min.	3.0
$Ti^{46}(n, p)Sc^{46}$	86 days	3.4
$Al^{27}(n, p)Mg^{27}$	9.5 min.	4.0
$Si^{28}(n, p)Al^{28}$	2.30 min.	4.5
$Fe^{56}(n, p)Mn^{56}$	2.58 hr.	5.1
$Ti^{48}(n, p)Sc^{48}$	44 hr.	5.1
$Mg^{24}(n, p)Na^{24}$	15 hr.	6.3
$Al^{27}(n, \alpha)Na^{24}$	15 hr.	6.5
$Tl^{203}(n, 2n)Tl^{202}$	12 days	8.5
$Pb^{204}(n, 2n)Pb^{203}$	52 hr.	9.0
$In^{115}(n, 2n)In^{114}$	49 days	9.3
$Mn^{55}(n, 2n)Mn^{54}$	291 days	11.0

emission were considered because the large number of foils used and the large amount of handling required would probably have complicated beta counting efforts owing to the combination of geometry and absorption effects. No reactions were actually eliminated for this reason since the only pure beta decay reactions which might have been used were $P^{31}(n,p)Si^{30}$ and $S^{32}(n,p)P^{32}$, and phosphorous and sulfur were not available in metallic form. Neptunium, which would have been a particularly desirable material because of its low threshold energy, could be obtained only in oxide form, clad in aluminum. (The use of neptunium is also complicated by the high background caused by the decay of neptunium, but Rydin (R1) has used it successfully.) There are also limitations because of the half-life of the activity produced. The maximum length of time available for a lattice run was approximately 90 hours. Hence, unless the cross section was quite large, reaction products with half-lives longer than a few days would reach only a fraction of saturation, and count rates would be too low. At the other extreme, activities with half-lives of a few minutes had to be ruled out because the minimum time attainable between shutting down the lattice and starting to count foils is approximately one hour. This results from the need to wait for the fission product activity of the fuel rods to decay sufficiently to permit handling and from the time required in handling of fuel rods and foils to prepare the foils for counting.

Still another criterion is that competing thermal or epithermal reactions must not predominate over the desired fast reaction. For example, iron and niobium would present difficulties because they are practically impossible to obtain free from manganese and tantalum, respectively. Both of the latter elements have very large neutron capture cross sections and the nuclides formed decay with the emission of energetic gamma rays.

For the reasons given above, the list of the reactions considered was narrowed to the following: $Rh^{103}(n,n')Rh^{103m}$, $In^{115}(n,n')In^{115m}$, $U^{238}(n,f)$, $Th^{232}(n,f)$, $Ni^{58}(n,p)Co^{58}$, $Nb^{93}(n,n')Nb^{93m}$, $Zn^{64}(n,p)Cu^{64}$, and $Pb^{204}(n,n')Pb^{204m}$. Early attempts to use the Rh, Th, Nb, and Pb reactions were unsuccessful owing to low counting rates. No further efforts were made to use Nb or Pb, since it appeared unlikely that

satisfactory results could be obtained. Furthermore, the energy ranges covered by the cross sections for these reactions are effectively covered by the cross sections for other reactions. Experiments with In, U^{238}, Ni, and Zn were generally successful, and these reactions are considered in more detail later in this chapter. The energy dependence of the cross sections for these reactions is shown in Figs. 2.3 and 2.4 from data compiled by Rydin (R1). The rhodium and thorium reactions were not successfully used but are discussed further below.

The energy dependence of the thorium fission cross section is shown in Fig. 2.5. The curve of thorium fission cross section as a function of energy is quite similar in shape to the cross-section curve for U^{238} fast fission. The thorium fission cross section has a slightly higher threshold energy and is smaller in magnitude than U^{238} by a factor of approximately four. The thorium fission reaction is of interest primarily for three reasons. First, reactors containing thorium for breeding are likely to be built in the future, and thorium fission will contribute to the multiplication factor. Second, the U^{235} concentration of the depleted foils used in the present work was 17 parts per million. This material is scarce and expensive and a more typical value for the U^{235} concentration is about 300 parts per million. The use of the more common foils for fast neutron detection requires a correction for U^{235} fission that may exceed 50% of the total count rate. Thorium, with its cross section similar to that of U^{238}, offers an inexpensive, readily available substitute that does not require corrections for a competing reaction. Another reason for persisting with efforts to utilize the thorium fast fission reaction is that it offers some additional flexibility in the counting procedure. As will be discussed below, when integral fission product gamma counting is used with the U^{238} (n, f) reaction, the cut-off energy is commonly set at 0.72 Mev. This is to ensure that only gamma rays resulting from fissions are counted and not those resulting from neutron capture. The decay sequence for thorium following neutron capture is:

$$Th^{232} + n \rightarrow Th^{233} \xrightarrow{23.3\ \text{min.}} Pa^{233} + \beta\ (1.23\ \text{Mev})$$

$$\xrightarrow{27.4\ \text{days}} U^{233} + \beta\ (0.57\ \text{Mev})$$

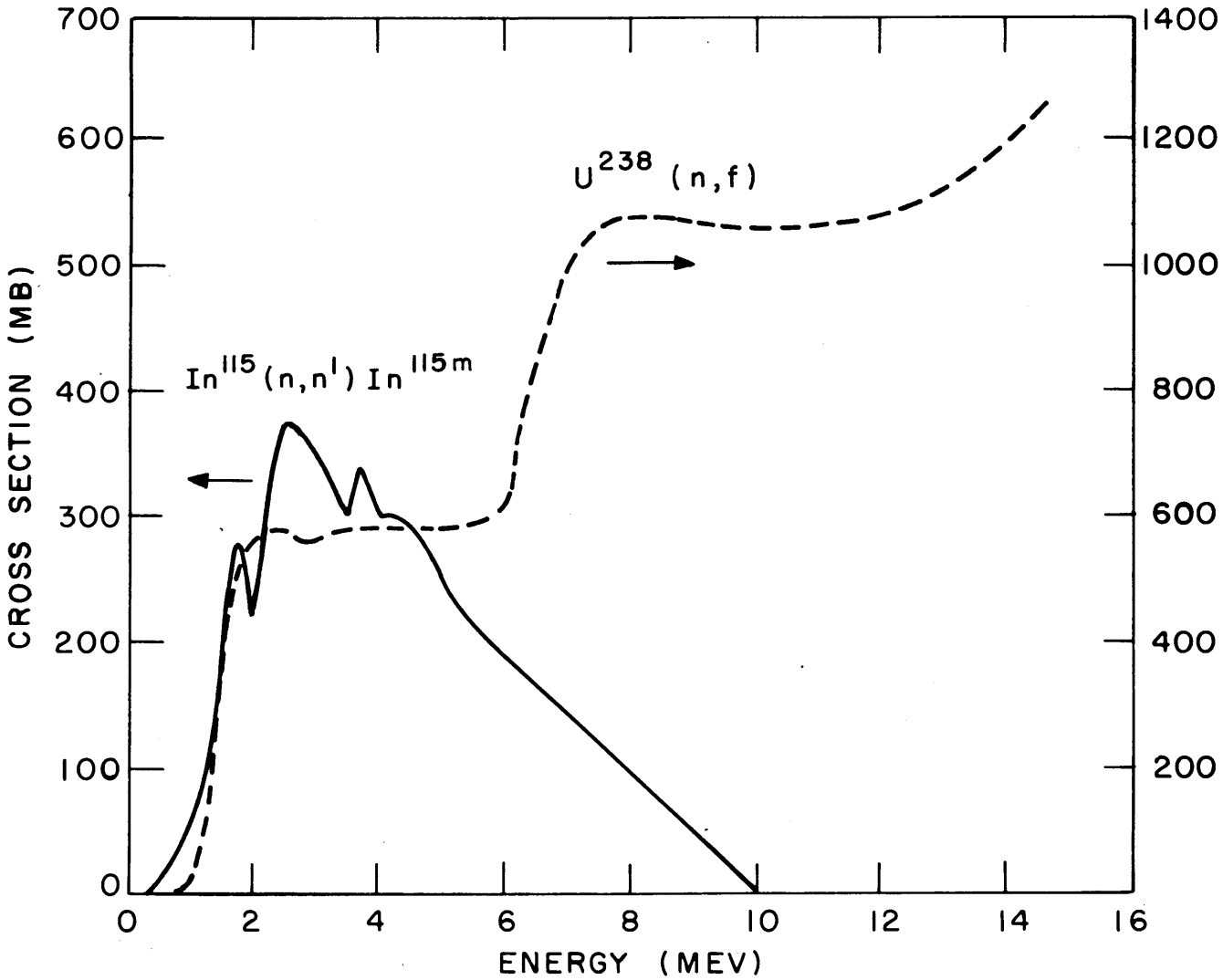

FIG. 2.3 CROSS SECTION VS. ENERGY FOR In^{115} (n,n^1) In^{115m} AND U^{238} (n,f)

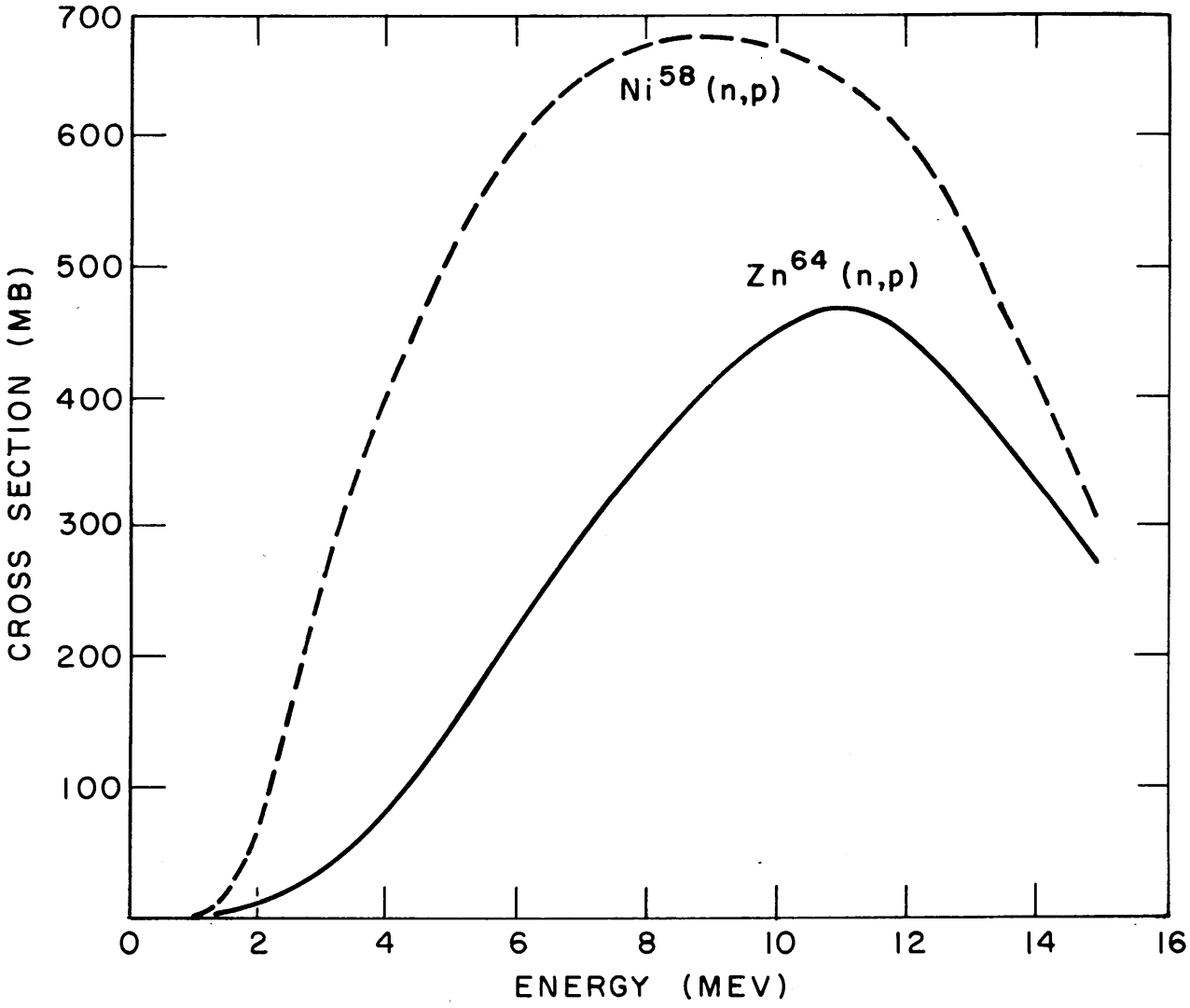

FIG. 2.4 CROSS SECTION VS. ENERGY FOR $Zn^{64}(n,p)\,Cu^{64}$ AND $Ni^{58}(n,p)\,Co^{58}$

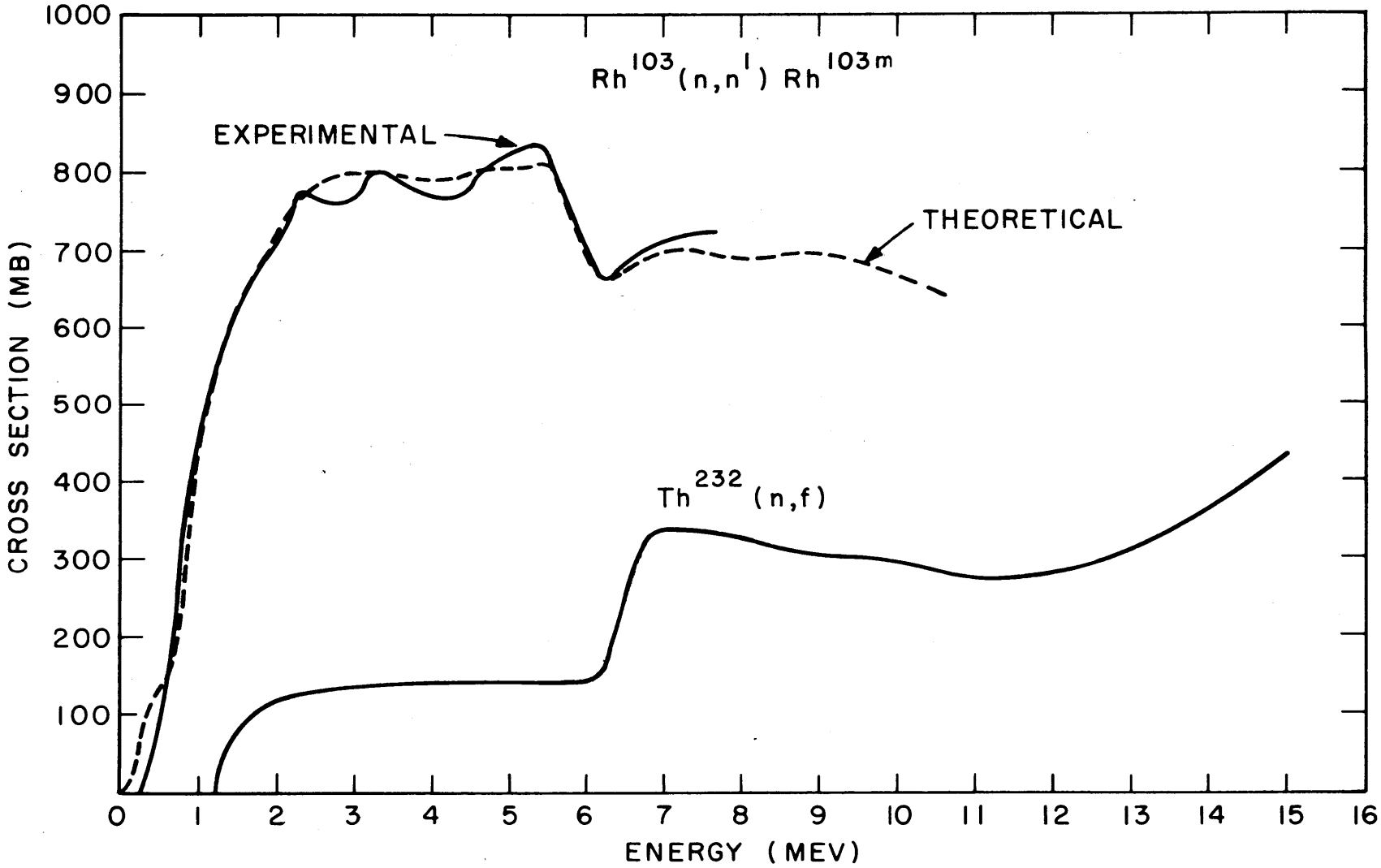

FIG. 2.5 CROSS SECTION VS. ENERGY FOR $Rh^{103}(n,n^1)\ Rh^{103m}$ AND $Th^{232}(n,f)$

The gamma rays associated with these beta decays have lower energies than the maximum beta energies; but even when a beta shield is used, there is bremsstrahlung with a maximum energy equal to the maximum energy of the betas. Hence, after a delay of two or three hours to allow for decay of Th^{233}, a discriminator setting of 0.57 Mev could be used with assurance that no gammas from the decay of Pa^{233} were being counted. This would seem to be an attractive way to increase the count rate so as to give statistical accuracy comparable, for example, to that obtained with the depleted uranium foils. Unfortunately, however, the natural background activity resulting from the decay of Th^{232} has a large peak just above 0.57 Mev (apparently resulting from Tl^{208}, one of the members of the thorium decay chain) and other peaks above that one. This increased background tends to offset the advantage of the increased count rate. Efforts were made to integral-count the thorium fission product gamma rays with energy cut-offs at 0.57 Mev, 0.65 Mev, and 0.72 Mev, respectively. No optimum setting was found and satisfactory results were not obtained with any of the settings. The natural background activity is, of course, independent of the experiment so that, for experiments performed in higher fluxes, the 0.57 Mev cut-off might well prove to be advantageous.

The cut-off energy for fission product counting of thorium might be lowered below 0.57 Mev without introducing significant errors from the bremsstrahlung associated with the beta decay of Pa^{233}. The bremsstrahlung associated with electrons of a given energy incident upon a target show a continuous energy spectrum. The maximum bremsstrahlung energy corresponds to the energy of the incident electron, but the most probable energy is lower (E2). Furthermore, the continuous beta energy spectra associated with beta decay have a most probable energy less than the maximum, the maximum energy having a very low probability. These two factors together imply that only a very small fraction of the bremsstrahlung associated with beta decay consists of X rays with energies near the maximum beta energy. Thus, it is likely that the integral fission product gamma counting of thorium foils could be extended to energies below 0.57 Mev, particularly if the foils have been covered with cadmium, without introducing

significant error. The above argument is only qualitative and analytical treatment of the bremsstrahlung activity counted would be exceedingly complex. However, suitable experiments could establish the acceptability of a lower cut-off energy.

The $Rh^{103}(n, n')Rh^{103m}$ reaction is of special interest because of its very low threshold energy. Two cross-section curves were found in the literature: one curve is theoretical (V1) and the other experimental (J2). The experimental curve represents a relative measurement only, so it has been normalized in Fig. 2.5 to give agreement with the theoretical curve at 1.5 Mev. Since the fast flux can be expected to increase with decreasing energy and since the threshold energy is low, a larger fraction of the rhodium reaction rate should be due to the portion of the neutron spectrum below 1 Mev than for most other reactions. This reaction should then be a useful tool for investigating the lower energy portion of the fast neutron spectrum. The neutrons below 1 Mev are especially interesting, not only because of the large value of the flux in this energy region, but also because the scattering-in from higher energies undoubtedly constitutes a major source for this group. For example, approximately 70% of the fission spectrum is above 1 Mev and the fraction of the rhodium reaction rate in a fission spectrum that is due to neutrons with energies less than 1 Mev is about 3%. The fraction of the rhodium reaction rate that is due to neutrons with energies less than 1 Mev is about 10% in neutron energy spectra typical of heavy water lattices (see section 4.4, for example). Although 10% is still a small fraction of the total reaction rate, it is a larger fraction than the percentage of the other reactions due to interactions with neutrons having energies below 1 Mev. Typical values of this fraction for the $In^{115}(n, n')In^{115m}$ and $U^{238}(n, f)$ reactions are 4% and 0.3%, respectively. The nickel and zinc reactions have cross sections with threshold energies above 1 Mev, so they provide no information regarding the neutrons below this energy.

Experimentally, the inelastic scattering of rhodium is a difficult reaction to use for three reasons. First, the half-life of 54 minutes causes a considerable loss of activity before counting. The smallest time interval between the end of the irradiation and the beginning of

counting was never less than one hour, even when elaborate preparations were taken beforehand. Thus, the count rate was less than one-half the saturated value for the first foil counted. In a typical experiment, approximately 18 foils had to be counted, so that subsequent count rates were decreased even more by decay before counting. Another difficulty stems from the low energy of the gamma ray emitted in the decay of Rh^{103m}, which is only 40 kev. This energy is not far above the noise threshold for typical counting arrangements with scintillation crystals and photomultiplier tubes. Furthermore, at this energy, gamma absorption within the foil limits the use of thicker foils as a means of increasing the count rate. In the experiments, two 0.005-inch-thick foils were used in each position and then counted side by side so as to increase the surface area for counting. Finally, the rhodium counting is complicated by the fact that it is difficult to obtain Rhodium foils free from iridium. Iridium has a thermal cross section of approximately 440 barns and a substantial resonance integral. The half life of Ir^{194} is 19 hours, and both produce gammas with energies greater than 40 kev - the energy of the gammas from Rh^{103m}.

2.4 Foil Fabrication Procedures

All foils were formed with hardened punches and dies machined to close tolerances and had clean, smooth edges. The foils were weighed on a Fisher precision microbalance (Model 1-912). With the exception of the depleted uranium foils, a completely new set of foils was punched out and weighed for each run. This served to keep to a minimum the background effect of competing (n,γ) activity. Because of their limited availability, the depleted uranium foils had to be re-used: the history of each was recorded. These foils were background-counted before irradiation and were always allowed to decay for at least six months between runs.

All foils were of high chemical purity, greater than 99.9%. The depleted uranium had a U^{235} content of 17.7 parts per million as determined by Wolberg (W4).

All the foils irradiated in the moderator region* were 0.25 inch in diameter. The zinc, nickel, and indium moderator foils were 0.020 inch thick; the thorium moderator foils were 0.010 inch thick; the depleted uranium and rhodium foils were 0.005 inch thick. In the lattices of 0.25-inch-diameter rods, all the fuel foils were 1/16 inch in diameter, while in the lattice of 0.75-inch-diameter rods, they were 1/8 inch in diameter. All fuel foils were 0.010 inch thick except the depleted uranium foils which were 0.005 inch thick.

2.5 Foil Holders

The fuel foils were positioned in special fuel slugs with depressions milled out for this purpose. Typical slugs used in the 0.25-inch fuel rod lattices are shown in Figs. 2.6 and 2.7. In the first three lattices studied (1.027%) fuel buttons of the type shown in Fig. 2.7, with depressions on the sides, were not available. When data from the earliest runs were analyzed, it was found that the steepest gradients in the fast flux distributions came near the edge of the fuel. It was desirable, therefore, to have additional foils positioned in this vicinity. At first, 1/16-inch-diameter foils were placed in the 0.006-inch air gap between the fuel and clad. This procedure was made difficult by the small space available. Only very thin foils could be used, and accurate positioning was difficult, owing to slippage that occurred when the rods were loaded and unloaded. There was insufficient space for catcher foils between the foils and the fuel; furthermore, it was not uncommon for the fuel slugs to jam up in the cladding when the fuel foils were unloaded. The depressions milled at the edge of the fuel slugs used in the lattices of 1.143% and 0.947% U^{235} concentration circumvented all these difficulties. The fuel buttons used in the lattice with 0.75-inch-diameter rods were similar to the type shown in Figs. 2.6 and 2.7 except for dimensions and the presence of five foil positions on each side rather than four as in Fig. 2.6.

---

*Hereafter, for the sake of brevity, the foils irradiated in the moderator are referred to as "moderator foils," and those irradiated in the fuel are called "fuel foils."

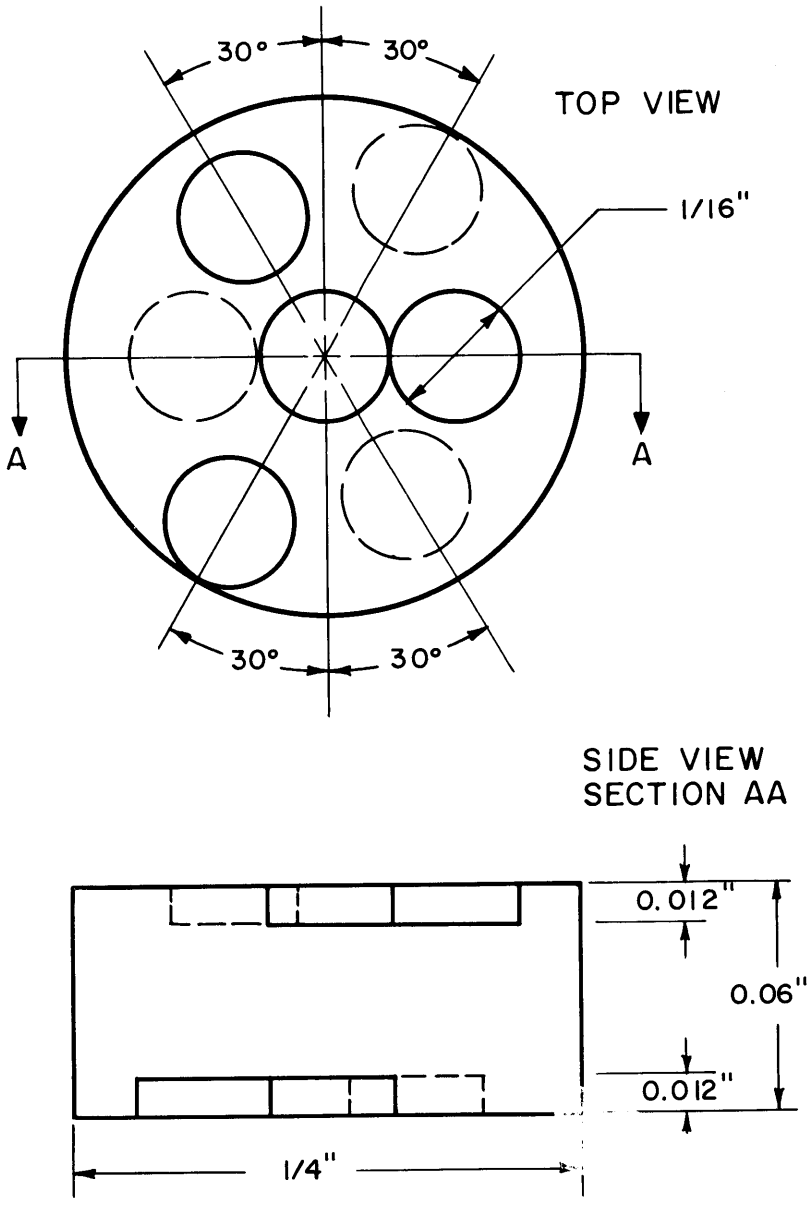

FIG. 2.6 FOIL HOLDER USED FOR INNER FUEL FOILS

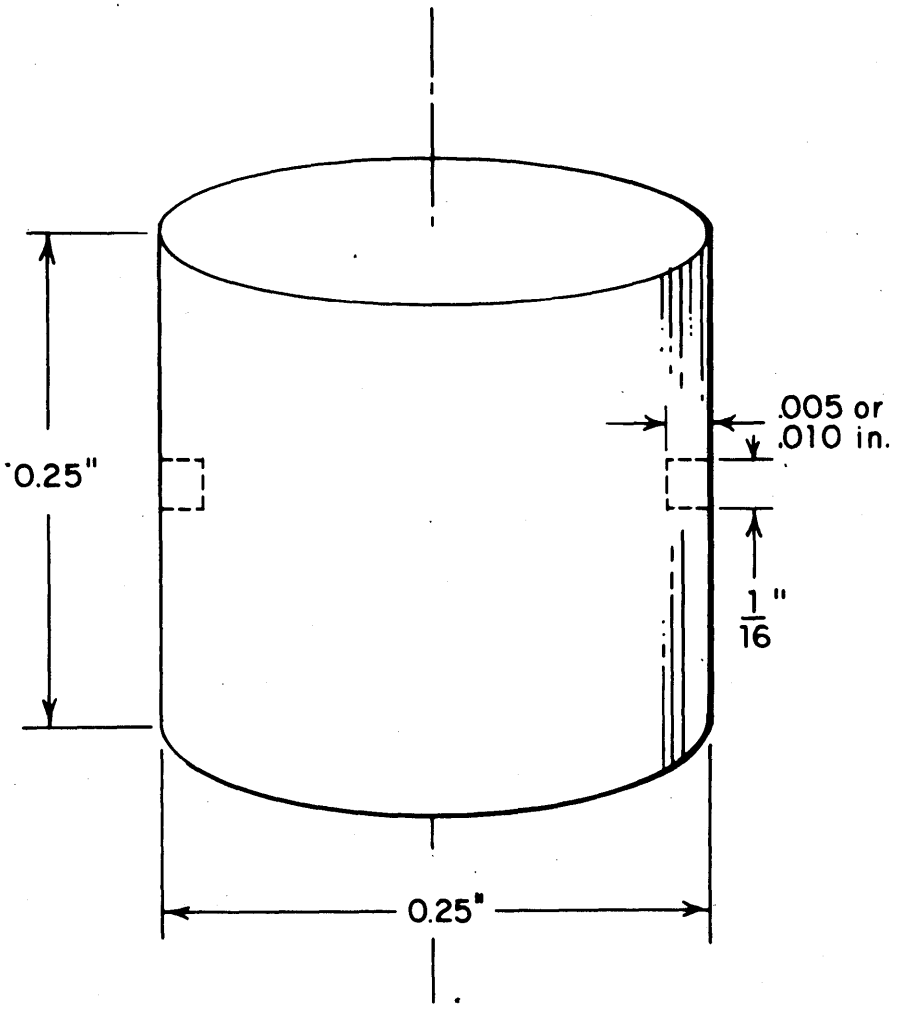

FIG. 2.7 FOIL HOLDER USED FOR FOILS AT THE SURFACE OF THE FUEL

It was found necessary to use catcher foils with the fuel slugs to prevent fission product contamination of the fuel foils in all cases. Wolberg (W4) found it necessary to have catcher foils in experiments in which fission product gamma rays were counted integrally, but catcher foils were not needed when gamma rays in photopeaks resulting from thermal activation were counted (S6). In the case of the threshold reactions, however, the activations are so low that the count rates from fission product contamination are significant when catcher foils are not used, even when the counting is limited to the gamma photopeak of the energy desired. The error resulting from this effect varies with the reaction but generally exceeds 30% of the total count rate when only one side of a detector foil is not covered with a catcher foil. Presumably, it is twice as large if both sides of the detector foil are exposed to fuel. In all cases reported here, a 0.001-inch-thick aluminum catcher foil was used on one side, while 0.001-inch-thick mylar tape was used on the other side and served also to secure the fuel foil in place.

The moderator foils were positioned in the lattices of 0.25-inch-diameter rods by holders of the type illustrated in Fig. 2.8. Since the foils were positioned at different heights, a height correction was required, as discussed in section 2.8. Mounting the foils on horizontal positioning strips would have eliminated this complication. However, for the 0.25-inch-diameter lattice, the design shown in Fig. 2.8 was deemed necessary in order to avoid excessive "shadowing" of the foils farthest from the rod and to obtain an adequate concentration of foil locations near the fuel. The moderator foil holders used in the lattice of 0.75-inch-diameter rods were similar except that the foils were all positioned at the same height since more space was available. Excessive shadowing was avoided in this case by bending the holder slightly to form a "v" as shown in Fig. 2.8.

The moderator foils were covered with cadmium in all cases in order to minimize the effect of competing capture reactions. The cadmium covers were assembled from a 0.060-inch-thick ring and two 0.020-inch-thick, 0.254-inch-diameter discs. This arrangement, while not necessarily either water-tight or "neutron-tight," minimized the amount of cadmium used and permitted rapid unloading of the foils for

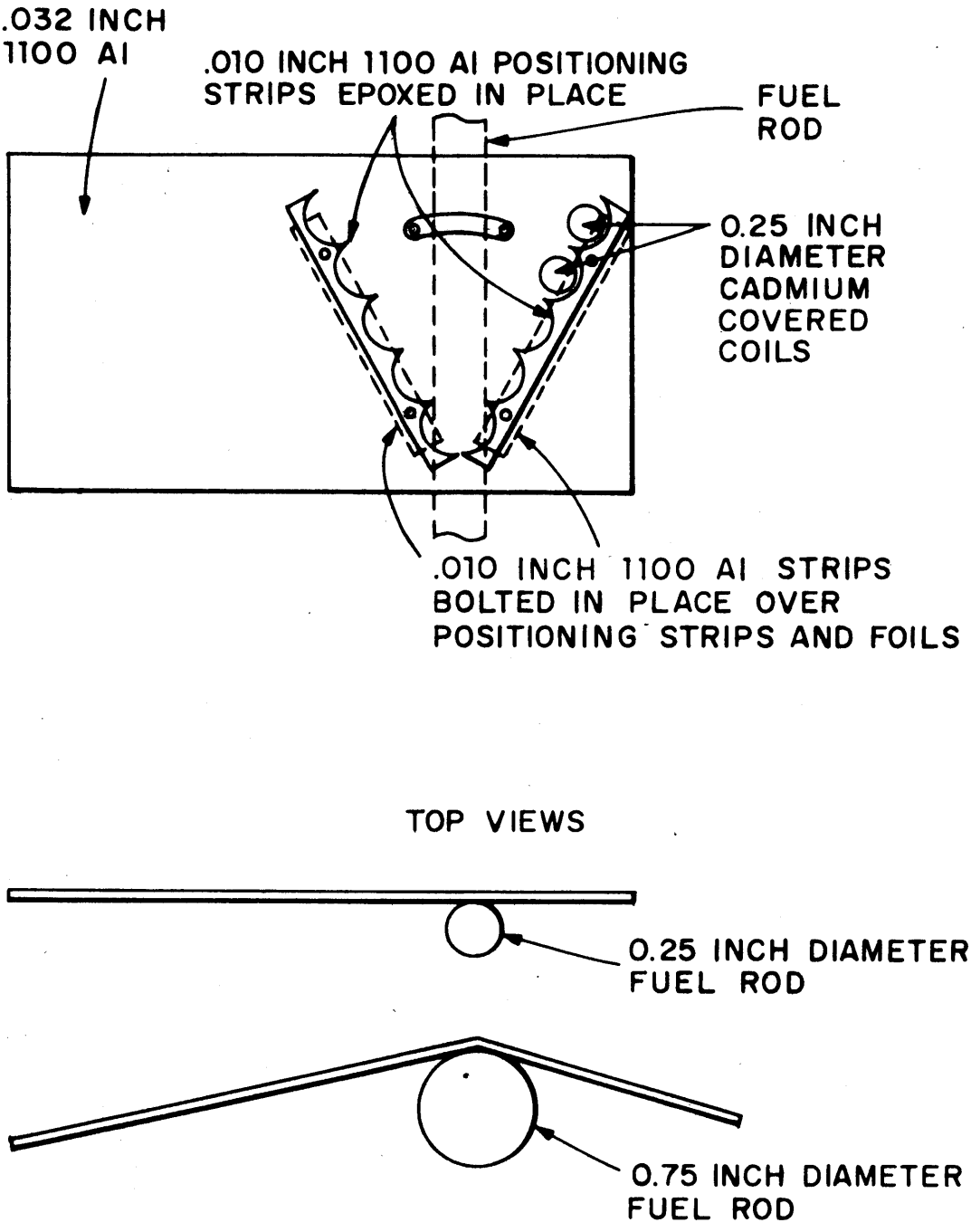

FIG. 2.8 FOIL HOLDER FOR MODERATOR FOILS (DIMENSIONS VARIABLE WITH LATTICE SPACING)

counting. Since the only purpose of the cadmium covers was to reduce thermal activation (no cadmium ratios were computed), this type of cover was satisfactory.

A rough estimate of the effectiveness of the cadmium covers can be obtained from estimates of the cadmium ratios of the competing capture reactions. The cadmium ratios are approximate, since they depend on the neutron energy spectra in the resonance and thermal regions and the spectra vary from lattice to lattice. As will be seen in sections 2.7.1 - 2.7.4, the competing reactions that are most troublesome include: $In^{115}(n, \gamma)In^{116}$ (cadmium ratio about 5); $U^{235}(n, f)$ (cadmium ratio about 20); and $Zn^{68}(n, \gamma)Zn^{69}$ (cadmium ratio about 17).

One additional moderator foil was taped flat against the outside of the cladding in order to obtain an additional data point nearer the fuel. This foil was left bare because a cadmium cover in this position would probably have produced a significant perturbation in the thermal flux in the rod to which it was attached.

The fuel foils were left bare in all cases. Since the thermal flux inside a rod constitutes the major source term for the fast flux originating in that rod, cadmium covers around the fuel slugs would have produced a substantial perturbation in the fast flux being measured. This perturbation would not only have been large but also would have been difficult to correct for. Furthermore, the thermal flux is depressed in the fuel, and, as will be seen, the fast flux peaks in the fuel, often quite sharply. Thus, the fast-to-thermal flux ratio is higher in the fuel, and there is less to be gained by the use of cadmium covers in the fuel.

2.6 Experimental Procedures

All detector foils were cleaned with acetone and then weighed on a microgram balance. The fuel buttons were cleaned with acetone and a 1-mil aluminum catcher foil was inserted into each foil position. The fuel foils were then mounted on the fuel buttons and secured in position with 1-mil mylar tape. The fuel buttons containing the fuel foils were then loaded into special, split fuel elements. The foils were always placed at a carefully measured height at least 16 inches from the bottom of the lattice. Higher counting rates could have been achieved by

irradiating at lower positions in the lattice where the thermal flux was greater, but the U^{238} cadmium ratio, R_{28}, has been found to be a function of axial position in these lattices (D2) up to a height of 16 inches. At about this height, the cadmium ratio reaches its equilibrium value and remains constant at higher positions. For this reason, a height of 16 inches in the lattice was considered to be the lowest at which measurements representative of the lattices studied should be made. The fuel rod containing the fuel foils was always located in either the center position of the lattice or else in the first ring out from the center position.

The holders for the moderator foils and the cadmium covers were cleaned with acetone before the foils were mounted. The holders containing the moderator foils were then attached to regular (non-split) fuel rods at a height such that the bottom edge of the holders was 16 inches from the bottom of the fuel. The fuel rods were loaded in either the second or third rings out from the center position of the lattice. The region in the immediate vicinity of the center rod of the lattice could not be used for the rods with the holders for the moderator foils because it was covered with a lucite plate in which holes were drilled for the rod positions. The holes were only slightly larger than the rod diameter and were therefore too small to permit the passage of the holders for the moderator foils when the rods were lowered into place. This arrangement reduced slightly the counting rates of the moderator foils and necessitated a radial correction in addition to the height corrections mentioned in section 2.8. On the other hand, it was desirable to have the moderator holders and the cadmium covers separated somewhat from the foils in the fuel in order to minimize the perturbation effects discussed in section 4.6.

The length of the various lattice experiments and cooling times are listed in Table 2.2. The experiments with depleted uranium, thorium and nickel were always combined in order to utilize the lattice facility more efficiently on long irradiations.

Upon removal of the rods from the lattice at the end of a run, the foils were extracted from the special rod, cleaned with acetone and mounted on special aluminum planchets for counting.

TABLE 2.2

Experimental Parameters for Threshold Detectors

Reaction	Approx. Threshold (Mev)	Approx. Fission Spectrum Cross Section (mb)	Irradiation Time	Cooling Time	γ Radiation Counted (Mev)	$T_{1/2}$
$In^{115}(n, n')In^{115m}$	0.5	290	8-12 hr	8 hr	0.335	4.5 hr
$U^{238}(n, f)$	1.0	580	1 wk	3 hr	fiss. prod.	–
$Th^{232}(n, f)$	1.2	140	1 wk	3 hr	fiss. prod.	–
$Ni^{58}(n, p)Co^{58}$	2.0	550	1 wk	3 d	0.81	71.3 d
$Zn^{64}(n, p)Cu^{64}$	3.0	269	12 hr	4 hr	0.551	12.8 hr
$Rh^{103}(n, n')Rh^{103m}$	0.2	840	90 min	1 hr	0.04	54 min

2.7 Counting Methods

All counting was done in a specially equipped counting room. The room was air-conditioned and furnished with its own independent electrical power supply to provide maximum stability of the counting equipment. A block diagram of the counting system is given in Fig. 2.9. The preamplifier was designed and built by Mr. David Gwinn.

Each foil had to be hand-counted in each run. No automatic counting equipment was available which combined the use of a multichannel analyzer, adequate shielding for high energy gamma rays, and at least a 3 X 3 inch sodium iodide scintillation crystal. As previously discussed in section 2.3, gamma-ray counting was used in all cases. Some of the pertinent counting data are given in Table 2.2. A more detailed discussion of the counting procedure for the thorium and rhodium detectors is given in section 2.3. The counting methods used for depleted uranium, indium, nickel, and zinc are discussed in more detail below.

2.7.1 The U^{238} (n, f) Reaction

The depleted uranium foils were integrally counted for fission product gamma rays. The energy cut-off of 0.72 Mev was used for the reasons given by Wolberg (W4); his arguments are similar to those which apply to thorium and were discussed in section 2.3 above. Neutron capture in U^{238} leads to the sequence of reactions:

$$U^{238} + n \rightarrow U^{239} \xrightarrow{23 \text{ min.}} Np^{239} + \beta(1.2 \text{ Mev})$$

$$\xrightarrow{2.3 \text{ days}} Pu^{239} + \beta(0.72 \text{ Mev}).$$

Arguments similar to those in section 2.3 can be used to support the use of a cut-off energy below 0.72 Mev. There is less incentive for using a lower cut-off energy with depleted uranium which has a larger fast fission cross section and consequently produces more fission product activity.

2.7.2 The $In^{115}(n, n')In^{115m}$ Reaction

The $In^{115}(n, n')In^{115m}$ reaction is complicated by the competing neutron capture reaction, $In^{115}(n, \gamma)In^{116}$. The magnitude of the capture cross section is approximately 150 barns for thermal neutrons and is

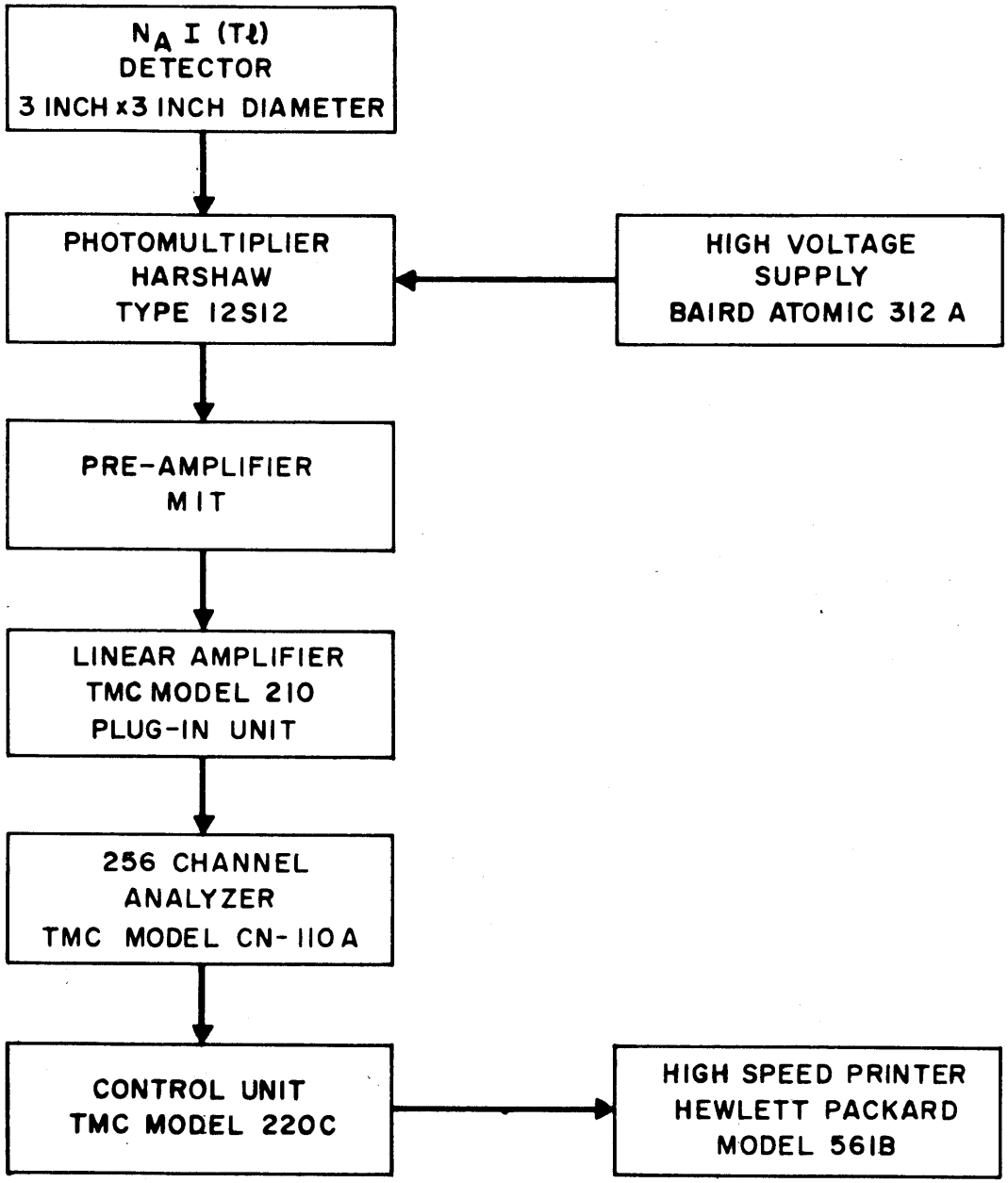

FIG. 2.9 BLOCK DIAGRAM OF COUNTING SYSTEM

substantial for resonance energies above the cadmium cut-off. As a result, the In^{116} activity ($T_{1/2}$ = 54 min.) is detectable even 8 to 12 hours after the end of the irradiation, when the counting of the In^{115m} activity must begin. The In^{116} activity consists of gamma rays with energies greater than the 0.335-Mev In^{115m} activity, so there are Compton effect counts from In^{116} activity underneath the 0.335-Mev photopeak. The contribution from the two decay schemes could be resolved by analysis of the 0.335-Mev photopeak data alone. An example of this method is the use of the FRANTIC code (R4). The method described in Appendix C, however, was found to be more desirable. In this method, the gamma rays under two photopeaks were counted for each foil – the 0.335-Mev In^{115m} photopeak and a 0.406-Mev photopeak from 54-minute In^{116}. One foil, usually a moderator foil with a relatively high count rate, was counted eight or ten times in order to get an accurate calibration as outlined in Appendix C. All other foils were usually counted on three passes; after that, the count rate had decayed too much for additional counting.

2.7.3 The $Ni^{58}(n, p)Co^{58}$ Reaction

The nickel foils presented little experimental difficulty. As stated in section 2.5, all the moderator foils were covered with cadmium to minimize the effects of thermal reactions. In the case of nickel, this was not necessary, but it was done for consistency and to study the possible perturbation caused by the cadmium covers.

The activity of the nickel foils was allowed to decay for approximately three days before counting. This permitted the decay of the 9-hour isomer of Co^{58}, thereby increasing the relative count rate of 71-day Co^{58} and simplifying decay-time corrections. Only the 0.81-Mev photopeak was counted because this method gave the best signal-to-noise ratio and an adequate count rate. The positron annihilation peak at 0.511 Mev is substantial, and in some cases, particularly when sodium iodide crystals smaller than 3 X 3 inches were used, greater accuracy could be obtained by counting the 0.511-Mev peak or both peaks.

No correction was needed for burn-up of Co^{58} and Co^{58m} by neutron capture because the thermal neutron flux in the lattices studied

was about 10^8 neut./cm^2-sec. For measurements in the presence of thermal fluxes greater than 10^{13} neut./cm^2-sec, cadmium covers must be used and/or burn-up corrections must be computed (M6).

2.7.4 The $Zn^{64}(n, p)Cu^{64}$ Reaction

The use of the $Zn^{64}(n, p)Cu^{64}$ reaction is complicated by the neutron capture reaction, $Zn^{68}(n, \gamma)Zn^{69}$. The presence of Zn^{69} is especially troublesome because its decay scheme is similar to that of Cu^{64}, both with respect to half-life (14 hours for Zn^{69} and 12.8 hours for Cu^{64}) and gamma energies (0.44 Mev for Zn^{69} and 0.511 Mev for Cu^{64}). When the gamma activities of these foils are counted, the two peaks can be resolved by standard scintillation counting. The peaks overlap at the lower edges, however, and the Cu^{64} activity must be corrected for counts resulting from the Zn^{69} activity. The method of determining this correction can be explained by reference to Fig. 2.10. The Cu^{64} activity counted corresponded to the gamma rays with energies between $E_{cut\text{-}off}$ and E_{max}, the part labeled A2 in Fig. 2.10. The correction that must be made is for the Zn^{69} activity that extends above $E_{cut\text{-}off}$. This activity corresponds to the part labeled A3 in Fig. 2.10. The first assumption made is that both the 0.44-Mev photopeak and the 0.511-Mev photopeak can be approximated by Gaussian distributions. The second assumption is that, since the energies of the two photopeaks are not very different, the standard deviation of the 0.44-Mev photopeak is the same as that of the 0.511-Mev photopeak. The desired correction was then made as follows:

1. The Cu^{64} activity of an activated copper foil was counted and the resulting 0.511-Mev photopeak was plotted. The combination of a high count rate and the absence of other photopeaks around the plotted photopeak made possible an accurate determination of the standard deviation:

$$\sigma = 1.177\ W, \tag{2.1}$$

where

σ = standard deviation (energy or channel)

W = half-width at half-maximum (energy or channels)

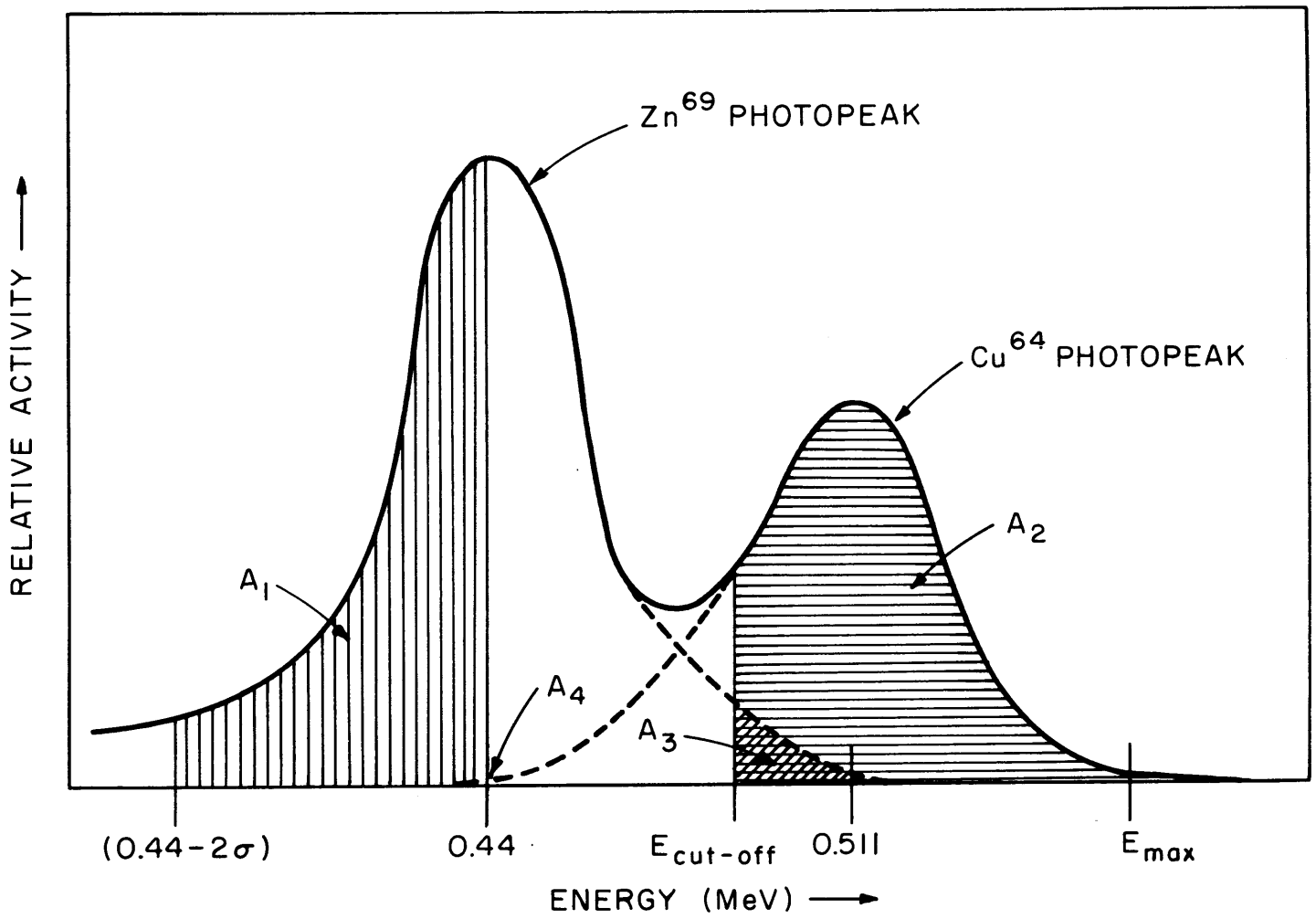

FIG. 2.10 TYPICAL SCINTILLATION COUNTER GAMMA SPECTRUM SHOWING 0.44 MeV AND 0.511 MeV PHOTOPEAKS

2. For each foil, the gamma rays were counted in the interval between 0.44 Mev and (0.44-2σ) Mev. This activity corresponds to the part labeled A1 in Fig. 2.10.

3. The distance between 0.44 Mev and $E_{cut-off}$ was measured in units of the standard deviation.

4. With the use of tabulated integrals of the Gaussian distribution, the ratio, R, was determined:

$$R = A3/A1 . \qquad (2.2)$$

5. The desired correction, A3, was obtained as the product of R and A1.

The activity, A1, counted in step 2, includes a contribution from the 0.511-Mev photopeak. This contribution is labeled A4 in Fig. 2.10. Once A3 has been determined and subtracted from A2, it is possible to use a procedure analogous to the one described above to determine A4. Then A1 is corrected by this amount, step 5 above is used to compute a new value of A3, and the process is iterated. In the foils counted in the present work, such iterations affected the final result by less than 0.1% because the 0.44-Mev photopeak was larger than the 0.511-Mev photopeak and because the distance between 0.44 Mev and 0.511 Mev was greater than the distance between 0.44 Mev and $E_{cut-off}$. Both of these factors tend to reduce the relative value of A4.

Two restrictions must be observed when the above procedure is used with this reaction. The counting is sensitive to gain shift in the counting equipment. This implies that both high count rates and long counting times must be avoided unless auxiliary gain-stabilizing equipment is used. The second limitation is that the fast-to-thermal flux ratio must be favorable. In typical lattices, the ratio of the height of the Zn^{69} peak to the height of the Cu^{64} peak varies from approximately two to four, depending on the lattice spacing and rod size. Measurements made in the highly thermal spectra available in the pneumatic tubes of the MITR and the MITR Medical Therapy Room show that for these spectra the Cu^{64} peak is barely detectable on the side of the Zn^{69} peak, even when the foils are covered with cadmium. In spectra such as these, with a lower fast-to-thermal ratio, analysis is possible only

by using other methods: for example, by using lithium-drifted-germanium diode detectors with higher energy resolution.

2.8 Data Processing Methods and Experimental Uncertainties

The following corrections were made to the count rates of all foils to obtain results normalized to a location at the center of the lattice at a height of 16 inches from the bottom of the lattice:

1. background (including foil background where applicable),
2. differences in activity decay from a common reference time,
3. differences in foil weight,
4. irradiation location relative to the macroscopic J_o flux distribution in the lattice, with the use of experimental results for the radial buckling (H9),
5. irradiation location relative to the axial flux distribution in the lattice (height of irradiation), with the use of experimental results for the axial buckling (H9).

No corrections for counter dead time were needed because a TMC-256 channel analyzer was always used in the "live-time" mode; i.e., dead-time corrections were made automatically.

No correction was necessary for pulse pile-up. This correction may be necessary in δ_{28} experiments when foils of natural uranium, or of higher U^{235} concentration, are irradiated and counted. Such foils may have count rates of 10^5 cpm or higher when they are integrally counted above some cut-off energy (0.72 Mev, for example). In these instances, a significant fraction of the count rate may be due to pulse pile-up counts (W4, D2). The count rate increases sharply with decreasing energy in such cases, and pairs of lower energy pulses can combine to produce a pulse above the cut-off energy. In the present work, the only uranium foils used had a U^{235} concentration of 17.7 parts per million. The maximum count rates achieved were approximately 10^3 cpm. Assuming a typical pulse pile-up factor of 3.3×10^{-5} μseconds/count (W4), the correction for pulse pile-up is less than 0.1% of the total for the maximum count rates. Since this correction would

be even less for the remainder of the foils counted, no attempt was made to correct for pulse pile-up.

No correction was made for the displacement of fuel by the detector foils as discussed by D'Ardenne (D2). The maximum correction, as determined by extrapolation from D'Ardenne's results, is less than 0.05% and applies to the lattices of 0.25-inch-diameter rods on 2.5-inch spacings.

All foils of a particular run were counted at the same distance from the scintillation crystal. The distances varied from approximately 1 cm to 2.5 cm. Tests showed no measurable geometric effects due to the different diameter foils used at these distances.

The activity of the depleted uranium foils irradiated in the fuel had to be corrected for U^{235} fission activity. For this purpose, δ_{28} was assumed to be constant inside the fuel. This assumption is a poor one but leads to negligible error, provided the depleted foils are sufficiently depleted. The fractions of the activity of the depleted uranium foils that resulted from U^{235} fission are listed in Table 2.3.

TABLE 2.3

U^{235} Fraction of Fission Rate in Depleted Uranium Foils

Rod Diameter (inch)	Lattice Spacing (inches)	U^{235} Concentration (%)	δ_{28}	F*
0.25	1.25	1.027	0.0259	0.060
	1.75		0.0232	0.066
	2.50		0.0181	0.083
0.25	1.25	1.143	0.02526	0.056
	1.75		0.02044	0.068
	2.50		0.01639	0.083
0.75	2.50	0.95	0.06091	0.028

* F is the U^{235} fraction of the fission rate in the depleted uranium foils.

The In^{115m} counting was also corrected for In^{116} activity as discussed in section 2.7.2 and Appendix C.

The fission product counting of the depleted uranium foils required additional data processing owing to the absence of a constant half-life for activity decay-time corrections. For this purpose, the time dependence of the fission product activity for each run was fitted to a polynomial by a least-squares computer code. A third-degree polynomial was found to give a reasonable fit. D'Ardenne (D2) also tried semi-log and log-log fits as well as higher order polynomials. There appears to be no significant difference in any of these forms for obtaining the time dependence of fission product gamma activity during a time interval of a few hours.*

A computer code was written early in the course of the work for making all the above corrections and analyzing the data. The code did not prove to be useful and much of the analysis was made with a desk calculator. Among the reasons for this were: all foils were counted by hand, without automatic sample changing equipment; a multichannel analyzer was used for all runs and detailed analysis of the output was generally required; no "foil library" was available – with the exception of the depleted uranium foils (which had to be repeatedly re-weighed, anyway) – all foils used were unirradiated and had to be weighed before each experiment; the moderator holders used in all of the seven lattices studied were such that the position of each individual foil had to be accurately measured and appropriate calculations and corrections made. The above factors combined to produce cases having little in common and requiring large amounts of computer input. This meant that the amount of time spent preparing input data and the delays that are sometimes encountered in the use of a computer frequently exceeded the amount of time required to do the computations on a desk calculator.

---

*This conclusion assumes that counting does not begin until at least two or three hours after the end of the irradiation. The time dependence of fission product gamma activity immediately after irradiation might be more difficult to fit.

The following factors contributed to the experimental uncertainties for all the foils counted:

1. the statistical uncertainty of the count rates,
2. the errors in weighing the foils,
3. the uncertainty in the height of irradiation in the lattice,
4. the uncertainty in the positions of the foils relative to the adjacent fuel rod (i. e., position within the lattice cell) during irradiation.

In addition, there were uncertainties that affected only certain reactions. These included:

1. the uncertainties introduced by fitting curves to the time dependence of the fission product activity of the depleted uranium foils,
2. the uncertainties in the calculation of the U^{235}(n, f) correction to the activity of the depleted uranium foils,
3. the uncertainties in the corrections for Zn^{69} activity in the use of the Zn^{64}(n, p)Cu^{64} reaction,
4. the uncertainty in the correction for In^{116} activity in the use of the In^{115}(n, n')In^{115m} reaction.

The statistical uncertainties in the count rates constituted the major part of the experimental uncertainty for most of the foils counted. The magnitude of the statistical uncertainties varied, not only with the different reactions used and with the different experiments with each reaction, but also with the different foils used in a given experiment. The variation in the uncertainties among the foils in a given experiment was especially large for some of the experiments in the lattices of 0.25-inch-diameter rods. In these lattices, the fuel foils were 1/16 inch in diameter and 0.010 inch or less in thickness, whereas the moderator foils were 1/4 inch in diameter and usually 0.020 inch thick. It was not unusual for the moderator foils to outweigh the fuel foils by a factor of 30. Even though the magnitude of the fast flux was greater in the fuel, the activity of the moderator foils was often 15 or 20 times greater than

that of the fuel foils. The largest values of statistical uncertainties came in counting some of the zinc foils. The gross count rates were sometimes as low as 50 cpm, with background count rates as high as 25 cpm. These values gave statistical uncertainties of about 25%. The smallest values obtained for statistical uncertainties were about 2% from counting some of the indium foils.

The uncertainty in weighing the foils was approximately 0.05 mg. The percentage uncertainty varied from about 1% for the smallest foils used to about 0.025% for the largest foils used.

The uncertainty in height of irradiation in the lattice was roughly 1/8 inch for the fuel foils and 1/4 inch for the moderator foils. These distances corresponded to uncertainties in the activation of about 0.5% for the fuel foils and 1.2% for the moderator foils.

The inaccuracy in the positioning of the foils relative to the adjacent fuel rod had little effect on the foils near the center of the rod and on the foils near the cell edge. At these positions, the gradients of the fast flux were small. Near the edge of the fuel rod, the gradients were large, and the maximum uncertainty due to inaccuracies of 0.010 inch in positioning of the foils in this region could be as high as 5%.

It was difficult to isolate the uncertainties resulting from the fitting of curves to the decay of the fission product activity of the depleted uranium foils. These uncertainties were not easily distinguished from the statistical uncertainties in counting these foils. The difficulty was compounded by the lack of any physical justification for the use of a polynomial for the time dependence of fission product activity decay. Since the true curve is not known to be a polynomial, certain analytical procedures (H6) for estimating this type of uncertainty cannot be used. By comparing the activities of individual foils calculated with polynomials of different order, a rough estimate of 2% can be made for the uncertainty in curve fitting.

The uncertainty associated with the correction of the activity of the depleted uranium foils for activity resulting from the U^{235}(n, f) reaction is considered negligible. The correction for U^{235} fission product activity was less than 9% in every experiment. The reported experimental uncertainties of the δ_{28} values used to calculate this correction were

usually less than 3%. The net uncertainty from this source was therefore much less than 1%.

The results of the zinc experiments are estimated to have an additional uncertainty of about 3% owing to inaccuracies in the corrections for Zn^{69} activity. One reason for this uncertainty is the sensitivity of the correction to the value of the standard deviation of the assumed Gaussian distribution of the gamma-ray photopeaks. A second reason is the sensitivity of the correction to any gain shift that occurs in the counting equipment while the foils are being counted. These two factors combined can change the correction for Zn^{69} by as much as 20%. Since the values of the corrections were about 15% of the total count rate in some cases, the net effect is the introduction of an additional 3% uncertainty.

The values of the correction of the indium foil results for the presence of In^{116} activity varied widely for different foils and for the same foils counted at different times. In a typical counting period, the contribution of the In^{116} activity was initially greater than 50% of the total count rate of the In^{115m} photopeak. As the 54-minute In^{116} decayed more rapidly than the 4.5-hour In^{115m}, this percentage decreased. The procedure described in Appendix C can be used to compute the required correction for In^{116} activity with an accuracy of at least 10%. Since, for most of the indium foils counted, the correction for In^{116} was less than 50% of the total count rate, the additional uncertainty from this source averaged less than 5%.

The combined effects of all the experimental uncertainties are shown with the results in section 4.1.

2.9 Perturbation Experiments

The moderator foils were 0.25 inch in diameter and were covered with cadmium. Any perturbation of the thermal flux in the nearest rod due to the presence of the cadmium directly affected the most important source of fast neutrons. To study this effect, axial flux traverses were made inside the fuel rod directly adjacent to the moderator foils. Measurements were made in each of the three lattices with 0.25-inch-diameter fuel rods. The foils used for the axial traverses were bare

foils made of Au(13.6%)-Pb alloy and were 0.25 inch in diameter. The foil counting and data analysis procedures were the standard ones used by the MIT Heavy Water Lattice Project; they are discussed in more detail in reference S6. The results of the experiments are discussed in section 4.6.

In addition to the above experiment, the $Ni^{58}(n, p)Co^{58}$ reaction was studied in the moderator with a modified foil holder. As discussed in section 2.7.3, the nickel foils can be left bare because competing thermal reactions do not interfere with the counting of the Co^{58} activity. Accordingly, a run was made with bare foils, with a moderator foil holder constructed of 0.012-inch-thick aluminum, the total weight of which was approximately 0.75 grams. This type of holder practically eliminated any possible depression of the fast neutron flux in the foils due to the cadmium covers and the aluminum holder, and avoided any thermal flux depression in the adjacent fuel rod.

Another experiment was performed to test the validity of the height correction procedure. A moderator foil holder was constructed similar to the type shown in Fig. 2.8 except that it was "inverted." The foils were positioned along a line slanting downward, going away from the fuel rod, rather than upward as in the normal holders. The foils closest to the fuel rod in this case were positioned higher in the lattice than those farthest from the fuel. The height corrections were therefore applied in reverse order; i.e., the closest foils had the largest correction and those farther away, the smallest correction. This situation is just the opposite of the normal holders and therefore provides a test of the height correction procedure.

The results of these experiments are given in section 4.6.

2.10 MITR Experiments

Measurements were made to obtain information on the macroscopic distribution of the fast flux in the MIT Reactor. Cadmium-covered, 0.0625-inch-diameter, nickel foils were irradiated for one hour in the thimble in Fuel Position #1, for one and one-half hours in Position #23, and for three hours in the pneumatic sample facility 1PH2 and the experimental facilities 3GV2, 3GV5, and 3GV6 which are located

in the graphite reflector of the MIT Reactor. The locations of these positions are shown in Fig. 2.11. The distances from each position to each of the fuel element positions are given in Table 2.4. The measurements were made in each facility at a height corresponding to the axial midpoint of the fuel. The values of the distances listed in Table 2.4 were taken from a blueprint for a cross section of the reactor at a point two inches below the midpoint of the fuel. Since the graphite vertical facilities are not parallel to the fuel, there is some error involved in those values; but the slant of the facilities is slight and the resulting error is probably negligible. Fuel element Positions 6 and 13 have also been included in Table 2.4. Although no measurements could be made at these positions at the time the data were obtained, they are sometimes used as sample facilities and are therefore of interest. Similarly, Position 20 is the present location of the MIT Organic Loop In-Pile Section. Foil data have been obtained by the Organic Loop Project for this position.

The foils were counted with the procedure described in section 2.7.3. It is important that cadmium covers be used for nickel irradiations to reduce the high thermal fluxes existing around the reactor core. Both Co^{58} with a half-life of 71 days and the 9.1-hour isomer, Co^{58m}, have large thermal neutron capture cross sections. Although corrections for the resulting burn-up of the activity counted can be made (M6), the corrections can be large and require knowledge of the neutron energy spectrum. The use of cadmium covers eliminated these complications.

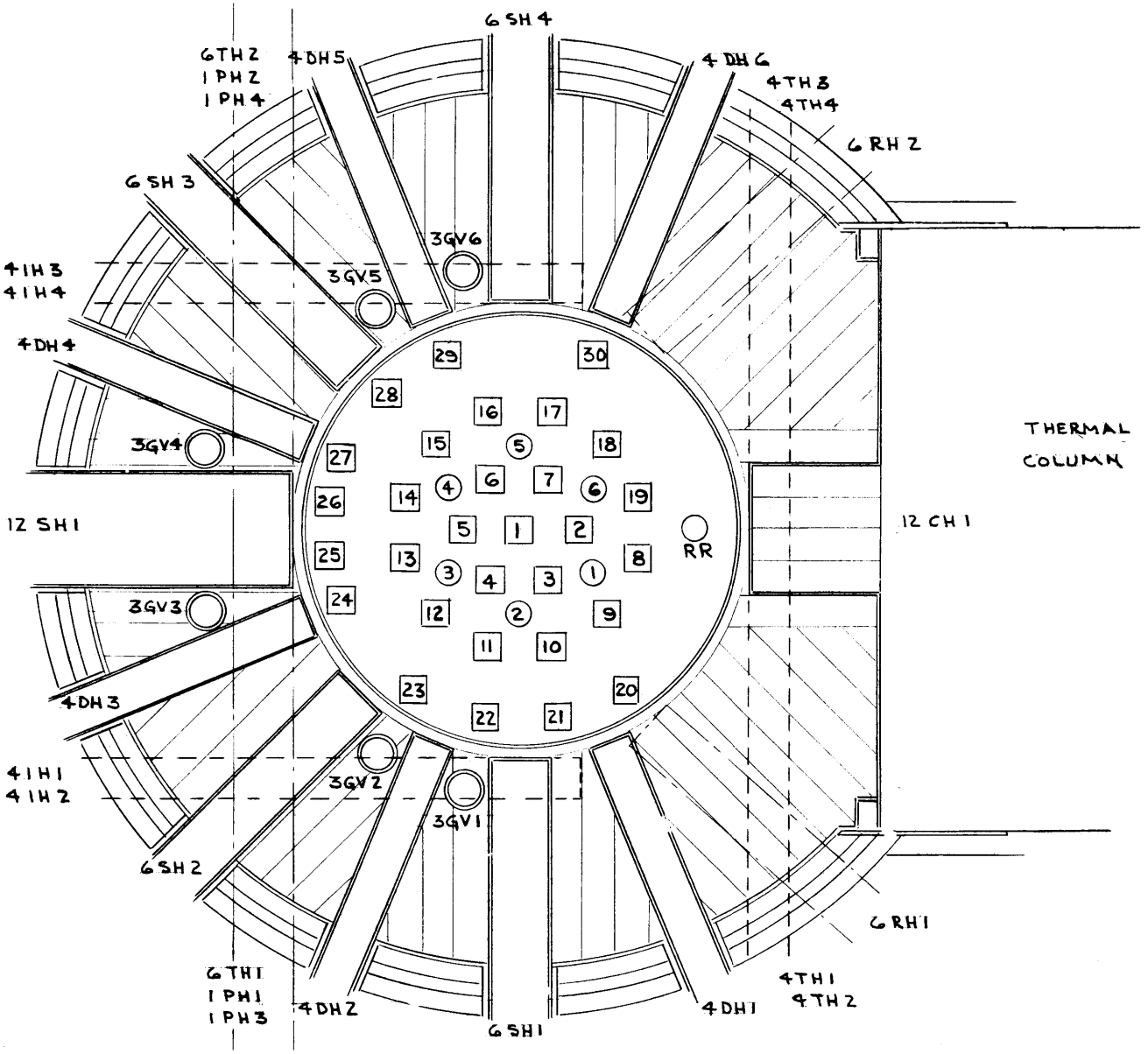

FIG. 2.11 MITR CORE

TABLE 2.4

Distances Between Foil Positions and MITR Fuel Elements

Distance in Inches	Fuel #1	Fuel #2	Fuel #3	Fuel #4	Fuel #5	Fuel #6	Fuel #7	Fuel #8	Fuel #9	Fuel #10	Fuel #11	Fuel #12	Fuel #13	Fuel #14	Fuel #15
Pos. 1	–	6.37	6.37	6.37	6.37	6.37	6.37	13.25	13.25	13.25	13.25	13.25	13.25	13.25	13.25
Pos. 6	6.37	11.00	12.75	11.00	6.37	–	6.37	18.18	19.31	19.31	19.31	16.06	13.12	9.81	7.31
Pos. 13	13.25	19.43	16.06	9.81	7.24	13.12	18.25	25.59	22.81	18.56	18.56	6.85	–	6.85	12.87
Pos. 20	20.93	18.12	14.56	18.87	24.87	27.18	24.31	14.00	8.37	9.43	9.43	22.37	28.00	31.93	33.87
Pos. 23	20.93	24.87	18.87	14.50	18.06	24.31	27.18	28.00	22.43	15.62	15.62	8.31	13.88	20.81	26.74
1PH2	26.56	31.93	29.75	23.81	19.31	22.43	28.68	38.68	36.81	32.68	32.68	20.18	14.12	12.68	17.25
3GV2	29.00	33.00	26.68	22.75	26.25	29.56	35.43	35.31	29.18	22.31	22.31	16.50	21.31	28.12	34.43
3GV5	29.00	32.87	35.37	32.44	26.19	22.62	26.68	42.75	44.94	44.68	44.68	34.31	28.06	21.25	16.37
3GV6	29.00	30.94	35.06	34.00	28.37	23.06	24.62	36.87	40.69	42.12	42.12	37.81	32.56	25.81	19.31
	#16	#17	#18	#19	#20	#21	#22	#23	#24	#25	#26	#27	#28	#29	#30
Pos. 1	13.25	13.25	13.25	13.25	20.93	20.93	20.93	20.93	20.93	20.93	20.93	20.93	20.93	20.93	20.93
Pos. 6	7.31	9.81	13.12	16.06	27.18	27.00	26.00	24.31	21.00	19.37	17.74	16.25	14.81	14.56	17.68
Pos. 13	18.56	22.81	25.59	26.37	28.00	23.93	19.12	13.87	7.87	7.93	10.00	13.12	18.31	23.18	30.75
Pos. 20	33.62	31.24	26.81	20.81	–	8.06	15.87	23.12	32.18	35.37	37.93	39.81	41.50	41.50	36.81
Pos. 23	31.12	33.56	33.87	31.93	23.12	15.93	7.75	–	12.00	17.06	21.93	26.31	32.18	36.75	41.50
1PH2	24.00	30.31	35.25	38.18	42.18	37.62	31.68	24.50	12.56	7.50	4.68	7.94	15.94	23.87	37.12
3GV2	39.25	41.81	42.06	39.81	28.06	20.00	12.25	8.19	16.94	23.12	27.75	32.68	39.38	44.50	49.81
3GV5	16.81	22.18	29.06	35.25	49.88	49.25	47.06	42.00	32.68	27.75	22.37	16.94	9.75	9.19	24.06
3GV6	15.81	18.19	24.44	31.18	49.25	52.94	48.87	46.00	38.68	34.50	29.56	24.38	16.18	10.88	15.87

Chapter III

THEORETICAL AND ANALYTICAL METHODS

3.1 Introduction

Two computer codes written in the course of this work, UNCOL and RATIO – and a third code, HEETR, written by Dr. H. K. Clark of the Savannah River Laboratory – are discussed in this chapter. The UNCOL code computes the relative spatial distribution of the fast flux in and around fuel rods. The HEETR code calculates fast flux distributions and other parameters for uniform lattices and for lattices of clustered rods. The RATIO code computes activation ratios from HEETR results.

3.2 The UNCOL Code

3.2.1 Introduction

Methods making use of transport theory can be divided into three general types: kernel methods, integral transport theory methods, and general transport theory methods. The relative merits of each type are discussed elsewhere (W1). The kernel methods are characterized by simplicity and directness. They have the disadvantages of being limited in their applicability and of requiring, in most cases, experimental data. Kernel methods are particularly suitable for treating fast neutrons because the cross sections involved are small and the number of interactions of interest are limited. For these reasons, a kernel method was selected for use in developing a theoretical representation of the fast flux. This effort resulted in the UNCOL code which computes the spatial distribution and magnitude of the uncollided fast flux. The computation consists of integrating a modified form of the single collision transport kernel for cylindrical shell sources. The integration is over the radius of all fuel rods in the assembly. The results are multiplied

by the appropriate weighting coefficients (usually a J_o distribution) and then summed to give the relative fast flux at points of interest.

The following assumptions are made:

(1) the kernel for cylinders of infinite length may be used for cylinders of finite length;

(2) the homogeneous kernel may be used for heterogeneous configurations by making suitable adjustments in the cross sections;

(3) the spatial distribution of the fission rate within a fuel rod may be expressed by the relation: $S(r') = C_o + C_1(r')^2$.

3.2.2 Applicability

The group of fast neutrons treated is not well defined. Some restrictions on the group can be specified, however, and qualitative boundaries can be defined.

Consider a source of fast neutrons with some energy spectrum, S(E). The neutrons with energies greater than some value, E_L, are of interest. It is assumed that all neutrons with energies above this value are either source neutrons which have undergone no interaction or neutrons which have experienced interactions that did not significantly affect their direction of travel. It is clear that this assumption is valid, provided E_L is sufficiently large. The cross sections of interest are then of the "removal" type used in multigroup calculations. If E_L is too small, the method will fail because a significant fraction of the neutrons with energies greater than E_L will have experienced interactions (notably, inelastic scattering and large angle elastic scattering) which significantly changed their direction of travel. Since no provision for treating changes in direction is included in the model, the latter group cannot be accurately calculated.

In the present case, the source group, S(E), is the fission neutron spectrum. The assemblies studied are cylindrical and are composed primarily of uranium and heavy water. Although the magnitude of E_L is not required for calculations, a rough estimate is useful in order to estimate the range of applicability of the results, For this purpose, it

is convenient to consider uranium and heavy water separately.

Murley (M3) has considered in detail the energy spectrum of the neutrons which have had one or two collisions in uranium. The spectra of these neutrons and of fission neutrons are shown in Fig. 3.1. More than 70% of the once-collided neutrons have energies below 1 Mev. Furthermore, this group does not include those neutrons which were captured in the first collision (i.e., it is smaller than the uncollided group). In addition, some (probably most) of the once-collided neutrons with energies greater than 1 Mev have changed their direction of travel only slightly. It is therefore reasonable to conclude that a large fraction of the neutrons above 1 Mev (perhaps 90% or more) are adequately covered in the model described above.

The treatment of the heavy water is more difficult. While in uranium elastic scattering can be almost completely ignored and the effects of inelastic scattering are not complicated, in heavy water this is not the case. Except for some inelastic scattering by oxygen (which poses no problem), the reaction of primary interest is elastic scattering. The analysis is complicated by the fact that in elastic scattering by heavy water, both the incident neutron energy, E, and the energy transfer, ΔE, must be considered. Furthermore, there is no fixed value of the scattering angle which provides a measure of change of direction below which the model can be said to be valid and above which the model fails. Accordingly, it is not particularly profitable to attempt a detailed analysis for the determination of E_L in heavy water. Instead, the model can be compared with experiments and some qualitative observations made.

The first observation is that both the fission spectrum and the elastic scattering cross section of heavy water decrease faster than linearly with increasing energy for energies greater than about 1 Mev. Both of these factors tend to limit the fraction of neutrons above 1 Mev which have been scattered through "large" angles. The second observation is that small angle scattering is favored by both high Z nuclides and low Z nuclides: the former because of the higher cross section for small angles, and the latter because of the translation from center-of-mass coordinates to laboratory coordinates.

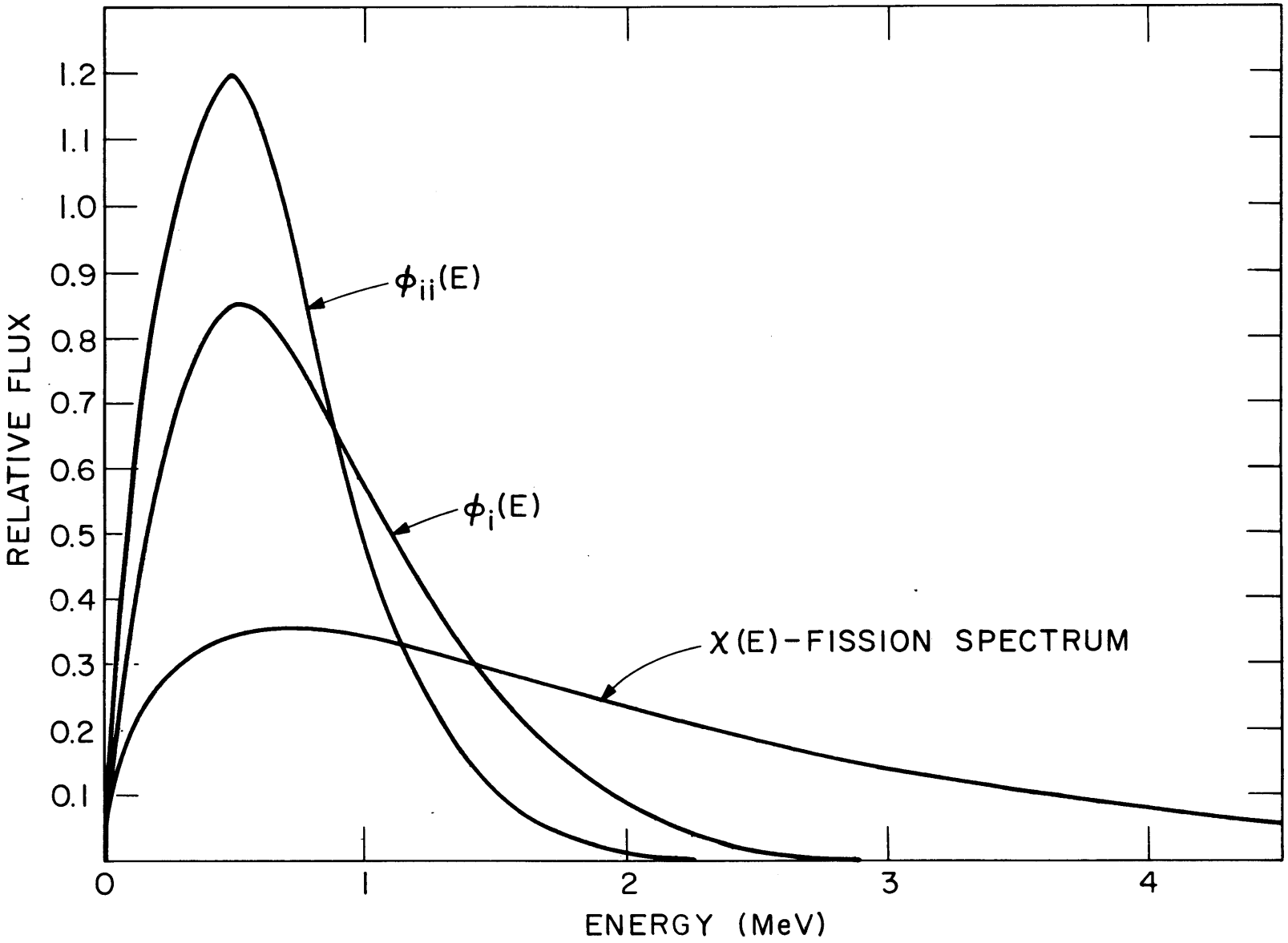

FIG. 3.1 ENERGY SPECTRA OF ONCE AND TWICE-COLLIDED NEUTRONS IN URANIUM

In view of the above arguments, it appears that the lower energy bound for the group of neutrons which can be treated by the present model is probably somewhere in the vicinity of 1 Mev.

3.2.3 Derivation

The single-collision transport kernel expresses the first collision neutron density at a point r, resulting from a cylindrical shell source of infinite length and of radius r'. The kernel has been tabulated by Weinberg and Wigner (W1); it has also been derived from the point kernel by Cady (C1).* It is:

$$\overline{T_c}(r, r') = \frac{\Sigma}{2\pi} \int_1^\infty K_o(\Sigma r y)\, I_o(\Sigma r' y)\, dy, \quad r > r', \tag{3.1}$$

$$\overline{T_c}(r, r') = \frac{\Sigma}{2\pi} \int_1^\infty K_o(\Sigma r' y)\, I_o(\Sigma r y)\, dy, \quad r < r'. \tag{3.2}$$

If we are interested, not in the first collision density, but rather in the fast neutron flux, we need only divide $\overline{T_c}(r, r')$ by Σ (the total cross section) to give the uncollided flux transport kernel, $T_c(r, r')$. This procedure is a straightforward one for monoenergetic source neutrons in a homogeneous medium. The consideration of an energy-dependent source in a multiregion assembly requires a definition of what is meant by the uncollided flux and an appropriate calculation of the cross section used. In this case, the uncollided flux is the integrated flux above a minimum energy, E_L. Then, for consistency, the cross section used must be the effective removal cross section.

If the source is not a cylindrical shell but a cylindrical rod, the uncollided flux at point r is obtained by integrating $T_c(r, r')$ over the radius of the rod:

$$T'_R(r) = \int_{R_1}^{R_2} dr'\, 2\pi r'\, T_c(r, r'). \tag{3.3}$$

---

*Some additional remarks concerning this kernel are made in Appendix B.

Equation 3.3 is valid only if the source is constant over the radius of the rod. This restriction can be removed by the introduction of a source term, S(r'), suitably normalized, which gives the radial dependence of the source. We may then write:

$$T_R(r) = \int_{R_1}^{R_2} dr'\ 2\pi r'\ S(r')\ T_c(r, r')\,. \tag{3.4}$$

The form of the source term S(r') is arbitrary. The only requirement is that it should give a reasonable approximation to the source distributions of interest. It is mathematically convenient to express S(r') in the form of a polynomial in even powers of r' :

$$S(r') = C_o + C_1(r')^2 + C_2(r')^4 + \ldots + C_N(r')^{2N}\,. \tag{3.5}$$

This form has the advantage that, being an even function of r', it better represents the source because, on physical grounds, the fission reaction rate distribution is symmetric about the center of the fuel rod except for macroscopic perturbations. In fact, as will be seen in section 4.1.1, truncation after the first two terms of Eq. 3.5 provides an excellent approximation for cases of interest.

Truncating Eq. 3.5 after two terms and substituting into Eq. 3.4 gives:

$$T_{Ra}(r) = \int_{R_1}^{R_2} dr' \left[C_o r' + C_1 r'^3\right] \int_1^\infty K_o(\Sigma r y)\ I_o(\Sigma r' y)\ dy, \quad r > r'; \tag{3.6}$$

$$T_{Rb}(r) = \int_{R_1}^{R_2} dr' \left[C_o r' + C_1 r'^3\right] \int_1^\infty K_o(\Sigma r' y)\ I_o(\Sigma r y)\ dy, \quad r < r'\,. \tag{3.7}$$

Reversing the order of integration in the last two equations gives:

$$T_{Ra}(r) = \int_1^\infty dy\ K_o(\Sigma r y) \int_{R_1}^{R_2} dr' \left[C_o r' + C_1 r'^3\right] I_o(\Sigma r' y)\,, \tag{3.8}$$

$$T_{Rb}(r) = \int_1^\infty dy\ I_o(\Sigma r y) \int_{R_1}^{R_2} dr' \left[C_o r' + C_1 r'^3\right] K_o(\Sigma r' y)\,. \tag{3.9}$$

The integrations over r′ can be performed analytically with the aid of the following relations:*

$$\int x\, I_o(x)\, dx = x\, I_1(x)\,, \tag{3.10}$$

$$\int x\, K_o(x)\, dx = -x\, K_1(x)\,, \tag{3.11}$$

$$\int x^3 I_o(x)\, dx = -4 \int x I_o(x)\, dx + \left[x^3 I_1(x) + 2x^2 I_o(x)\right], \tag{3.12}$$

$$\int x^3 K_o(x)\, dx = 4 \int x K_o(x)\, dx - \left[x^3 K_1(x) + 2x^2 K_o(x)\right]. \tag{3.13}$$

Making the appropriate change of variables and using Eqs. 3.10 - 3.13, we get:

$$T_{Ra}(r) = \int_1^\infty dy\, K_o(\Sigma r y)\, P_{Ra}(R_1, R_2, \Sigma, y), \tag{3.14}$$

$$T_{Rb}(r) = \int_1^\infty dy\, I_o(\Sigma r y)\, P_{Rb}(R_1, R_2, \Sigma, y)\,, \tag{3.15}$$

where

$$P_{Ra}(R_1, R_2, \Sigma, y) = \frac{I_1(\Sigma R_2 y)}{\Sigma y}\left[C_o R_2 + C_1 R_2^3 - \frac{4C_1 R_2}{(\Sigma y)^2}\right] + \frac{2C_1 R_2^2}{(\Sigma y)^2} I_o(\Sigma R_2 y)$$
$$- \frac{I_1(\Sigma R_1 y)}{\Sigma y}\left[C_o R_1 + C_1 R_1^3 - \frac{4C_1 R_1}{(\Sigma y)^2}\right] - \frac{2C_1 R_1^2}{(\Sigma y)^2} I_o(\Sigma R_1 y)\,; \tag{3.16}$$

$$P_{Rb}(R_1, R_2, \Sigma, y) = \frac{K_1(\Sigma R_1 y)}{\Sigma y}\left[C_o R_1 + \frac{4C_1 R_1}{(\Sigma y)^2} + C_1 R_1^3\right] + \frac{2C_1 R_1^2}{(\Sigma y)^2} K_o(\Sigma R_1 y)$$
$$- \frac{K_1(\Sigma R_2 y)}{\Sigma y}\left[C_o R_2 + \frac{4C_1 R_2}{(\Sigma y)^2} + C_1 R_2^3\right] - \frac{2C_1 R_2^2}{(\Sigma y)^2} K_o(\Sigma R_2 y)\,. \tag{3.17}$$

---

*Equations 3.12 and 3.13 are special cases of a general reduction formula due to Watson (W5).

The integrations in Eqs. 3.14 and 3.15 are done numerically in UNCOL. The parabolic rule for integration is used (H6), but the mesh spacing is left arbitrary to be included as input to the code. These points are discussed in greater detail in Appendix A.

For points inside the fuel rod, the uncollided flux is the sum of integrals of three types. Equation 3.14, with $R_1 = 0$ and $R_2 = r$, gives the contribution from the cylindrical portion of the rod from the center out to the radius r. Equation 3.15, with $R_1 = r$ and $R_2 = R_o$, gives the contribution of the annular section of the fuel rod "outside" the point of interest. The third type of integral gives the contribution from fuel rods other than the one in which the point is located. For this, Eq. 3.14 is used repeatedly with $R_1 = 0$, $R_2 = R_o$ and with r equal to the distance to the center of each rod.

For points outside the fuel, Eq. 3.14 is used repeatedly for each rod with $R_1 = 0$, $R_2 = R_o$ and r the distance to the center of each rod calculated.

Until now, the procedure for the calculation of the cross section, Σ, has been left open. For a homogeneous medium, Σ should be the effective removal cross section consistent with the considerations of section 3.2.2. It is probably best determined by experiment, but it should be closely approximated by the removal cross section of the highest energy group in a set of multigroup constants. As stated in section 3.2.1, the group should be one with a lower boundary at approximately 1 Mev.

The extension to two regions requires further definition of Σ. The accuracy of the method is probably improved if the values of Σ for the two regions are not very different. Fortunately, cross sections for fast neutrons (especially if averaged over an energy interval) do not show the extreme variations that are often seen in thermal cross sections. In UNCOL, Σ is treated as a function of distance from the center of the fuel rod for which the calculation is made. The weighted average of the fuel and moderator values is calculated by using the fractions of the straight line distance as weights:

$$\Sigma(r) = \frac{\Sigma_F R_o + \Sigma_M (r - R_o)}{r} . \qquad (3.18)$$

For points inside the fuel rod for which the calculation is made, $\Sigma = \Sigma_F$.

Results of UNCOL calculations for the lattices studied, as well as for the MIT Reactor core, are given in Chapter IV. A FORTRAN listing of the code is given in Appendix A which also includes sample input and output for several different types of calculations.

3.3 The HEETR Code

The HEETR code is an integral transport code used to calculate high energy events in thermal reactors (C9, C10). A brief description follows.

HEETR is a multigroup, multiregion code for cylindrical assemblies and is written in FORTRAN II. The basic assumptions used in the code are:

(1) scattering in the laboratory system is isotropic;

(2) the distribution of secondary neutrons is uniform within each region;

(3) the distribution of currents at interfaces is uniform over the interface;

(4) the number of neutrons passing through an interface per unit solid angle is proportional to the cosine of the angle that the direction of travel makes with the normal to the interface;

(5) the reactor is infinite.

The neutron current leaving a region is expressed, in terms of the current entering the region, by means of transmission probabilities and, in terms of sources within the region, by means of escape probabilities. For regular lattice arrays, a cell boundary condition is used (net current at outer interface of outer region equals zero). For clusters of cylindrical fuel elements, Dancoff factors are used to approximate the interaction between elements.

The code requires as its input values of microscopic group cross sections, dimensions, and nuclide concentrations. The relative spatial distribution of thermal fissions is also required. For each neutron group, the code computes disadvantage factors in each region. The

spatially averaged flux integrated over energy, and spatial averages of nuclear parameters are also calculated. In particular, the ratio of U^{238} fissions to U^{235} fissions, δ_{28}, is calculated for each fuel region as well as for the entire fuel rod. The lower energy bound for which the code is applicable is not specified, but the code is probably useful down to the energies at which resonance self-shielding becomes significant.

Some modifications were made in the code for use at MIT, so that the program used is somewhat different from the one listed in reference C10. The modifications are limited mainly to control sequencing and parameter dimensions. A listing of the FORTRAN deck and sample input and output are given in Appendix A. The results of HEETR calculations made for the lattices studied in this work are given in section 4.1.1.

3.4 The RATIO Code

The RATIO code was written to analyze the energy spectra calculated by the HEETR code in terms of various fast reactions. It calculates a matrix of the ratios of the fast reaction rates. It also calculates for each reaction and spectrum the relative contribution by each energy group to the total activation. The boundaries of the energy groups are variable. The code was written for a five-group structure, but the extension to a greater number of groups is straightforward.

In RATIO, the multigroup energy spectrum is converted into a "fine-mesh" differential energy spectrum as follows. In all except the highest energy group, the spectrum is treated as a histogram consistent with the relative values of the different groups; i. e., the flux is assumed constant over the energy range of each individual group. The highest energy group is treated as a portion of the fission neutron energy spectrum. The highest energy group is then normalized so that its integral is consistent with the relative fluxes in the groups computed by HEETR. This procedure involves the assumption that the lower bound of the highest energy group is sufficiently high so that the spectrum above this point does, in fact, correspond to part of a fission spectrum. As will be seen in Chapter IV, this criterion seems to be satisfied in the cases considered. Some sort of special treatment such as this one is needed for the first group. This group has no specified upper energy

bound. If, for example, in the calculation of activation integrals, an upper bound is chosen and it is arbitrarily set too low, the activation due to neutrons above this energy is completely ignored. Conversely, if some value is set for the upper energy bound and this value is too high, then it is likely that the activation occurring at the lower energies in the group will be underestimated. The source of this difficulty is the exponential nature of the energy spectrum of the flux at the higher energies. The choice of the fission spectrum shape is then not only logical on physical grounds but is needed for consistent calculations.

With the above procedure, a fine-mesh flux is computed in increments of 0.25 Mev. The saturated specific activation for a given reaction, denoted by i, is then:

$$A_i = \int_0^\infty \phi(E)\, \sigma_i(E)\, dE\,. \tag{3.19}$$

The integration of Eq. 3.19 is done with the aid of the trapezoidal rule. The cross-section data used are identical with those compiled by Rydin (R1) except for the $Rh^{103}(n, n')Rh^{103m}$ data which were compiled from the theoretical curve by Vogt and Cross (V1).

A print-out of the FORTRAN source program and sample input and output of RATIO are given in Appendix A.

Chapter IV

EXPERIMENTAL RESULTS AND COMPARISON WITH ANALYTICAL METHODS

4.1 Spatial Distributions of Fast Neutrons

4.1.1 Lattice Results

The intracellular spatial distributions for the $In^{115}(n, n')In^{115m}$, $U^{238}(n, f)$, $Ni^{58}(n, p)Co^{58}$, and $Zn^{64}(n, p)Cu^{64}$ reactions are given in Figs. 4.1 - 4.4 for the lattices of 0.25-inch-diameter rods containing 1.027% U^{235}. The intracellular spatial distributions for these reactions in the lattices of 0.25-inch-diameter rods containing 1.143% U^{235} are given in Figs. 4.5 - 4.8. For both U^{235} concentrations, the lattices with 0.25-inch-diameter rods had spacings of 1.25, 1.75, and 2.50 inches, respectively. The results for the one lattice of 0.75-inch diameter rods containing 0.947% U^{235} are given in Figs. 4.9 - 4.12; the spacing in this lattice was 2.50 inches.

The experimental results are normalized at the edge of the lattice cell because the results obtained with the moderator foils were more accurate (mainly because of their larger size) than the results obtained with the fuel foils. It is important to keep this normalization in mind when interpreting the results. For example, it might be concluded from Fig. 4.1 that the magnitude of the fast flux inside the fuel rod of the lattice with 2.50-inch spacing is greater than the fast flux inside the fuel rod of the lattice with 1.25-inch spacing. In fact, the contrary is true: since the interaction effect between rods increases as the rod spacing decreases, the magnitude of the fast flux also increases.* The magnitude of the fast flux in the fuel of the lattice with 1.25-inch spacing is

---

*The actual magnitude of the fast flux also depends on a number of other things. The MIT Reactor is the source of neutrons for the lattice, so the magnitude of the fast flux in the lattice varies with the power level of the reactor. Similarly, the height of the regulating rod of the reactor is a factor because it is located near the end of the thermal

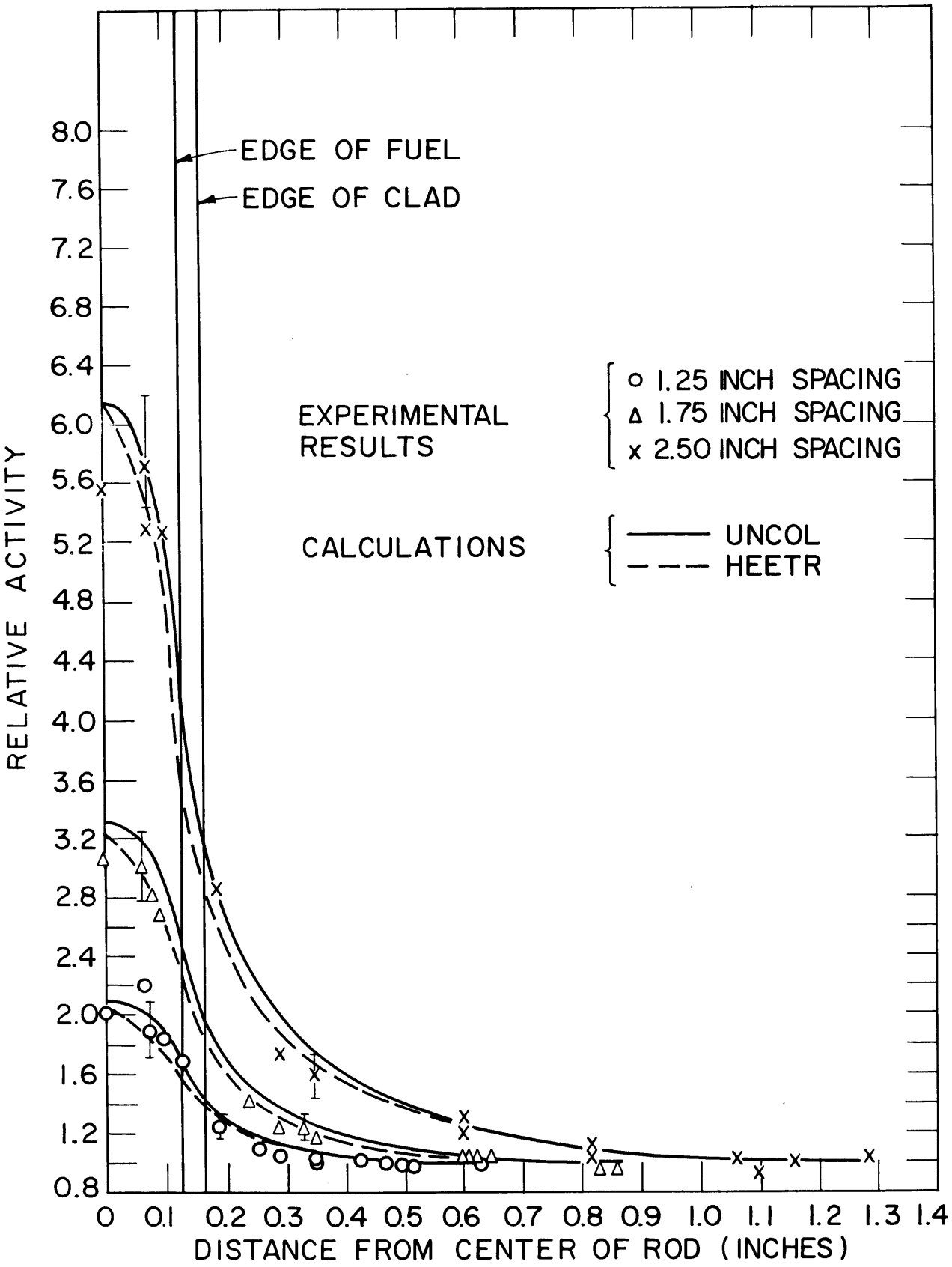

FIG. 4.1 $In^{115}(n,n^{1})\ In^{115m}$ ACTIVITY DISTRIBUTION FOR LATTICES OF 0.25 INCH DIAMETER, 1.027% U^{235} RODS

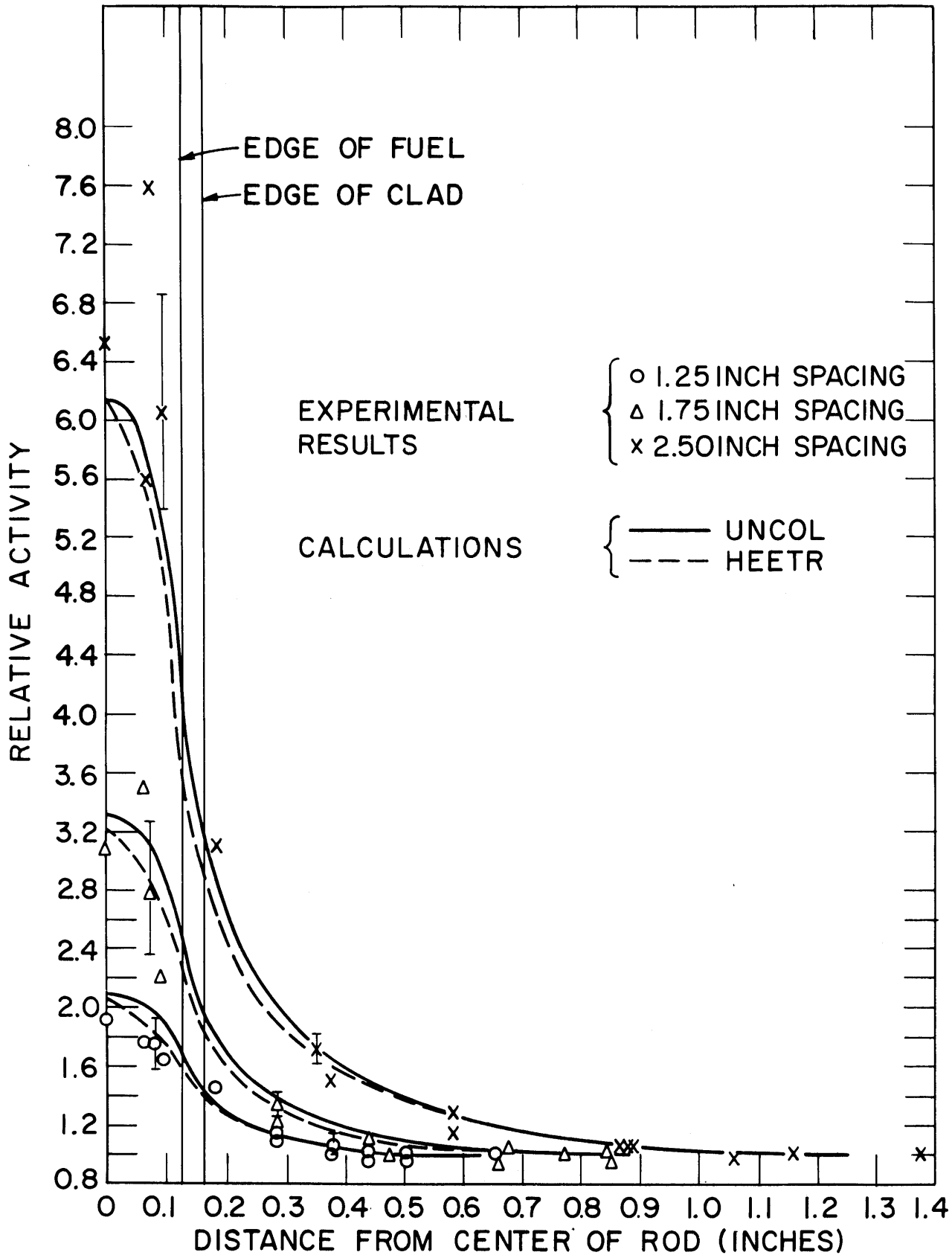

FIG. 4.2 $U^{238}(n,f)$ ACTIVITY DISTRIBUTION FOR LATTICES OF 0.25 INCH DIAMETER, 1.027 % U^{235} RODS.

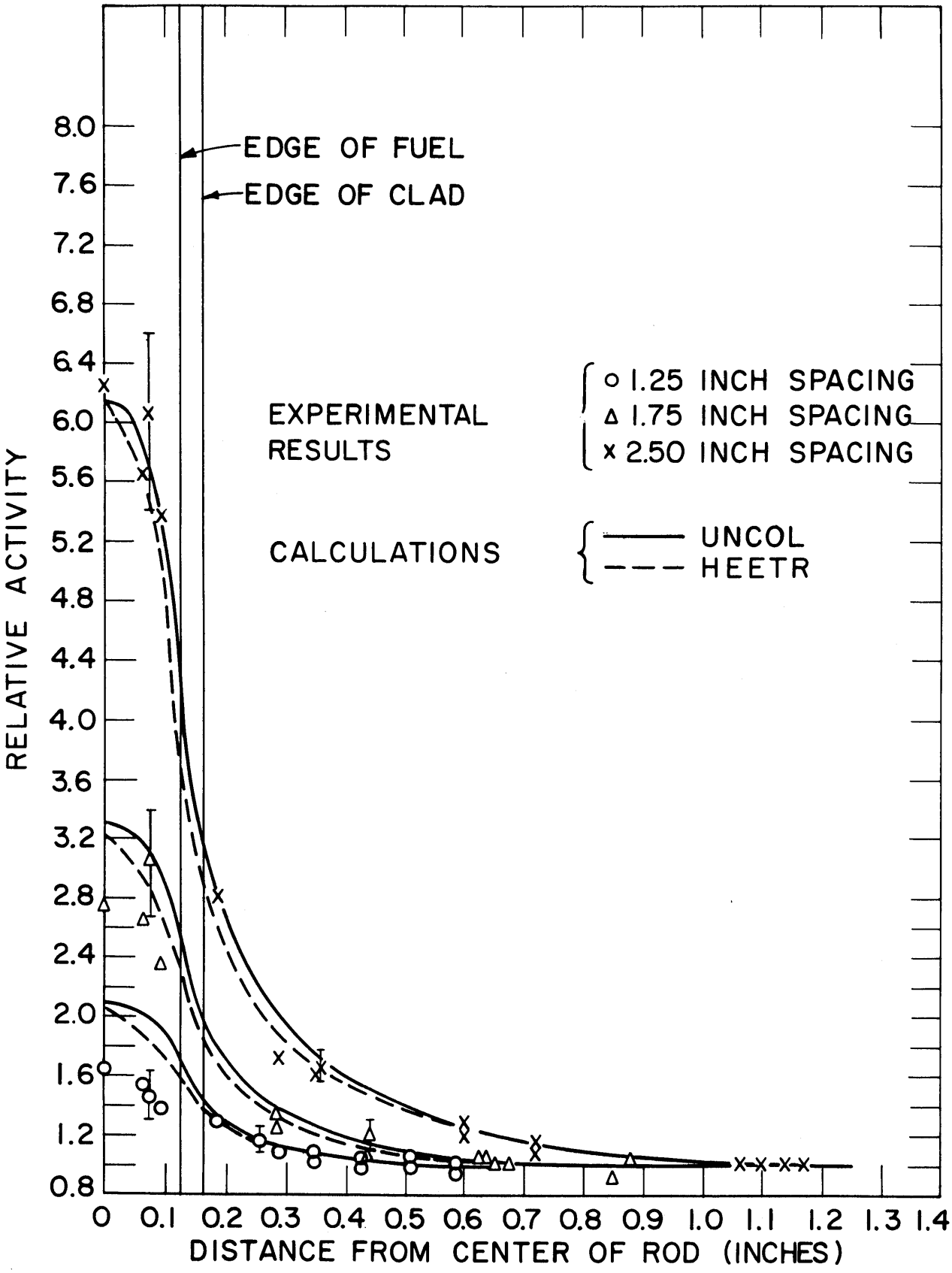

FIG. 4.3 Ni^{58} (n, p) Co^{58} ACTIVITY DISTRIBUTION FOR LATTICES OF 0.25 INCH DIAMETER, 1.027 % U^{235} RODS

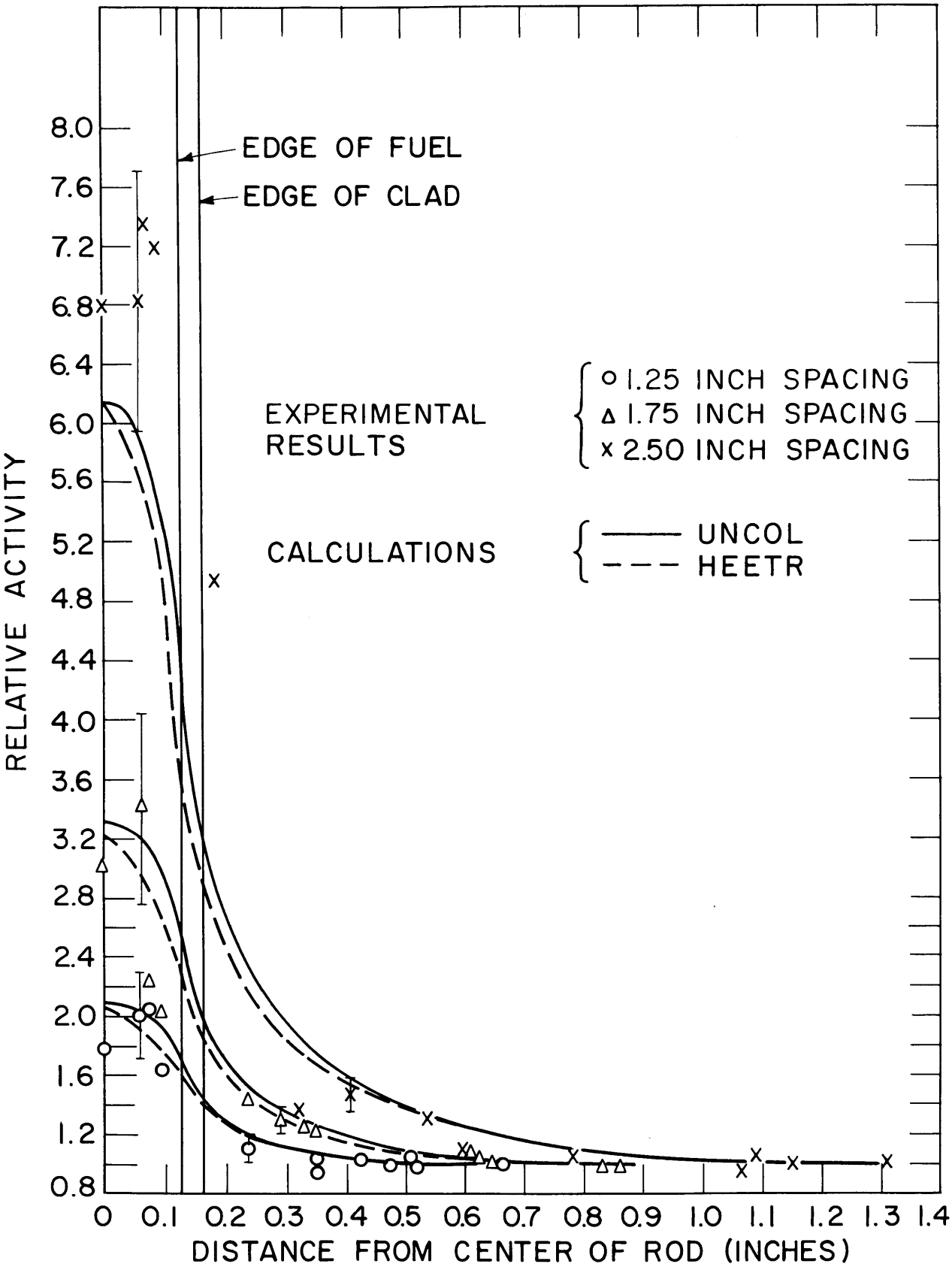

FIG. 4.4 $Zn^{64}(n,p)Cu^{64}$ ACTIVITY DISTRIBUTION FOR LATTICES OF 0.25 INCH DIAMETER, 1.027% U^{235} RODS

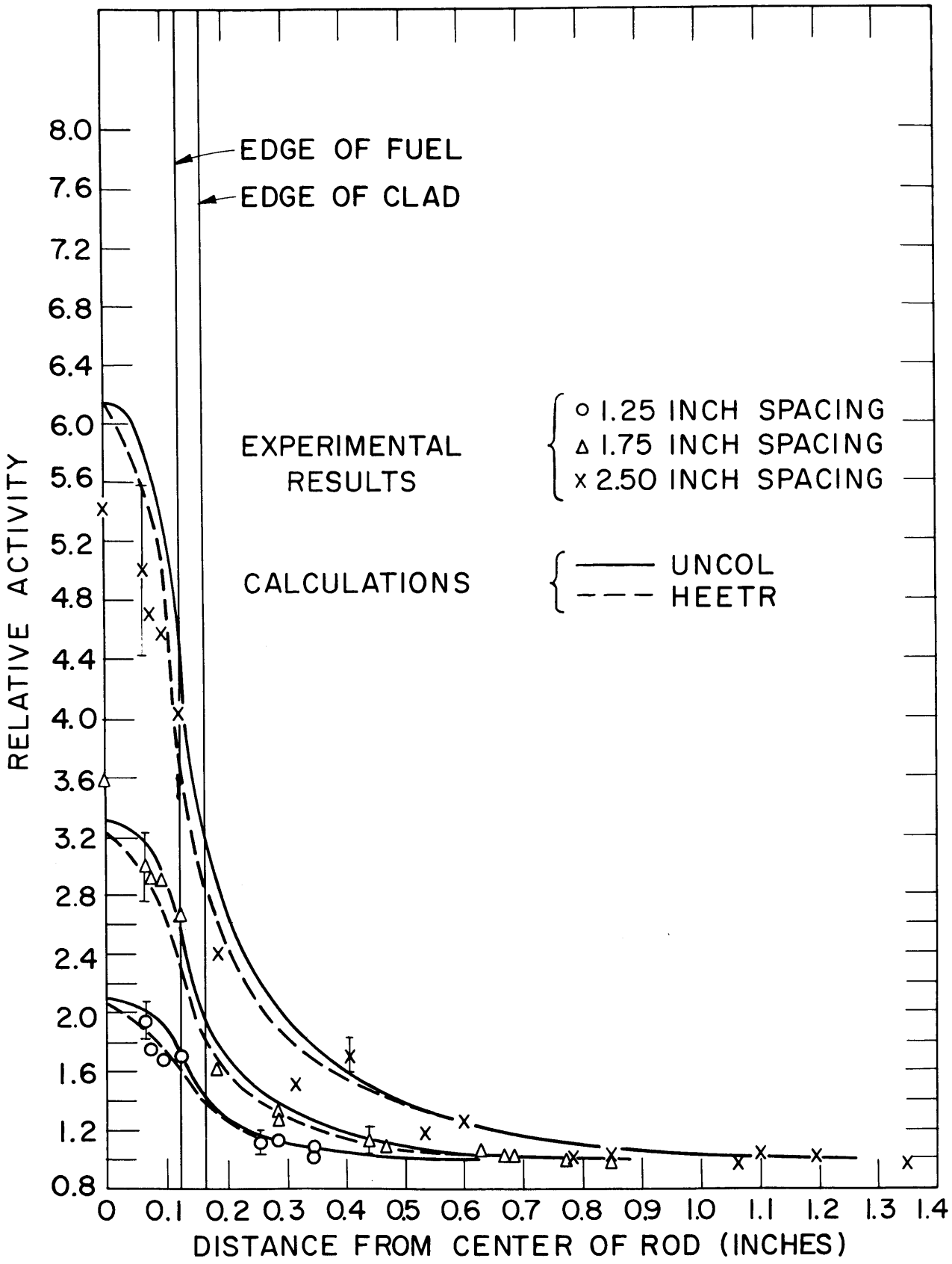

FIG. 4.5 $In^{115}(n,n^{1})\ In^{115m}$ ACTIVITY DISTRIBUTION FOR LATTICES OF 0.25 INCH DIAMETER, 1.143 % U^{235} RODS

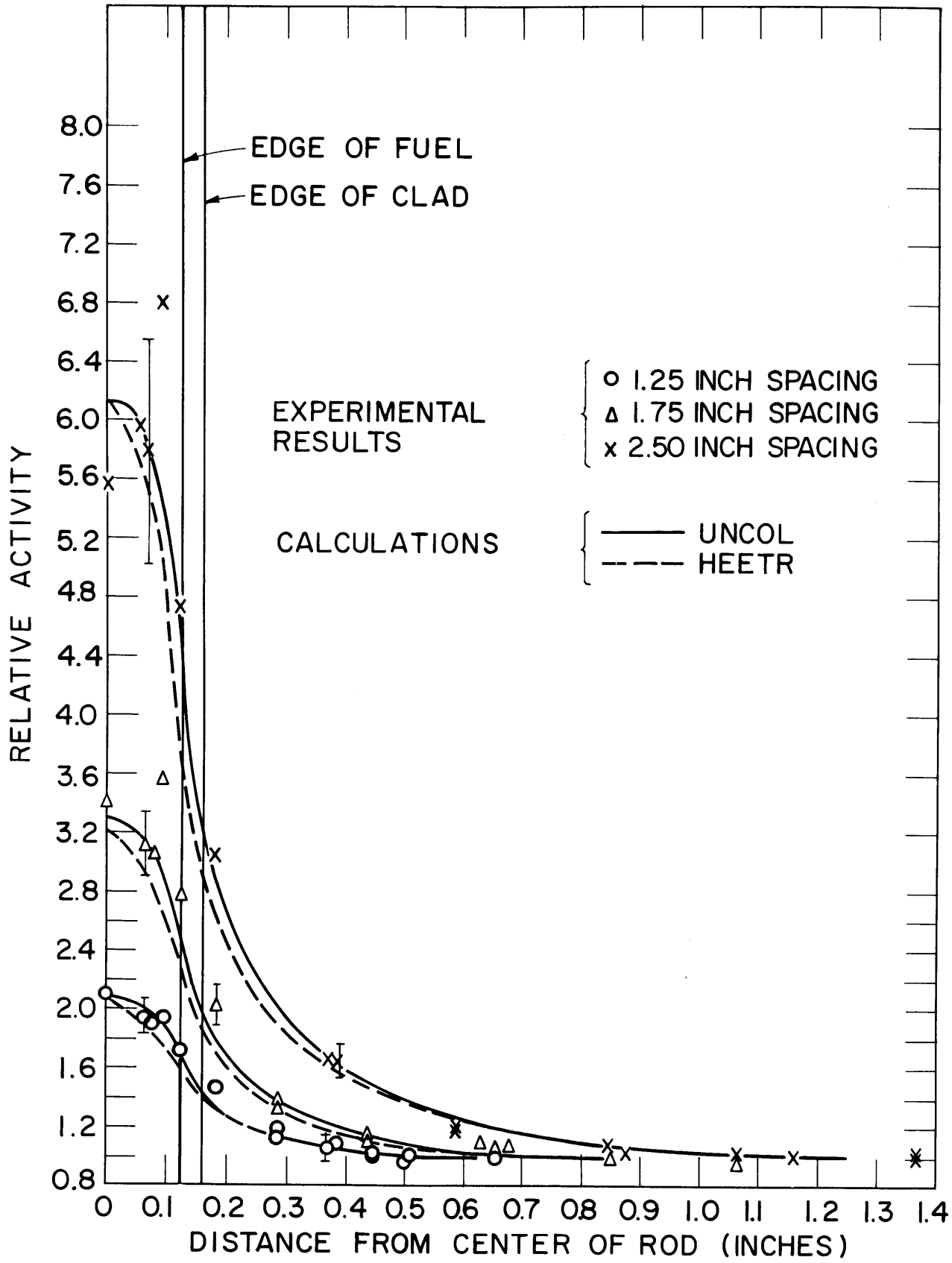

FIG. 4.6 $U^{238}(n,f)$ ACTIVITY DISTRIBUTION FOR LATTICES OF 0.25 INCH DIAMETER, 1.143% U^{235} RODS

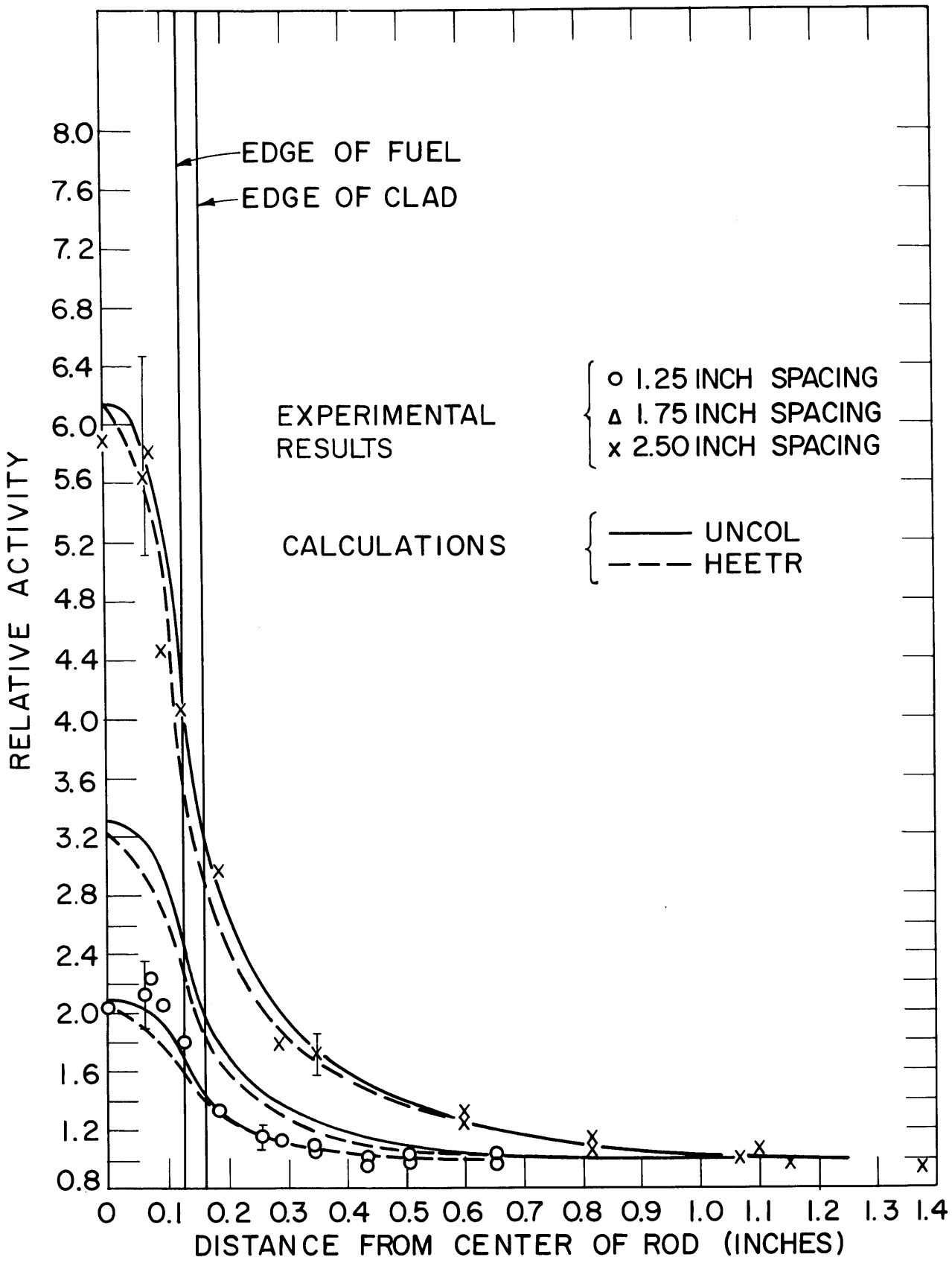

FIG. 4.7 $Ni^{58}(n,p)Co^{58}$ ACTIVITY DISTRIBUTION FOR LATTICES OF 0.25 INCH DIAMETER, 1.143% U^{235} RODS

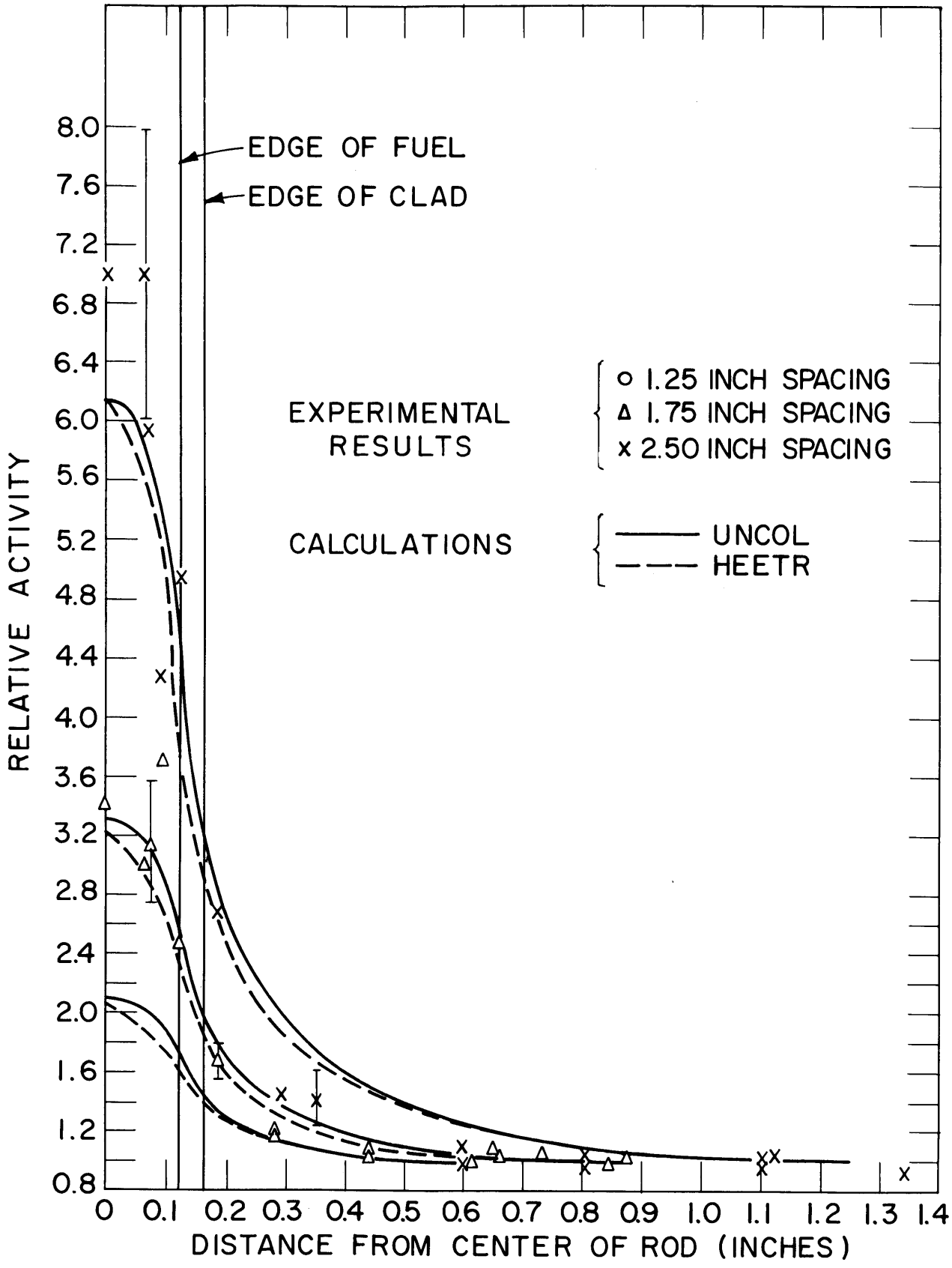

FIG.4.8 $Zn^{64}(n,p)Cu^{64}$ ACTIVITY DISTRIBUTION FOR LATTICES OF 0.25 INCH DIAMETER, 1.143 % U^{235} RODS

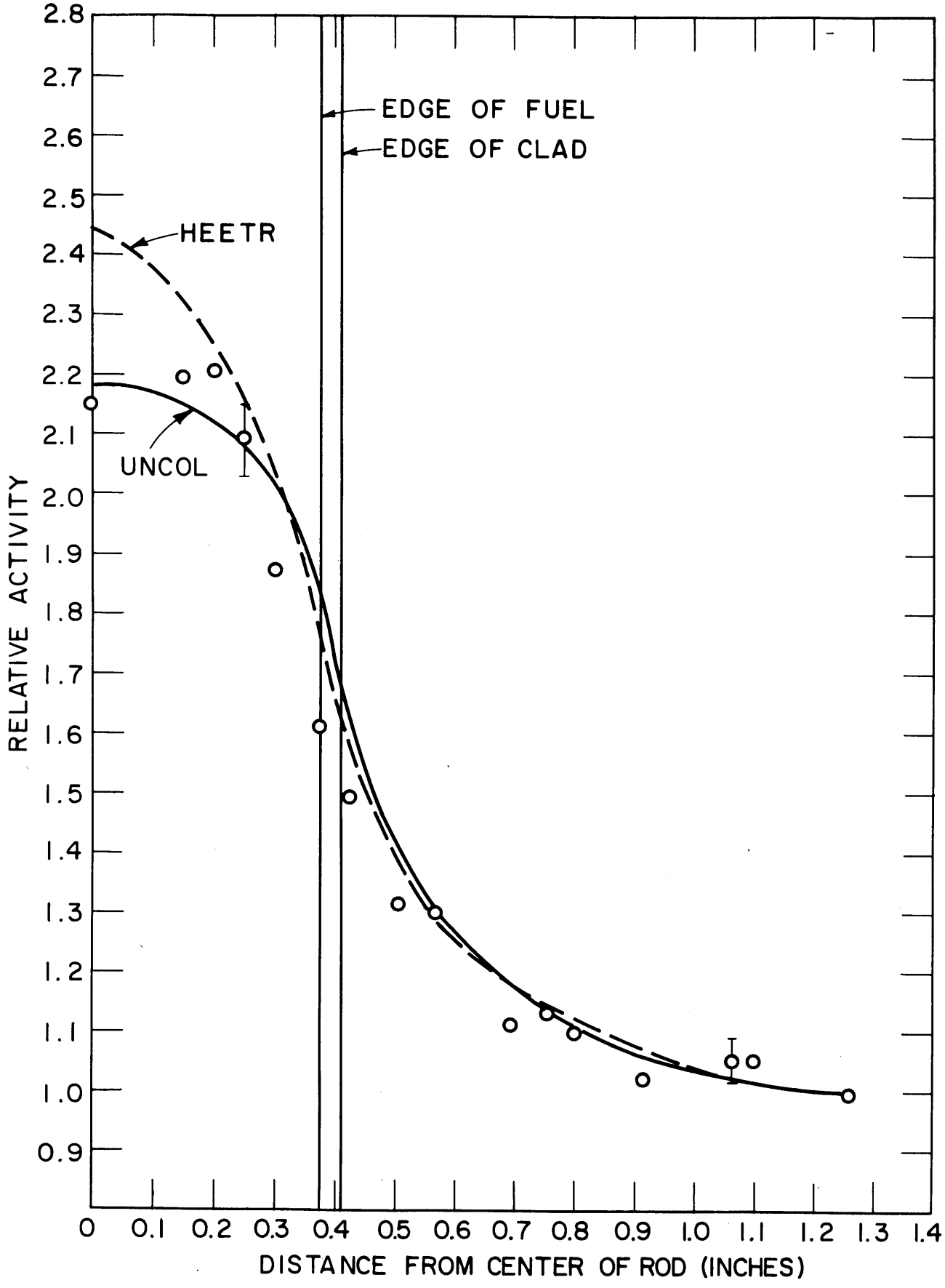

FIG. 4.9 $In^{115}(n,n')In^{115m}$ ACTIVITY DISTRIBUTION FOR THE LATTICE OF 0.75 INCH DIAMETER, 0.947% U-235 RODS.

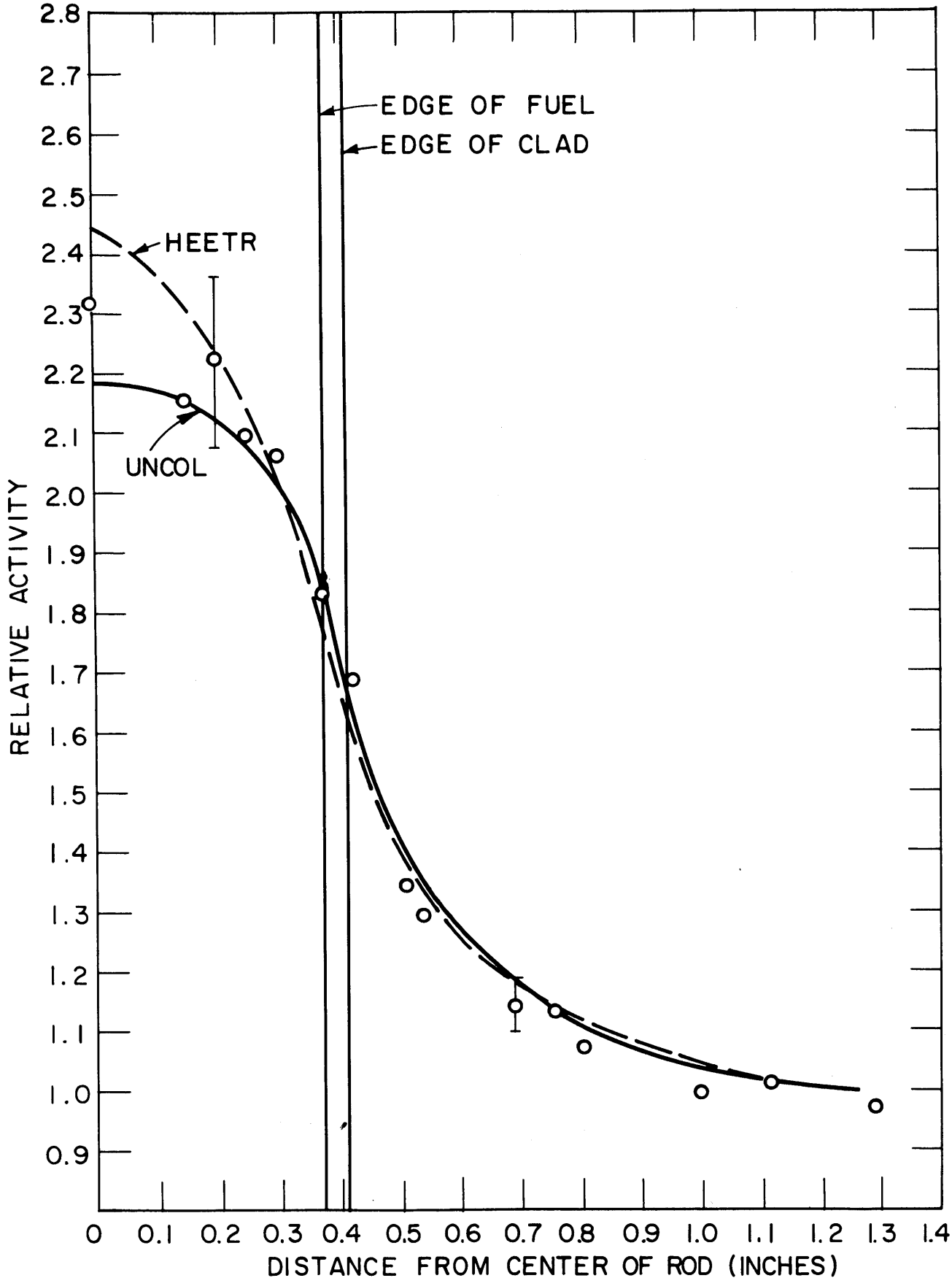

FIG. 4.10 $U^{238}(n,f)$ ACTIVITY DISTRIBUTION FOR THE LATTICE OF 0.75 INCH DIAMETER, 0.947 % U-235 RODS.

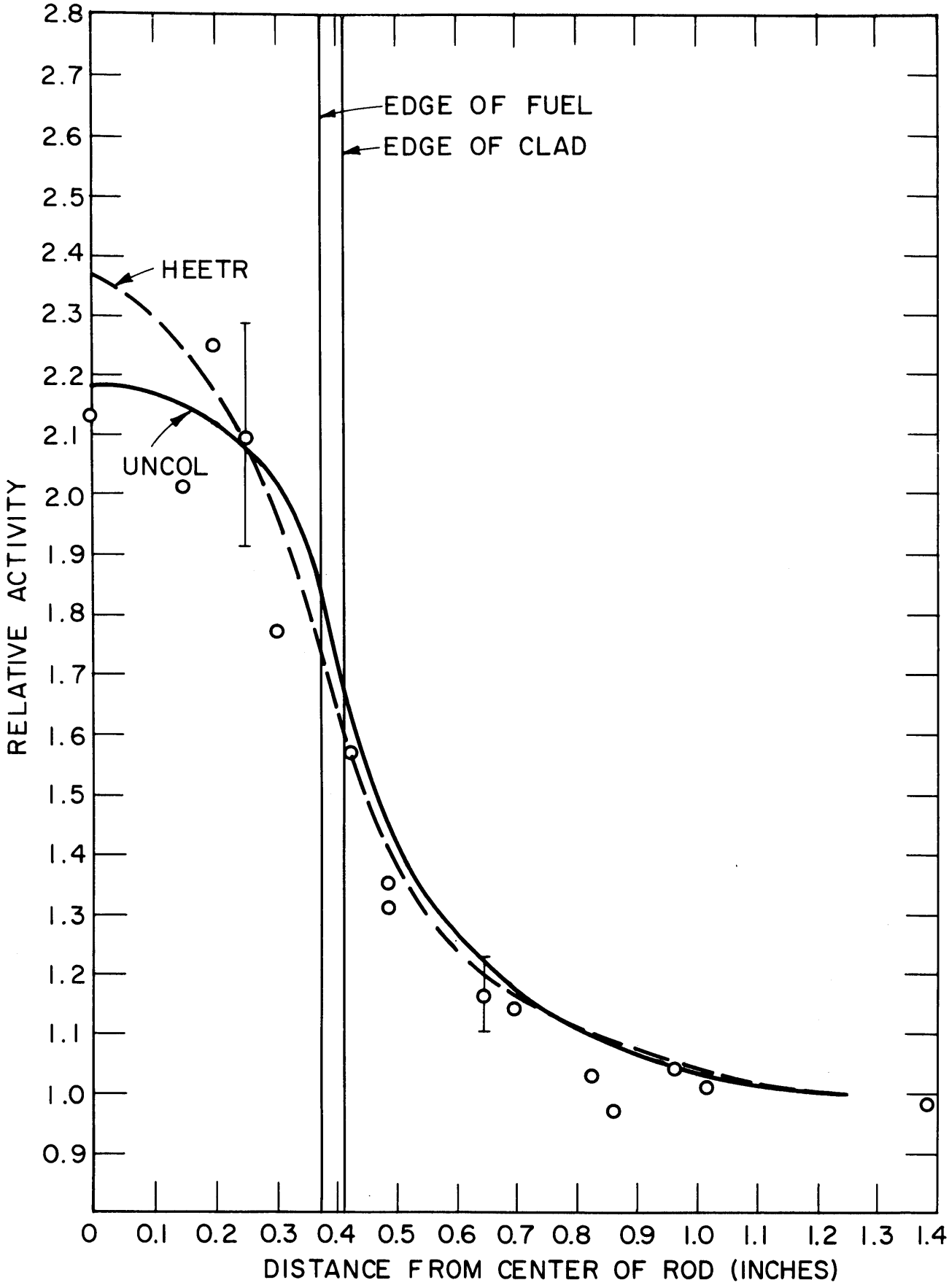

FIG. 4.11 Ni^{58} (n,p) Co^{58} ACTIVITY DISTRIBUTION FOR THE LATTICE OF 0.75 INCH DIAMETER, 0.947 % U-235 RODS.

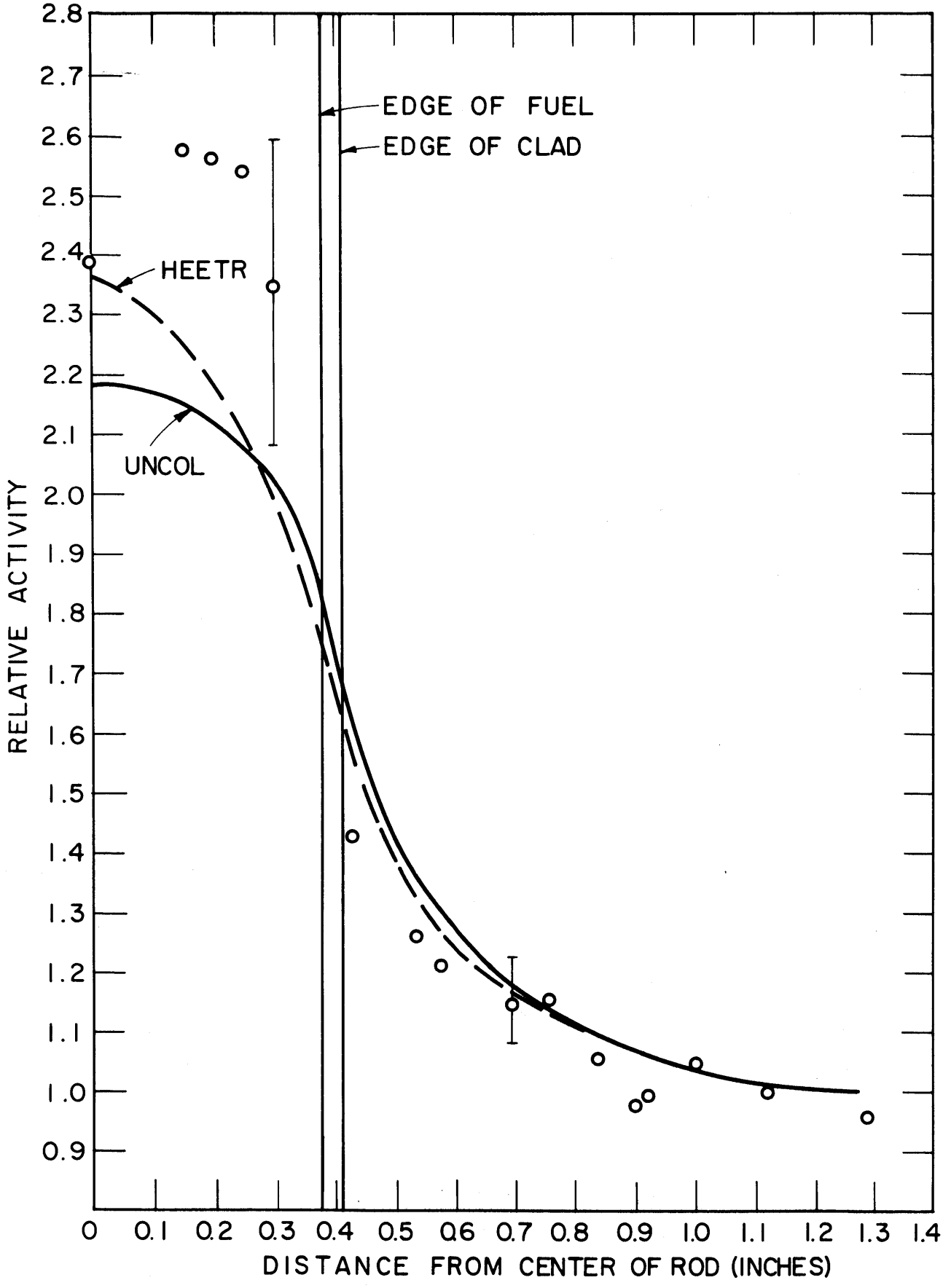

FIG. 4.12 $Zn^{64}(n,p)\ Cu^{64}$ ACTIVITY DISTRIBUTION FOR THE LATTICE OF 0.75 INCH DIAMETER, 0.947% U-235 RODS.

therefore greater than in the fuel of the lattice with 2.50-inch spacing.

The results of the UNCOL and HEETR calculations are plotted together with the experimental results. These results are also normalized at the cell edge to be consistent with the experimental results.

The UNCOL results plotted in Figs. 4.1-4.12 were obtained with a consistent set of removal cross sections as discussed in section 3.2.2. Calculations were made with many values of the removal cross sections: the removal cross sections of the fuel and the moderator were varied independently from 0.05 cm^{-1} to 0.2 cm^{-1}. The values of 0.1 cm^{-1} and 0.093 cm^{-1} for the removal cross sections of the fuel and moderator, respectively, led to the best correlation of experimental results obtained under widely varying conditions. In particular, as discussed in section 4.5 below, this set of values also provides a satisfactory comparison with results obtained in the MITR core and experimental facilities. The conditions in the reactor and at the experimental facilities contrast sharply with those in the lattices studied, both with respect to dimensions of the fuel elements and moderator-to-fuel volume ratio. The values of the removal cross sections that led to the best correlation are close to the calculated values of group removal cross sections published by other workers. For example, ANL few-group calculations give, for a single group lying above 1.35 Mev,* removal cross sections of 0.0899 cm^{-1} for D_2O and 0.1039 for U^{238} (A4, C9). Some insight into the sensitivity of the calculations to changes in the values of the cross sections can be gained from the results discussed in section 4.13 and Appendix D.

The only other input data for the UNCOL calculations that require explanation are the polynomial coefficients for the spatial distribution of fissions inside a fuel rod. As discussed in section 3.2.3, it has been assumed that this distribution may be expressed by means of a polynomial of the form:

---

column through which the source neutrons must pass on their way to the lattice. The diameter of the fuel rods in the lattice is also a factor, and the fast flux in the fuel increases with increasing rod size. Finally, the fast flux decreases toward the top and the edges of the lattice because the thermal flux decreases in these areas.

*This is the most appropriate group for comparison for which calculations were found.

$$S(r') = C_o + C_1 r'^2 . \tag{4.1}$$

It is convenient to normalize the distribution so that C_o is equal to unity; then only C_1 must be determined. For a first approximation, S(r') could be expressed by the thermal flux distribution within a fuel rod as determined either experimentally or by calculation, for example, with THERMØS (H7). In the more tightly spaced lattices, however, there is significant fast and resonance fission. The resonance fission may be assumed to be independent of position within the fuel rod (S6); the fast fission distribution is the same as that being calculated. Thus, we may write:

$$\begin{aligned} S(r') &= 1.0 + C_1 r'^2 \\ &= \phi_{TH}(r') + \delta_{25} + \delta_{28}\phi_F(r') . \end{aligned} \tag{4.2}$$

This formulation assumes that δ_{28} is constant within the fuel rod. Although this assumption is not justified, its use leads to a negligible error because δ_{28} is much smaller than unity. Since Eq. 4.2 involves $\phi_F(r')$, the distribution being calculated, the procedure is an iterative one. An estimate is made of $\phi_F(r')$; C_1 is then calculated (by a least-squares method, for example); then $\phi_F(r')$ is calculated. If the assumed distribution differs from the one calculated, the assumed distribution is corrected and the process repeated. Since δ_{28} is always much smaller than unity, the process converges rapidly and, at most, only a few iterations are needed. The procedure described was used in the present work because it gives a more accurate fission distribution when the experimental values of δ_{25} and δ_{28} are available than if only thermal fissions are included. In the lattices studied, the omission of fast and resonance fission leads to errors of less than 1% in the calculation of the fast flux distribution. Hence, if δ_{25} and δ_{28} are not known, they can be estimated or taken as zero. On the other hand, the assumption that the fission rate is constant inside the fuel rod (setting C_2 to zero) will, in general, affect the results significantly. The effect on the results is greatest for the larger rod diameters and may be as much as 5% in terms of the peak-to-minimum ratio for lattices of one-inch-diameter rods. It is important, therefore, to obtain some estimate of

the thermal flux distribution inside the fuel rod. In the present work, therefore, THERMØS was used to calculate the thermal flux distribution (H10), and measured values of δ_{28} and δ_{25} were used. The fission distributions, as computed by the above procedure, are compared with the polynomial approximations in Table 4.1.

The calculated spatial distributions shown in Figs. 4.1 - 4.12 are for intracellular rod-to-rod traverses, i. e., the distributions along a line from the center of a fuel rod toward the center of an adjacent rod in the lattice. These distributions are consistent with the experimental ones because the holders for the moderator foils were always positioned to correspond to a rod-to-rod traverse. An option in the UNCOL code permits the calculation of the spatial distribution for a rod-to-moderator traverse along a line from the center of a fuel rod toward the midpoint between two adjacent rods in the lattice. Calculations for rod-to-moderator traverses gave results that were not very different from those for rod-to-rod traverses. The spatial distributions within the fuel rods were the same for both types of calculations. The calculations for rod-to-moderator traverses gave distributions that were slightly lower in the moderator than those for rod-to-rod traverses. The differences were greatest for the region near the cell edge where they ranged from 0.8% to 1.6%. The slightly lower values for positions in the moderator for the rod-to-moderator traverses are a result of the slightly greater distances between these positions and nearby rods compared with the distances for the corresponding positions on rod-to-rod traverses.

The HEETR results are the calculated activity distributions for each reaction considered, in contrast to the UNCOL results which are fast flux distributions. A HEETR calculation provided the neutron energy spectrum for a lattice cell and the spatial distribution, within the lattice cell, of each of the five energy groups described in Table 4.2. (In this table, the fission spectrum component for each group is also given with the spectrum normalized so that its integral is unity.) With the HEETR energy spectrum as input, the RATIO code computed, for each reaction, the percentage of the total activation due to each of the five energy groups. These results were then used with the spatial distribution of the five energy groups computed by HEETR to compute the activity distributions.

TABLE 4.1

Comparisons of the Fission Distributions Inside the Fuel Rod with the Polynomial Approximations to the Distributions

Rod Diameter (Inch)	Lattice Spacing (Inches)	δ_{25}	δ_{28}	C_1	r (cm)	S_{exp} (1.)	S_{pol} (2.)
0.25	1.25	0.0525	0.0274	0.90	0.0	1.0	1.0
					0.079	1.0054	1.0055
					0.159	1.0224	1.0226
					0.238	1.0503	1.0509
					0.3175	1.0879	1.0907
0.25	1.75	0.0310	0.0217	0.90	0.0	1.0	1.0
					0.079	1.0055	1.0055
					0.159	1.0236	1.0226
					0.238	1.0515	1.0509
					0.3175	1.0901	1.0907
0.25	2.50	0.0188	0.0183	0.92	0.0	1.0	1.0
					0.079	1.0057	1.0057
					0.159	1.0239	1.0231
					0.238	1.0527	1.0520
					0.3175	1.0922	1.0927
0.75	2.50	0.060*	0.061	0.2782	0.0	1.0	1.0
					0.254	1.0188	1.0179
					0.508	1.0758	1.0717
					0.762	1.1636	1.1615
					0.9525	1.2533	1.2523
0.75	3.50	0.045*	0.052*	0.290	0.0	1.0	1.0
					0.254	1.0188	1.0187
					0.508	1.0760	1.0760
					0.762	1.1710	1.1683
					0.9525	1.2643	1.2630

*Estimated.

(1.) $S_{exp} = \phi_{TH}(r) + \delta_{25} + \delta_{28}\phi_F(r)$ (Normalized at r = 0).

(2.) $S_{pol} = 1.0 + C_1 r^2$.

TABLE 4.1 (continued)

Rod Diameter (Inches)	Lattice Spacing (Inches)	δ_{25}	δ_{28}	C_1	r (cm)	S_{exp}	S_{pol}
0.75	5.00	0.03*	0.047	0.30	0.0	1.0	1.0
					0.254	1.0192	1.0193
					0.508	1.0776	1.0774
					0.762	1.1745	1.1741
					0.9525	1.2700	1.2721
1.0	Single rod	0.01*	0.0551	0.186	0.0	1.0	1.0
					0.127	1.0031	1.0029
					0.381	1.0196	1.0269
					0.635	1.0719	1.0749
					0.889	1.1453	1.1469
					1.1430	1.2430	1.2429
1.0	4.5	0.0479	0.0597	0.190	0.0	1.0	1.0
					0.127	1.0027	1.0030
					0.381	1.0277	1.0275
					0.635	1.0772	1.0766
					0.889	1.1507	1.1501
					1.143	1.2443	1.2482
1.0	5.0 and 5.75	0.0340 0.0268	0.0596 0.0583	0.190	0.0	1.0	1.0
					0.127	1.0028	1.0030
					0.381	1.0281	1.0275
					0.635	1.0782	1.0766
					0.889	1.1527	1.1501
					1.143	1.2474	1.2482

*Estimated.

TABLE 4.2

Limits of the Energy Groups in the HEETR Calculations

Group	E_L (Mev)	Normalized* N(E) Fission Spectrum
1	3.679	0.14659
2	2.231	0.20703
3	1.353	0.22383
4	0.8208	0.17596
5	0.4979	0.11346

*The fraction of the fission spectrum below 0.4979 Mev is 0.13313.

As noted in section 4.4, the spatial distributions of the first four energy groups are similar. Since these four groups contribute nearly all the activation for the reactions studied, there is very little variation in the different activity distributions. This result is especially evident for the lattices with rods 0.25 inch in diameter.

The HEETR calculations were made with the cell boundary approximation as discussed in section 3.3 and the transport cross section option. The results of calculations with total cross sections showed no significant differences from those obtained with the transport approximation. The microscopic cross-section input data used were from a 15 energy group set supplied by H. K. Clark from data in references Y1, O2, and O3. The calculations reported here were made with the first five groups (i. e., the high energy range) of the fifteen-group structure for which the data were compiled. It was necessary, therefore, to change only the transfer cross sections. The transfer cross sections affected were those of the type (i→j), where i denotes groups 1 - 5 and j denotes values greater than 5. Each 5-group (i→6) transfer cross-section value is the sum of all the 15-group (i→j) values for j greater than 5.

In comparing the experimental and calculated results, there are two conspicuous examples of discrepancies. These two examples are results with the zinc reaction in the lattices with 2.5-inch spacing and

those with the nickel reaction in the lattice with 0.25-inch-diameter rods containing 1.027% U^{235}, at the spacing of 1.25 inches. The results with the zinc reaction include higher normalized fluxes in the fuel for the 2.5-inch lattices, as shown in Figs. 4.4, 4.8 and 4.12, than predicted by the calculations. This result could be due in part to the perturbation effects discussed in section 4.6. But this effect is too small to account for all of the difference, which is as high as 20%, and should affect the results of all the reactions equally. There are two experimental factors that are unique with the zinc reaction in comparison with the others utilized. The first is the necessity for correcting for the Zn^{69} activity as discussed in section 2.7.4. The second factor is the low statistical accuracy that could be attained with the zinc reaction. As shown in Fig. 2.4, the cross section for the $Zn^{64}(n, p)Cu^{64}$ reaction has a relatively high threshold energy and is not large for any energy. Both the correction for Zn^{69} activity and the statistical uncertainty are greatest in the lattices with 2.5-inch spacing. The ratio of Zn^{69} activity is higher in these lattices than in the others because the ratio of the thermal flux to the fast flux is higher. The statistical uncertainty is larger than in other lattices because the fast flux is lower, owing to the smaller interaction effect between rods and to the lower values of the multiplication factor in these lattices.

It is difficult to explain physically why the spatial distribution of the zinc reaction in the lattice of 2.50-inch spacings should be very different from the distributions of the other reactions in these lattices. A difference in the intracellular distributions of the different reactions implies a spectral shift going from one region of the lattice cell to another region. As will be shown in section 4.4, such spectral shifts do occur, but only in the energy range below about 1 Mev. The relatively high value of the threshold energy of the zinc reaction means that spectral shifts would have to occur in the energy range above about 3 Mev to account for a different distribution of this reaction as compared with the others, and such a spectral shift in this energy range seems very unlikely. In fact, it is difficult to see how the neutron spectrum above about 3 Mev can be very different from a fission spectrum. The possibility of a different spatial distribution for the neutrons of

higher energies could be explored by changing the HEETR group structure so that the highest energy group would be subdivided into several groups. This procedure would require a new set of nuclear data consistent with the new group structure. An experimental test of the spatial distribution of the neutrons of higher energies could be made by using additional reactions having sufficiently high threshold energies. Among the possibilities in Table 2.1, the $Mg^{24}(n, p)Na^{24}$ reaction and the $Al^{27}(n, \alpha)Na^{24}$ reaction appear to be the most attractive due to their suitable threshold energies, values of half-life of the products that are convenient for experiments, and availability in metallic form. The use of these reactions was not possible in the present work, owing to insufficient activation and resulting low counting rates. The increase in the power of the MITR to 5 MW might permit their use in future lattices, however, especially in lattices of larger diameter rods, and also provide greater activation of the zinc reaction with corresponding improvement in the accuracy of the experimental results.

The discrepancy between theory and experiment for the $Ni^{58}(n, p)Co^{58}$ results for the lattice of rods of 1.03% U^{235} on 1.25-inch spacings may have been due to a systematic experimental error. It would be difficult to construct a physically meaningful curve through the data points. The discrepancy is probably too great to attribute to experimental scatter, especially since the accuracy attained in the more closely packed lattices was generally higher than in the others. It appears, judging from the computed curves and the other distributions, as though the experimental points in the fuel are all too low by a factor of approximately 1.3. This factor is too large to be due to a mistake in the correction for radial location in the lattice tank. These corrections are usually less than 5%. Furthermore, since the rod supporting the foils in the moderator was always farther from the center of the lattice than the rod containing the fuel foils, the radial correction factor tends to reduce slightly the relative peaking in the fuel. In this case, the rod containing the fuel foils would have had to have been located in the seventh ring rather than in the center position in order to account for the difference. A more likely explanation is that the moderator foil holder slipped at some point before or during the run. If the moderator foils were actually located about six inches lower than assumed, an

error of this magnitude would result. This possibility was recognized after the first two lattices were studied. In subsequent experiments, the position of the moderator holder was measured both before and after the experiment. The results in question were obtained with the second lattice studied, and the height of the moderator holder was measured only before the run. No opportunity afforded itself to repeat this experiment.

The accuracy attained in the lattice with 0.75-inch-diameter rods is generally higher than that for the lattices with 0.25-inch-diameter rods. This result is expected for two reasons. All other factors being equal, the magnitude of the fast flux increases with increasing rod size. The increase in fuel area per unit cell (by a factor of nine) significantly increased the fast flux. Furthermore, the larger rods made possible the use of 1/8-inch-diameter foils inside the fuel, whereas only 1/16-inch-diameter foils could be used inside the 0.25-inch-diameter rods. The total count rate per foil was thereby increased by a factor of four.

Wolberg (W4) measured the intracellular distribution of the $U^{238}(n,f)$ reaction in and around a single 1.00-inch-diameter, natural uranium rod in D_2O. The results together with the UNCOL results are plotted in Fig. 4.13. The experimental results inside the fuel rod are more accurate than those in the moderator and the results are therefore normalized at the center of the rod.

Except as discussed above, there appear to be no large differences between the experimental results, the results of the UNCOL calculations, and those of the HEETR calculations. The HEETR results give distributions with a greater slope inside the fuel than do the UNCOL results. The HEETR results show some slight variations among the different reactions, at least in the lattice of 0.75-inch-diameter rods. The UNCOL results, on the other hand, represent flux distributions and cannot discriminate among the different reactions. These differences between UNCOL and HEETR are not large, however, and the two methods can be said to match the experimental results with comparable accuracy. The fact that agreement between UNCOL results and experimental results was obtained in so many cases using a consistent set of values for the removal cross sections is evidence that the assumptions made in the derivation of UNCOL in section 3.2 were justified.

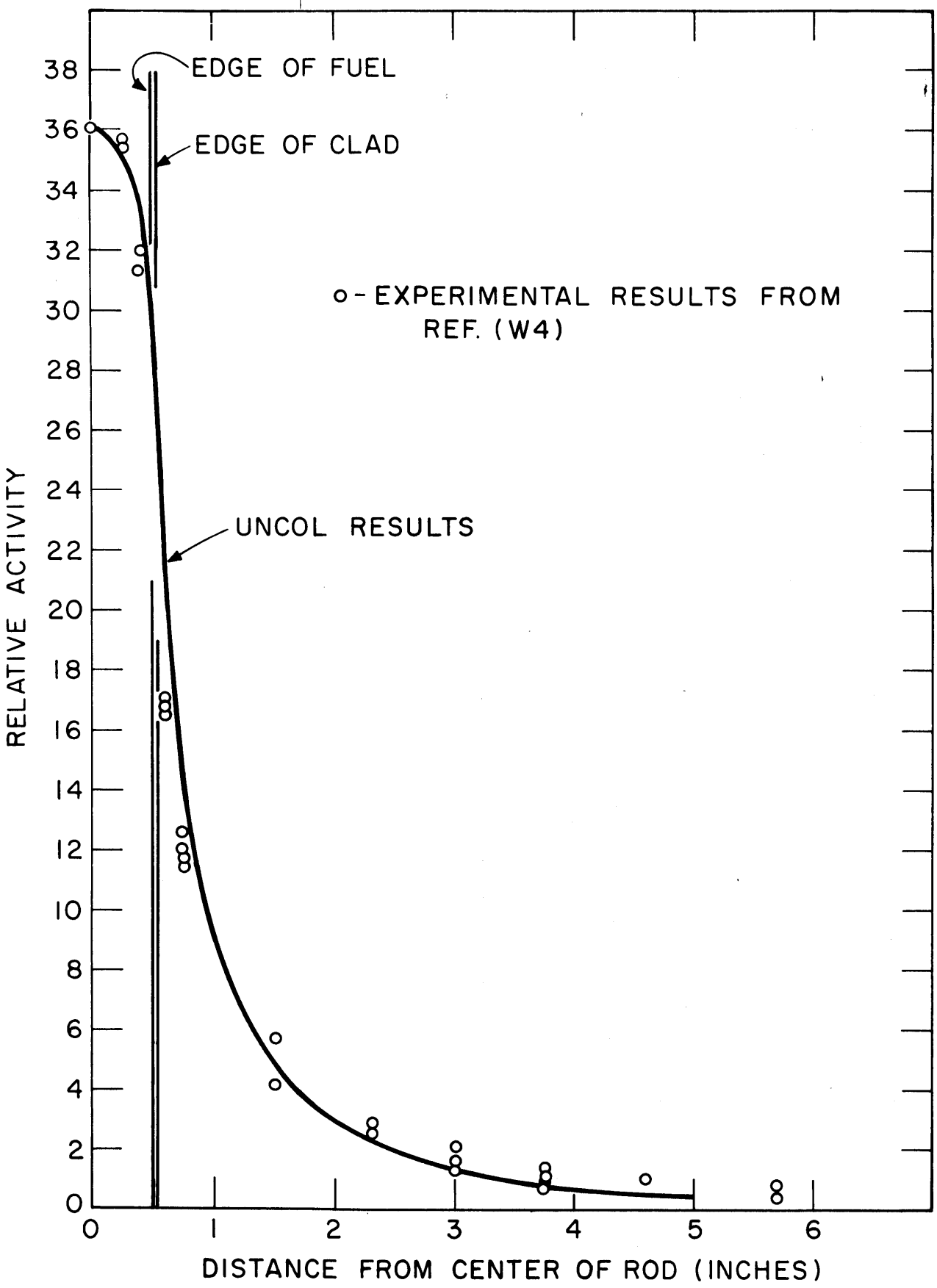

FIG. 4.13 U^{238} (n,f) ACTIVITY DISTRIBUTION FOR A 1.0 INCH DIAMETER SINGLE ROD (W4) OF NATURAL URANIUM

4.1.2 Leakage Effects

The UNCOL code is well suited for studying fast neutron leakage effects in lattice assemblies of different diameter. The diameter of the lattice assembly enters into the calculations in two ways. First, the diameter determines the extrapolated radius of the assembly, which affects the argument of the J_o source distribution and thereby influences the weighting coefficients for the contribution to the fast flux at a point in the lattice from the surrounding fuel rods. Second, for a given fuel rod spacing, the diameter determines the number of rods in the lattice assembly and, therefore, the number of rods contributing to the fast flux at a given point. Thus, as the size of the lattice is increased, the contribution of the interaction effect between fuel rods is increased because the number of fuel rods contributing to the interaction effect is increased and because the weighting coefficients for these interaction contributions are increased. An increase in the interaction effect between fuel rods tends to reduce the peak-to-minimum ratio of the fast flux in the lattice cell because the contribution of the interaction effect is nearly the same for different points in the lattice cell. An increase in the interaction effect also tends to increase the value of δ_{28} because the magnitude of the fast flux in the fuel is increased relative to the thermal flux.

These effects can be illustrated by comparing results of calculations around the center rod for lattices of 0.25-inch-diameter fuel rods spaced 2.50 inches apart. Results obtained with UNCOL are plotted in Fig. 4.14 for a miniature lattice, a lattice occupying a three-foot tank (as in the results of section 4.1.1), and an "infinite" lattice. The miniature lattice has an extrapolated radius of 10.55 inches and only three rings, for a total of 37 fuel rods. The lattice in the three-foot tank has an extrapolated radius of 19.317 inches and seven rings for a total of 169 rods. The "infinite" lattice has 22 rings for a total of 1,519 rods, and has a (nearly) constant macroscopic source distribution as opposed to a J_o source distribution for the other two lattices. The contribution from the entire outer ring of the infinite lattice is less than one part per million of the total. The approximation to an infinite lattice is, therefore, very good. The results are the relative values of the fast flux around the center rod when the thermal flux in the center rod has the

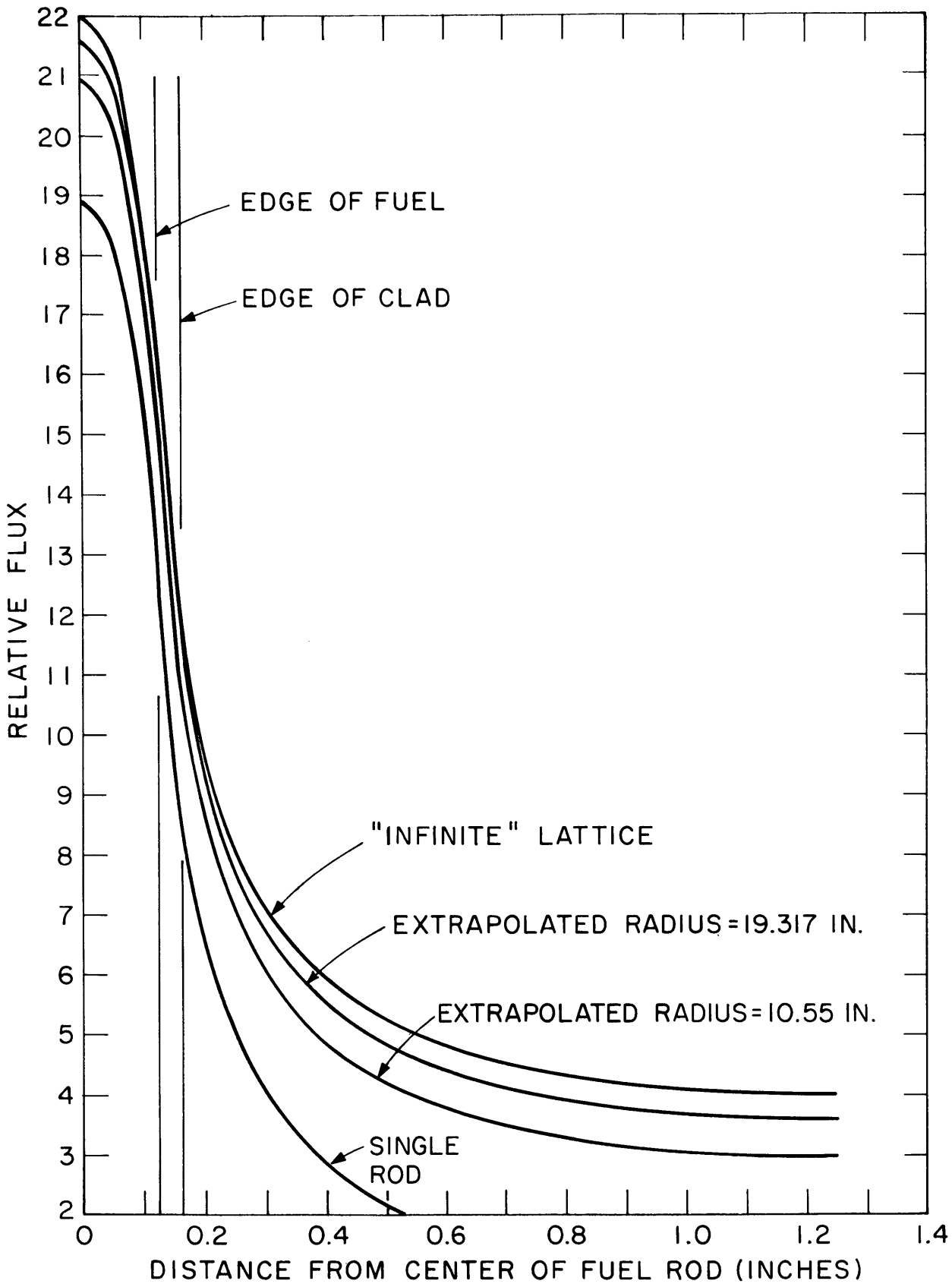

FIG. 4.14 LEAKAGE EFFECTS ON THE INTRACELLULAR DISTRIBUTION OF THE FAST FLUX IN LATTICES OF 0.25 INCH DIAMETER RODS ON 2.50 INCH SPACING

same value for all three lattices.

The fractional differences in the values of the fast flux are not large for points inside the central fuel rod. Even the value of the fast flux in the fuel in the miniature lattice is only about 5% less than for corresponding points in the "infinite" lattice. This result shows that δ_{28} measurements can be made in miniature lattices without the need for a large correction for leakage.

The fractional differences in the values of the fast flux are greater for points located in the moderator. At the midpoint between rods, 1.25 inches from the center of the central rod, the miniature lattice has a fast flux that is only about 75% of the flux at the corresponding point in an infinite lattice. It is possible that this difference in the distributions also affects the resonance flux distributions and, consequently, the effective resonance integral. This effect may be smaller for neutrons of lower energies, however, so that differences in the effective resonance integrals may be relatively small.

It is worth while noting that the actual difference in the values of the fast flux in the fuel that is observed between two different sized assemblies is almost the same for different points within the lattice cell. For instance, the difference in the values of the fast flux in the fuel and in the moderator for the "infinite" lattice and the lattice with an extrapolated radius of 10.55 inches is about one unit in the relative flux. This result suggests that the spatial distributions of the fast flux in different sized assemblies can be obtained by adding to the results for a single rod, a value of the fast flux due to interaction effects that is the same for different points in the lattice cell.

The results for a single 0.25-inch-diameter rod in D_2O are also included in Fig. 4.14. A comparison of this curve with the three other curves shows that in all the lattices with 2.50-inch spacing, most of the fast flux inside a 0.25-inch-diameter fuel rod comes from the rod, itself; in other words, the interaction between rods is small. On the other hand, no single rod contributes the greater part of the fast flux at points well out into the moderator. The calculation shows, for example, that at a point 1.25 inches from the center rod, the single rod value is only 2.13%, 1.73%, and 1.55% of the values for the miniature lattice, the

three-foot lattice, and the infinite lattice, respectively.

The effects of axial leakage are also of interest. It was assumed in the derivation of the equations used in the UNCOL code that the fuel rods were infinitely long so that the axial flux in the fuel rods was constant. The lattices in which the experiments were done were four feet in length and had axial flux distributions that were exponential functions of height. The axial relaxation length of the flux varied slightly from lattice to lattice but was approximately 30 cm. Simms (S6) has derived a modification of the THERMØS code to account for the effect of this difference on the spatial distribution of the thermal flux, since THERMØS assumed a constant axial flux. Simms' results indicate that an exponential axial flux gives an intracellular distribution of the thermal flux that differs from that resulting from a constant axial flux by less than 0.3% in terms of the peak-to-minimum ratio (cell edge to cell center). While these results are not directly applicable to the intracellular distribution of fast neutrons, it can be argued on physical grounds that this distribution should be even less sensitive to the axial variation than is the intracellular thermal neutron distribution. The mean-free path of fast neutrons is approximately 10 cm in a uranium-heavy water assembly. The age to thermal energy in uranium-heavy water lattices is approximately 100 cm^2. The mean-square displacement between the point of origin and the point of thermalization is then about 600 cm^2, so the crow-flight distance between these points is about 25 cm. Thermal neutrons at a given point, therefore, have come from farther away than the fast neutrons at the same point. The deviation of an exponential function from linearity increases with distance. Since the thermal flux depends more strongly than the fast flux on neutrons coming from distant points, the effect of the exponential axial flux on the spatial distribution of the thermal flux should be greater than on the corresponding distribution of the fast flux. Hence, by using Simms' results, we may conclude that the presence of an exponential axial flux in the experiments caused an effect on the intracellular distribution of the fast flux that should be less than 0.3% in terms of the peak-to-minimum ratio. This conclusion is supported by the results of experiments in which δ_{28} has been measured at different heights in the lattice

(W4, D2, H9). The experimental values of δ_{28} have been found to be constant above a height of 12 inches in the lattice. This result indicates that the thermal flux and the fast flux had the same axial dependence.

The effect of the finite length of the lattice on comparisons with calculations in which the lattice was assumed to be infinite in length can be approximated by additional UNCOL calculations. The calculations consist of computing the fast flux at a given point (corresponding to the point at which the experiments were done) that results from an array of fuel rods disposed as shown in Fig. 4.15. These rods form two slabs, each three feet in width, which are infinite in the horizontal direction. The upper slab extends upward an infinite distance from a height that is 32 inches above the location of the experiment. The lower slab extends downward an infinite distance from a height that is 16 inches below the location of the experiment. The UNCOL code can be used to calculate the fast flux at the experimental point that results from the fuel rods arranged as shown in Fig. 4.15 because they are infinitely long in the horizontal direction. These rods not only fill the space that would be occupied by the extension of the lattice into one of infinite length, but also fill an infinite volume outside such an extension. It can be argued, therefore, that the fast flux at the experimental point computed for such an arrangement is greater than the fast flux resulting from that part of an infinite lattice that is outside the four-foot length of the experimental lattice. Calculations for this type of arrangement were made in which the diameter and spacings of the fuel rods corresponded to the diameter and spacings of the fuel rods in the lattices studied. In every instance, the magnitude of the fast flux calculated for these arrangements was less than 0.4% of the values of the fast flux calculated for the corresponding infinite lattice. These results do not provide a basis for a complete comparison of the infinite lattice assumed for the UNCOL calculations and the finite lattices used in the experiments because the exponential axial flux has not been accounted for. The results are a further indication, however, that for lattices as large as those studied in the present work, the axial leakage effect on intracellular distributions of the fast flux can probably be neglected.

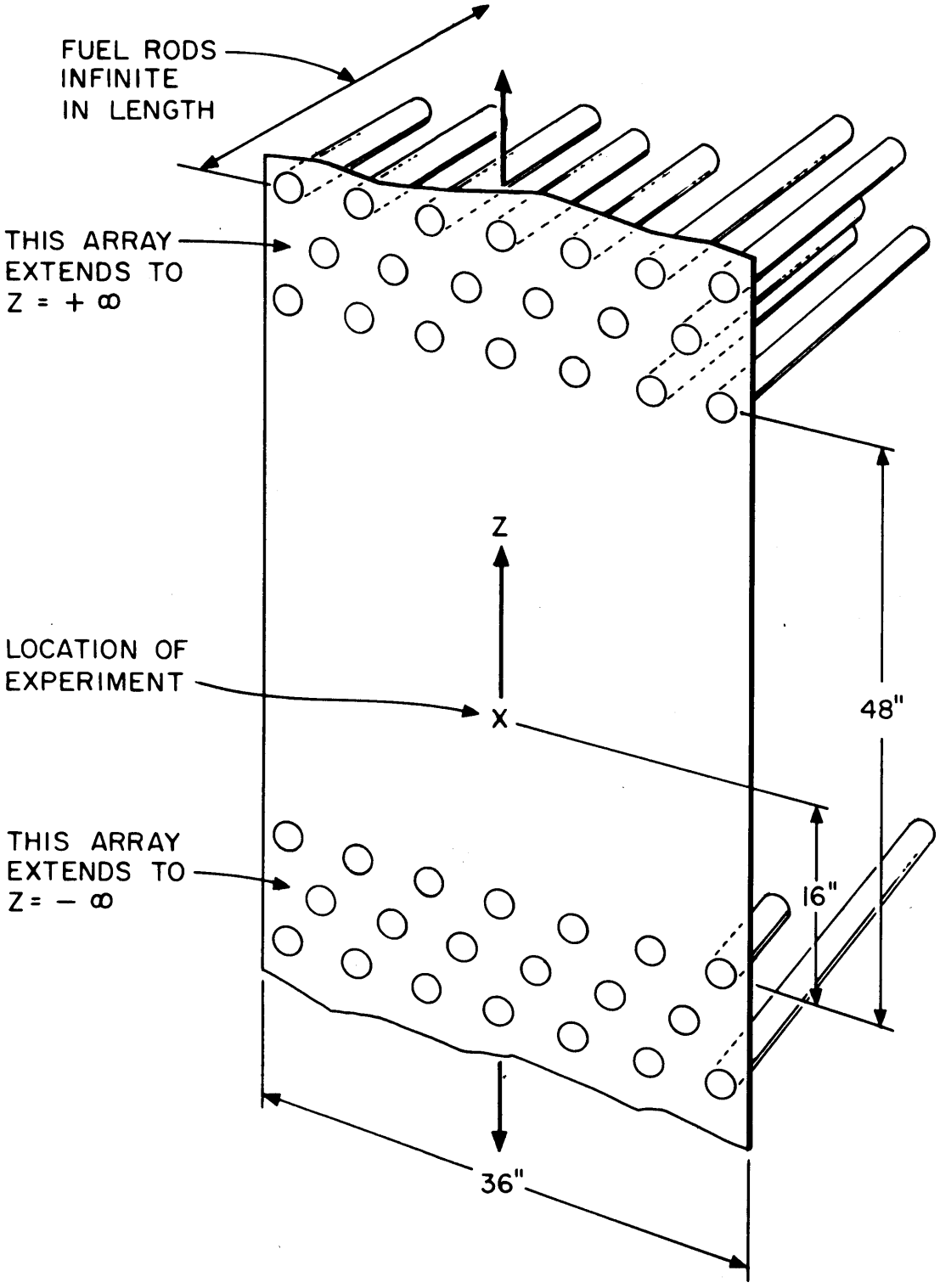

FIG. 4.15 FUEL ROD ARRANGEMENT FOR CORRECTION FOR FINITE LATTICE LENGTH.

4.1.3 Results Obtained in Water-Moderated Lattices

The only information found for the distribution, in lattice cells with water moderator, of the activations induced by fast neutrons was due to Klein (K7). He measured the $U^{238}(n, f)$ reaction rate in and around a 0.387-inch-diameter fuel rod in a water-moderated lattice with a moderator-to-fuel volume ratio of 4:1. The results are given in Fig. 4.16, together with the results of UNCOL and HEETR calculations. The agreement between the UNCOL results and the experimental results is improved by increasing the removal cross section of the moderator from 0.093 cm^{-1} to 0.098 cm^{-1}. This increase is to be expected because water has a higher removal cross section than heavy water. (The values for heavy water and light water values from the LASL 16-group set for a single group above 1.4 Mev are approximately 0.0815 cm^{-1} and 0.0935 cm^{-1}, respectively, depending upon how the first two groups are combined (A4).)

The HEETR results also agree well with the experimental results. The curve calculated with HEETR has a steeper slope than the curve obtained with UNCOL inside the fuel rod. A similar result was found for the D_2O lattices, although the difference is small. The experimental results deviate by less than 10% from either of the two theoretical curves over the entire lattice cell.

The value of δ_{28} computed with HEETR for the water-moderated lattice is 0.076, which agrees with the experimental value of 0.076 ± 0.002 obtained at Brookhaven (H2).

4.2 Advantage Factors for Fast Neutrons

In many theoretical analyses, the calculation of parameters expressing high energy events – for example, fast fission – depends on multigroup calculations of the fast neutron energy spectrum in homogenized lattices. The homogenization procedure involves volume-weighting the regions of the lattice. This approximation is reasonable in the high energy range, especially for water-moderated lattices, because the mean-free paths are long for neutrons in the Mev energy range and are comparable with the dimensions of the lattice cells. Heterogeneous effects, however, introduce some error in this procedure. In an attempt

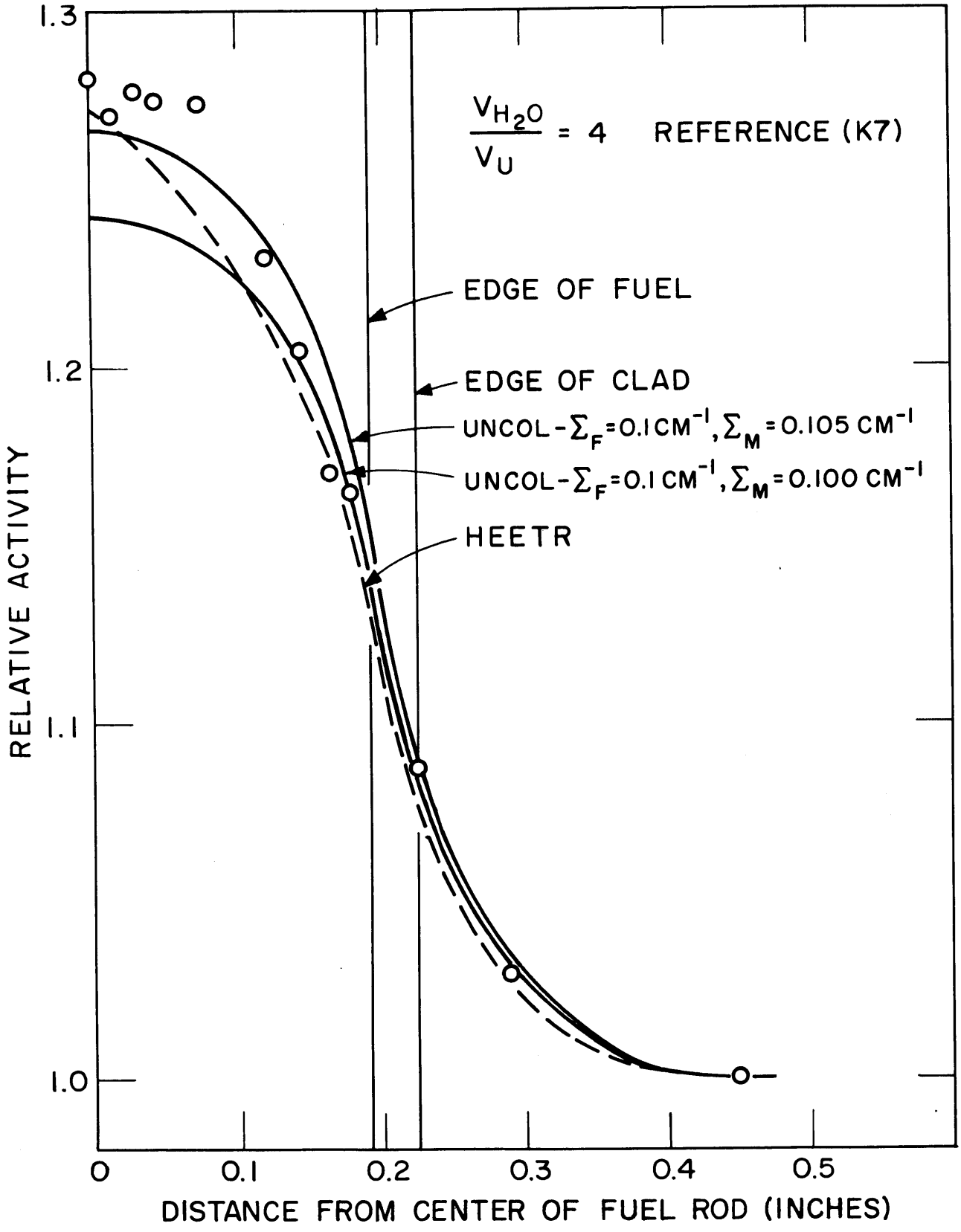

FIG. 4.16 U^{238} (n,f) ACTIVITY DISTRIBUTION FOR AN H_2O LATTICE

to account properly for these effects, Hellens and Honeck have proposed a simple one-group theory (H2) with which they have been able to correlate experimental information about fission ratios in water-moderated lattices. One result of the theory is Eq. 4.3 which gives the ratio of the average fast flux in the fuel to the average in the moderator. This ratio may be called the "advantage factor for fast neutrons:"

$$\frac{\overline{\phi}_F}{\overline{\phi}_M} = 1.0 + \beta\Sigma_1 \ell_o \frac{V_M}{V_F}, \tag{4.3}$$

where

ℓ_o = average chord length of fuel rod (cm),

Σ_1 = removal cross section (cm^{-1}) of the moderator,

$\frac{V_M}{V_F}$ = moderator-to-fuel volume ratio,

β = a numerical factor (related to chord length distributions in fuel and moderator) which serves to improve the accuracy of Eq. 4.3.

The value of β has been inferred from experiment and from Monte Carlo calculations (H8, H2): it varies from approximately 0.45 for tightly packed lattices to 0.667 for single rods.

Good agreement has been observed between the values predicted from Eq. 4.3 and the experiments by Klein at Bettis and Bliss and Price at Brookhaven (B5) for water-moderated lattices.

The predictions of Eq. 4.3 applied to heavy water-moderated lattices are plotted in Fig. 4.17 with $\Sigma_1 = 0.093\ cm^{-1}$ and $\beta = 0.4$, 0.5, and 0.6. Also included in Fig. 4.17 are the experimental results and the results of UNCOL calculations for the seven lattices studied. The results of several additional UNCOL calculations are also included: those for two additional lattices of the 0.75-inch-diameter fuel rods (3.5-inch and 5.0-inch spacings, respectively); and those for three lattices of 1.0-inch-diameter fuel rods (4.5-inch, 5.0-inch, and 5.75-inch spacings, respectively).

The agreement with the predictions of Eq. 4.3 is reasonably good although the results of the UNCOL calculations indicate a variation with

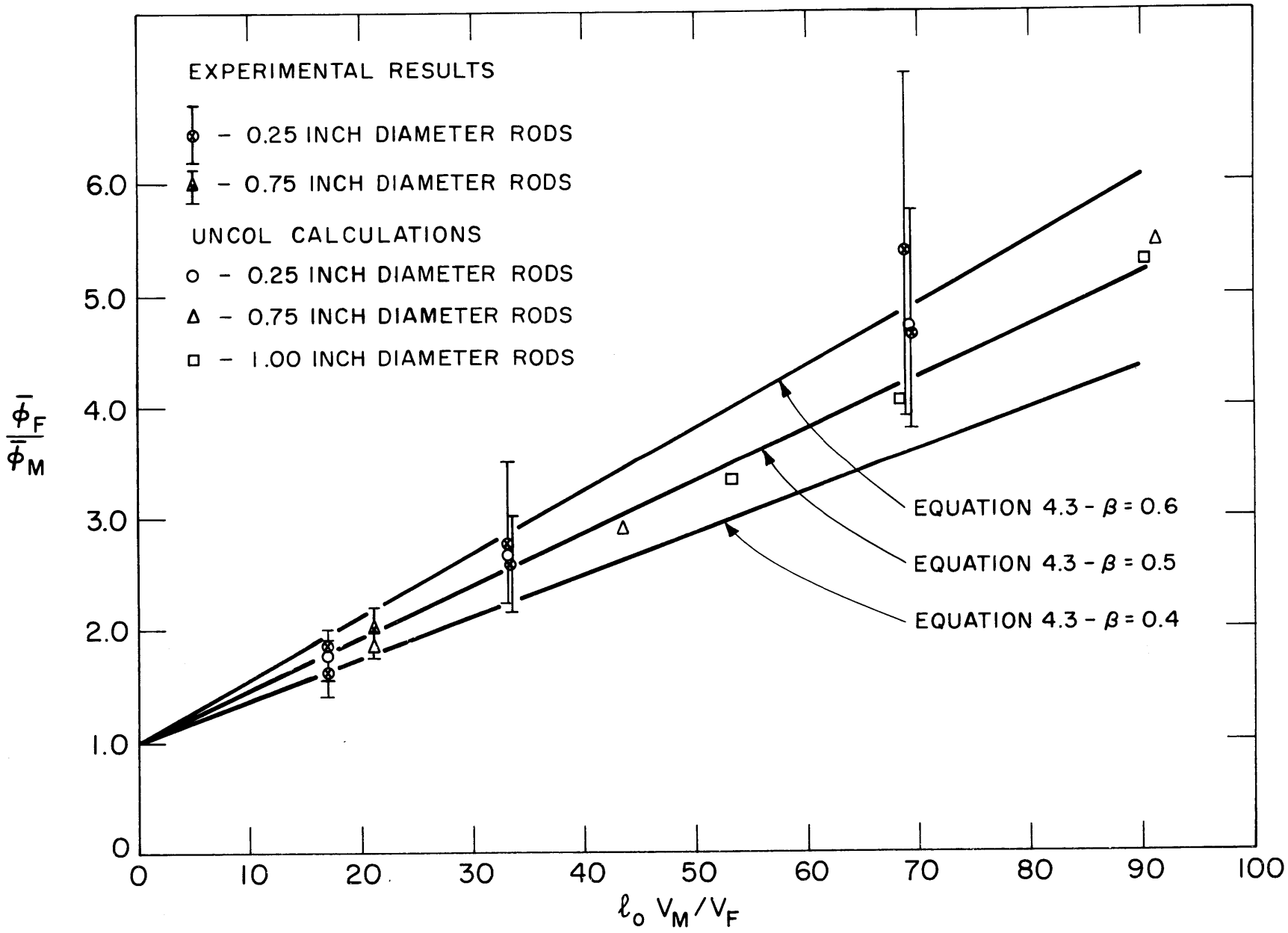

FIG. 4.17 ADVANTAGE FACTORS FOR FAST NEUTRONS

rod size that is not accounted for by Eq. 4.3. The agreement with the predictions of Eq. 4.3 is improved if β is increased as the lattice spacing is increased, in accordance with results reported for water-moderated lattices. In fact, the range of values for β from 0.45 to 0.667, to give agreement with results from water-moderated lattices as the lattice spacing is increased from small values to infinity (single rods), appears to hold equally well for heavy water-moderated lattices.

4.3 Correlation of Experimental and Theoretical Values of δ_{28}

Measurements of δ_{28}, the ratio of U^{238} fission to U^{235} fission, have been an integral part of the program of the MIT Heavy Water Lattice Project. Results and experimental details are reported in references 1, 2, 3, 4, 9, 14, 21, 28, 30, and 31 of Appendix E.

The HEETR code has been used to compute δ_{28} for all the lattices studied up to August, 1965. The results are compared with the experimental results in Table 4.3, which also contains values of δ_{28}^{∞}, the value that would have been measured in the same type of lattice but with an infinite diameter. The procedure used for this calculation is discussed in more detail later in this section.

The agreement between the experimental values of δ_{28} and those calculated with the HEETR code are fair, with the HEETR values consistently falling somewhat below the measured values. The discrepancy in each lattice amounts to less than 5% of the calculated value except for two of the lattices of the 1.027% enriched rods and one of the lattices of 1.143% enriched rods. There is some evidence of a trend toward better agreement between calculation and experiment as the rod diameter is increased, but not of any apparent pattern for the discrepancies in terms of the lattice spacings. The trend toward better agreement as the fuel rod diameter is increased could be the result of greater accuracy in the experiments for these lattices, since the magnitude of the fast flux (and of δ_{28}) increases with increasing rod size. Another possibility is that the assumptions used in the HEETR code are better at the larger rod diameters, particularly the assumption about the directional dependence of the neutron current at the interfaces. Clark has reported comparisons of values of δ_{28} calculated with HEETR with those measured

TABLE 4.3

Calculated and Experimental Results for δ_{28}

Rod Diameter (Inches)	Lattice Spacing (Inches)	U^{235} Concentration (%)	δ_{28} HEETR Calculations	δ_{28} Experimental Results	δ_{28}^{∞}
0.25	1.25	1.027	0.02467	0.0259 ± .0011	0.02725
	1.75		0.01863	0.0232 ± .0016	0.0240
	2.50		0.01566	0.0181 ± .0004	0.0185
0.25	1.25	1.143	0.02464	0.02526 ± .0023	0.02657
	1.75		0.01861	0.02044 ± .00075	0.02119
	2.50		0.01564	0.01639 ± .0010	0.01678
0.75	2.50	0.947	0.05866	0.06091 ± .001826	0.06402
1.00	4.50	0.72	0.05904	0.0597 ± .0020	0.0608
	5.00		0.05745	0.0596 ± .0017	0.0605
	5.75		0.05602	0.0583 ± .0012	0.0590

in heavy water-moderated lattices of 1.0-inch-diameter, natural uranium rods and clusters of these rods at the Savannah River Laboratory (C10). In these comparisons, the calculated values consistently exceeded the experimental values by as much as 8%. As mentioned in section 4.1.3, the HEETR result for the water-moderated lattice discussed was in good agreement with the experimental value of δ_{28}.

The UNCOL code cannot be used to calculate δ_{28} directly. It is possible, however, to derive a relationship between δ_{28} and the magnitude of the fast flux as computed by UNCOL:

$$\delta_{28} = \frac{\text{fission rate in } U^{238}}{\text{fission rate in } U^{235}} = \frac{F^{28}}{F^{25}} , \tag{4.4}$$

or

$$\delta_{28} = \frac{1}{F^{25}} \int_{E_L}^{\infty} N^{28}\sigma_f^{28}(E)\, \phi(E)\, dE . \tag{4.5}$$

If it is assumed that the shape of the energy spectrum above E_L is the same for all cases of interest,

$$\delta_{28} = \frac{kN^{28}\Phi}{F^{25}} , \tag{4.6}$$

where Φ denotes the integral flux above the threshold energy, and k is a constant.

The source term for the UNCOL fast flux calculation is S. In terms of the physical events taking place:

$$S = \nu^{25}F^{25} + \nu^{28}F^{28} \tag{4.7}$$

$$= F^{25}(\nu^{25}+\nu^{28}\delta_{28}) . \tag{4.7a}$$

Hence, we get:

$$F^{25} = \frac{S}{(\nu^{25}+\nu^{28}\delta_{28})} , \tag{4.8}$$

or

$$\delta_{28} = \frac{kN^{28}\Phi(\nu^{25}+\nu^{28}\delta_{28})}{S} . \tag{4.9}$$

If the source terms are normalized consistently for different calculations, S can be treated as a constant. Such a normalization can be made by computing an average source value for the fuel rod. For the input to UNCOL, we have:

$$S = 1.0 + C_1 r^2 , \tag{4.10}$$

and it follows that:

$$\overline{S} = \frac{\int_0^R S\ 2\pi r\ dr}{\int_0^R 2\pi r\ dr} = \frac{\int_0^R (r+C_1 r^3)\ dr}{\int_0^R r\ dr} , \tag{4.11}$$

$$\overline{S} = 1.0 + 0.5\ C_1\ R^2 , \tag{4.12}$$

where R is the rod radius in centimeters.

If $\overline{S}$ is now substituted for S in Eq. 4.9, an implicit relationship is obtained for δ_{28}. The value of δ_{28} can be considered to be a function only of Φ, the magnitude of the fast flux computed by UNCOL. In fact, the relationship between δ_{28} and Φ is nearly linear because the effect of δ_{28} on the right-hand side is very small for the lattices studied. It is convenient to plot Eq. 4.9 in the form:

$$\delta_{28} = kG\Phi , \tag{4.13}$$

where

$$G = \frac{N^{28}}{S}\left(\nu^{25}+\nu^{28}\delta_{28}\right).$$

Many measured values of δ_{28} are available and G can easily be calculated for these values. Then, if the model is valid, it should be possible to plot δ_{28} versus $G\Phi$ and obtain a straight line.

In Fig. 4.18, the experimental values of δ_{28} from Table 4.3, as well as single rod values for 0.25-inch, 0.75-inch, and 1.00-inch-diameter fuel rods, are plotted against $G\Phi$.* In the calculation of G, a value of 2.45 was used for ν^{25} and a value of 2.84 was used for ν^{28} (S7). The value of the fast flux used is the average value inside the fuel rod computed from UNCOL results averaged in a manner identical to that used to compute $\overline{S}$.

This method appears to work well for values of δ_{28} less than approximately 0.055. Above this value, there appears to be a systematic deviation, with the measured values falling below the predicted values.

It is not clear why this method should fail to correlate experimental values of δ_{28} above 0.055. One possible explanation is that the assumption of a constant spectral shape at energies above the U^{238}(n,f) threshold energy becomes increasingly less valid as lattice parameters are changed to give values of δ_{28} greater than 0.055. The lattice

---

*The point corresponding to an experimental value of 0.0479 for δ_{28} is for a lattice of 0.75-inch-diameter rods on 5.0-inch spacings and having a U-235 concentration of 0.937%. This is a preliminary result and may be revised after additional data analysis (D6).

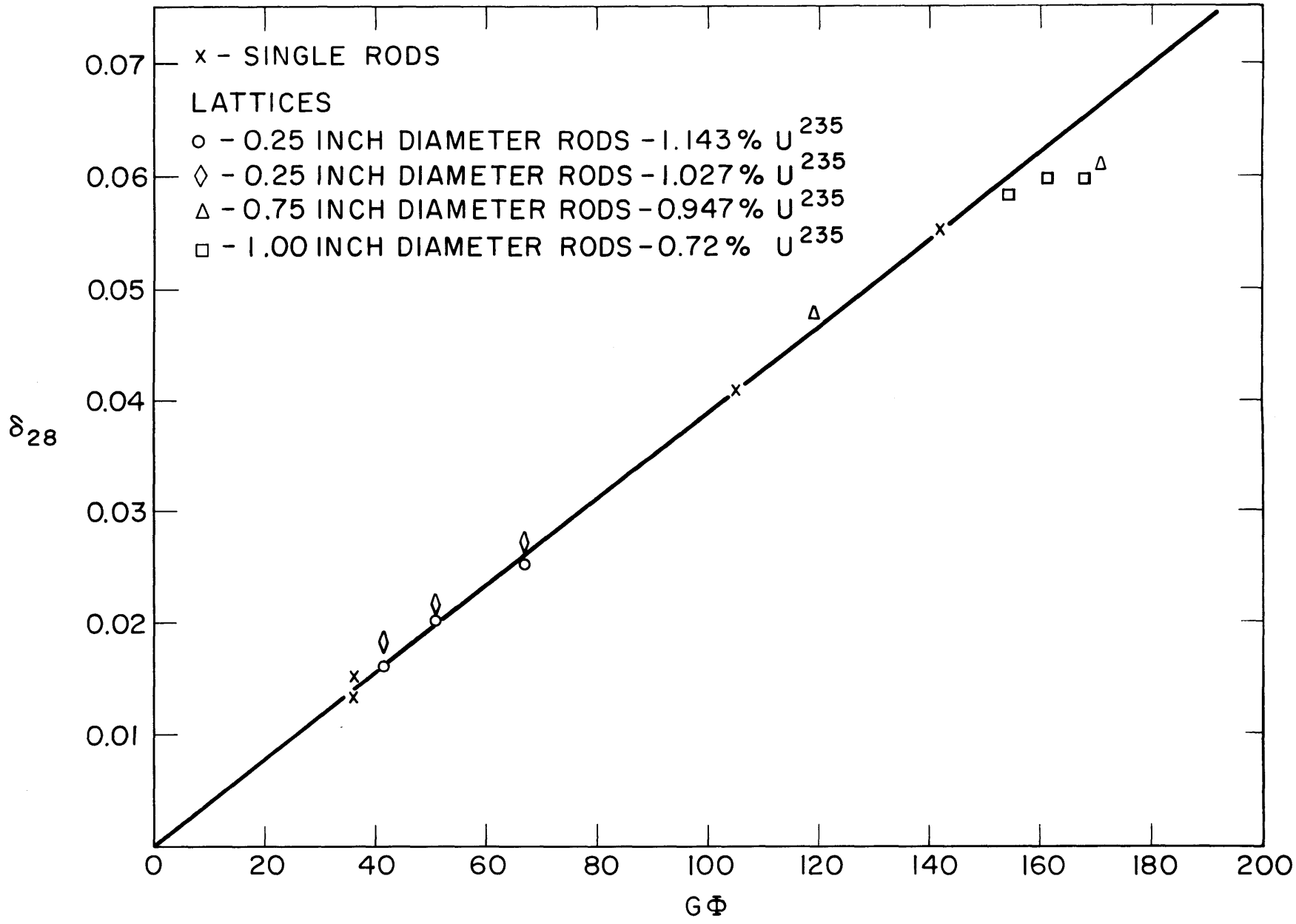

FIG. 4.18 δ_{28} VERSUS UNCOL FLUX PARAMETER

parameters that have the greatest effect on δ_{28} are the fuel rod diameter, fuel rod spacing, and the U^{235} concentration. In the lattices studied in the present work, the U^{235} concentration varies only slightly. An increase in the fuel rod diameter and/or a decrease in the rod spacing tend to increase δ_{28} and also tend to increase the relative amount of inelastic scattering for neutrons with energies above the U^{238} fast fission threshold. As will be shown in section 4.4, this increase in inelastic scattering in the lattices of larger rod diameters and smaller spacings produces neutron spectra that are softer, for energies greater than 1 Mev, than the spectra in lattices of smaller rods and greater spacings. In fact, there is very little spectral shift among the lattices having values of δ_{28} less than about 0.055, but a significant softening for just those lattices with values of δ_{28} greater than 0.055. Furthermore, this spectral shift is consistent with the systematic disagreement between the experimental values of δ_{28} greater than 0.055 and those predicted by the UNCOL method. The U^{238} fission rate can be written:

$$F^{28} = \int_{E_L}^{\infty} N^{28}\sigma_f^{28}(E)\,\phi(E)\,dE\,. \tag{4.14}$$

The assumption that the spectral shape above E_L does not change made it possible to eliminate the integral:

$$F^{28} = kN^{28}\phi\,. \tag{4.15}$$

As an aid to understanding the effects of spectral shift on the U^{238} fission rate, $\sigma_f^{28}(E)$ may be considered a weighting coefficient. In comparisons involving no spectral shift, Eq. 4.15 is useful because the constant term, k, does not change. If the spectrum is then softened, however, the value of k decreases because $\sigma_f^{28}(E)$ is smaller for lower energies (see Fig. 2.3) and has the effect of a smaller weighting coefficient in the integral of Eq. 4.14. Thus, the UNCOL method tends to predict values of δ_{28} that are greater than experimental results because the method does not account for spectral softening that occurs in lattices of large rods that are closely packed.

Two additional points deserve mention. First, both the results from HEETR and those of the UNCOL method indicate that in comparisons

of one lattice of rods of 1.027% U^{235} with another lattice of rods of 1.143% U^{235} but identical in all other respects, the values of δ_{28} should not be very different. The HEETR results show a difference of about 0.1% between lattices that are identical except for U^{235} concentration. This 0.1% difference is almost exactly the difference in the U^{238} concentration of the two enrichments, which is the only factor that varies in the UNCOL treatment of these lattices. The significantly higher experimental values for the rods of 1.027% U^{235} are in disagreement with these theoretical results. Papay has noted that the higher values for the rods of 1.027% U^{235} are difficult to explain physically and has suggested that the differences in the experimental values may be due to mistakes in the enrichment of the fuel slugs used in the experiments (P6).

Second, as described in section 4.1.2, the UNCOL code may be used for calculations in which the diameter of the lattice assembly is effectively infinite. Combination of this procedure with the one described above for the calculation of δ_{28} makes it possible to calculate δ_{28}^{∞}, the value that would exist in a lattice of infinite diameter. This procedure amounts to a correction of the experimental value of δ_{28} for the effects of leakage. Heretofore, the treatment of fast leakage effects has been based on diffusion theory which may not treat accurately the behavior of the fast neutrons involved (H2). It is important to note that the assumption regarding the shape of the spectrum above the U^{238} fission threshold should be valid for comparisons of experimental lattices with the infinite (but otherwise identical) lattice, even for lattices of large-diameter fuel rods and tight spacings. For example, the neutron spectrum above 1 Mev in a lattice of 1.0-inch-diameter, natural uranium rods on 5.0-inch spacings, contained in a four-foot-diameter tank, should not be significantly different from the spectrum in a lattice that is identical except for an infinite diameter. Thus, although the UNCOL method does not correlate accurately the experimental values of δ_{28} for lattices of 1.0-inch-diameter rods, the ratio of the fast flux calculated by UNCOL for the infinite lattice to that obtained for the experimental lattice provides a correction factor that can be used to correct the experimental value of δ_{28} for leakage. Values of δ_{28}^{∞} obtained in this way are included in Table 4.3.

4.4 Calculations of Energy Spectra

The HEETR code has been used to calculate spectra for the lattices studied. Differential energy spectra are obtained by means of the procedure described in section 3.4. The spectra are in the form of histograms except for the highest energy group. This group is assumed to have the same shape as that portion of the fission spectrum covering the same energy interval.

The results of calculations for all three lattices of 0.25-inch-diameter fuel rods, and for one lattice each of the 0.75-inch-diameter and 1.00-inch-diameter fuel rods, are shown in Figs. 4.19 - 4.21. Spectra have been calculated for three different locations in each lattice cell for which calculations were made: the middle of the moderator region, the cladding, and the center of the fuel rod. All spectra have been normalized to the same value for the highest energy group to facilitate the observation of trends. The spectrum of the fission neutron flux has been included for comparison in each figure.

All the spectra show an increasing deviation from a fission spectrum as the neutron energy is decreased. The spectra of the highest two energy groups deviate little from a fission spectrum, so the assumption that the first group has the same shape as a fission spectrum over that energy range is probably justified.

A definite trend toward softer spectra is evident as the lattice spacing is decreased and/or the fuel rod diameter is increased. This trend is more evident for spectra inside the fuel than elsewhere in the lattice cell and can be explained on the basis of increased inelastic scattering. As discussed in section 4.3, the trend toward softer spectra for the larger rods and tighter spacings is consistent with the failure of the UNCOL method to correlate accurately the experimental values of δ_{28} in lattices of such rods. As shown in Fig. 4.19, there is practically no difference in the spectra above 1 Mev inside the fuel for the lattices of 0.25-inch-diameter rods. The spectra inside the fuel in the lattices of the larger rods are increasingly softer as the energy is decreased below about 2 Mev.

The HEETR results have also been used with the RATIO code to compute activation ratios in the various spectra for the fast neutron

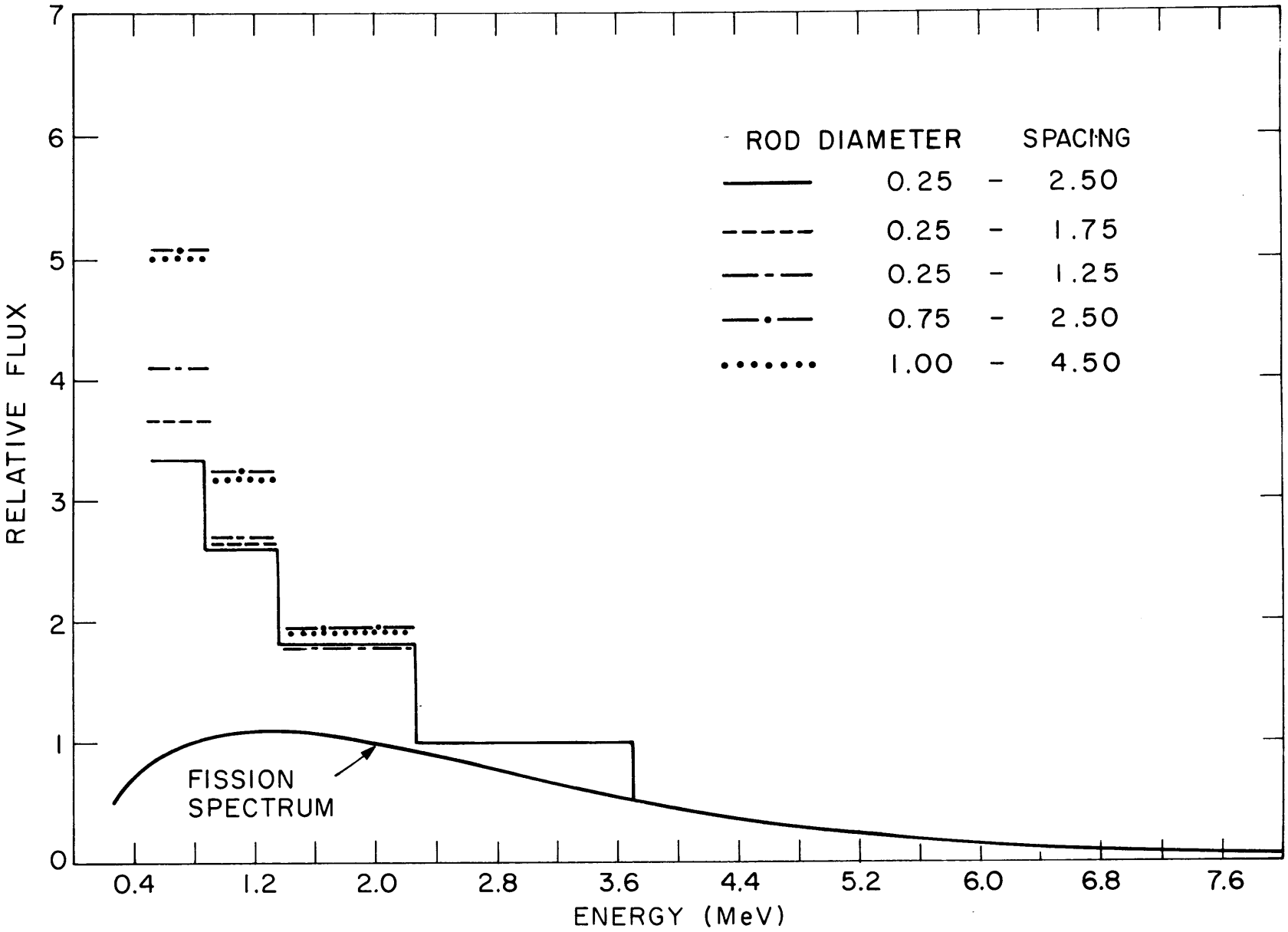

FIG. 4.19 ENERGY SPECTRA IN THE FUEL FOR VARIOUS LATTICES

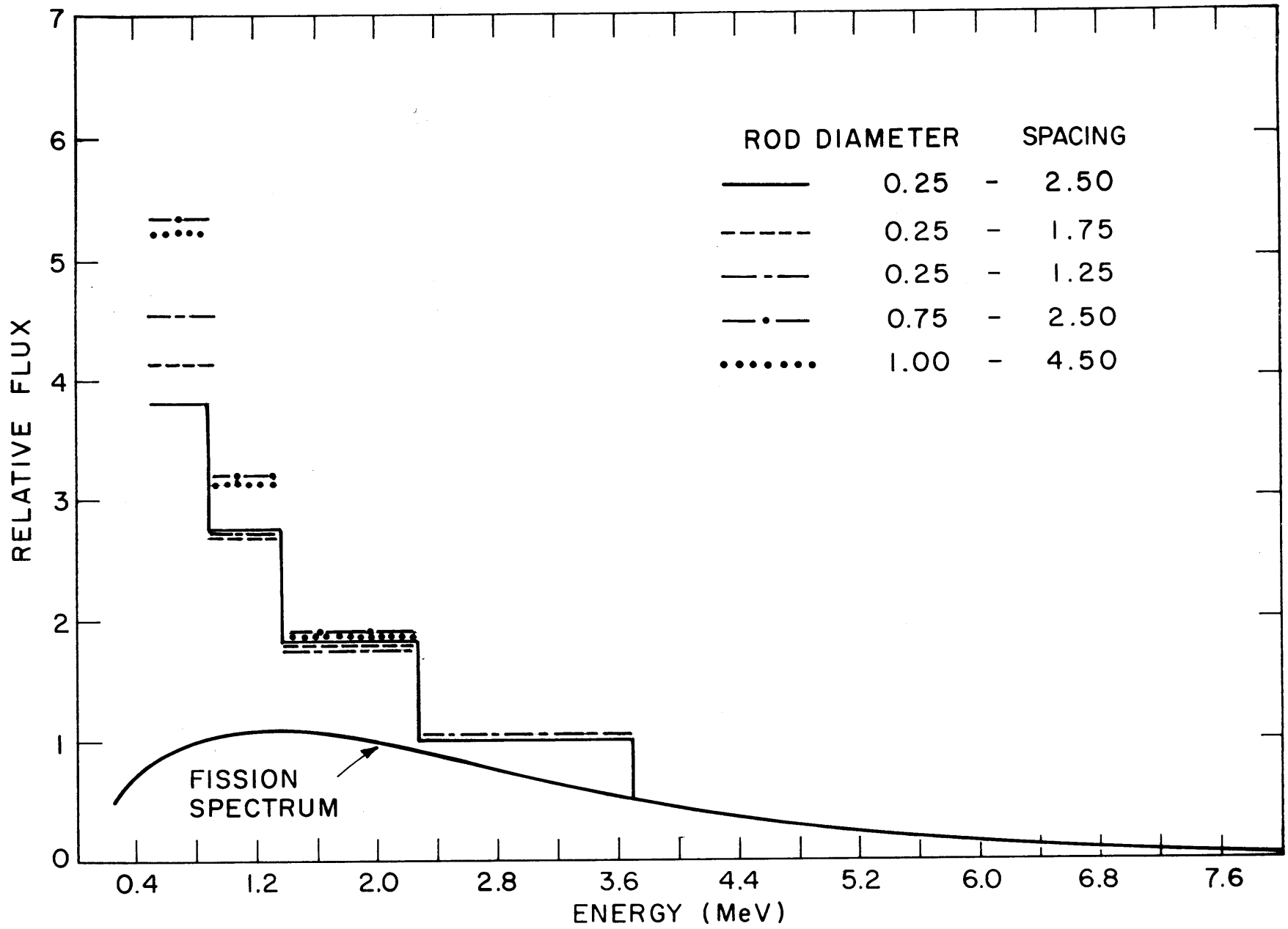

FIG. 4.20 ENERGY SPECTRA IN THE CLADDING FOR VARIOUS LATTICES

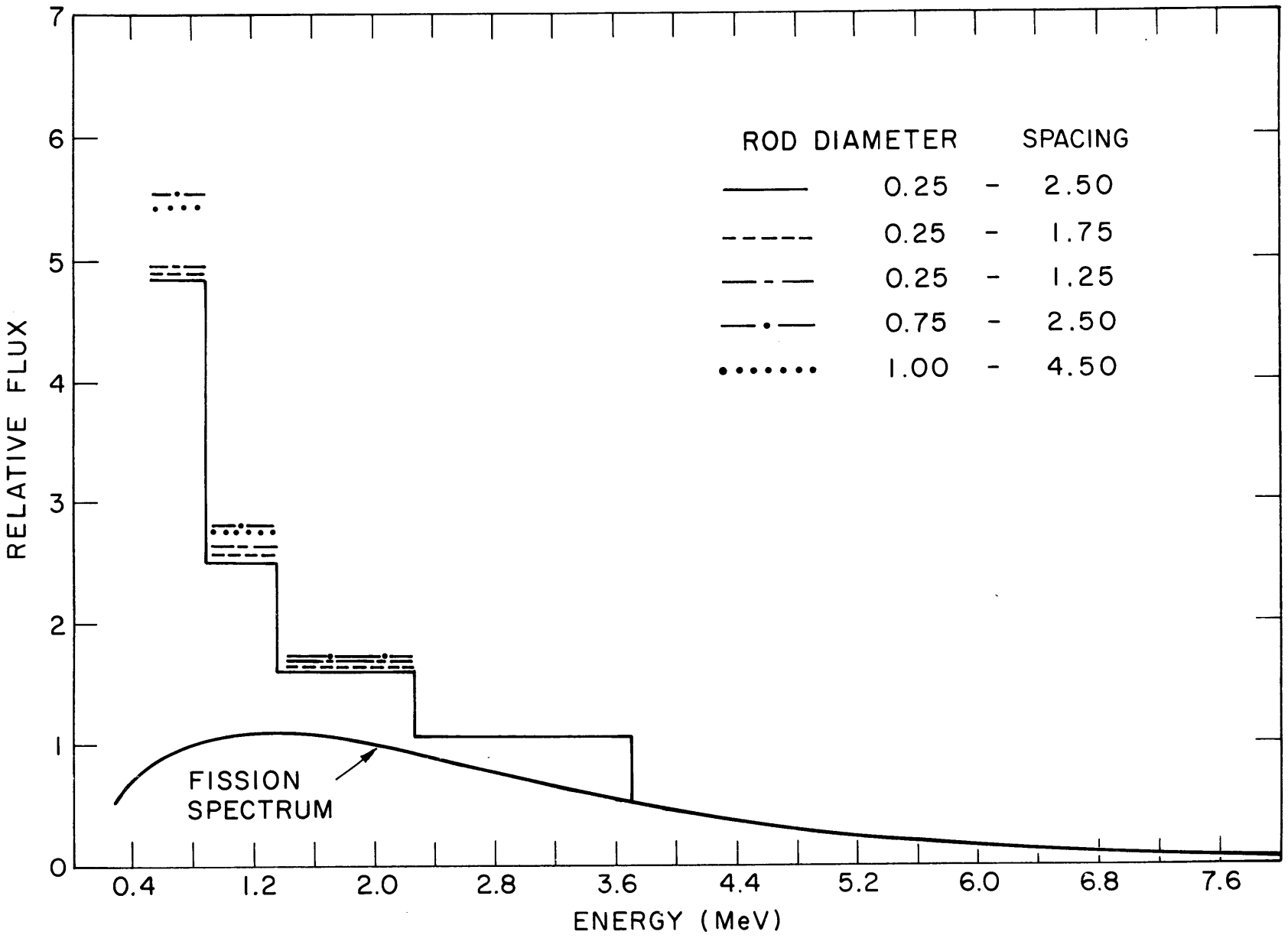

FIG. 4.21 ENERGY SPECTRA IN THE MODERATOR FOR VARIOUS LATTICES

threshold reactions used in the present work. These results are given in Table 4.4 in terms of the $U^{238}(n, f)$ reaction rate. The rhodium reaction has also been included because of its relatively low threshold energy. Attempts were also made to obtain experimental values of these ratios. To do so, however, it was necessary to determine absolute counting rates. The experimental conditions involved – small foils, low counting rates, long time intervals between runs, substantial variations in counting equipment, and irregular lattice shutdowns, to mention just a few – introduced such large experimental uncertainties in the absolute counting rates as to make such comparisons of little value. Furthermore, it is evident from Table 4.4 that the variation in these ratios is very small for the cases calculated. Table 4.4 includes results over a wide range of lattices with possibly different spectra, and also values corresponding to a fission spectrum. The HEETR calculations show some spectral shift in this list. It can be concluded, therefore, that threshold reactions do not provide a sensitive method of detecting small changes in fast neutron energy spectra.

4.5 UNCOL Calculations for the MITR

A distinct advantage of kernel methods, such as the UNCOL code, is that they can be used for calculations in nonuniform arrays. An example is the MIT Reactor, a horizontal section of which is shown in Fig. 2.11. The central fuel element (#1) and the first ring of six fuel elements (#2 through #7) constitute a regular lattice array with a triangular spacing of 6.375 inches. The second ring of twelve fuel elements (#8 through #19) departs slightly from this pattern. The reactor shim control rods are positioned between the first and second rings. The spacings between the elements of the second ring are therefore increased to 6.85 inches to form a circle of radius 13.250 inches around the central element. The spacing is further increased in the outer ring of ten elements (#20 through #30). These elements fall on a circle of radius 20.935 inches about the central element and are not uniformly spaced along the circle. The design of the reactor is discussed in greater detail in reference T6.

The fast neutron distributions of interest in the MITR are not the distributions in and around a fuel element as in the lattices (although these could also be calculated). Instead, the relative values in the

TABLE 4.4

Activation Ratios for Various Spectra

Lattice Configuration		Location in Lattice Cell	$U^{238}(n,f)$/Reaction			
Rod Diameter (Inches)	Rod Spacing (Inches)		$In^{115}(n,n')$	$Ni^{58}(n,p)$	$Zn^{64}(n,p)$	$Rh^{103}(n,n')$
0.25	2.50	Cell average	1.81	2.51	9.03	0.617
0.25	1.75	Cell average	1.80	2.51	9.04	0.613
0.25	1.25	Cell average	1.80	2.52	9.06	0.610
0.75	2.50	Cell average	1.79	2.55	9.17	0.595
0.75	5.00	Cell average	1.79	2.54	9.11	0.602
1.00	4.50	Cell average	1.79	2.55	9.17	0.595
Fission Spectrum			1.97	2.20	7.60	0.735
0.25	2.50	Fuel	1.83	2.55	9.13	0.629
0.25	2.50	Cladding	1.82	2.56	9.20	0.621
0.25	2.50	Moderator	1.81	2.49	8.96	0.618
0.25	1.75	Fuel	1.82	2.54	9.11	0.625
0.25	1.75	Cladding	1.81	2.55	9.15	0.618
0.25	1.75	Moderator	1.80	2.50	9.00	0.613
0.25	1.25	Fuel	1.81	2.54	9.12	0.618
0.25	1.25	Cladding	1.80	2.54	9.13	0.613
0.25	1.25	Moderator	1.80	2.51	9.04	0.610
0.75	2.50	Fuel	1.78	2.61	9.35	0.592
0.75	2.50	Cladding	1.78	2.60	9.33	0.592
0.75	2.50	Moderator	1.79	2.53	9.08	0.598
0.75	5.0	Fuel	1.79	2.62	9.41	0.598
0.75	5.0	Cladding	1.78	2.65	9.51	0.592
0.75	5.0	Moderator	1.80	2.47	8.89	0.613

different fuel element positions and the experimental facilities are of interest. The calculation of these relative values requires several modifications of the UNCOL procedure used for the lattice calculations as well as an additional approximation. The approximation involves the cylindricalization of the rectangular fuel elements and the modifications include the following:

(1) calculations must be made for annular shape to properly treat reduced-plate elements;

(2) the distances between a point of interest and the individual fuel elements must be read into the code;

(3) the weighting coefficients for the individual fuel elements must be read into the code;

(4) the nuclear properties of graphite must be taken into account when calculations are done for positions 3GV2, 3GV5, and 3GV6.

The cylindricalization of the rectangular fuel elements is reasonably straightforward. The elements are assumed to be cylinders with a cross-sectional area equal to that of the rectangular elements: cylinders with a diameter of approximately 3.1 inches. This equivalence relation is not unique and others could be used, such as equating the outer perimeter of the element with the circumference of the cylinder, which would give a diameter of about 3.5 inches. Areas (or unit volumes) are the standard basis for unit cell calculations, however, and this is probably the most meaningful basis for the present application because it preserves the fuel-to-moderator volume ratio.

The consideration of annuli is a consequence of the use of "reduced-plate" elements as experimental facilities in the MITR. For this purpose, either six or eight of the sixteen fuel-bearing plates are removed from the center of the element and a sample thimble inserted. The resulting arrangement can be treated conveniently as an annulus. The inner diameter is computed so that the area of the annulus is the same fraction of the cylindrical area as the percentage of the remaining plates. For example, if eight of the sixteen plates are removed, then the area of the annulus must be one-half the area of the cylinder.

The distances between the fuel elements and points of interest are taken from blueprints of the reactor as discussed in section 2.10. They are given in Table 2.3.

The weighting coefficients have been taken to be the actual power produced by the individual elements. Since the U^{235} content varies from one element to the next, relative thermal fluxes are not an adequate index of the fast neutron source, even if they are known. The MITBURN code (M7), which was written to compute fuel burn-up in the MITR, provides the individual element power for any configuration and power level of the MITR that is of interest. But the weighting coefficients for the "annular" reduced-plate elements must be adjusted because the weighting coefficient as used in UNCOL is a specific unit, or intensive, quantity. In other words, if the cross-sectional area of the reduced-plate elements is reduced to an annulus and the weighting coefficient is not proportionately increased, the specific power of the element will be too low because the decrease in the size of the element will have been accounted for twice.

The modification to include a third region composed of graphite is necessary because the lattice calculations were based on a two-region treatment. There are approximately five inches of graphite between the vertical sample facilities (3GV2, 3GV5, and 3GV6) and the core tank. In the first set of calculations, no allowance was made for the presence of this graphite, and the calculations predicted relative values of the fast flux in these facilities that were lower than the experimental values by a factor of about five. These calculations were based on the assumption that the space between the fuel elements and the facilities were completely filled with heavy water. The low results were a consequence of the much higher fast neutron removal cross section of heavy water as compared to that of graphite.

To account for the presence of the graphite, two additional quantities are required. The first is an effective removal cross section for graphite. The second requirement is an effective thickness of graphite through which the neutrons pass in reaching the facilities. The procedure used was first to calculate the graphite thickness and then to vary the cross section until acceptable agreement with experiment was obtained.

The exact graphite thickness could have been measured between each facility and each fuel element. The result would have been a matrix similar to the matrix of Table 2.3. Instead, an average value was calculated and used for the calculations for all the fuel elements. This method is somewhat more general, in the sense that it does not restrict use of the code to the MITR; the results are not affected. It is assumed that the edge of the core tank is a straight line in the immediate vicinity of the graphite facility. Then, as shown in Fig. 4.22, d is the perpendicular distance between the facility and the core tank, θ is the angle between the perpendicular and the direction of interest, and r is the graphite thickness of interest.

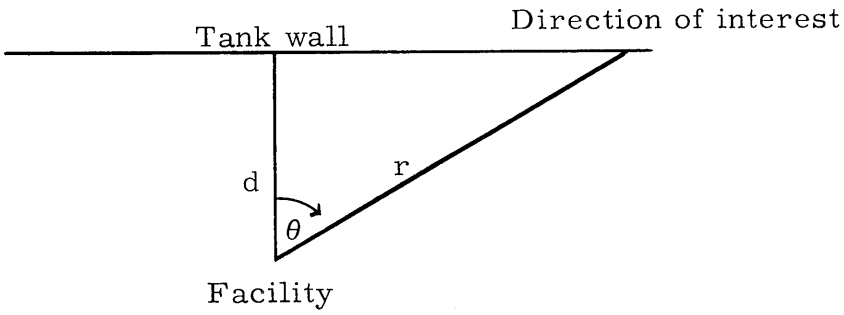

FIG. 4.22 Theoretical arrangement for graphite facility calculations.

We are interested in an average value of r; therefore, we write:

$$R_G = \bar{r} = \frac{\int_0^{\theta_o} r\, d\theta}{\int_0^{\theta_o} d\theta} = \frac{1}{\theta_o} \int_0^{\theta_o} \frac{d}{\cos\theta}\, d\theta, \tag{4.16}$$

or,

$$R_G = \frac{d}{\theta_o} \left\{ \ln \left| \sec\theta + \tan\theta \right| \right\}_{\theta=0}^{\theta=\theta_o}. \tag{4.17}$$

Taking $\theta_o = 45°$, d = 5 inches, we get:

$$\bar{r} = 1.12d = 5.6 \text{ inches} = R_G.$$

The graphite thickness and cross section enter into the calculation of the over-all cross section in a manner similar to that discussed in section 3.2.2 for the two-region case; i. e.,

$$\Sigma(r) = \frac{\Sigma_F R_F + \Sigma_G R_G + \Sigma_M(r-R_F-R_G)}{r} . \qquad (4.18)$$

Equation 4.18 is exact for the case of pure attenuation (no "build-up factor"), which is consistent with the model for the UNCOL code. In fact, within the limitations of the model, there is no restriction to the number of regions to which an equation of the type of Eq. 4.18 can be extended.

There are two sets of experimental data with which results of the above calculations can be compared. The first set involves the $Ni^{58}(n, p)Co^{58}$ measurements described in section 2.10. These measurements were performed August 12, 1965. The fuel arrangement at that time corresponded to MITR Core Configuration #62, for which the weighting coefficients (power per element in MW) are given in Table 4.5. The results of the measurements are compared with the UNCOL calculations in Table 4.6 where both are normalized to the value at Fuel Element Position #1. The agreement between calculations and experiment is quite good with the exception of the results for 3GV6. In all the other experimental facilities, the results of the calculations are slightly higher relative to Position #1 than the experimental results. The calculated value for 3GV6 is approximately 20% lower than the experimental value.

The value of the removal cross section for graphite used for the calculations for 3GV2, 3GV5, and 3GV6 was 0.030 cm^{-1}. This value gives results that agree well with experiment and is not very different from the value of the removal cross section for carbon calculated from the first two groups of the LASL 16-group set (A4). The theoretical value so determined is 0.0348 cm^{-1} for one group of fast neutrons above 1.4 Mev.

The second set of experiments with which UNCOL calculations for the MITR have been compared is a series of foil measurements made by personnel of the MIT Organic Loop Project (T7). These foil measurements

TABLE 4.5

Weighting Coefficients for MITR Core Configuration #62

Fuel Element Position	Weighting Coefficient
1	0.1250*
2	0.1252
3	0.1210
4	0.1158
5	0.1172
6	0.1191
7	0.1240
8	0.0629
9	0.0703
10	0.0670
11	0.0867
12	0.0726
13	0.0633
14	0.0836
15	0.0899
16	0.0651
17	0.0891
18	0.0740
19	0.0818
22	0.0422
26	0.0375
28	0.0436
29	0.0328
30	0.0307
20, 21, 23, 24, 25, 27	0.0000

*10-plate element

TABLE 4.6

Experimental and Calculated Relative Fast Fluxes for MITR Core Configuration #62

Experimental Facility	Experimental Results (Relative)	Results of UNCOL Calculations (Relative)
Position 1	1.0	1.0
Position 23	3.025×10^{-2}	3.114×10^{-2}
1PH2	3.090×10^{-2}	3.229×10^{-2}
3GV2	1.017×10^{-2}	1.116×10^{-2}
3GV5	3.816×10^{-2}	3.834×10^{-2}
3GV6	1.988×10^{-2}	1.586×10^{-2}

were based on the $Ni^{58}(n, p)Co^{58}$ reaction. The measurements were made in experimental thimbles and in monitor tubes of the organic loop in-pile section. The irradiations were made in Fuel Position 1 and Fuel Position 20 of the MIT Reactor between April 1963 and August 1965. The results are normalized to the first experiment and are compared in Table 4.7.

TABLE 4.7

Comparison of UNCOL Calculations and Organic Loop Data

Core Configuration	Experimental Facility	Experimental Results (Relative)	Results of UNCOL Calculations (Relative)	Remarks
39	Position 1	1.0	1.0	10-plate element in Position 1
50	Position 1	0.766	0.833	
52	Position 1	0.289	0.241	No fuel in Position 1
61	Position 20	0.0236	0.0204	A cadmium-lined sample assembly and in-pile section occupied Position 20.
61	Position 20	0.0211	0.0204	

The UNCOL calculations for the MITR cannot be more accurate than the MITBURN code from which the weighting coefficients are taken. The generally good agreement between the results of UNCOL calculations and experimental results provides additional confidence in the accuracy of MITBURN calculations as well as some assurance that the UNCOL code can be successfully used for calculations in the MITR.

4.6 Perturbation Effects

Measurements were made as described in section 2.9 in an effort to determine perturbation effects on results obtained with the cadmium-covered foils in the moderator.

In the first set of measurements, the axial distribution of the $Au^{197}(n, \gamma)Au^{198}$ reaction was measured with bare Pb-Au (13%) foils, 0.010 inches thick. The results for the three lattices with the 0.25-inch-diameter fuel rods are shown in Fig. 4.23. The flux is depressed locally in the vicinity of the moderator foils, with a maximum deviation of about 10% (below the normal value). The results are similar for all three lattices, although the lattice with 1.75-inch spacing seems to have a slightly greater depression than the other two. The 1.25-inch spacing might have been expected to show the greatest depression, since the cadmium covers were closer to the fuel and since they occupied a greater percentage of the moderator volume in the lattice cell. But the neutron spectrum in the thermal and resonance range is different for the three lattices; it is harder for the tighter lattices and, as will be shown in the discussion that follows, this accounts for the apparent discrepancy.

In retrospect, the choice of gold foils for use in measuring the effect of the cadmium covers on the axial distribution of the thermal flux does not appear to have been a wise one. The thermal flux is the parameter of interest because nearly all of the fissions occurring in these lattices (which are the sources of the fast neutrons) are in U^{235}. The value of the thermal fission cross section for U^{235} is about 570 barns (A4) and the value of the effective resonance integral for infinite dilution is about 274 barns (A5). The value of the thermal cross section for the $Au^{197}(n, \gamma)Au^{198}$ reaction is 98.8 barns (A4). The effective resonance integral is a strong function of the foil thickness. If it is assumed

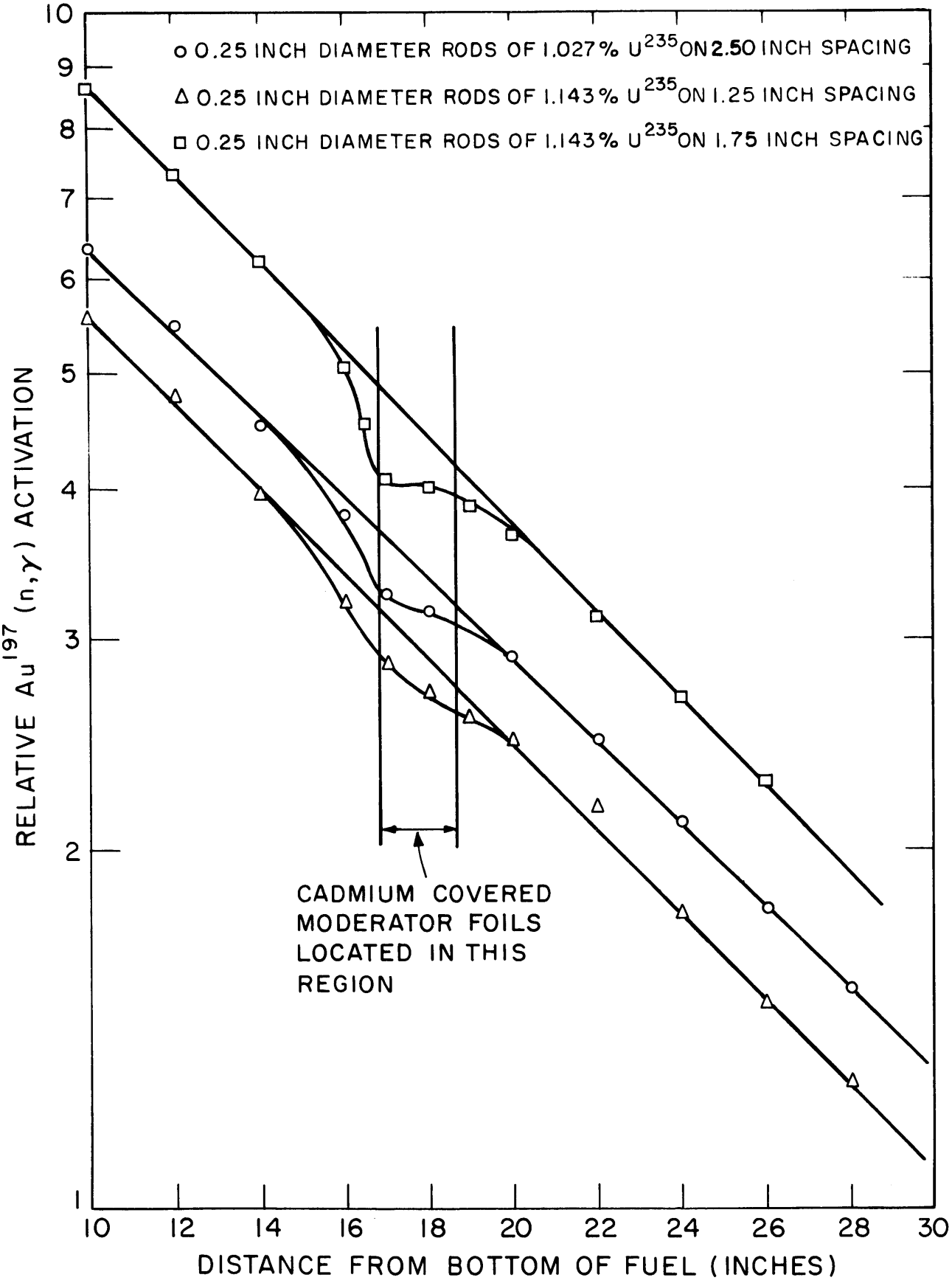

FIG. 4.23 EFFECT OF CADMIUM COVERS ON THE AXIAL DISTRIBUTION OF THE THERMAL FLUX

that a Pb-Au (13%) foil, 0.010 inch thick, is equivalent to a pure gold foil, 0.0016 inch thick (this assumption should cause the value of effective resonance integral to be overestimated), a value of 394 barns is appropriate (S6). The ratios of the effective resonance integral to the thermal cross section are about 0.475 for U^{235} fission and 3.9 for the gold reaction used in the experiment. These ratios show that a larger fraction of the gold reaction results from interactions with resonance neutrons than is the case for the U^{235}(n, f) reaction.* The fraction of the gold reaction that is due to interactions with resonance neutrons can be calculated by using Eq. 4.19 and the experimental values of δ_{25}, the ratio of the U^{235} fission rate in foils covered with cadmium to the U^{235} fission rate in bare foils. The ratio of epicadmium to subcadmium activation can be written:**

$$\frac{\text{epicadmium activation}}{\text{subcadmium activation}} = \frac{\frac{\text{ERI}}{\sigma_o}\beta}{(0.886 \quad 0.414\beta)}, \tag{4.19}$$

where,

β = the ratio of the integral resonance flux to the integral thermal flux.

The experimental values of δ_{25} vary from about 0.02 to 0.05 for the lattices of 0.25-inch-diameter rods (H9). The solution of Eq. 4.19 for β gives values of 0.038 to 0.1 for these lattices; these values can then be used to compute the epicadmium-to-subcadmium activation ratios for the gold reaction. Results of these calculations indicate that the ratio of epicadmium to subcadmium activation for the gold foils used in the experiments varied from 0.16 to 0.42 as the rod spacing is decreased from 2.50 inches to 1.25 inches in the lattices of 0.25-inch-diameter rods. These results indicate that a reduction of 10% in the activation of the gold foils corresponded to a reduction in the thermal flux of 12% for the widely spaced lattices and of 17% for the tightly spaced lattices.

---

*The Na^{23}(n, γ)Na^{24} reaction would have been a better choice than gold for use in the experiment because the ratio of the effective resonance integral to the thermal cross section is about 0.514 (A4, A5).

**The effective energy for "cadmium cut-off" is assumed to be 0.4 ev.

The activity distribution in the moderator of the $Ni^{58}(n, p)Co^{58}$ reaction, measured by using bare foils and a modified foil holder, is shown in Fig. 4.24 together with the results from an experiment with cadmium covers on the foils. It appears that the activation of the foils nearest the fuel rod may be decreased by approximately 10% by the presence of the cadmium. The foils farther from the rod are affected little, if any. This result is to be expected in view of the axial distributions described above. The activation of the foils nearest the rod should be decreased as a result of the presence of the cadmium covers, more than the foils further away, for two reasons. First, since they are closer to the rod, a greater percentage of the contribution from the rod comes from their immediate vicinity. This is a consequence of the roughly exponential attenuation of the fast neutrons as they leave their point of birth. Second, the foils nearest the rod receive a higher percentage of their total activation from that rod, the other rods in the lattice playing a relatively smaller role.

It would be difficult to obtain an analytic correction for the perturbation caused by the cadmium covers. Such a correction would be a complicated function of rod diameter, lattice spacing, and distance from the foil to the rod. Even the data of Fig. 4.23 are of limited value for this purpose, since their use requires treatment of an axially dependent source.

The desired corrections could have been obtained empirically with data similar to those shown in Fig. 4.24. This procedure was not adopted because the number of experiments required would have been prohibitive. A separate correction curve would have been required for every lattice studied, and more than one experiment would have been necessary in each case in order to obtain an accurate correction. The net effect would have been almost to double the amount of experiments required. Since lattice experimental time was at a premium, it was decided not to perform these experiments.

This decision is further supported by additional considerations. The foils inside the fuel rod were not affected by this perturbation. As described in section 2.6, the fuel foils were always positioned in a separate rod at least one cell away from the moderator holders. Only those

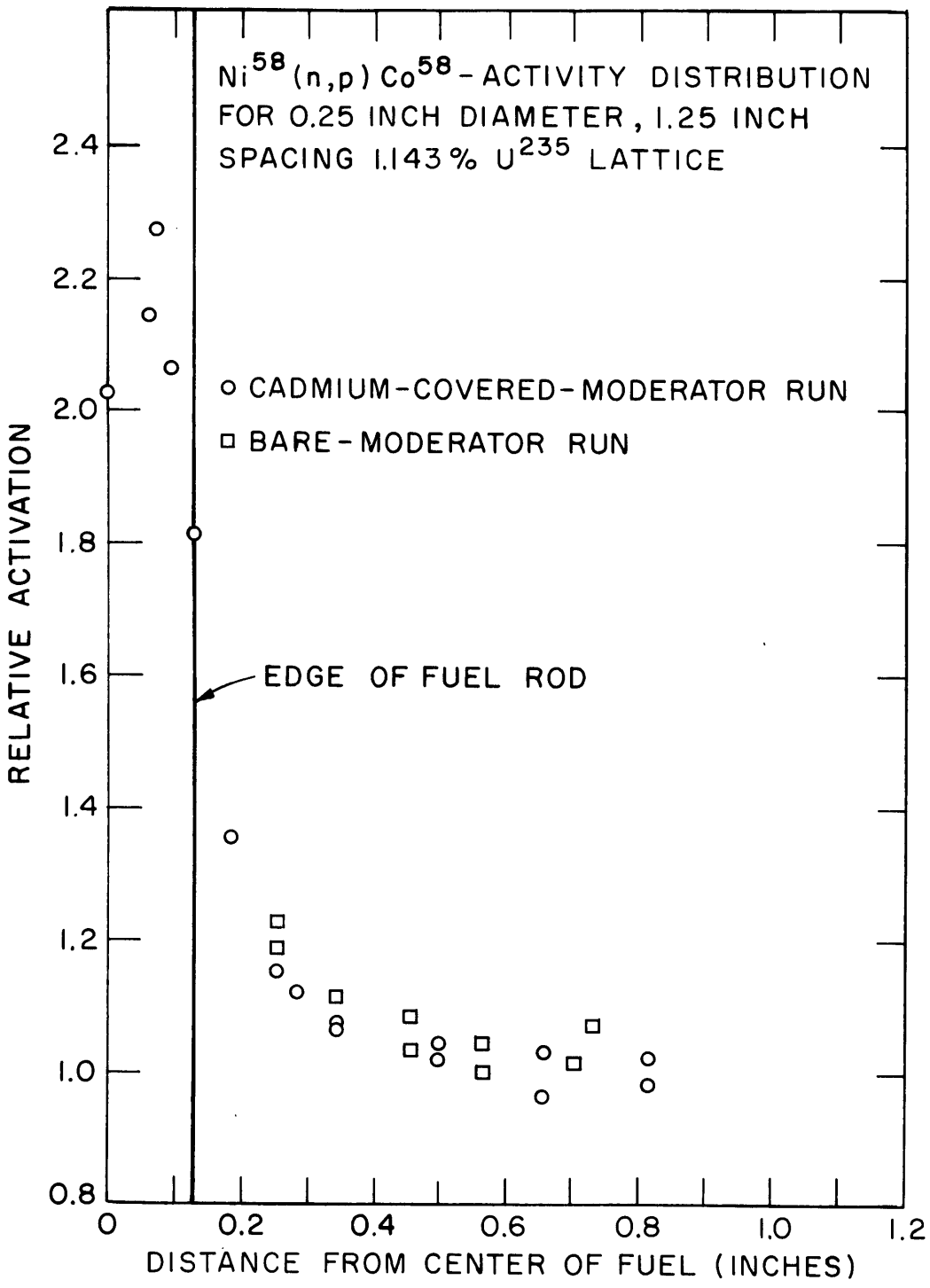

FIG. 4.24 COMPARISON OF RESULTS FOR CADMIUM COVERED AND BARE MODERATOR FOILS

moderator foils closest to the rod were substantially affected. This result is to be expected and is supported by the data shown in Figs. 4.23 and 4.24. The foil locations closest to the fuel rod were not the most important ones for determining either the fast neutron distributions in the lattice cells or the fast fission rate inside the fuel. Finally, the results of Fig. 4.23, together with the calculations discussed above, effectively establish a reasonably accurate upper limit on the magnitude of this effect. In accordance with these data, the effect could not exceed 12% to 17% (depending on the lattice), even if the fast flux activating the foil originated entirely from within the adjacent rod and from within a very small volume inside the rod. Neither of these conditions existed in any of the lattices studied.

The results of the test of the "inverted" moderator foil holder are given in Fig. 4.25. There is no detectable difference between the results for the two kinds of holders. This is to be expected, provided the measurements are made sufficiently high in the lattice.

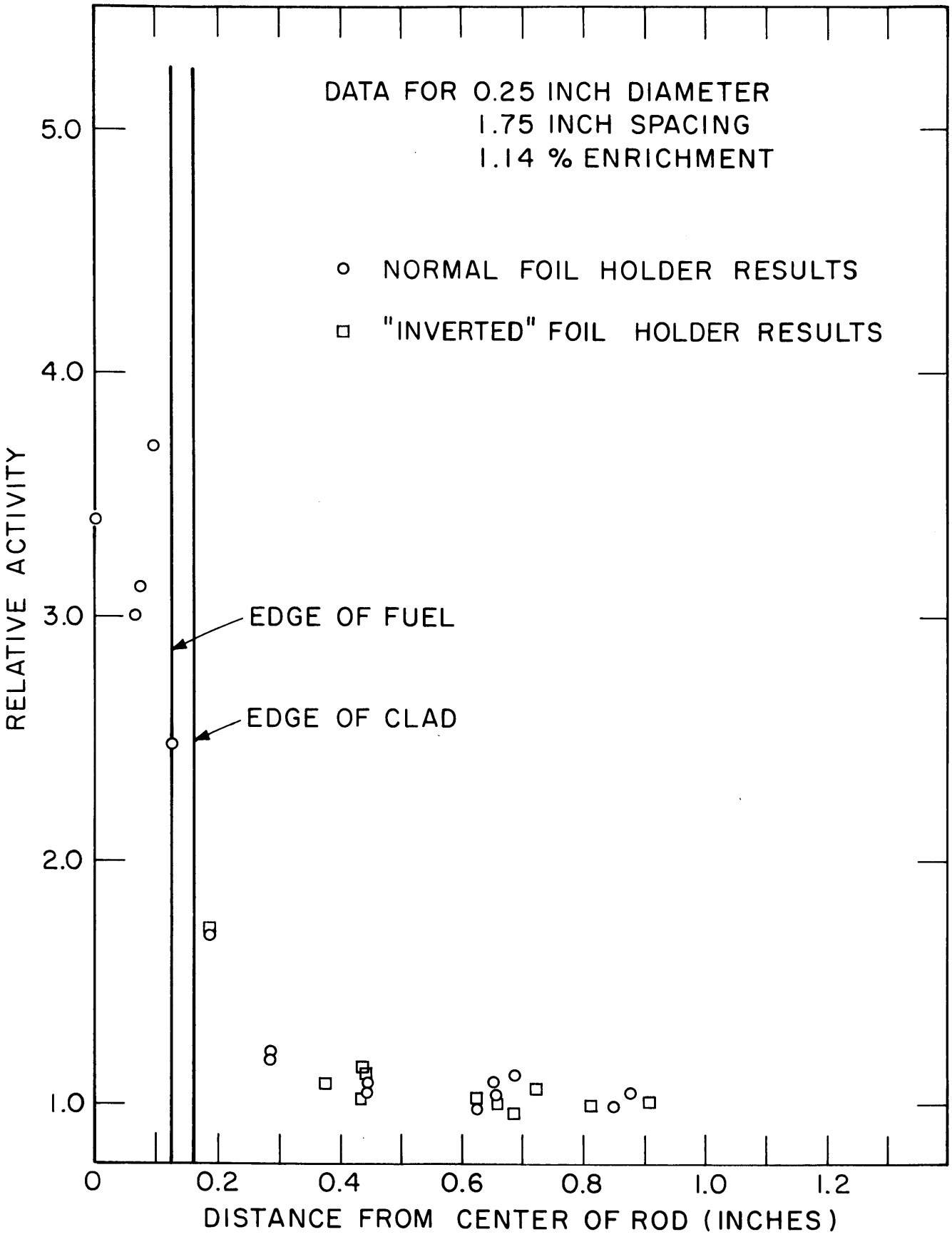

FIG.4.25 COMPARISON OF RESULTS FOR NORMAL AND INVERTED FOIL HOLDERS

Chapter V

RECOMMENDATIONS FOR FUTURE WORK

It is recommended that additional measurements be made of the intracellular distributions of the activation of threshold detectors. Such measurements would provide experimental information of direct use for calculations of radiation damage rates and of certain reactor physics parameters, such as resonance capture in homogenized lattice cells as done, for example, in reference D2. Measurements of the intracellular distribution of the fast flux could also be used to extend the application of the UNCOL code by providing values of effective removal cross sections for other materials besides slightly enriched uranium and heavy water. The values of the effective removal cross section for uranium and heavy water used in the present work were close to calculated values found in the literature for a group of neutrons with energies above 1.35 Mev (see section 4.1.1). As discussed in Appendix D, however, the results of the UNCOL calculations are quite sensitive to changes in the values of the effective removal cross sections used, and it is not obvious that the calculated values found in the literature for other materials are sufficiently accurate. If comparisons with additional experiments show that calculated values of removal cross sections for some other materials besides uranium and heavy water can be used in UNCOL to give satisfactory agreement, a better basis would be established for the application of the UNCOL code to assemblies of different types. The removal cross sections used in the UNCOL code are those consistent with one energy group having a lower limit of about 1 Mev. In sets of multigroup constants, the neutrons with energies greater than 1 Mev are usually divided into two or more groups. The values of the removal cross section for such groups must be combined, so that an effective value is obtained that includes only transfer from energies above 1 Mev to lower energies. Viewed from another standpoint, the procedure used for determining the values of the removal

cross sections to give agreement between UNCOL results and experimental results can be considered a procedure for the experimental measurement of removal cross sections. Thus, as discussed in Appendix D, the experimental values of the removal cross sections for a group of neutrons above 1 Mev are 0.093 ± 0.003 cm^{-1} and 0.100 ± 0.005 cm^{-1} for heavy water and uranium, respectively. Additional materials in which measurements would be of particular interest include: water (the results shown in Fig. 4.16 are probably not sufficient to justify assigning a value of 0.098 cm^{-1} as the removal cross section for water), graphite, organic compounds similar to those used as coolants in reactors, thorium, and the oxides of both uranium and thorium. Single rod measurements, preferably with rods at least 0.75 inch in diameter, are well suited for experiments of this type, require less material than even miniature lattices, and should provide results from which values of the effective removal cross sections may be deduced. Single rod measurements are useful for determining values of the effective removal cross sections for both fuel and moderator materials: inside the fuel, the spatial distribution of the fast flux is determined primarily by the properties of the fuel, while far from the fuel rod the distribution is a strong function of the properties of the material surrounding the fuel rod.

It would be worth while to attempt to use the $Rh^{103}(n, n')Rh^{103m}$ reaction and one or more of the reactions with cross sections having relatively high threshold energies in any additional measurements of intracellular distributions of fast neutrons in lattice assemblies. The rhodium reaction has a lower threshold energy than any of the reactions used in the present work. Use of this reaction would provide experimental information about the spatial distribution of the neutrons with energies below 1 Mev as well as some reaction rate ratios more sensitive to the lower portion of the neutron spectrum than those involving only the reactions with higher threshold energies. The use of reactions with cross sections having higher threshold energies, such as the $Mg^{24}(n, p)Na^{24}$ and $Al^{27}(n, \alpha)Na^{24}$ reactions, would extend the experimental results into the higher energy portion of the spectrum. It appears as though the spatial distributions of all the reactions induced by neutrons

with energies greater than 1 Mev are similar, but the results of the experiments with the zinc reaction, discussed in section 4.1.1, introduce some doubt about the distribution of the neutrons with energies greater than about 5 Mev. The use of the rhodium reaction as well as the reaction with higher threshold energies was not possible in the present work, owing to insufficient activation for counting. The increase in power of the MIT Reactor to 5 MW might permit the use of these reactions in future lattices, however, and they could also be used in critical assemblies.

The measurement of axial and radial activity distributions with threshold detectors would provide useful information about the separability of the energy and spatial dependence of neutrons in multiplying assemblies. Measurements of the axial and radial distribution of the thermal flux are usually made when lattice assemblies are studied, and comparable measurements of the fast flux would make possible interesting comparisons. Although the effort made in the present work to measure the radial distribution of the indium reaction was unsuccessful because the count rates were too low, such measurements can probably now be made with reasonable accuracy. The recent increase in power of the MIT Reactor to 5 MW and the use of a specially designed foil holder for larger foils would increase the count rates, probably enough to make the measurements feasible. The use of the nickel reaction, with the foils left in the lattice during the course of a number of other lattice experiments in order to achieve a higher percentage of the saturated activity than is possible with shorter irradiations, might be a better method than the use of the indium reaction. The nickel reaction has the advantage of not requiring the use of cadmium covers; these would produce an unacceptable perturbation for other experiments being done simultaneously in the lattice. Furthermore, the long half-life (71 days) of the Co^{58} formed by the reaction makes it possible to use long counting periods for a large number of foils to improve the statistical accuracy of the results.

An interesting problem for which the UNCOL code seems well suited is that of calculating the spatial distribution of the $D^2(\gamma, n)H^1$ reaction in a heavy water assembly. Some experiments have recently

been done at MIT in which the effects of the spatial distribution of this reaction were studied (S8). The threshold for this reaction in heavy water is 2.2 Mev. Gamma rays originating with energies greater than the threshold energy are likely to be degraded below this amount in a single interaction. Thus, the spatial distribution of the gamma rays capable of producing photoneutrons should be amenable to treatment in the same manner as the uncollided neutron flux. The experimental determination of the correct attenuation coefficients to be used in this type of calculation would probably present difficulties. But there is probably less need for experimental values than in the case of fast neutrons. Gamma-ray attenuation coefficients are well tabulated as functions of energy and it should be possible to compute reasonably accurate values for use in UNCOL.

The use of the UNCOL code with the method described in section 4.3 to correlate experimental values of δ_{28} in lattices of clusters of rods moderated by heavy water would be worth while. Other analytical methods are available for calculating δ_{28}, such as the HEETR code and the MOCA-2 code (D1), but their application to nonuniform arrays, such as clusters, is not straightforward. The large amount of experimental work on heavy water-moderated lattices of clusters of rods at the Savannah River Laboratory has produced many experimental values of δ_{28} with which calculations can be compared. The UNCOL code could be used in its present form for calculations of lattices with clusters of rods but would be relatively inefficient in terms of computer time compared with a modified form more compatible with arrangements of rods in clusters. Such calculations would also require knowledge of the spatial distribution of the fission rates inside the fuel rods. These distributions are different for different rod positions within the clusters and could probably be calculated with THERMØS if experimental results are not available.

The Monte Carlo code, MOCA-2A, (D1) can be used to compute spatial distributions, δ_{28}, and energy spectra, as well as other data. It should, therefore, provide comparisons for all the results reported here. In particular, the use of MOCA-2A might be combined effectively with the use of HEETR for spectral calculations. Since MOCA-2A involves fewer assumptions, it is probably more accurate than HEETR. On the other hand, HEETR calculations can be made in a fraction of the

computer time required for a Monte Carlo code like MOCA-2A. Thus, HEETR might be used to study effects of varying parameters over a wide range; then specific calculations of interest could be made with MOCA-2A.

Appendix A

COMPUTER CODES

A.1 UNCOL, Uncollided Flux Approximation

The UNCOL code computes the spatial distribution of the uncollided fast flux in accordance with the assumptions and the mathematical derivation given in section 3.2. The code was programmed in FORTRAN and compiled and run on an IBM 7094 computer at the MIT Computation Center. The amount of computer time required is obviously a function of the complexity of the problem but is typically about 0.2 minutes per problem. The required input data are described in section A.1.1. A listing of the FORTRAN source deck and a brief description of each of the subroutines is given in section A.1.2, and input and output data for sample problems are given in sections A.1.3 and A.1.4.

A.1.1 Input Data for UNCOL

The input data are given below in the order required. The names of the variables for each FORMAT statement are given, followed by the required FORMAT in parentheses, and then by a brief description of the variables.

ID(I), I = 1, 12 (12A6)

ID(I) is an arbitrary identification statement of 72 spaces or less used to label each set of data. It will be printed out as the first line of the output data.

NF, NM, MORE, IRG, JCON, NMESH1, NMESH2, KAN, KREAD, KGRPH, KASIG, KRTM, INF (16I4)

NF is the number of points for which calculations are to be made inside the fuel rod and must be greater than one. The location of the points is determined by the number of points and the radius of the rod.

The radius is divided into (NF-1) equal increments. The points are then equally spaced from the center of the fuel rod* outward to the surface of the rod.

NM is the number of points to be calculated in the moderator. NM can be any number including zero. The moderator points are located at equal intervals between the surface of the fuel rod and the midpoint between fuel rods (i. e., one-half the lattice spacing).

MORE is a control character for additional data. If MORE is non-zero, the program will re-cycle and read in a new set of input data at the end of the problem. The algebraic sign of MORE is important if JCON is negative, as described below.

IRG is the total number of "rings" of fuel rods to be computed minus two (i. e., if the total is three, IRG = 1). The central rod – the one containing the fuel points – is not counted as a ring. The number of rings determines the size of the lattice when a lattice calculation is being made. In the "read-in" case (see the discussion for JCON), the definition of the rings is arbitrary, and the number of rings to be used is arbitrary. In such cases, the rods can be grouped into rings in any arrangement that is convenient for use of the results (see discussion of NRPR(K)).

JCON is the control character for the macroscopic source distribution. If JCON is zero, a J_o distribution is assumed. The central rod is given the weight unity. The rings of additional rods are weighted with a J_o distribution according to their distance from the central rod, with EXTP used as the extrapolated radius. If JCON is positive, the central rod and all the rings are weighted as unity. If JCON is negative, a "read-in" problem is calculated, and the weighting coefficients for each rod are read in with WTRD(J) as described below. The magnitude of JCON gives the total number of rods for which calculations are to be made. If JCON is negative and MORE is negative, a non-lattice array is assumed. In this case, both the weighting coefficients for each rod, (WTRD(J)), and the distance in inches of each rod, (R(2, K)), from the

*The "center" point is actually slightly offset from the center to avoid mathematical difficulties that accompany zero arguments.

nearest rod,* must be read in as described below. The number of rods per ring, NRPR(K), and the labels, LABEL(K), must also be read in as described below. The magnitude of JCON gives the total number of rods to be calculated.

NMESH1 is the number of mesh points to be used in the numerical integration (using the parabolic formula) of Eqs. 3.14 and 3.15 for the nearest rod. For the calculations reported in the present work, NMESH1 was 121. Results with 241 and 481 for NMESH1 differed by less than 0.5%. NMESH1 must be an odd number.

NMESH2 is the number of mesh points to be used in the numerical integration of Eq. 3.14 for all rods other than the nearest rod. In the present work, the value of NMESH2 was 21. The use of 41 and 81 for NMESH2 affected the results by less than 0.5%. NMESH2 must be an odd number. The amount of computer time required for a given problem is almost a linear function of the magnitudes of NMESH1 and NMESH2.

KAN is the control character for annular fuel. If KAN is negative, all the fuel rods are annular. If KAN is positive, only the nearest rod is annular and all others are solid rods. If KAN is non-zero, the inner diameter in inches must be read in (DAN) as described below. If KAN is non-zero, its magnitude is the number of fuel rod points that are inside the annular fuel section. This must be computed to be consistent with NF, DIAM, and DAN (see discussion of NF).

KREAD is a control character for calculations for a single point that is not located in a fuel region. If KREAD is non-zero, no calculations are made for the nearest rod. This can greatly reduce the amount of running time required if, for example, a series of points corresponding to experimental facilities in the MITR is being calculated. It is still necessary to have NF greater than one. Use NF = 2 and NM = 0 for such cases.

KGRPH is a control character for calculations for a point located in a third region. An example is a MITR graphite vertical facility. If

*In nonuniform arrays, there may not be a central rod or, even if there is one, it may not coincide with the location of interest. In such instances, the distribution of the fast flux is calculated in and around the "nearest" rod.

KGRPH is non-zero, the value of the cross section (in cm^{-1}) of the material comprising the third region (SGRPH) and the effective thickness in inches of the third region (GRAD) must be read in as described below.

KASIG is a control character for calculations for an annular fuel region in which the center region is a void rather than moderator. If KASIG is non-zero, the center region is treated as a void when KAN is non-zero.

KRTM is a control character for calculations for a rod-to-moderator lattice cell traverse rather than a rod-to-rod traverse which is the normal case. If KRTM is non-zero, a rod-to-moderator traverse is calculated.

INF is a control character for the calculation of the correction for the finite axial length of the lattice. If INF is non-zero, only this calculation is made, and the following additional data must be read in as described below: the distance in inches to the edge of the lattice (HGT) and the convergence criterion (CONV).

SIGF, SIGM, SPA, DIAM, EXTP, DAN (6E12.6)

SIGF is the value of the fuel removal cross section in cm^{-1}.

SIGM is the value of the moderator removal cross section in cm^{-1}.

SPA is the value of the lattice spacing in inches. For non-lattice problems, it does not enter into the calculations.

DIAM is the value of the diameter of the fuel rod in inches.

EXTP is the value of the extrapolated radius of the lattice in inches for calculations in which the macroscopic source follows a J_o distribution. If JCON is non-zero, EXTP does not enter into the calculations.

DAN is the value of the inner diameter in inches of the annular fuel region. If KAN is zero, DAN does not enter into the calculations.

C0, C1 (6E12.5)

C0 and C1 are the source distribution coefficients discussed in sections 3.2.3 and 4.1.1.

NOTE: All the input data below are option data. If JCON is zero or positive, and KGRPH and INF are zero, no more data are required.

If JCON is negative:

WTRD(J), J = 1, JNO (6E12.5)

WTRD(J) are the values of the read-in weighting coefficients. JNO is the absolute value of JCON; i. e., the magnitude of JCON controls the number of rods to be calculated.

If JCON and MORE are both negative:

R(2, K), K = 1, JNO (6E12.5)

R(2, K) are the values of the distances in inches from the other rods to the nearest rod.

NRPR(K), K = 1, 8 (16I4)

NRPR(K) is the number of rods in ring K. The rods for which distances from the nearest rod are read in with R(2, K) above can be grouped arbitrarily into as many as eight rings for convenience in use of the output data.

LABEL(K), K = 1, JNO (12A6)

LABEL(K) is a label, using 6 spaces or less, for rod K.

If KGRPH is non-zero:

SGRPH, GRAD (6E12.6)

SGRPH is the value of the removal cross section in cm^{-1} of the material constituting the third region.

GRAD is the effective thickness in inches of the third region, i. e., the effective distance between the point for which calculations are being made and the moderator region.

If INF is non-zero:

HGT, CONV (6E12.6)

HGT is the distance in inches between the point for which calculations are being made and the base of the cylindrical

lattice. For example, if measurements have been made at an axial height of 16 inches, setting HGT equal to 16.0 permits the calculation of the appropriate correction for the finite dimension. More specifically, the correction computed is the total contribution from distances greater than 16 inches.

CONV is the convergence criterion that determines the number of rows that are included for the correction for finite length. In CONV = 10^{-4}, as was used in the present work, rows will be added until the contribution of the additional row drops below 0.01% of the total.

A.1.2 Fortran Listing and Summary of UNCOL

The UNCOL code consists of a MAIN program, three subroutines, and five function subprograms. The subroutines are called QUAD, SUM, and AXIAL, and the function subprograms are called BI0, BI1, BK0, BK1, and BESS. A brief description of each part of the program is given below, followed by a FORTRAN listing of the entire program.

The MAIN program has been labeled UNCFAP. It does the following operations:

1. The input data are read in, printed out, and converted to a consistent set of units (inches to centimeters, etc.).
2. For calculations in lattices, the locations of all the points in the lattice cell are computed, as well as the distances from each point to the rods in the lattice.
3. The values of the removal cross sections are computed by Eq. 3.18.
4. All necessary subroutines are called.
5. For calculations in lattices, the average flux in the fuel and in the moderator are computed and printed out, as well as the ratio of these quantities. The calculation of the average fluxes uses the trapezoidal rule for integration and uses the locations in the lattice cell as mesh points for which calculations are made.

The subroutine QUAD does the following:

1. The fast flux contributed by the nearest rod to points in the moderator is computed by numerically integrating Eq. 3.14. The parabolic rule is used for the integration with the number of mesh points determined by NMESH1. The infinite limit for the dummy variable is replaced by a finite limit, ϵ, which is computed as follows:

$$\epsilon = \frac{16.0}{\Sigma(r) \cdot r} . \tag{A.1}$$

This value of the upper limit ensures that the value of the integrand at the last mesh point is less than 0.01% of the value at the first mesh point for problems encountered in the present work. The integration is extrapolated past the upper limit by assuming that the integrand is linear at that point. Since the integrand approaches zero asymptotically, this extrapolation procedure underestimates any remaining portion of the integral.

2. For each point inside the fuel rod, the fast flux contributed by that part of the fuel rod inside the point is calculated. The procedure is analogous to that of step 1.

3. For each point inside the fuel rod, the fast flux contributed by that part of the fuel rod outside the point is calculated. This calculation involves the use of Eq. 3.15 but is in other respects analogous to step 1.

4. The fast flux contributed by all rods except the nearest rod is computed for each point. This calculation uses Eq. 3.14 but replaces the infinite limit of the dummy variable by ϵ where,

$$\epsilon = \frac{8.0}{\Sigma(r) \cdot r} . \tag{A.2}$$

This reduction in the upper limit is consistent with the previous criterion for Eq. A.1. The function being integrated consists of products of the modified Bessel functions of the

first kind, I, and modified Bessel functions of the second kind, K. The I functions asymptotically approach infinity as the arguments are increased without limit, while the K functions asymptotically approach zero as the arguments are increased without limit. The products of two such functions converge only if the arguments of the K function exceed those of the I function. This criterion is automatically satisfied by Eq. 3.14. The convergence is more rapid for equal values of the dummy variable in the calculations involved in this step as compared with step 1 because the distances from the points to the rods are larger than those of step 1 (i. e., the K arguments are larger) while the rod diameters (and therefore the I arguments) have not increased.

The use of Eq. A.2 involves one constraint. For r sufficiently large, the upper limit as defined by Eq. A.2 becomes less than unity, the lower limit, and the integral is negative and meaningless. Physically, these cases are relatively unimportant because the fast flux contributed by rods at such distances is usually insignificant. Nevertheless, to avoid this complication, the upper limit is never permitted to decrease below a value of two. This constraint, along with the linear extrapolation, ensures adequate treatment of points at distances of more than 100 cm from the rod being calculated.

The subroutine SUM does the following:

1. The appropriate macroscopic weighting coefficients are computed and applied.
2. The final form of the output data is obtained and the results printed out.

The subroutine AXIAL does the following:

1. The magnitude of the fast flux at the location of the experiment that is contributed by the fuel rods arranged as shown in Fig. 4.15 is calculated.

2. The additional input data required for the calculations of step 1 are printed out together with the results.

The function subprograms BI0, BI1, BK0, BK1, and BESS are used to compute the Bessel functions I_0, I_1, K_0, K_1, and J_0, respectively. The polynomial approximations from reference A1 are used.

```
*      LIST8
*      LABEL
*      SYMBOL TABLE
C UNCFAP
       DIMENSION R(15,100),SIG(15,100),PH(30,100),TPH(100),FPH(100)
       DIMENSION SPH(100),WTC(1000),ID(12),QD(1000),RPH(1   ),WTRD(100)
       DIMENSION NRPR(8),NOR(100),LABEL(100)
       COMMON R,SIG,PH,TPH,FPH,SPH,NRPR,RD,NF,NM,NO,NOR,NZ
       COMMON WTRD,EXTP,JCON,SIGA,JJN ,SPA,IRG,CO,C1,NMESH1,NMESH2,RNORM
       COMMON KAN,KREAD,LABEL,RAN,KASIG
     2 FORMAT(12A6)
     3 FORMAT(1H1,12A6)
     4 FORMAT(16I4)
     5 FORMAT(6E12.5)
     6 FORMAT(86H0PTS. FUEL PTS. SIGMAF(CM-1) SIGMAM(CM-1) ROD-SP(IN) ROD
      1 DIAM(IN)  EXTRAP. RADIUS(IN) )
     8 FORMAT( 25H    NMESH1       NMESH2    ,/I8,I11)
     7 FORMAT(I4,I10,2E13.5,E11.5,E13.5,2E13.4)
    10 FORMAT(46H MICROSCOPIC SOURCE DISTRIBUTION COEFFICIENTS )
    11 FORMAT(4H CO= ,E12.6,4H C1= ,E12.6)
    13 FORMAT(I4,E16.5)
    14 FORMAT(90H THIS CALCULATION USES READ IN WEIGHTING COEFFICIENTS FO
      1R MACROSCOPIC SOURCE DISTRIBUTION  )
    22 FORMAT(70H THIS CALCULATION ASSUMES A J0 MACROSCOPIC RADIAL SOURCE
      1 DISTRIBUTION )
    23 FORMAT(76H THIS CALCULATION ASSUMES A CONSTANT MACROSCOPIC RADIAL
      1SOURCE DISTRIBUTION )
    65 FORMAT(31H FUEL VOLUME WEIGHTED AVERAGE= ,F7.3/,36H MODERATOR VOLU
      1ME WEIGHTED AVERAGE= ,F7.3/,8H RATIO= ,F7.3)
   105 FORMAT(43H NEAREST ROD IS ANNULAR, INNER RADIUS(CM)= ,F7.3)
   106 FORMAT(41H ALL RODS ARE ANNULAR, INNER RADIUS(CM)= ,F7.3)
   126 FORMAT(53H THIS CALCULATION IS FOR A ROD TO MODERATOR TRAVERSE  )
C    NMESH1 AND NMESH2 MUST BE ODD
C    IRG IS TOTAL NO. OF RINGS COMPUTED MINUS 2
C    IF JCON=0-J0 DIST. COMPUTED, IF POS.-INFINITE CASE, IF NEG.-READ IN
C         DISTRIBUTION WITH WTRD, JCON IS NO. OF RODS
C    KAN IS CONTROL FOR ANNULAR CASE, IF NEGATIVE ALL RODS ARE ANNULAR,
C         IF POSITIVE ONLY NEAREST ROD IS ANNULAR, MAGNITUDE OF KAN IS
C         THE NUMBER OF FUEL PTS. CONTAINING SOURCES
C    IF JCON AND MORE ARE NEG.,    ·NON-LATTICE ARRAY EXISTS, DISTANCES
C         MUST BE READ IN, NO PTS. OUTSIDE FUEL ARE CALC., -JCON IS NO.
C         OF RODS
C    MORE IS ALSO CONTROL FOR ADDITIONAL RUNS
C    KREAD IS CONTROL FOR DATA PT. OUTSIDE OF ALL FUEL LOCATIONS
C    KGRPH IS CONTROL FOR PRESENCE OF THIRD REGION
C    KASIG IS CONTROL FOR VOID INSIDE ANNULAR ELEMENT
C    KRTM IS CONTROL FOR ROD TO MODERATOR TRAVERSE
C    INF IS CONTROL FOR CALCULATING INFINITE AXIAL CORRECTION
     1 READ INPUT TAPE 4,2,(ID(I),I=1,12)
       WRITE OUTPUT TAPE 2,3,(ID(I),I=1,12)
       READ INPUT TAPE 4,4,NF,NM,MORE,IRG,JCON,NMESH1,NMESH2,KAN,KREAD,
      1KGRPH,KASIG,KRTM,INF
       NO=NF+NM
       READ INPUT TAPE 4,5,SIGF,SIGM,SPA,DIAM,EXTP,DAN
       WRITE OUTPUT TAPE 2,6
```

```
      WRITE OUTPUT TAPE 2,7,NO,NF,SIGF,SIGM,SPA,DIAM,EXTP
      WRITE OUTPUT TAPE 2,8,NMESH1,NMESH2
      READ INPUT TAPE 4,5,CO,C1
      WRITE OUTPUT TAPE 2,10
      WRITE OUTPUT TAPE 2,11,CO,C1
      IF(INF) 209,9,209
  209 CALL AXIAL (SIGF,SIGM,DIAM)
      GO TO 68
    9 RAN=2.54*DAN/2.0
      JJN=0
      IF(JCON) 12,16,18
   12 JNO=-JCON
      JJN=JNO*MORE
      READ INPUT TAPE 4,5,(WTRD(J),J=1,JNO)
      WRITE OUTPUT TAPE 2,14
      GO TO 19
   16 WRITE OUTPUT TAPE 2,22
      GO TO 19
   18 WRITE OUTPUT TAPE 2,23
   19 SP=SPA*2.54
      RD=2.54*DIAM/2.0
      DRF=RD/FLOATF(NF-1)
      DO 20 N=2,NF
   20 R(1,N)=DRF*FLOATF(N-1)
      R(1,1)=R(1,2)/10.0
      IF(JJN) 27,21,21
   27 READ INPUT TAPE 4,5,(R(2,K),K=1,JNO)
      READ INPUT TAPE 4,4,(NRPR(K),K=1,8)
C    NRPR(K) IS NO. OF RODS IN RING K, MAX. NO. OF RINGS IS 8
      READ INPUT TAPE 4,2,(LABEL(K),K=1,JNO)
      DO 29 K=1,JNO
   29 R(2,K)=R(2,K)*2.54
      GO TO 32
   21 IF(NM) 32,32,122
  122 DRM=((SP/2.0)-RD)/FLOATF(NM)
      NL=NF+1
      DO 25 N=NL,NO
   25 R(1,N)=RD+DRM*FLOATF(N-NF)
      A=SP**2
      IF(KRTM) 26,30,26
   26 WRITE OUTPUT TAPE 2,126
      DO 28 N=1,NO
      B=R(1,N)**2
      ARG=A+B-1.732*SP*R(1,N)
      R(2,N)=SQRTF(ARG)
      R(5,N)=R(2,N)
      ARG=A+B
      R(3,N)=SQRTF(ARG)
      ARG=A+B+1.732*SP*R(1,N)
      R(4,N)=SQRTF(ARG)
      ARG=B+3.0*A-1.732*SP*R(1,N)
      R(6,N)=SQRTF(ARG)
      ARG=ARG+3.464*SP*R(1,N)
```

```
      R(7,N)=SQRTF(ARG)
      ARG=B+4.0*A+3.464*SP*R(1,N)
      R(8,N)=SQRTF(ARG)
      ARG=ARG-6.928*SP*R(1,N)
      R(9,N)=SQRTF(ARG)
      ARG=B+4.0*A
      R(10,N)=SQRTF(ARG)
      R(11,N)=1.732*SP-R(1,N)
   28 R(12,N)=1.732*SP+R(1,N)
      GO TO 32
   30 DO 31 N=1,NO
      R(2,N)=SP-R(1,N)
      B=R(1,N)**2
      ARG=A-R(1,N)*SP+B
      R(3,N)=SQRTF(ARG)
      ARG=A+B+R(1,N)*SP
      R(4,N)=SQRTF(ARG)
      R(5,N)=SP+R(1,N)
      ARG=3.0*A+B-3.0*R(1,N)*SP
      R(6,N)=SQRTF(ARG)
      ARG=B+3.0*A
      R(7,N)=SQRTF(ARG)
      ARG=3.0*A+B+1.7320508*R(1,N)*SP
      R(8,N)=SQRTF(ARG)
      ARG=(SP-R(1,N))**2+3.0*A
      R(9,N)=SQRTF(ARG)
      ARG=3.0*A+(SP+R(1,N))**2
      R(10,N)=SQRTF(ARG)
      R(11,N)=2.0*SP-R(1,N)
   31 R(12,N)=2.0*SP+R(1,N)
   32 IF(KAN) 33,37,34
   33 NZ=NF+KAN+1
      WRITE OUTPUT TAPE 2,106,RAN
      GO TO 35
   34 NZ=NF-KAN+1
      WRITE OUTPUT TAPE 2,105,RAN
   35 FR=(RD-RAN)/RD
      SGF=SIGF*FR+SIGM*(1.0-FR)
      DO 36 N=1,NF
   36 SIG(1,N)=SGF
      GO TO 43
   37 DO 42 N=1,NF
   42 SIG(1,N)=SIGF
      SGF=SIGF
   43 IF(JJN) 90,41,41
   90 IF(KGRPH) 190,91,190
  190 READ INPUT TAPE 4,5,SGRPH,GRAD
      GRD=GRAD*2.54
      WRITE OUTPUT TAPE 2,199,SGRPH,GRAD
  199 FORMAT(49H THIS CALCULATION IS FOR A PT. IN A THIRD REGION  /,8X,
     18H SIGMA= ,E12.6,13H DIST.(IN.)= ,E12.6)
      DO 192 K=1,JNO
  192 SIG(2,K)=(RD*SGF+GRD*SGRPH+(R(2,K)-(RD+GRD))*SIGM)/R(2,K)
```

```
      GO TO 59
   91 DO 92 K=1,JNO
   92 SIG(2,K)=(RD*SGF+(R(2,K)-RD)*SIGM)/R(2,K)
      GO TO 59
   41 IF(NM) 48,48,141
  141 NN=NF+1
      DO 44 N=NN,NO
   44 SIG(1,N)=(RD*SIGF+(R(1,N)-RD)*SIGM)/R(1,N)
   48 DO 50 M=2,12
      DO 50 N=1,NO
   50 SIG(M,N)=(RD*SIGF+(R(M,N)-RD)*SIGM)/R(M,N)
      M=13
      DO 55 N=1,IRG
      LX=(N+2)*3
      R(13,N)=SP*FLOATF(LX)/3.14159
   55 SIG(M,N)=(RD*SIGF+(R(M,N)-RD)*SIGM)/R(M,N)
   59 CALL QUAD
      CALL SUM
      IF(NM) 68,68,159
  159 IF(KAN) 68,60,68
   60 IF(JJN)68,61,61
   61 QD(1)=R(1,2)/4.0
      DO 62 N=2,NO
   62 QD(N)=R(1,N)
      AFN=(TPH(1)*QD(1)**2 +TPH(NF)*QD(NF)**2)/2.0
      AFD=(QD(1)**2+QD(NF)**2)/2.0
      AMN=(TPH(NF+1)*QD(NF+1)**2+TPH(NO)*QD(NO)**2)/2.0
      AMD=(QD(NF+1)**2+QD(NO)**2)/2.0
      N1=NF-1
      N2=NF+2
      DO 63 N=2,N1
      AFN=AFN+TPH(N)*QD(N)**2
   63 AFD=AFD+QD(N)**2
      AF=RNORM*AFN/AFD
      NN=NO-1
      DO 64 N=N2,NN
      AMN=AMN+TPH(N)*QD(N)**2
   64 AMD=AMD+QD(N)**2
      AM=RNORM*AMN/AMD
      FAF=AF/AM
      WRITE OUTPUT TAPE 2,65,AF,AM,FAF
   68 IF(MORE) 1,70,1
   70 CALL EXIT
      END
*      LIST8
*     LABEL
*     SYMBOL TABLE
      SUBROUTINE QUAD
      DIMENSION R(15,100),SIG(15,100),PH(30,100),TPH(100),FPH(100)
      DIMENSION SPH(100),WTC(1000),ID(12),QD(1000),RPH(1   ),WTRD(100)
      DIMENSION NRPR(8),NOR(100),LABEL(100)
      COMMON R,SIG,PH,TPH,FPH,SPH,NRPR,RD,NF,NM,NO,NOR,NZ
      COMMON WTRD,EXTP,JCON,SIGA,JJN ,SPA,IRG,CO,C1,NMESH1,NMESH2,RNORM
```

```
      COMMON KAN,KREAD,LABEL,RAN,KASIG
      WTC(1)=1.0
      WTC(NMESH1)=1.0
      KU=NMESH1-1
      DO 10 K=2,KU,2
   10 WTC(K)=4.0
      KU=KU-1
      DO 12 K=3,KU,2
   12 WTC(K)=2.0
      IF(KREAD) 15,11,15
   11 IF(JJN) 55,14,14
   15 M=1
      DO 16 N=1,NF
   16 PH(M,N)=0.0
      GO TO 103
   14 IF(NM) 214,55,214
C  NEAREST ROD MODERATOR PTS. CALCULATED
  214 FA=C1*RD**3
      FB=C0*RD
      FC=2.0*C1*RD**2
      FD=4.0*C1*RD
      M=1
      NL=NF+1
      DO 17 N=NL,NO
   17 PH(M,N)=0.0
      VR=RD
      KCON=0
   18 DO 50 N=NL,NO
      U=SIG(M,N)*R(M,N)
      V=SIG(M,N)*VR
      EP=16.0/U
      YD=(EP-1.0)/FLOATF(NMESH1-1)
      DO 25 K=1,NMESH1
      Y=1.0+YD*FLOATF(K-1)
      A=U*Y
      B=V*Y
      C=SIG(M,N)*Y
      QD(K)=BK0(A)*(BI1(B)*(FA+FB-FD/(C**2))+FC*BI0(B)/C)/C
   25 PH(M,N)=PH(M,N)+WTC(K)*QD(K)
      PH(M,N)=PH(M,N)*4.0*YD/3.0
      DH=QD(K-1)-QD(K)
   50 PH(M,N)=PH(M,N)+0.5*(QD(K)**2)*YD/DH
      IF(KAN) 51,55,51
   51 KCON=KCON+1
      GO TO (52,55),KCON
   52 VR=RAN
      FA=-C1*RAN**3
      FB=-C0*RAN
      FC=-2.0*C1*RAN**2
      FD=-4.0*C1*RAN
      GO TO 18
C  FUEL PTS.- CONTRIBUTION FROM INSIDE
   55 NW=1
```

```
      IF(KAN) 57,60,57
   57 GA=C1*RAN**3
      GB=CO*RAN
      GC=2.0*C1*RAN**2
      GD=4.0*C1*RAN
      NW=NZ
   60 M=1
      DO 61 N=1,NF
   61 PH(M,N)=0.0
      DO 100 N=NW,NF
      UV=SIG(M,N)*R(M,N)
      EP=16.0/UV
      YD=(EP-1.0)/FLOATF(NMESH1-1)
      FA=C1*R(M,N)**3
      FB=CO*R(M,N)
      FC=2.0*C1*R(M,N)**2
      FD=4.0*C1*R(M,N)
      DO 75 K=1,NMESH1
      Y=1.0+YD*FLOATF(K-1)
      AB=UV*Y
   63 C=SIG(M,N)*Y
      QD(K)=BK0(AB)*(BI1(AB)*(FA+FB-FD/(C**2))+FC*BI0(AB)/C)/C
      PH(M,N)=PH(M,N)+WTC(K)*QD(K)
      IF(KAN) 65,75,65
   65 BB=SIG(M,N)*RAN*Y
      QD(K+2)=BK0(AB)*(BI1(BB)*(GA+GB-GD/(C**2))+GC*BI0(BB)/C)/C
      PH(M,N)=PH(M,N)-WTC(K)*QD(K+2)
   75 CONTINUE
  100 PH(M,N)=PH(M,N)*4.0*YD/3.0
C  FUEL PTS.-CONTRIBUTION FROM OUTSIDE, IN ROD
      FD=4.0*C1*RD
      FE=CO*RD
      FF=C1*RD**3
      FG=2.0*C1*RD**2
      M=1
      NL=NF-1
      DO 150 N=1,NL
      REF=R(M,N)
      IF(KAN) 101,202,101
  101 REF=MAX1F(R(M,N),RAN)
      IF(KASIG) 201,202,201
  201 W=SIG(M,N)*REF
      GO TO 102
  202 W=SIG(M,N)*R(M,N)
  102 FA=CO*REF
      FB=4.0*C1*REF
      FC=C1*REF**3
      FH=2.0*C1*REF**2
      U=SIG(M,N)*REF
      V=SIG(M,N)*RD
      EP=16.0/V
      YD=(EP-1.0)/FLOATF(NMESH1-1)
      QQ=0
```

```
      DO 125 K=1,NMESH1
      Y=1.0+YD*FLOATF(K-1)
      A=U*Y
      B=V*Y
      C=SIG(M,N)*Y
      D=W*Y
      QD(K)=BI0(D)*(BK1(A)*(FA+FB/(C**2)+FC)+BK1(B)*(-FD/(C**2)-FE-FF)-
     1BK0(B)*FG/C+BK0(A)*FH/C)/C
  125 QQ=QQ+WTC(K)*QD(K)
      QQ=QQ*4.0*YD/3.0
      DH=QD(K-1)-QD(K)
  150 PH(M,N)=PH(M,N)+QQ+0.5*(QD(K)**2)*YD/DH
      KCON=0
      IF(JJN) 103,104,104
  103 ML=2
      MU=2
      NL=2
      NU=-JCON
      II=2
      GO TO 120
C  ALL EXCEPT NEAREST ROD CALCULATED
  104 WTC(NMESH2)=1.0
      II=1
  105 GO TO (110,115,170),II
  110 ML=2
      MU=12
      NL=1
      NU=NO
      GO TO 120
  115 ML=13
      MU=13
      NL=1
      NU=IRG
  120 DO 121 M=ML,MU
      DO 121 N=NL,NU
  121 PH(M,N)=0.0
      FA=C1*RD**3
      FB=C0*RD
      FC=2.0*C1*RD**2
      FD=4.0*C1*RD
      VR=RD
  122 DO 160 M=ML,MU
      DO 160 N=NL,NU
      U=SIG(M,N)*R(M,N)
      V=SIG(M,N)*VR
      EP=8.0/U
      GO TO 310
  305 EP=EP*2.0
  310 IF(EP-2.0) 305,305,315
  315 YD=(EP-1.0)/FLOATF(NMESH2-1)
      DO 135 K=1,NMESH2
      Y=1.0+YD*FLOATF(K-1)
      A=U*Y
```

```
      B=V*Y
      C=SGI*Y
      C=SIG(M,N)*Y
      QD(K)=BK0(A)*(BI1(B)*(FA+FB-FD/(C**2))+FC*BI0(B)/C)/C
  135 PH(M,N)=PH(M,N)+WTC(K)*QD(K)
      PH(M,N)=PH(M,N)*4.0*YD/3.0
      DH=QD(K-1)-QD(K)
  160 PH(M,N)=PH(M,N)+0.5*(QD(K)**2)*YD/DH
      IF(KAN) 162,168,168
  162 KCON=KCON+1
      GO TO (164,168,164,168,164,168,164,168),KCON
  164 VR=RAN
      FA=-C1*RAN**3
      FB=-C0*RAN
      FC=-2.0*C1*RAN**2
      FD=-4.0*C1*RAN
      GO TO 122
  168 II=II+1
      GO TO 105
  170 RETURN
      END
*     LIST8
*     LABEL
*     SYMBOL TABLE
      SUBROUTINE SUM
      DIMENSION R(15,100),SIG(15,100),PH(30,100),TPH(100),FPH(100)
      DIMENSION SPH(100),WTC(1000),ID(12),QD(1000),RPH(1   ),WTRD(100)
      DIMENSION NRPR(8),NOR(100),LABEL(100)
      COMMON R,SIG,PH,TPH,FPH,SPH,NRPR,RD,NF,NM,NO,NOR,NZ
      COMMON WTRD,EXTP,JCON,SIGA,JJN ,SPA,IRG,C0,C1,NMESH1,NMESH2,RNORM
      COMMON KAN,KREAD,LABEL,RAN
      DO 4 M=1,12
    4 WTC(M)=1.0
      WTC(3)=2.0
      WTC(4)=2.0
      DO 8 M=6,10
    8 WTC(M)=2.0
      QD(1)=18.0
      DO 9 M=2,IRG
    9 QD(M)=QD(M-1)+6.0
      DO 10 N=1,NO
      TPH(N)=0.0
      FPH(N)=0.0
   10 SPH(N)=0.0
      DO 11 N=1,IRG
   11 RPH(N)=0.0
      IF(JCON) 150,160,170
  150 IF(JJN   ) 300,300,151
  151 WTC(1)=WTC(1)*WTRD(1)
      WTC(2)=WTC(2)*WTRD(2)
      WTC(3)=WTC(3)*(WTRD(3)+WTRD(7))/2.0
      WTC(4)=WTC(4)*(WTRD(4)+WTRD(6))/2.0
      WTC(5)=WTC(5)*WTRD(5)
```

```
      WTC(6)=WTC(6)*(WTRD(9)+WTRD(19))/2.0
      WTC(7)=WTC(7)*(WTRD(11)+WTRD(17))/2.0
      WTC(8)=WTC(8)*(WTRD(13)+WTRD(15))/2.0
      WTC(9)=WTC(9)*(WTRD(10)+WTRD(18))/2.0
      WTC(10)=WTC(10)*(WTRD(12)+WTRD(16))/2.0
      WTC(11)=WTC(11)*WTRD(8)
      WTC(12)=WTC(12)*WTRD(14)
      DO 152 K=1,IRG
      KW=K+19
  152 QD(K)=QD(K)*WTRD(KW)
      GO TO 170
  300 JNO=-JCON
      NRS=1
      DO 400 N=1,NO
      PH(1,N)=PH(1,N)*WTRD(1)
  400 TPH(N)=PH(1,N)
      KU=NRPR(1)+1
      DO 301 K=2,KU
      DO 401 N=1,NO
      FPH(N)=FPH(N)+PH(2,K)*WTRD(K)
  401 TPH(N)=TPH(N)+PH(2,K)*WTRD(K)
  301 NOR(K)=1
      IF(NRPR(2)) 350,350,302
  302 NRS=2
      KL=KU+1
      KU=KU+NRPR(2)
      DO 303 K=KL,KU
      DO 402 N=1,NO
      SPH(N)=SPH(N)+PH(2,K)*WTRD(K)
  402 TPH(N)=TPH(N)+PH(2,K)*WTRD(K)
  303 NOR(K)=2
      IF(NRPR(3)) 350,350,304
  304 DO 306 NN=1,IRG
      NRS=NRS+1
      KL=KU+1
      KU=KU+NRPR(NRS)
      DO 306 K=KL,KU
      RPH(NN)=RPH(NN)+PH(2,K)*WTRD(K)
  306 NOR(K)=NRS
  350 DO 355 K=1,IRG
      DO 355 N=1,NO
  355 TPH(N)=TPH(N)+RPH(K)
      WRITE OUTPUT TAPE 2,390
  390 FORMAT (38H DIMENSIONS AND WEIGHTING COEFFICIENTS ,/ 51H ROD DIST.
     1(CM) DIST.(IN) RING WEIGHT.COEFF.  LABEL     )
      DO 352 K=1,JNO
  352 QD(K)=R(2,K)/2.54
      DO 354 K=1,JNO
  354 WRITE OUTPUT TAPE 2,391,K,R(2,K),QD(K),NOR(K),WTRD(K),LABEL(K)
  391 FORMAT( 1X,I2,F10.2,F10.2,I5,F11.4,7X,A6)
      GO TO 440
  160 ARG=2.405*SPA/EXTP
      WTRD(1)=BESS(ARG,1)
```

```
    DO 163 M=2,5
163 WTC(M)=WTC(M)*WTRD(1)
    ARG=2.405*2.0*SPA*3.0/(3.14159*EXTP)
    DO 164 M=6,12
    WTRD(M)=BESS(ARG,1)
164 WTC(M)=WTC(M)*WTRD(M)
    DO 165 N=1,IRG
    ARG=2.405*FLOATF(N+2)*3.0*SPA/(3.14159*EXTP)
    WTRD(N)=BESS(ARG,1)
165 QD(N)=QD(N)*WTRD(N)
170 DO 12 N=1,NO
    DO 12 M=1,12
 12 TPH(N)=TPH(N)+PH(M,N)*WTC(M)
    DO 20 N=1,NO
    DO 20 M=2,5
 20 FPH(N)=FPH(N)+PH(M,N)*WTC(M)
    DO 28 N=1,NO
    DO 28 M=6,12
 28 SPH(N)=SPH(N)+PH(M,N)*WTC(M)
    DO 30 N=1,IRG
 30 RPH(N)=RPH(N)+PH(13,N )*QD(N)
    DO 31 N=1,NO
    DO 31 I=1,IRG
 31 TPH(N)=TPH(N)+RPH(I)
440 WRITE OUTPUT TAPE 2,60
 60 FORMAT(19H UN-NORMALIZED FLUX )
    WRITE OUTPUT TAPE 2,44
    DO 65 N=1,NO
    DN=R(1,N)/2.54
 65 WRITE OUTPUT TAPE 2,70,N,R(1,N),DN,TPH(N),PH(1,N),FPH(N),SPH(N)
 70 FORMAT(I3,F7.3,F10.4,4E12.5)
    WRITE OUTPUT TAPE 2,80
 80 FORMAT(17H ADDITIONAL RINGS )
    WRITE OUTPUT TAPE 2,82
 82 FORMAT(5X2H 1,10X2H 2,10X2H 3,10X2H 4,10X2H 5,10X2H 6,10X2H 7,
   110X2H 8,10X2H 9,9X3H 10)
    IF(IRG-10) 83,83,85
 83 WRITE OUTPUT TAPE 2,84,(RPH(N),N=1,IRG)
    GO TO 98
 84 FORMAT(10E12.5)
 85 WRITE OUTPUT TAPE 2,84,(RPH(N),N=1,10)
    WRITE OUTPUT TAPE 2,86
 86 FORMAT(4X3H 11,9X3H 12,9X3H 13,9X3H 14,9X3H 15,9X3H 16,9X3H 17,9X3
   1H 18,9X3H 19,9X3H 20)
    WRITE OUTPUT TAPE 2,84,(RPH(N),N=11,IRG)
 98 DO 16 N=1,IRG
 16 RPH(N)=RPH(N)/TPH(NO)
    DO 24 N=1,NO
 24 FPH(N)=FPH(N)/TPH(NO)
    DO 32 N=1,NO
 32 SPH(N)=SPH(N)/TPH(NO)
    DO 36 N=1,NO
 36 PH(1,N)=PH(1,N)/TPH(NO)
```

```
      RNORM=TPH(NO)
      DO 90 N=1,NO
   90 TPH(N)=TPH(N)/TPH(NO)
      WRITE OUTPUT TAPE 2,40
   40 FORMAT(38H RELATIVE FLUX NORMALIZED TO CELL EDGE )
      WRITE OUTPUT TAPE 2,44
   44 FORMAT(68H PT. DIST.(CM) DIST.(IN)    TOTAL NEAREST ROD FIRST RING
     1 SECOND RING )
      DO 50 N=1,NO
      DN=R(1,N)/2.54
      WRITE OUTPUT TAPE 2,48,N,R(1,N),DN,TPH(N),PH(1,N),FPH(N),SPH(N)
   48 FORMAT(I3,F7.3,F10.4,F12.4,3E12.5)
   50 CONTINUE
      WRITE OUTPUT TAPE  2,80
      WRITE OUTPUT TAPE 2,82
      IF(IRG-10) 101,101,120
  101 WRITE OUTPUT TAPE 2,84,(RPH(N),N=1,IRG)
      GO TO 200
  120 WRITE OUTPUT TAPE 2,84,(RPH(N),N=1,10)
      WRITE OUTPUT TAPE 2,86
      WRITE OUTPUT TAPE 2,84,(RPH(N),N=11,IRG)
  200 RETURN
      END
*     LIST8
*     LABEL
*     SYMBOL TABLE
      SUBROUTINE AXIAL (SIGF,SIGM,DIAM)
      DIMENSION R(15,100),SIG(15,100),PH(30,100),TPH(100),FPH(100)
      DIMENSION SPH(100),WTC(1000),ID(12),QD(1000),RPH(1  ),WTRD(100)
      DIMENSION NRPR(8),NOR(100),LABEL(100)
      COMMON R,SIG,PH,TPH,FPH,SPH,NRPR,RD,NF,NM,NO,NOR,NZ
      COMMON WTRD,EXTP,JCON,SIGA,JJN ,SPA,IRG,CO,C1,NMESH1,NMESH2,RNORM
      COMMON KAN,KREAD,LABEL,RAN,KASIG
    2 FORMAT (6E12.6)
      READ INPUT TAPE 4,2,HGT,CONV,GAM
      WRITE OUTPUT TAPE 2,5,HGT,CONV,GAM
    5 FORMAT(13H HEI)HT(IN) = ,F5.2,7H CONV = ,E12.6,14H GAMMA(CM-1) =
     1 ,E12.6)
      WTC(1)=1.0
      WTC(NMESH2)=1.0
      KU=NMESH2-1
      DO 3 K=2,KU,2
    3 WTC(K)=4.0
      KU=KU-1
      DO 4 K=3,KU,2
    4 WTC(K)=2.0
      SP=SPA*2.54
      RD=2.54*DIAM/2.0
      FA=C1*RD**3
      FB=CO*RD
      FC=2.0*C1*RD**2
      FD=4.0*C1*RD
      LR=EXTP/SPA
```

```
      DO 8 J=1,LR
      ARG=SPA*2.405*FLOATF(J)/EXTP
    8 WTRD(J)=BESS(ARG,1)
      RNORM=0.0
      VR=RD
      AV=HGT*2.54
      RW=SP*0.86603
   12 FLX=0.0
      DO 137 J=1,LR
      AH=SP*FLOATF(J)
   20 ARG=AV**2+AH**2
      RA=SQRTF(ARG)
      SGI=(RD*SIGF+(RA-RD)*SIGM)/RA
      U=SGI*RA
      V=SGI*VR
      EP=8.0/U
      GO TO 28
   26 EP=EP*2.0
   28 IF(EP-2.0) 26,26,29
   29 YD=(EP-1.0)/FLOATF(NMESH2-1)
      FX=0.0
      DO 135 K=1,NMESH2
      Y=1.0+YD*FLOATF(K-1)
      A=U*Y
      B=V*Y
      C=SGI*Y
      QD(K)=BK0(A)*(BI1(B)*(FA+FB-FD/(C**2))+FC*BI0(B)/C)/C
  135 FX=FX+WTC(K)*QD(K)
      FX=FX*4.0*YD/3.0
      DH=QD(K-1)-QD(K)
      FX=FX+0.5*(QD(K)**2)*YD/DH
  137 FLX=FLX+FX*WTRD(J)
      RNORM=RNORM+FLX
  200 AVIN=AV/2.54
      WRITE OUTPUT TAPE 2,211,   AVIN
  211 FORMAT (12H DIST.(IN) = ,F8.2)
      ARG=AV*GAM
      FLX=FLX*2.0
      FLXP=FLX*EXPF(ARG)
      FLXM=FLX*EXPF(-ARG)
      WRITE OUTPUT TAPE 2,212,FLX,FLXP,FLXM
  212 FORMAT (18H LINEAR CONTRIB. = ,E12.6,21H WEIGHTED CONTRIB.S = ,2E1
     12.6)
      AV=AV+RW
      IF(CONV-FLX/RNORM) 12,12,303
  303 RETURN
      END
*     LIST8
*     LABEL
*     SYMBOL TABLE
      FUNCTION BESS(ARG,J)
      GO TO (1,1),J
    1 IF(ARG-3.0)7,7,6
```

```
C       J0 FOR ARG LESS THAN 3
      7 T=ARG/3.0
        BESS=1.0-2.2499997*(T**2.0)+1.2656208*T**4.0-.3163866*T**6.0+.0444
       1479*T**8.0-.0039444*T**10.0+.0002100*T**12.0
        RETURN
      6 T=3.0/ARG
        PRINT 11
     11 FORMAT(26H J0 ARG GREATER THAN 3.0    )
        F0=.79788456-.00000077*T-.00552740*T**2.0-.00009512*T**3.0+.001372
       137*T**4.0-.00072805*T**5.0+.00014476*T**6.0
        THETA0=ARG-.78539816-.04166397*T-.00003954*T**2.0+.00262573*T**3.0
       1-.00054125*T**4.0-.00029333*T**5.0+.00013558*T**6.
C   J0FOR ARG GREATER THAN 3
      8 BESS=F0*COSF(THETA0)/SQRTF(ARG)
        RETURN
        END
```

A.1.3 Sample Lattice Problem Treated with UNCOL

```
*      DATA
    10/10/65, 0.75-2.5
0005001000100005000002410021
0.          0.093       2.5         0.75        19.32
1.          0.2782
   10/10/65, 0.75-2.5

PTS. FUEL PTS. SIGMAF(CM-1) SIGMAM(CM-1) ROD-SP(IN) ROD DIAM(IN)  EXTRAP. RADIUS(IN)
 15         5  1.0000E-01   .93000E-01 .25000E 01   .75000E 00    .1932E 02
   NMESH1      NMESH2
    241          21
MICROSCOPIC SOURCE DISTRIBUTION COEFFICIENTS
CO= .10000E 01 C1= .27820CE CO
THIS CALCULATION ASSUMES A JO MACROSCOPIC RADIAL SOURCE DISTRIBUTION
UN-NORMALIZED FLUX
PT. DIST.(CM) DIST.(IN)    TOTAL NEAREST ROD FIRST RING SECOND RING
 1    .024      .0094   .81109E 02  .54983E 02  .13876E C2  .72265E 01
 2    .238      .0937   .80882E 02  .54718E 02  .13889E C2  .72515E 01
 3    .476      .1875   .79178E 02  .52943E 02  .13928E C2  .72833E 01
 4    .714      .2812   .76068E 02  .49732E 02  .13993E C2  .73193E 01
 5    .952      .3750   .68296E 02  .41827E 02  .14086E C2  .73599E 01
 6   1.175      .4625   .56055E 02  .29432E 02  .14198E C2  .74021E 01
 7   1.397      .5500   .49782E 02  .22973E 02  .14336E C2  .74487E 01
 8   1.619      .6375   .45787E 02  .18761E 02  .14502E C2  .75000E 01
 9   1.841      .7250   .43C30E 02  .15750E 02  .14700E C2  .75562E 01
10   2.064      .8125   .41C53E 02  .13480E 02  .14932E C2  .76175E 01
11   2.286      .9000   .39619E 02  .11705E 02  .15205E C2  .76842E 01
12   2.508      .9875   .38587E 02  .10281E 02  .15526E C2  .77566E 01
13   2.730     1.0750   .37875E 02  .91143E 01  .15903E C2  .78349E 01
14   2.953     1.1625   .37434E 02  .81423E 01  .16349E C2  .79193E 01
15   3.175     1.2500   .37237E 02  .73215E 01  .16881E C2  .80102E 01
ADDITIONAL RINGS
      1            2            3            4            5            6            7
 .29880E 01  .12850E C1  .51688E 00  .18415E CO  .49841E-01
RELATIVE FLUX NORMALIZED TO CELL EDGE
PT. DIST.(CM) DIST.(IN)    TOTAL NEAREST ROD FIRST RING SECOND RING
 1    .024      .0094      2.1782  .14766E 01  .37264E CO  .19407E 00
 2    .238      .0937      2.1721  .14695E C1  .37299E CO  .19474E 00
 3    .476      .1875      2.1263  .14218E 01  .37403E CO  .19559E 00
 4    .714      .2812      2.0428  .13356E 01  .37579E CO  .19656E 00
 5    .952      .3750      1.8341  .11233E 01  .37827E CO  .19765E 00
 6   1.175      .4625      1.5054  .79040E 00  .38128E CO  .19878E 00
 7   1.397      .5500      1.3369  .61696E 00  .38499E CO  .20004E 00
 8   1.619      .6375      1.2296  .50383E 00  .38946E CO  .20141E 00
 9   1.841      .7250      1.1556  .42296E 00  .39477E CO  .20292E 00
10   2.064      .8125      1.1025  .36200E 00  .40102E CO  .20457E 00
11   2.286      .9000      1.0640  .31435E 00  .40834E CO  .20636E 00
12   2.508      .9875      1.0363  .27610E 00  .41694E CO  .20831E 00
13   2.730     1.0750      1.0172  .24477E 00  .42707E CO  .21041E 00
14   2.953     1.1625      1.0053  .21866E CO  .43905E CO  .21268E 00
15   3.175     1.2500      1.0000  .19662E 00  .45335E CO  .21512E 00
ADDITIONAL RINGS
      1            2            3            4            5            6            7
 .80242E-01  .34508E-01  .13881E-01  .49453E-02  .13385E-02
FUEL VOLUME WEIGHTED AVERAGE=  74.036
MODERATOR VOLUME WEIGHTED AVERAGE=  39.936
RATIO=   1.854
```

A.1.4 Sample MITR Problem Treated with UNCOL

```
*      DATA
 10/10/65  MITR POS. 1, CORE CONFIGURATION 62
000400000-1000010-30012100210002          0010
0.1           0.093         6.375         3.16          24.0          1.935
1.            0.015
0.12496       0.12524       0.12097       0.11584       0.11725       0.11910
0.12401       0.06286       0.07032       0.06697       0.08669       0.0726
0.06335       0.08359       0.08987       0.06510       0.08910       0.07398
0.08185       0.            0.            0.04221       0.            0.
0.            0.03755       0.            0.04359       0.03284       0.03072
0.            6.375         6.375         6.375         6.375         6.375
6.375         13.25         13.25         13.25         13.25         13.25
13.25         13.25         13.25         13.25         13.25         13.25
13.25         20.935        20.935        20.935        20.935        20.935
20.935        20.935        20.935        20.935        20.935        20.935
000600120011
POS  1POS  2POS  3POS  4POS  5POS  6POS  7POS  8POS  9POS 10POS 11POS 12
POS 13POS 14POS 15POS 16POS 17POS 18POS 19POS 20POS 21POS 22POS 23POS 24
POS 25POS 26POS 27POS 28POS 29POS 30
```

```
 10/10/65  MITR POS. 1, CORE CONFIGURATION 62

PTS. FUEL PTS. SIGMAF(CM-1) SIGMAM(CM-1) ROD-SP(IN) ROD DIAM(IN)  EXTRAP. RADIUS(IN)
  4          4  1.00000E-01   .93000E-01 .63750E 01   .31600E 01    .2400E 02
   NMESH1       NMESH2
    121          21
MICROSCOPIC SOURCE DISTRIBUTION COEFFICIENTS
CO= .100000E 01 C1= .150000E-01
THIS CALCULATION USES READ IN WEIGHTING COEFFICIENTS FOR MACROSCOPIC SOURCE DISTRIBUTION
NEAREST ROD IS ANNULAR, INNER RADIUS(CM)=   2.457
DIMENSIONS AND WEIGHTING COEFFICIENTS
ROD DIST.(CM) DIST.(IN) RING WEIGHT.COEFF.  LABEL
 1       0.        0.      0      .1250       POS  1
 2      16.19      6.37    1      .1252       POS  2
 3      16.19      6.37    1      .1210       POS  3
 4      16.19      6.37    1      .1158       POS  4
 5      16.19      6.37    1      .1172       POS  5
 6      16.19      6.37    1      .1191       POS  6
 7      16.19      6.37    1      .1240       POS  7
 8      33.65     13.25    2      .0629       POS  8
 9      33.65     13.25    2      .0703       POS  9
10      33.65     13.25    2      .0670       POS 10
11      33.65     13.25    2      .0867       POS 11
12      33.65     13.25    2      .0726       POS 12
13      33.65     13.25    2      .0633       POS 13
14      33.65     13.25    2      .0836       POS 14
15      33.65     13.25    2      .0899       POS 15
16      33.65     13.25    2      .0651       POS 16
17      33.65     13.25    2      .0891       POS 17
18      33.65     13.25    2      .0740       POS 18
19      33.65     13.25    2      .0818       POS 19
20      53.17     20.93    3     0.           POS 20
21      53.17     20.93    3     0.           POS 21
22      53.17     20.93    3      .0422       POS 22
23      53.17     20.93    3     0.           POS 23
24      53.17     20.93    3     0.           POS 24
25      53.17     20.93    3     0.           POS 25
26      53.17     20.93    3      .0375       POS 26
27      53.17     20.93    3     0.           POS 27
28      53.17     20.93    3      .0436       POS 28
29      53.17     20.93    3      .0328       POS 29
30      53.17     20.93    3      .0307       POS 30
UN-NORMALIZED FLUX
PT. DIST.(CM) DIST.(IN)    TOTAL NEAREST ROD FIRST RING SECOND RING
 1   .134      .0527   .15954E 02  .11823E 02  .37839E 01  .34166E 00
 2  1.338      .5267   .15954E 02  .11823E 02  .37839E 01  .34166E 00
 3  2.675     1.0533   .17254E 02  .13122E 02  .37839E 01  .34166E 00
 4  4.013     1.5800   .16235E 02  .12103E 02  .37839E 01  .34166E 00
ADDITIONAL RINGS
     1           2           3           4           5           6           7           8
 .60672E-02
RELATIVE FLUX NORMALIZED TO CELL EDGE
PT. DIST.(CM) DIST.(IN)    TOTAL NEAREST ROD FIRST RING SECOND RING
 1   .134      .0527       .9827  .72823E 00  .23307E 00  .21045E-01
 2  1.338      .5267       .9827  .72823E 00  .23307E 00  .21045E-01
 3  2.675     1.0533      1.0628  .80827E 00  .23307E 00  .21045E-01
 4  4.013     1.5800      1.0000  .74551E 00  .23307E 00  .21045E-01
ADDITIONAL RINGS
     1           2           3           4           5           6           7           8
 .37371E-03
```

A.2 HEETR, High Energy Events in Thermal Reactors

A brief discussion of the HEETR code is given in section 3.3 and more detailed discussions are available in references C9 and C10. The copy of the code supplied by Dr. H. K. Clark was modified slightly, as described below, for use in the present work. The changes in the input data required by these modifications are given in section A.2.1, and a FORTRAN listing of the entire code as used in the present work is given in section A.2.2.

The dimensions of the subscripted variables were changed to be consistent with the use of five energy groups, as many as 20 regions, and only one "symmetry class" (i. e., calculations for lattices of clusters of rods are excluded). This modification reduced the storage requirements of the code sufficiently to permit loading the entire code into the IBM 7094 at the MIT Computation Center. By so doing, it was possible to avoid the use of "chain jobs" and thereby to reduce greatly the amount of computer time required per problem.

The control of the sequence of operations in the code was modified in two ways. First, in accordance with the above discussion, the chain nature of the code was eliminated by making PART 1 the main program and PART 2 a subroutine which is called by PART 1. Second, a control option was introduced which permits the calculation of a series of problems with the same nuclear data without the necessity for reading in the nuclear data with each set of data for a new problem. This modification reduces considerably the number of input data cards and computer time required for a series of problems with the same nuclear data.

A.2.1 Input Data for HEETR

A detailed discussion of the input data required for the HEETR code is given in reference C10. The additional input data required as a result of the modifications to HEETR for use in the present work are discussed in this section. The name of the required input variable is given first, followed by the format to be used, and then by a brief description of the variable.

MORE (14I5)

MORE is a control character that permits the calculation of a series of problems with one batch of input data. If MORE is zero, the program will terminate at the completion of the calculation for the first set of data. If MORE is negative, at the completion of the calculation for the first set of data, the code will read in a complete new set of data, including the nuclear data. If MORE is positive, the code will repeatedly read in new sets of input data, except for the nuclear data, at the end of each problem. MORE is read in on the first card of input data together with NG and NM as described in reference C10.

ID(I), I = 1, 12 (12A6)

ID(I) is an identification statement used to label the output of the problem. ID(I) will be printed at the top of the list of the output. ID(I) is read in on the second card following the nuclear data.

T (7F10.6)

T is the temperature in Mev of the Maxwellian distribution assumed for the fission neutron spectrum. The subroutine, FNSPM, which is used to calculate the shape of the fission neutron spectrum, was modified by Clark in a later version of HEETR than the one reported in reference C10. The newer version of FNSPM assumes a Maxwellian distribution for the fission neutron spectrum and requires the use of a library routine to calculate values of the Error Function. The Error Function is not available as a library routine at the MIT Computation Center, so the newer version of FNSPM was further modified so that the Error Function is computed by the appropriate series representation.

A.2.2 Fortran Listing of HEETR

A Fortran listing of the version of the HEETR code used in the present work is given below.

```
*      LIST8
*      LABEL
*      SYMBOL TABLE
CPT-1    MAIN  HEETR CODE
  301 FORMAT(14I5)
  302 FORMAT(7F10.6)
  303 FORMAT(/////)
  304 FORMAT(24F3.2)
  305 FORMAT(12A6)
  310 FORMAT(50X14HPROBLEM NUMBERI5)
  311 FORMAT(1H065X18HWEIGHT FRACTION OF)
  312 FORMAT(30H   TYPE NO.     DENSITY(G/CC) ,2XA6,8(4XA6))
  313 FORMAT(I8,F18.5,F13.6,8F10.6)
  314 FORMAT(46H1PRINTOUT OF LIBRARY TAPE AND FISSION SPECTRUM)
  315 FORMAT(98H1 GROUP   EL(MEV)    FISSION SOURCE   SIGMA-T     SIGMA-
     1TR    SIGMA-C     SIGMA-F        NU         A6,F16.3)
  316 FORMAT(I5,1PE14.4,0PF12.5,1PE15.3,3E12.3,0PF9.3)
  317 FORMAT(104H0          SIGMA-IJ (TRANSFER TO GROUP I FROM GROUP J),
     1ARRANGED AS 11, 21, 22, 31, 32, 33,...,(NG+1)(NG))
  318 FORMAT(10X11F10.4)
  319 FORMAT(74H1PRINTOUT OF MACROSCOPIC CROSS SECTIONS AND FISSION SPEC
     1TRUM FOR EACH TYPE)
  320 FORMAT(112H1 GROUP   EL(MEV)    FISSION SOURCE   SIGMA-T     SIGMA
     1-TR    SIGMA-C     SIGMA-F    NUSIGMA-F      TYPE NUMBER I1)
  321 FORMAT(I5,1PE14.4,0PF12.5,F15.7,4F12.7)
  322 FORMAT(120H1HEETR CODE                    COMPUTES EVENTS IN CYLINDR
     1ICAL CELLS FROM ESCAPE AND TRANSMISSION PROBABILITIES          )
  323 FORMAT(31H1END OF LAST PROBLEM OF SERIES I2/////)
  324 FORMAT(120H0SOURCE SUPPLIED FOR EACH REGION IS RELATIVE NUMBER OF
     1NEUTRONS PRODUCED BY FISSIONS OCCURRING IN GROUP NG+1.          )
  325 FORMAT(120H0SOURCE SUPPLIED FOR EACH REGION IS ESTIMATE OF RELATIV
     1E NUMBER OF NEUTRONS PRODUCED BY FISSIONS OCCURRING IN NG GROUPS.)
  326 FORMAT(120H0TRANSMISSION AND ESCAPE PROBABILITIES ARE COMPUTED FRO
     1M TOTAL CROSS SECTIONS.                                         )
  327 FORMAT(120H0TRANSMISSION AND ESCAPE PROBABILITIES ARE COMPUTED FRO
     1M TRANSPORT CROSS SECTIONS.                                     )
  328 FORMAT(120H0DANCOFF FACTORS ARE EMPLOYED FOR INTERACTION BETWEEN E
     1LEMENTS IMMERSED IN MODERATOR.                                  )
  329 FORMAT(120H0THE CELL APPROXIMATION IS MADE WITH ZERO CURRENT AT TH
     1E CELL BOUNDARY.                                                )
  330 FORMAT(19X20HTHERMAL VALUE OF NU=F5.3,10X43HTEMPERATURE OF FISSION
     1 SPECTRUM MAXWELLIAN=F5.3)
  331 FORMAT(12A6)
  332 FORMAT(1H0,12A6)
      DIMENSION ST( 5,25),STR( 5,25),SC( 5,25),SF( 5,25),VNU( 5,25),SIJ(
     1020,25),AWT(25),COMP(26,10),EL( 5),SGMT( 5,10),SGMTR( 5,10),SGMC(
     25,10),SGMB( 5,10),VSGMB( 5,10),SGMIJ( 20,10),SPRM( 5),NWSC(1)
      DIMENSION NR(10),INT(20,1) ,RAD(20,1) ,FS(20,1) ,ATAS(24),WTS(24,1
     1,1)  ,WIL(24),CC(25),NOUT(5),ID(12)
      COMMON SGMT,SGMTR,SGMC,SGMB,VSGMB,SGMIJ,SPRM,NG,NSC,NR,NWSC
      COMMON NRT,NST,EL,INT,RAD,RADC,FS,FSM,ATAS,WTS,WIL,NSA,NSR,NCC
      COMMON NOUT,VNUTH,NTIN,NTOUT,MORE
C     NG=NO. OF GROUPS, NSC=NO. OF SYMMETRY CLASSES, NR(I)=NO. OF
C     REGIONS IN EACH CLASS, NRT=NO. OF DIFFERENT TYPES OF REGIONS IN .
C     CELL, NM=NO. OF MATERIALS FOR WHICH DATA ARE TO BE READ, NWSC(I)=
```

```
C      NO. OF UNITS WITHIN EACH SYMMETRY CLASS, ST(I,J)= SIGMA TOTAL OF
C      MATERIAL J IN GROUP I. SIMILARLY STR, SC, SF, AND VNU REPRESENT
C      SIGMA TRANSPORT, SIGMA CAPTURE, SIGMA FISSION, AND NU. SIJ(I,J)
C      REPRESENTS TRANSFER CROSS SECTIONS OF MATERIAL J ARRANGED IN THE
C      ORDER 11, 21, 22, 31, 32, 33,...,(NG+1)(NG).   INT(J,I) IS THE
C      REGION TYPE INDEX FOR SYMMETRY CLASS I. INT(J,I) ASSUMES A TYPE
C      NO. FOR EACH REGION J. AWT(I)=ATOMIC WEIGHT OF MATERIAL I.
C      COMP(I,J)=DENSITY OF TYPE J FOLLOWED IN ORDER BY WEIGHT FRACTIONS
C      OF VARIOUS MATERIALS I-1. RAD(I,J)=OUTER RADIUS OF REGION I OF
C      SYMMETRY CLASS J. EL(I)=LOWER BOUND OF GROUP I IN MEV. FS(I,J)=
C      ESTIMATED OR ACTUAL FISSION SOURCE IN EACH REGION I OF EACH
C      SYMMETRY CLASS J. NP=PROBLEM NO. NST=SOLUTION TYPE(IF NST IS EVEN,
C      FS IS ACTUAL SOURCE IN NG+1 GROUP. IF ODD FS IS ESTIMATE. 0 THRU 3
C      INDICATE TRANS. APPROX.). ATAS(I)=POSSIBLE AXIS TO AXIS SEPARATION
C      VALUES IN INCREASING ORDER. WTS(I,J,K)=NO. OF UNITS IN SYMMETRY
C      CLASS K TRANSMITTING NEUTRONS TO UNIT OF SYMMETRY CLASS J AT A
C      SEPARATION ATAS(I). FSM=ACTUAL OR ESTIMATED FISSION SOURCE IN
C      MODERATOR.
C      INTRACELL SPACINGS MUST BE LISTED FIRST IN INCREASING ORDER FOL-
C      LOWED BY INTERCELL SPACINGS, EVEN IF SOME INTER ARE LESS
C      UATAS=UNIT AXIS TO AXIS SEPARATION. RADC=RADIUS OF CELL
C      VNUTH=THERMAL VALUE OF NU. T=TEMPERATURE OF FISSION SPECTRUM.
C      IF NST=2,3,6,OR 7,(AND IF NSC=NWSC(NSC)=1) CODE USES CELL BOUNDARY
C      IF RATIO OF U-238 TO U-235 FISSIONS IS DESIRED, NST IS INCREASED
C      BY 10. THE URANIUM MUST BE MATERIAL TYPE 2, AND MATERIAL TYPE 3
C      MUST BE PURE U-238 HAVING THE SAME ATOMIC DENSITY AS IN MATERIAL
C      TYPE 2. THIS OPTION IS AVAILABLE ONLY WHEN NST IS EVEN.
C      NCC IS NEGATIVE EXPONENT OF 10 FOR CONVERGENCE CRITERION
C      MODERATOR REGION IS ALWAYS TYPE 1. NSA=NO. OF INTRA CELL SPACINGS.
C      NSR=NO. OF INTERCELL SPACINGS
C      NOUT SPECIFIES OUTPUT. IT CONSISTS OF 5 NUMBERS.IF FIFTH NUMBER IS
C      NON-ZERO, LIBRARY TAPE IS PRINTED. IF FOURTH NUMBER IS NON-ZERO
C      MACROSCOPIC SIGMAS FOR TYPES EMPLOYED ARE PRINTED. IF THIRD NUMBER
C      IS NON-ZERO, TPOO, TPOI, AND DTP ARE PRINTED. IF SECOND NUMBER IS
C      NON-ZERO, ATAS, WTS, AND WIL ARE PRINTED. IF FIRST NUMBER IS NON-
C      ZERO, FISSION SOURCES AND DISADVANTAGE FACTORS ARE PRINTED.
       NLIB=4
       NTIN=4
       NTOUT=2
  500  READ INPUT TAPE NLIB,301,NG,NM,MORE
       NIJ=((NG+1)*(NG+2))/2-1
       DO 2 I=1,NM
    2  READ INPUT TAPE NLIB,302,(ST(J,I),J=1,NG),(STR(J,I),J=1,NG),(SC(J,
      1I),J=1,NG),(SF(J,I),J=1,NG),(VNU(J,I),J=1,NG),(SIJ(J,I),J=1,NIJ)
      2,AWT(I)
       READ INPUT TAPE NLIB,302,                    (EL(I),I=1,NG)
       READ INPUT TAPE NLIB,305,(CC(I),I=1,NM)
  502  READ INPUT TAPE NTIN,301,NSC,(NR(I),I=1,NSC),(NWSC(I),I=1,NSC),NRT
      1,NST,NSA,NSR,NCC,NP,(NOUT(I),I=1,5)
       IF(NSC)21,21,22
   21  WRITE OUTPUT TAPE NTOUT,323,NR(1)
       CALL EXIT
   22  WRITE OUTPUT TAPE NTOUT,322
```

```
      READ INPUT TAPE 4,331,(ID(I),I=1,12)
      K=NM+1
      DO 4 I=1,NRT
    4 READ INPUT TAPE NTIN,302,(COMP(J,I),J=1,K)
      DO 3 I=1,NSC
      K=NR(I)
      READ INPUT TAPE NTIN,301,(INT(J,I),J=1,K)
      READ INPUT TAPE NTIN,302,(RAD(J,I),J=1,K)
    3 READ INPUT TAPE NTIN,302,(FS(J,I),J=1,K)
      READ INPUT TAPE NTIN,302,UATAS,FSM,RADC,VNUTH,T
      NATAS=NSA+NSR
      READ INPUT TAPE NTIN,302,(ATAS(I),I=1,NATAS)
      READ INPUT TAPE NTIN,304,(WIL(I),I=1,NSA)
      DO 5 I=1,NSC
      DO 5 J=1,NSC
    5 READ INPUT TAPE NTIN,304,(WTS(K,I,J),K=1,NATAS)
      DO 18 I=1,NATAS
   18 ATAS(I)=UATAS*ATAS(I)
      DO 14 I=1,NRT
      DO 7 J=1,NG
      SGMT(J,I)=0.
      SGMTR(J,I)=0.
      SGMC(J,I)=0.
      SGMB(J,I)=0.
    7 VSGMB(J,I)=0.
      DO 8 J=1,NIJ
    8 SGMIJ(J,I)=0.
      DO 14 J=1,NM
      IF(COMP(J+1,I))14,14,10
   10 XN=COMP(1,I)*COMP(J+1,I)*.6023/AWT(J)
      DO 11 L=1,NG
      SGMT(L,I)=SGMT(L,I)+XN*ST(L,J)
      SGMTR(L,I)=SGMTR(L,I)+XN*STR(L,J)
      SGMC(L,I)=SGMC(L,I)+XN*SC(L,J)
      SGMB(L,I)=SGMB(L,I)+XN*SF(L,J)
   11 VSGMB(L,I)=VSGMB(L,I)+XN*SF(L,J)*VNU(L,J)
      DO 12 L=1,NIJ
   12 SGMIJ(L,I)=SGMIJ(L,I)+XN*SIJ(L,J)
   14 CONTINUE
      SM=0.
      DO 17 I=1,NG
      IF(I-1)15,15,16
   15 SPRM(I)=FNSPM(EL(I),T)
      GO TO 17
   16 SM=SM+SPRM(I-1)
      SPRM(I)=FNSPM(EL(I),T)-SM
   17 CONTINUE
      IF(NST-10)101,100,100
  100 MST=NST
      NST=MST-10
  101 WRITE OUTPUT TAPE NTOUT,303
      WRITE OUTPUT TAPE NTOUT,310,NP
      WRITE OUTPUT TAPE 2,332,(ID(I),I=1,12)
```

```
   IF(FLOATF(NST/2)-FLOATF(NST)/2.+.1)23,23,24
23 WRITE OUTPUT TAPE NTOUT,325
   GO TO 25
24 WRITE OUTPUT TAPE NTOUT,324
25 N=NST/4+1
   GO TO (26,27),N
26 WRITE OUTPUT TAPE NTOUT,327
   GO TO 28
27 WRITE OUTPUT TAPE NTOUT,326
28 N=NST+1
   GO TO (29,29,30,30,29,29,30,30),N
29 WRITE OUTPUT TAPE NTOUT,328
   GO TO 42
30 WRITE OUTPUT TAPE NTOUT,329
42 WRITE OUTPUT TAPE NTOUT,303
   NST=MST
   IF(NM-9)31,31,32
31 N=NM
   GO TO 33
32 N=9
33 WRITE OUTPUT TAPE NTOUT,311
   WRITE OUTPUT TAPE NTOUT,312,(CC(I),I=1,N)
   DO 34 I=1,NRT
34 WRITE OUTPUT TAPE NTOUT,313,I,COMP(1,I),(COMP(J+1,I),J=1,N)
   WRITE OUTPUT TAPE NTOUT,303
   IF(NM-9)45,45,35
35 IF(NM-18)36,36,37
36 N=NM-9
   GO TO 38
37 N=9
38 WRITE OUTPUT TAPE NTOUT,311
   WRITE OUTPUT TAPE NTOUT,312,(CC(I+9),I=1,N)
   DO 39 I=1,NRT
39 WRITE OUTPUT TAPE NTOUT,313,I,COMP(1),(COMP(J+10),J=1,N)
   IF(NM-18)45,45,40
40 N=NM-18
   WRITE OUTPUT TAPE NTOUT,303
   WRITE OUTPUT TAPE NTOUT,311
   WRITE OUTPUT TAPE NTOUT,312,(CC(I+18),I=1,N)
   DO 41 I=1,NRT
41 WRITE OUTPUT TAPE NTOUT,313,I,COMP(1),(COMP(J+19),J=1,N)
45 WRITE OUTPUT TAPE NTOUT,303
   WRITE OUTPUT TAPE NTOUT,330,VNUTH,T
   IF(NOUT(5))46,60,46
46 WRITE OUTPUT TAPE NTOUT,314
   DO 48 I=1,NM
   WRITE OUTPUT TAPE NTOUT,315,CC(I),AWT(I)
   DO 47 J=1,NG
47 WRITE OUTPUT TAPE NTOUT,316,J,EL(J),SPRM(J),ST(J,I),STR(J,I),SC(J,
  1I),SF(J,I),VNU(J,I)
   WRITE OUTPUT TAPE NTOUT,317
48 WRITE OUTPUT TAPE NTOUT,318,(SIJ(II,I),II=1,NIJ)
60 IF(NOUT(4))61,80,61
```

```
   61 WRITE OUTPUT TAPE NTOUT,319
      DO 63 I=1,NRT
      WRITE OUTPUT TAPE NTOUT,320,I
      DO 62 J=1,NG
   62 WRITE OUTPUT TAPE NTOUT,321,J,EL(J),SPRM(J),SGMT(J,I),SGMTR(J,I),
     1SGMC(J,I),SGMB(J,I),VSGMB(J,I)
      WRITE OUTPUT TAPE NTOUT,317
   63 WRITE OUTPUT TAPE NTOUT,318,(SGMIJ(II,I),II=1,NIJ)
   80 CALL PART2
      IF(MORE) 500,550,502
  550 CALL EXIT
      END
*     LIST8
*     LABEL
*     SYMBOL TABLE
CPART2   HEETR CODE
      SUBROUTINE PART2
      DIMENSION SGMT( 5,10),SGMTR( 5,10),SGMC( 5,10),SGMB( 5,10),VSGMB(
     15,10),SGMIJ( 20,10),SPRM( 5),NR(10),INT(20,1) ,RAD(20,1) ,ABT(20,1
     2, 20),FS(20,1) ,AA(19,10),AQ(19,10),VA(2,10),ATAS(24),WTS(24,1,
     31)  ,WIL(24),TPOI(19,1, 20),TPOO(20,1, 20),DTP(24,20),NWSC(1) ,ABM
     4(20),VQ(2,10),V(20,1) ,UFS(20,1) ,PFS(20,1) ,DFS(2 ,1) ,NOUT(5),
     5PHI(20),EL( 5),IH(20),FDU(20,1) ,FNU(20,1) ,DLTA(2 ,1) ,IS(7),
     6IR(7),DA(7)
      COMMON SGMT,SGMTR,SGMC,SGMB,VSGMB,SGMIJ,SPRM,NG,NSC,NR,NWSC
      COMMON NRT,NST,EL,INT,RAD,RADC,FS,FSM,ATAS,WTS,WIL,NSA,NSR,NCC
      COMMON NOUT,VNUTH,NTIN,NTOUT,MORE
C     ABT(I,J,K)=ABSORPTIONS IN REGION I, SYMMETRY CLASS J, AND GROUP K.
C     ABM(I)=ABSORPTIONS IN MODERATOR IN GROUP I.
  301 FORMAT(40H1          PRINTOUT OF AVERAGED CONSTANTS/////)
  302 FORMAT(30H0    MODERATOR    CELL RADIUS=F8.4 ,13H   VOL FRACT=F7.5
     1,19H   THRML FISS SRCE=F7.5,14H    LAST ITER=F7.5)
  303 FORMAT(30H0    MODERATOR    CELL RADIUS=F8.4, 13H   VOL FRACT=F7.5
     1,19H   FINAL FISS SRCE=F7.5,14H    PREV ITER=F7.5)
  304 FORMAT(7H0CLASS I1,6H  NO.=I2,7H   REGNI3,7H   TYPEI2,10H   RADIUS
     1=F8.4,13H   VOL FRACT=F7.5,19H   THRML FISS SRCE=F7.5,13H   LAST I
     2TER=F7.5)
  305 FORMAT(7H0CLASS I1,6H  NO.=I2,7H   REGNI3,7H   TYPEI2,10H   RADIUS
     1=F8.4,13H   VOL FRACT=F7.5,19H   FINAL FISS SRCE=F7.5,13H   PREV I
     2TER=F7.5)
  306 FORMAT(10X7HGROUP  10I10)
  307 FORMAT(120H0GROUP     EL(MEV)   SPECTRUM      FLUX      SIGMA-T
     1  SIGMA-TR     SIGMA-C     SIGMA-F     NU*SIGMA-F        NU      )
  308 FORMAT(I4,1PE15.3,0PF10.5,1PE13.4,0PF10.4,F12.4,F13.5,F12.5,F13.5,
     1F15.4)
  309 FORMAT(104H0          SIGMA-IJ (TRANSFER TO GROUP I FROM GROUP J),
     1ARRANGED AS 11, 21, 22, 31, 32, 33,...,(NG+1)(NG))
  310 FORMAT(10X11F10.4)
  311 FORMAT(1H0///40X41HPARAMETERS AVERAGED OVER SPACE AND ENERGY//9H S
     1IGMA-T=F8.5,13H    SIGMA-TR=F8.5,14H    1/(TRMFP)=F8.5,12H    SIGM
     2A-C=F9.6,12H    SIGMA-F=F9.6,7H    NU=F7.4/6X11HNU*SIGMA-F=F9.6,18
     3H    SIGMA-REMOVAL=F9.6,39H    TAU (TRMFP/(3*SIGMA (C+F+R-NU*F)))=
     4F8.3/11X58HFRACTION OF SOURCE NEUTRONS ARISING FROM THERMAL FISSIO
```

```
   5NS=F9.6/11X34HRATIO OF FAST TO THERMAL FISSIONS=F8.5)
312 FORMAT(41H1PRINTOUT OF DANCOFF FACTORS IN MODERATOR)
313 FORMAT(12H0    RADIUS=F7.4,29H     AXIS-TO-AXIS SEPARATION=F7.4)
314 FORMAT(5X15HDANCOFF FACTOR 10F10.5)
315 FORMAT(39H1PRINTOUT OF TRANSMISSION PROBABILITIES)
316 FORMAT(7H0CLASS I1,11H    REGION I2)
317 FORMAT(10X10HTPOI      10F10.5)
318 FORMAT(46H1PRINTOUT OF AXIS-TO-AXIS SPACINGS AND WEIGHTS)
319 FORMAT(30H0AXIS-TO-AXIS SEPARATION      8F11.4)
320 FORMAT(81H0WTS(I,J,K) ARRANGED WITHIN ROWS BY I. ROWS ADVANCE BY J
   1, AND GROUPS OF ROWS BY K)
321 FORMAT(24F5.1)
322 FORMAT(5X15HDISADVNTG FCTR 10F10.5)
323 FORMAT(30H NO. IN INF. REG. LATTICE     8F11.4)
324 FORMAT(10X10HTPOO      10F10.5)
325 FORMAT( 1H0//40X41HDISADVANTAGE FACTORS AND VOLUME FRACTIONS)
326 FORMAT(11X 41HOVERALL RATIO OF U-238 TO U-235 FISSIONS=F8.5)
327 FORMAT(21X 22HSYMMETRY CLASS, REGION    I5,1H,I2,6(I7,1H,I2))
328 FORMAT(21X 22H  U-238/U-235 FISSIONS 7F10.5)
    IDA=0
    IF(NST-10)111,110,110
110 NST=NST-10
    IDA=1
111 CALL TRP(NST,NSC,NR,INT,NG,NSA,NSR,WTS,WIL,ATAS,RAD,RADC,SGMT,
   1SGMTR,TPOO,TPOI,DTP,L)
    IF(L)2,2,1
  1 FS(L,1)=FSM
  2 SUMA=0.
    DO 31 I=1,NSC
    KK=NR(I)
    DO 31 J=1,KK
 31 SUMA=SUMA+FS(J,I)*FLOATF(NWSC(I))
    IF(L)32,32,33
 32 SUMA=SUMA+FSM
    FSM=FSM/SUMA
 33 DO 34 I=1,NSC
    KK=NR(I)
    DO 34 J=1,KK
 34 FS(J,I)=FS(J,I)/SUMA
    IF(FLOATF(NST/2)-FLOATF(NST)/2.+.1)38,38,35
 35 DO 36 I=1,NSC
    KK=NR(I)
    DO 36 J=1,KK
 36 DFS(J,I)=FS(J,I)
    IF(L)37,37,38
 37 DFSM=FSM
 38 VM=0.
    DO 7 I=1,NSC
    K=NR(I)
    DO 7 J=1,K
    IF(J-1)3,3,4
  3 V(1,I)=(RAD(1,I)/RADC)**2
    GO TO 5
```

```
 4 V(J,I)=(RAD(J,I)**2-RAD(J-1,I)**2)/RADC**2
 5 IF(L)6,6,7
 6 VM=VM+V(J,I)*FLOATF(NWSC(I))
 7 CONTINUE
   IF(L)8,8,9
 8 VM=1.-VM
 9 N=NST/4
40 CALL SOLN(L,NG,NSC,NST,NSA,NSR,NR,INT,NWSC,SGMT,SGMTR,SGMIJ,FS,FSM
  1,SPRM,DTP,TPOO,TPOI,RAD,RADC,ABT,ABM,WTS)
   DO 12 I=1,NSC
   KK=NR(I)
   DO 12 J=1,KK
   JJ=INT(J,I)
   UFS(J,I)=0.
   DO 12 K=1,NG
   IF(N)10,10,11
10 ABT(J,I,K)=ABT(J,I,K)/(SGMTR(K,JJ)*V(J,I))
   GO TO 12
11 ABT(J,I,K)=ABT(J,I,K)/(SGMT(K,JJ)*V(J,I))
12 UFS(J,I)=UFS(J,I)+VSGMB(K,JJ)*ABT(J,I,K)*V(J,I)
   IF(L)13,13,17
13 UFSM=0.
   DO 16 I=1,NG
   IF(N)14,14,15
14 ABM(I)=ABM(I)/(SGMTR(I,1)*VM)
   GO TO 16
15 ABM(I)=ABM(I)/(SGMT(I,1)*VM)
16 UFSM=UFSM+ABM(I)*VSGMB(I,1)*VM
17 IF(FLOATF(NST/2)-FLOATF(NST)/2.+.1)51,51,18
18 SUMA=0.
   DO 19 I=1,NSC
   KK=NR(I)
   DO 19 J=1,KK
   PFS(J,I)=FS(J,I)-UFS(J,I)
19 SUMA=SUMA+PFS(J,I)*FLOATF(NWSC(I))
   IF(L)20,20,21
20 PFSM=FSM-UFSM
   SUMA=SUMA+PFSM
   UFSM=UFSM/SUMA
   PFSM=PFSM/SUMA
21 SUMC=0.
   DO 22 I=1,NSC
   KK=NR(I)
   DO 22 J=1,KK
   UFS(J,I)=UFS(J,I)/SUMA
   PFS(J,I)=PFS(J,I)/SUMA
22 SUMC=SUMC+ABSF(DFS(J,I)-PFS(J,I))*FLOATF(NWSC(I))
   IF(L)23,23,24
23 SUMC=SUMC+ABSF(DFSM-PFSM)
24 IF(SUMC-10.**(-NCC))60,60,25
25 SUMC=0.
   DO 41 I=1,NSC
   KK=NR(I)
```

```
      DO 41 J=1,KK
      FS(J,I)=DFS(J,I)+UFS(J,I)
   41 SUMC=SUMC+FS(J,I)*FLOATF(NWSC(I))
      IF(L)42,42,43
   42 FSM=DFSM+UFSM
      SUMC=SUMC+FSM
      FSM=FSM/SUMC
   43 DO 44 I=1,NSC
      KK=NR(I)
      DO 44 J=1,KK
   44 FS(J,I)=FS(J,I)/SUMC
      GO TO 40
   51 SUMA=0.
      SUMC=0.
      DO 52 I=1,NSC
      KK=NR(I)
      DO 52 J=1,KK
   52 SUMA=SUMA+UFS(J,I)*FLOATF(NWSC(I))
      IF(L)53,53,54
   53 SUMA=SUMA+UFSM
      UFSM=UFSM/SUMA
      SUMC=ABSF(FSM-UFSM)
   54 DO 55 I=1,NSC
      KK=NR(I)
      DO 55 J=1,KK
      UFS(J,I)=UFS(J,I)/SUMA
   55 SUMC=SUMC+ABSF(FS(J,I)-UFS(J,I))*FLOATF(NWSC(I))
      IF(SUMC-10.**(-NCC))60,60,56
   56 DO 57 I=1,NSC
      KK=NR(I)
      DO 57 J=1,KK
   57 FS(J,I)=UFS(J,I)
      IF(L)58,58,40
   58 FSM=UFSM
      GO TO 40
   60 DO 63 I=1,NG
      PHI(I)=0.
      DO 61 J=1,NSC
      KK=NR(J)
      DO 61 JJ=1,KK
   61 PHI(I)=PHI(I)+ABT(JJ,J,I)*V(JJ,J)*FLOATF(NWSC(J))
      IF(L)62,62,63
   62 PHI(I)=PHI(I)+ABM(I)*VM
   63 CONTINUE
      DO 66 I=1,NG
      DO 64 J=1,NSC
      KK=NR(J)
      DO 64 JJ=1,KK
   64 ABT(JJ,J,I)=ABT(JJ,J,I)/PHI(I)
      IF(L)65,65,66
   65 ABM(I)=ABM(I)/PHI(I)
   66 CONTINUE
      DO 69 I=1,NG
```

```
      SGMT(I,10)=0.
      SGMTR(I,10)=0.
      SGMC(I,10)=0.
      SGMB(I,10)=0.
      VSGMB(I,10)=0.
      DO 67 J=1,NSC
      F=FLOATF(NWSC(J))
      KK=NR(J)
      DO 67 JJ=1,KK
      LL=INT(JJ,J)
      SGMT(I,10)=SGMT(I,10)+SGMT(I,LL)*V(JJ,J)*ABT(JJ,J,I)*F
      SGMTR(I,10)=SGMTR(I,10)+SGMTR(I,LL)*V(JJ,J)*ABT(JJ,J,I)*F
      SGMC(I,10)=SGMC(I,10)+SGMC(I,LL)*V(JJ,J)*ABT(JJ,J,I)*F
      SGMB(I,10)=SGMB(I,10)+SGMB(I,LL)*V(JJ,J)*ABT(JJ,J,I)*F
   67 VSGMB(I,10)=VSGMB(I,10)+VSGMB(I,LL)*V(JJ,J)*ABT(JJ,J,I)*F
      IF(L)68,68,69
   68 SGMT(I,10)=SGMT(I,10)+SGMT(I,1)*VM*ABM(I)
      SGMTR(I,10)=SGMTR(I,10)+SGMTR(I,1)*VM*ABM(I)
      SGMC(I,10)=SGMC(I,10)+SGMC(I,1)*VM*ABM(I)
      SGMB(I,10)=SGMB(I,10)+SGMB(I,1)*VM*ABM(I)
      VSGMB(I,10)=VSGMB(I,10)+VSGMB(I,1)*VM*ABM(I)
   69 CONTINUE
      NIJ=((NG+1)*(NG+2))/2-1
      K=NG+1
      DO 72 I=1,NG
      LL=((I-1)*I)/2+1
      DO 72 J=I,K
      LL=LL+J-1
      SGMIJ(LL,10)=0.
      DO 70 II=1,NSC
      KK=NR(II)
      DO 70 JJ=1,KK
      MM=INT(JJ,II)
   70 SGMIJ(LL,10)=SGMIJ(LL,10)+SGMIJ(LL,MM)*V(JJ,II)*ABT(JJ,II,I)*FLOAT
     1F(NWSC(II))
      IF(L)71,71,72
   71 SGMIJ(LL,10)=SGMIJ(LL,10)+SGMIJ(LL,1)*VM*ABM(I)
   72 CONTINUE
      SMP=0.
      SGT=0.
      SGTR=0.
      SGC=0.
      SGB=0.
      VSGB=0.
      SGIJ=0.
      PH=0.
      DO 73 I=1,NG
      PH=PH+PHI(I)
      SGT=SGT+SGMT(I,10)*PHI(I)
      SGTR=SGTR+SGMTR(I,10)*PHI(I)
      SGC=SGC+SGMC(I,10)*PHI(I)
      SMP=SMP+PHI(I)/SGMTR(I,10)
      SGB=SGB+SGMB(I,10)*PHI(I)
```

```
    VSGB=VSGB+VSGMB(I,10)*PHI(I)
    KK=(NG*(NG+1))/2+I
 73 SGIJ=SGIJ+SGMIJ(KK,10)*PHI(I)
    PH=1./PH
    DO 74 I=1,NG
 74 PHI(I)=PHI(I)*PH
    SGT=SGT*PH
    SGTR=SGTR*PH
    SGC=SGC*PH
    SGB=SGB*PH
    VSGB=VSGB*PH
    SGIJ=SGIJ*PH
    SMP=1./(SMP*PH)
    KK=NG/11+1
    WRITE OUTPUT TAPE NTOUT,301
    WRITE OUTPUT TAPE NTOUT,307
    DO 75 I=1,NG
 75 IH(I)=I
    DO 80 I=1,NG
    VV=VSGMB(I,10)/SGMB(I,10)
 80 WRITE OUTPUT TAPE NTOUT,308,I,EL(I),SPRM(I),PHI(I),SGMT(I,10),
   1SGMTR(I,10),SGMC(I,10),SGMB(I,10),VSGMB(I,10),VV
    WRITE OUTPUT TAPE NTOUT,309
    WRITE OUTPUT TAPE NTOUT,310,(SGMIJ(I,10),I=1,NIJ)
    IF(FLOATF(NST/2)-FLOATF(NST)/2.+.1)87,87,81
 81 VV=VSGB/SGB
    FTNR=(1.-SUMA)/SUMA
    FTFR=FTNR*VNUTH/VV
    TAU=1./(3.*SMP*(SGC+SGB+SGIJ-VSGB))
    WRITE OUTPUT TAPE NTOUT,311,SGT,SGTR,SMP,SGC,SGB,VV,VSGB,SGIJ,TAU,
   1SUMA,FTFR
    IF(IDA)126,126,112
112 DO 113 I=1,NG
    IF(SGMB(I,3))114,114,113
113 CONTINUE
114 NFG=I-1
    SA=0.
    SB=0.
    SC=0.
    DO 118 J=1,NSC
    NK=NR(J)
    DO 118 K=1,NK
    IF(INT(K,J)-2)118,115,118
115 FDU(K,J)=0.
    FNU(K,J)=0.
    DO 116 I=1,NFG
116 FDU(K,J)=FDU(K,J)+SGMB(I,3)*ABT(K,J,I)*PHI(I)
    FDU(K,J)=FDU(K,J)*V(K,J)*FLOATF(NWSC(J))*(1.-SUMA)/VSGB
    DO 117 I=1,NG
117 FNU(K,J)=FNU(K,J)+SGMB(I,2)*ABT(K,J,I)*PHI(I)
    FNU(K,J)=FNU(K,J)*V(K,J)*FLOATF(NWSC(J))*(1.-SUMA)/VSGB
    X=DFS(K,J)*FLOATF(NWSC(J))*SUMA/VNUTH+FNU(K,J)-FDU(K,J)
    DLTA(K,J)=FDU(K,J)/X
```

```
      SA=SA+FDU(K,J)
      SB=SB+FNU(K,J)
      SC=SC+DFS(K,J)*FLOATF(NWSC(J))*SUMA
  118 CONTINUE
      DELTA=SA/(SC/VNUTH+SB-SA)
      WRITE OUTPUT TAPE NTOUT,326,DELTA
      IL=0
      I=0
      IJ=1
      IK=1
  119 DO 123 J=IJ,NSC
      NK=NR(J)
      DO 122 K=IK,NK
      IF(INT(K,J)-2)122,120,122
  120 I=I+1
      IF(I-7)121,124,124
  121 IS(I)=J
      IR(I)=K
      DA(I)=DLTA(K,J)
  122 CONTINUE
  123 IK=1
      IL=1
      IF(I)126,126,124
  124 WRITE OUTPUT TAPE NTOUT,327,(IS(JJ),IR(JJ),JJ=1,I)
      WRITE OUTPUT TAPE NTOUT,328,(DA(JJ),JJ=1,I)
      IF(IL)125,125,126
  125 I=0
      IJ=J
      IK=K
      GO TO 119
  126 IF(NOUT(1))82,93,82
   82 WRITE OUTPUT TAPE NTOUT,325
      IF(L)83,83,85
   83 WRITE OUTPUT TAPE NTOUT,302,RADC,VM,DFSM,PFSM
      DO 84 I=1,KK
      JJ=XMINOF(NG,10*I)
      K=10*(I-1)+1
      WRITE OUTPUT TAPE NTOUT,306,(IH(J),J=K,JJ)
   84 WRITE OUTPUT TAPE NTOUT,322,(ABM(J),J=K,JJ)
   85 DO 86 I=1,NSC
      LL=NR(I)
      DO 86 J=1,LL
      MM=INT(J,I)
      WRITE OUTPUT TAPE NTOUT,304,I,NWSC(I),J,MM,RAD(J,I),V(J,I),DFS(J,I
     1),PFS(J,I)
      DO 86 JJ=1,KK
      LM=XMINOF(NG,10*JJ)
      K=10*(JJ-1)+1
      WRITE OUTPUT TAPE NTOUT,306,(IH(II),II=K,LM)
   86 WRITE OUTPUT TAPE NTOUT,322,(ABT(J,I,II),II=K,LM)
      GO TO 93
   87 IF(NOUT(1))88,93,88
   88 IF(L)89,89,91
```

```
 89 WRITE OUTPUT TAPE NTOUT,303,RADC,VM,UFSM,FSM
    DO 90 I=1,KK
    JJ=XMINOF(NG,10*I)
    K=10*(I-1)+1
    WRITE OUTPUT TAPE NTOUT,306,(IH(J),J=K,JJ)
 90 WRITE OUTPUT TAPE NTOUT,322,(ABM(J),J=K,JJ)
 91 DO 92 I=1,NSC
    LL=NR(I)
    DO 92 J=1,LL
    MM=INT(J,I)
    WRITE OUTPUT TAPE NTOUT,305,I,NWSC(I),J,MM,RAD(J,I),V(J,I),UFS(J,I
   1),FS(J,I)
    DO 92 JJ=1,KK
    LM=XMINOF(NG,10*JJ)
    K=10*(JJ-1)+1
    WRITE OUTPUT TAPE NTOUT,306,(IH(II),II=K,LM)
 92 WRITE OUTPUT TAPE NTOUT,322,(ABT(J,I,II),II=K,LM)
 93 NATAS=NSA+NSR
    IF(NOUT(2))94,98,94
 94 IF(L)994,994,98
994 WRITE OUTPUT TAPE NTOUT,318
    LM=(NSA+NSR)/9+1
    DO 96 I=1,LM
    JJ=XMINOF(NSA+NSR,8*I)
    LL=XMINOF(NSA,8*I)
    K=8*(I-1)+1
    WRITE OUTPUT TAPE NTOUT,319,(ATAS(J),J=K,JJ)
    IF(NSA-K)96,95,95
 95 WRITE OUTPUT TAPE NTOUT,323,(WIL(J),J=K,LL)
 96 CONTINUE
    WRITE OUTPUT TAPE NTOUT,320
    DO 97 K=1,NSC
    DO 97 J=1,NSC
 97 WRITE OUTPUT TAPE NTOUT,321,(WTS(I,J,K),I=1,NATAS)
 98 IF(NOUT(3))99,105,99
 99 IF(L)100,100,102
100 WRITE OUTPUT TAPE NTOUT,312
    K=NR(1)
    R=RAD(K,1)
    DO 101 LL=1,NATAS
    WRITE OUTPUT TAPE NTOUT,313,R,ATAS(LL)
    DO 101 I=1,KK
    JJ=XMINOF(NG,10*I)
    K=10*(I-1)+1
    WRITE OUTPUT TAPE NTOUT,306,(IH(J),J=K,JJ)
101 WRITE OUTPUT TAPE NTOUT,314,(DTP(LL,J),J=K,JJ)
102 WRITE OUTPUT TAPE NTOUT,315
    IF(J-1)104,104,103
103 WRITE OUTPUT TAPE NTOUT,317,(TPOI(J-1,I,LM),LM=MM,LL)
104 WRITE OUTPUT TAPE NTOUT,324,(TPOO(J,I,LM),LM=MM,LL)
105 RETURN
    DO 104 I=1,NSC
    K=NR(I)
```

```
      DO 104 J=1,K
      WRITE OUTPUT TAPE NTOUT,316,I,J
      DO 104 JJ=1,KK
      LL=XMINOF(NG,10*JJ)
      MM=10*(JJ-1)+1
      WRITE OUTPUT TAPE NTOUT,306,(IH(LM),LM=MM,LL)
      END
*     LIST8
*     LABEL
*     SYMBOL TABLE
CFNSPM
      FUNCTION FNSPM(E,T)
C     FRACTION OF FISSION NEUTRONS ABOVE E CALCULATED FROM
C     N(E)=A*SQRTF(E)*EXPF(-E/T) WHERE T IS TEMPERATURE OF MAXWELLIAN
      X=E/T
      SX=SQRTF(X)
      IF(SX-3.0) 1,1,11
    1 ANS=1.0
      S=0.0
      D=1.0
    2 S=S+1.0
      D=D*S
      TM=((-1.0)**S)*(SX**(2.0*S))/(D*(2.0*S+1.0))
      ANS=ANS+TM
      TEST=ABSF(TM/ANS)
      IF(TEST-0.000001) 5,2,2
    5 ANS=ANS*2.0*SX/1.7724539
    6 FNSPM=1.0+1.1283792*SX*EXPF(-X)-ANS
      RETURN
   11 ANS=1.0-1.0/(2.0*(SX**2))+3.0/(4.0*(SX**4))-15.0/(8.0*(SX**6))+105
     1.0/(16.0*(SX**8))-945.0/(32.*(SX**10))+10395./(64.*(SX**12))-
     2 135135./(128.*(SX**14))+2027025./(256.*(SX**16))
      EX=-(SX**2)
      ANS=1.0-EXPF(EX)*ANS/(SX*1.7724539)
      GO TO 6
      END
*     LIST8
*     LABEL
*     SYMBOL TABLE
CMOD
      SUBROUTINE MOD(IG,NSC,NST,NSA,NSR,NR,NWSC,SGMT,SGMTR,SGMIJ,WTS,DTP
     1,RAD,RADC,ABM,SPRM,FSM,G,EQ,HII,C,Q)
      DIMENSION H(10),TS(10,10),SPRM( 5)
      DIMENSION NR(10),RAD(20,1 ),SGMT( 5,10),SGMTR( 5,1 ),SGMIJ( 20,10)
     1,ABM(20),NWSC(1) ,WTS(24,1,1)  ,DTP(24,20),        G(10,10),EQ(10)
      M=(IG*(IG+1))/2
      K=NR(1)
      R=RAD(K,1)
      SUM=0.
      DO 1 I=1,NSC
    1 SUM=SUM+FLOATF(NWSC(I))
      V=RADC**2-SUM*R**2
      N=NST/4
```

```
      IF(N)2,2,3
    2 C=(SGMTR(IG,1)-SGMT(IG,1)+SGMIJ(M,1))/SGMTR(IG,1)
      B=SGMTR(IG,1)*R
      GO TO 4
    3 C=SGMIJ(M,1)/SGMT(IG,1)
      B=SGMT(IG,1)*R
    4 EF=.5*R**2/(B*V)
      L=NSA+NSR
      DO 6 I=1,NSC
      DO 6 J=1,NSC
      TS(I,J)=0.
      DO 6 K=1,L
      IF(WTS(K,I,J))6,6,5
    5 TS(I,J)=TS(I,J)+WTS(K,I,J)*DTP(K,IG)
    6 CONTINUE
      SUM=0.
      DO 8 I=1,NSC
      H(I)=0.
      DO 7 J=1,NSC
    7 H(I)=H(I)+TS(I,J)
    8 SUM=SUM+FLOATF(NWSC(I))*EF*(1.-H(I))
      EE=1.-C*(1.-SUM)
      HII=EE
      DO 10 I=1,NSC
   10 G(I,I)=-(EE*TS(I,I)+C*FLOATF(NWSC(I))*EF*(1.-H(I))**2)
      DO 12 I=1,NSC
      DO 12 J=1,NSC
      IF(I-J)11,12,11
   11 G(I,J)=-(EE*TS(I,J)+C*FLOATF(NWSC(J))*EF*(1.-H(I))*(1.-H(J)))
   12 CONTINUE
      Q=SPRM(IG)*FSM
      K=IG-1
      IF(K)17,17,13
   13 DO 16 I=1,K
      M=(IG*(IG+1))/2-K-1+I
      IF(N)14,14,15
   14 Q=Q+ABM(I)*SGMIJ(M,1)/SGMTR(I,1)
      GO TO 16
   15 Q=Q+ABM(I)*SGMIJ(M,1)/SGMT(I,1)
   16 CONTINUE
   17 DO 18 I=1,NSC
   18 EQ(I)=Q*EF*(1.-H(I))
      RETURN
      END
*     LIST8
*     LABEL
*     SYMBOL TABLE
      SUBROUTINE TRP(NST,NSC,NR,INT,NG,NSA,NSR,WTS,WIL,ATAS,RAD,RADC,
     1SGMT,SGMTR,TPOO,TPOI,DTP,KK)
CTRP
      DIMENSION NR(10),INT(20,1) ,WTS(24,1,1)  ,WIL(24),ATAS(24),RAD(20,
     11) ,SGMT( 5,10),SGMTR( 5,10),TPOI(19,1, 20),TPOO(2 ,1, 20),DTP(24,
     220)
```

```
      N=NST/4
      KK=NST+1
      GO TO (31,31,32,32,31,31,32,32),KK
   31 KK=0
      GO TO 25
   32 NR(1)=NR(1)+1
      KK=NR(1)
      RAD(KK,1)=RADC
      INT(KK,1)=1
   25 DO 8 I=1,NSC
      M=NR(I)
      DO 8 J=1,M
      L=INT(J,I)
      IF(J-1)2,2,1
    1 A=RAD(J-1,I)/RAD(J,I)
    2 DO 8 K=1,NG
      IF(N)3,3,4
    3 B=SGMTR(K,L)*RAD(J,I)
      GO TO 5
    4 B=SGMT(K,L)*RAD(J,I)
    5 IF(J-1)6,6,7
    6 TPOO(1,I,K)=TCYL(B)
      GO TO 8
    7 TPOO(J,I,K)=TOO(A,B)
      TPOI(J-1,I,K)=TOI(A,B)
    8 CONTINUE
      IF(KK)26,26,24
   26 M=NSA+NSR
      K=NR(1)
      R=RAD(K,1)
C     TO BE ABLE TO USE DANCOFF FACTOR ALL OUTERMOST RADII MUST BE EQUAL
      X=0.
      DO 16 I=1,NSA
      A=R/ATAS(I)
      Y=DCFR(A,0.)*WIL(I)
      X=X+Y
      IF(X-1.)10,10,9
    9 Y=(1.-(X-Y))/Y
   10 DO 15 L=1,NG
      IF(N)11,11,12
   11 B=SGMTR(L,1)*R
      GO TO 13
   12 B=SGMT(L,1)*R
   13 DTP(I,L)=DCFR(A,B)
      IF(X-1.)15,15,14
   14 DTP(I,L)=DTP(I,L)*Y
   15 CONTINUE
      IF(X-1.)16,16,17
   16 CONTINUE
      GO TO 20
   17 IF(I-NSA)18,20,20
   18 J=I+1
      DO 19 I=J,NSA
```

```
      DO 19 L=1,NG
   19 DTP(I,L)=0.
   20 J=NSA+1
      IF(M-J)24,27,27
   27 DO 23 I=J,M
      A=R/ATAS(I)
      DO 23 L=1,NG
      IF(N)21,21,22
   21 B=SGMTR(L,1)*R
      GO TO 23
   22 B=SGMT(L,1)*R
   23 DTP(I,L)=DCFR(A,B)
   24 RETURN
      END
*     LIST8
*     LABEL
*     SYMBOL TABLE
CJVECTR
      SUBROUTINE JVECTR(NR,INT,IG,ISC,NST,SGMT,SGMTR,SGMIJ,SPRM,FS,TPOO,
     1TPOI,RAD,ABT,AA,AQ,VA,VQ)
C     IG=GROUP INDEX, ISC=SYMMETRY CLASS INDEX,JVECTR=VA*ABSORPTION IN
C     REGION 1 + VQ. ABSORPTION IN REGION I=AA*ABSORPTION IN REGION 1+AQ
      DIMENSION TPOO(20,1, 20),TPOI(19,1, 20),NR(1) ,INT(20,1) ,AA(19,10
     1),AQ(19,10),AUX(2),SGMT( 5,10),SGMTR( 5,10),SGMIJ( 20,10),SPRM( 5)
     2,ABT(20,1, 20),VA(2,10),DMX(2,2),SIMX(2,2),FS(20,1) ,RAD(20,1)
     3,VQ(2,10)
      M=(IG*(IG+1))/2
      N=NST/4
      L=INT(1,ISC)
      IF(N)2,2,3
    2 C=(SGMTR(IG,L)-SGMT(IG,L)+SGMIJ(M,L))/SGMTR(IG,L)
      B=RAD(1,ISC)*SGMTR(IG,L)
      GO TO 4
    3 C=SGMIJ(M,L)/SGMT(IG,L)
      B=RAD(1,ISC)*SGMT(IG,L)
    4 X=TPOO(1,ISC,IG)
      E=(1.-X)/(2.*B)
      VA(1,ISC)=((1.-C)*X+C*E)/(1.-X)
      VA(2,ISC)=(1.-C+C*E)/(1.-X)
      Q=SPRM(IG)*FS(1,ISC)
      K=IG-1
      IF(K)9,9,5
    5 DO 8 I=1,K
      M=(IG*(IG+1))/2-K-1+I
      IF(N)6,6,7
    6 Q=Q+ABT(1,ISC,I)*SGMIJ(M,L)/SGMTR(I,L)
      GO TO 8
    7 Q=Q+ABT(1,ISC,I)*SGMIJ(M,L)/SGMT(I,L)
    8 CONTINUE
    9 VQ(1,ISC)=(E-X)*Q/(1.-X)
      VQ(2,ISC)=(E-1.)*Q/(1.-X)
      MM=NR(ISC)-1
      IF(MM)26,26,1
```

```
    1 DO 25 I=1,MM
      CALL MATS(INT,I+1,ISC,IG,NST,SGMT,SGMTR,SGMIJ,TPOO,TPOI,RAD,DMX,
     1SIMX,EO,EI,C)
      L=INT(I+1,ISC)
   10 AA(I,ISC)=(VA(1,ISC)-VA(2,ISC))/(1.-C)
      AQ(I,ISC)=(VQ(1,ISC)-VQ(2,ISC))/(1.-C)
      Q=SPRM(IG)*FS(I+1,ISC)
      IF(K)15,15,11
   11 DO 14 J=1,K
      M=(IG*(IG+1))/2-K-1+J
      IF(N)12,12,13
   12 Q=Q+ABT(I+1,ISC,J)*SGMIJ(M,L)/SGMTR(J,L)
      GO TO 14
   13 Q=Q+ABT(I+1,ISC,J)*SGMIJ(M,L)/SGMT(J,L)
   14 CONTINUE
   15 DO 16 J=1,2
      AUX(J)=0.
      DO 16 JJ=1,2
   16 AUX(J)=AUX(J)+DMX(J,JJ)*VQ(JJ,ISC)
      AUX(1)=AUX(1)+Q*EO
      AUX(2)=AUX(2)+Q*EI
      DO 17 J=1,2
      VQ(J,ISC)=0.
      DO 17 JJ=1,2
   17 VQ(J,ISC)=VQ(J,ISC)+SIMX(J,JJ)*AUX(JJ)
      DO 18 J=1,2
      AUX(J)=0.
      DO 18 JJ=1,2
   18 AUX(J)=AUX(J)+DMX(J,JJ)*VA(JJ,ISC)
      DO 19 J=1,2
      VA(J,ISC)=0.
      DO 19 JJ=1,2
   19 VA(J,ISC)=VA(J,ISC)+SIMX(J,JJ)*AUX(JJ)
      AA(I,ISC)=AA(I,ISC)+(VA(2,ISC)-VA(1,ISC))/(1.-C)
      AQ(I,ISC)=AQ(I,ISC)+(VQ(2,ISC)-VQ(1,ISC)+Q)/(1.-C)
   25 CONTINUE
   26 RETURN
      END
*     LIST8
*     LABEL
*     SYMBOL TABLE
CMATS
      SUBROUTINE MATS(INT,I,J,K,NST,SGMT,SGMTR,SGMIJ,TPOO,TPOI,RAD,DMX,
     1SIMX,EO,EI,C)
C     I,J,K ARE REGION,SYMMETRY CLASS AND GROUP INDICES. DMX IS RIGHT
C     MATRIX. SIMX IS INVERSE OF LEFT MATRIX
      DIMENSION SGMT( 5,10),SGMTR( 5,10),SGMIJ( 20,10),TPOO(20,1, 20),
     1TPOI(19,1, 20),INT(20,1) ,DMX(2,2),SIMX(2,2),RAD(2 ,1)
      M=(K*(K+1))/2
      N=NST/4
      L=INT(I,J)
      A=RAD(I-1,J)/RAD(I,J)
    1 IF(N)2,2,3
```

```
     2 C=(SGMTR(K,L)-SGMT(K,L)+SGMIJ(M,L))/SGMTR(K,L)
       B=RAD(I,J)*SGMTR(K,L)
       GO TO 4
     3 C=SGMIJ(M,L)/SGMT(K,L)
       B=RAD(I,J)*SGMT(K,L)
     4 X=TPOI(I-1,J,K)
       Y=TPOO(I,J,K)
       DEN=2.*B*(1.-A**2)
       G=A*X+Y
       EO=(1.-G)/DEN
       EI=(1.-X)*A/DEN
       DMX(1,1)=X*(1.-C*(1.-EI))+C*EO
       DMX(1,2)=0.
       DMX(2,1)=C*EI*(1.-X)
       DMX(2,2)=-(1.-C*(1.-EO-EI))
       SIMX(1,1)=-1./DMX(2,2)
       SIMX(2,2)=-1./(A*X*(1.-C*(1.-EO))+C*EI*(1.-Y))
       SIMX(1,2)=(Y*(1.-C*(1.-EI))+C*EO*(1.-A*X))*SIMX(1,1)*SIMX(2,2)
       SIMX(2,1)=0.
    21 RETURN
       END
*      LIST8
*      LABEL
*      SYMBOL TABLE
       SUBROUTINE SOLN (L,NG,NSC,NST,NSA,NSR,NR,INT,NWSC,SGMT,SGMTR,SGMIJ
      1,FS,FSM,SPRM,DTP,TPOO,TPOI,RAD,RADC,ABT,ABM,WTS)
CSOLN
       DIMENSION NR(10),INT(20,1),NWSC(1),SGMT( 5,10),SGMTR( 5,10),
      1     FS(20,1),         DTP(24,20),TPOO(20,1,20),TPOI(19,1,20),RAD(2
      20,1),ABT(20,1,20),ABM(20),AA(19,10),AQ(19,10),VA(2,10),VQ(2,10),
      3AUX(10,10),ANC(10,1),G(10,10),EQ(10),WTS(24,1,1) ,
      4SGMIJ(135,10),SPRM( 5)
       DO 18 IG=1,NG
       IF(L) 13,13,14
    13 CALL MOD(IG,NSC,NST,NSA,NSR,NR,NWSC,SGMT,SGMTR,SGMIJ,WTS,DTP,RAD,
      1RADC,ABM,SPRM,FSM,G,EQ,HII,C,Q)
    14 DO 1 ISC=1,NSC
     1 CALL JVECTR(NR,INT,IG,ISC,NST,SGMT,SGMTR,SGMIJ,SPRM,FS,TPOO,TPOI,
      1RAD,ABT,AA,AQ,VA,VQ)
       IF(L) 15,15,16
    15 DO 2 I=1,NSC
       DO 2 J=1,NSC
     2 AUX(I,J)=G(I,J)*VA(1,J)
       DO 3 I=1,NSC
     3 AUX(I,I)=AUX(I,I)+HII*VA(2,I)
       DO 4 I=1,NSC
       ANC(I,1)=0.0
       DO 4 J=1,NSC
     4 ANC(I,1)=ANC(I,1)+G(I,J)*VQ(1,J)
       DO 5 I=1,NSC
     5 ANC(I,1)=-ANC(I,1)-HII*VQ(2,I)+EQ(I)
       IF(NSC-1) 20,20,21
    21 PRINT 100
```

```
  100 FORMAT(17H LEQ WAS REACHED      )
      CALL EXIT
   20 ANC(1,1)=ANC(1,1)/AUX(1,1)
      GO TO 10
   16 ANC(1,1)=(VQ(2,1)-VQ(1,1))/(VA(1,1)-VA(2,1))
   10 DO 7 I=1,NSC
      K=NR(I)-1
      ABT(1,I,IG)=ANC(I,1)
      IF(K) 7,7,6
    6 DO 9 J=1,K
    9 ABT(J+1,I,IG)=AA(J,I)*ANC(I,1)+AQ(J,I)
    7 CONTINUE
      IF(L) 17,17,18
   17 ABM(IG)=Q
      DO 8 I=1,NSC
    8 ABM(IG)=ABM(IG)+FLOATF(NWSC(I))*(ANC(I,1)*(VA(1,I) VA(2,I))+VQ(1,I
     1)-VQ(2,I))
      ABM(IG)=ABM(IG)/(1.0-C)
   18 CONTINUE
      RETURN
      END
*     LIST8
*     LABEL
*     SYMBOL TABLE
CDCFR
      FUNCTION DCFR(R,S)
C     COMPUTES DANCOFF FACTOR AS FUNCTION OF R=RADIUS/(AXIS-TO-AXIS SEP-
C     ARATION) AND OF S=SIGMA*RADIUS
      RADF(U,V)=SQRTF(1./R**2-(U+V)**2)
      DANF(U,V)=BEKI3(S*(RADF(U,V)-SQRTF(1.-U**2)-SQRTF(1.-V**2)))/RADF(
     1U,V)
      DIMENSION A(8),H(8)
      A(1)=0.98940093
      A(2)=0.94457502
      A(3)=0.86563120
      A(4)=0.75540441
      A(5)=0.61787624
      A(6)=0.45801678
      A(7)=0.28160355
      A(8)=0.09501251
      H(1)=0.02715246
      H(2)=0.06225352
      H(3)=0.09515851
      H(4)=0.12462897
      H(5)=0.14959599
      H(6)=0.16915652
      H(7)=0.18260342
      H(8)=0.18945061
      IF(S)4,5,4
    4 SUM=0.
      DO 3 I=1,8
      DO 3 J=1,I
      IF(I-J)2,2,1
```

```
     1 SUM=SUM+4.*H(I)*H(J)*(DANF(A(I),A(J))+DANF(A(I),-A(J)))
       GO TO 3
     2 SUM=SUM+2.*H(J)**2*(DANF(A(J),A(J))+DANF(A(J),-A(J)))
     3 CONTINUE
       DCFR=.10132118*SUM
       GO TO 8
     5 B=2.*R
       E=SQRTF(1.-B**2)
       IF(E)6,6,7
     6 DCFR=.18169012
       GO TO 8
     7 C=ATANF(B/E)
       DCFR=.31830988*(C-SINF(.5*C)/COSF(.5*C))
     8 RETURN
       END
*      LIST8
*      LABEL
*      SYMBOL TABLE
CBEKI3
       FUNCTION BEKI3(X)
       IF(X-.1)1,2,2
     1 BEKI3=.73665545/(.93793888+X*(1.1941916+X*(.58824515+X*(.57033719+
      1X*(-1.5791166+X*4.292469)))))
       GO TO 9
     2 IF(X-.4)3,4,4
     3 BEKI3=.57149776/(.72767871+X*(.92546909+X*(.474152 8+X*(.25082036+
      1X*(-.025930075+X*.055707999)))))
       GO TO 9
     4 IF(X-1.)5,6,6
     5 BEKI3=.32724738/(.41667409+X*(.52956551+X*(.27542730+X*(.12837751+
      1X*(.011919149+X*.013920954)))))
       GO TO 9
     6 IF(X-2.5)7,8,8
     7 BEKI3=(.22159402+X*(-.093883791+X*(.014738215-X*.0  85765003)))/(
      1.28267237+X*(.23563203+X*(.063402052+X*.013600324)))
       GO TO 9
     8 Y=1./(X+3.25)
       BEKI3=1.2684458*SQRTF(Y)*EXPF(-X)/(1.0120742+Y*(-.  0325432+Y*(
      1-1.1646323+Y*(1.3873864-Y*4.4655208))))
     9 RETURN
       END
*      LIST8
*      LABEL
*      SYMBOL TABLE
CTCYL
       FUNCTION TCYL(B)
       IF(B-5.)1,1,2
     1 IF(B-.001) 5,4,4
     4 T0=BI0(B)
       T1=BI1(B)
       U0=BK0(B)
       U1=BK1(B)
       TCYL=1.-4.*B**2/3.*(2.*(B*(U1*T1+U0*T0)-1.)+U1*T1/B-U0*T1+U1*T0)
```

```
      GO TO 3
    5 TCYL=1.-B*(2.-B*(2.6666667-B*(1.3659315-LOGF(B))))
      GO TO 3
    2 TCYL=3./(16.*B**2)*(1.+5./(8.*B**2))
    3 RETURN
      END
*     LIST8
*     LABEL
*     SYMBOL TABLE
CTOO
      FUNCTION TOO(A,B)
      DIMENSION X(7),H(7)
      X(1)=.98628381
      X( 2)=.92843488
      X( 3)=.82720132
      X( 4)=.68729290
      X( 5)=.51524864
      X( 6)=.31911237
      X( 7)=.10805495
      H(1)=.035119460
      H( 2)=.080158087
      H( 3)=.12151857
      H( 4)=.15720317
      H( 5)=.18553840
      H( 6)=.20519846
      H( 7)=.21526385
      SUM=0.
      IF(B-.001) 2,2,4
    2 DO 3 I=1,7
      Y=B*2.*SQRTF(1.-X(I)**2)
      Z=B*2.*SQRTF(1.-(A*X(I))**2)
    3 SUM=SUM+(Y**3*(.32487747*(1.+.024358732*Y**2)-LOGF(Y)*(1.+.025*Y**
     12)/6.)-Z**3*(.32487747*(1.+.024358732*Z**2)-LOGF(Z)*(1.+.025*Z**2)
     2/6.)*A)*H(I)
      TOO=  -1.2732395*SUM
      C=SQRTF(1.-A**2)
      TERM=    A+B*(2.-1.2732395*(A*C+ATANF(A/C)))-4.*B**2*(2.-3.*A+A**3)
     1/3.
      TERM=1.-TERM
      TOO=TOO+TERM
      GO TO 5
    4 DO 1 I=1,7
    1 SUM=SUM+BEKI3(2.*B*SQRTF(1.-(A*X(I))**2))*H(I)
      TOO=TCYL(B)-1.2732395*A*SUM
    5 RETURN
      END
*     LIST8
*     LABEL
*     SYMBOL TABLE
CTO1
      FUNCTION TOI(A,B)
      DIMENSION X(7),H(7)
      X(1)=.98628381
```

```
      X( 2)=.92843488
      X( 3)=.82720132
      X( 4)=.68729290
      X( 5)=.51524864
      X( 6)=.31911237
      X( 7)=.10805495
      H(1)=.035119460
      H( 2)=.080158087
      H( 3)=.12151857
      H( 4)=.15720317
      H( 5)=.18553840
      H( 6)=.20519846
      H( 7)=.21526385
      TOI=0.
      IF(B-.001) 2,2,4
    2 DO 3 I=1,7
      Y=B*(SQRTF(1.-(A*X(I))**2)-A*SQRTF(1.-X(I)**2))
    3 TOI=TOI+Y**2*(.78539816-.32487747*Y*(1.+.024358732*Y**2)+Y*LOGF(Y)
     1*(1.+.025*Y**2)/6.)*H(I)
      TOI=TOI*1.2732395
      C=SQRTF(1.-A**2)
      TERM=B*(.63661976*(C+ATANF(A/C)/A)-A)
      TERM=1.-TERM
      TOI=TOI+TERM
      GO TO 5
    4 DO 1 I=1,7
    1 TOI=TOI+H(I)*BEKI3(B*(SQRTF(1.-(A*X(I))**2)-A*SQRTF(1.-X(I)**2)))
      TOI=TOI*1.2732395
    5 RETURN
      END
*     LIST8
*     LABEL
*     SYMBOL TABLE
CBI0
      FUNCTION BI0 (X)
      IF (X - 3.75) 2, 2, 3
    2 Z = (X / 3.75)**2
      BI0 = 1.0 + Z * (3.5156229 + Z * (3.0899424 + Z * (1.2067492 +
     1      Z * (0.2659732 + Z * (0.0360768 + Z * 0.0045813)))))
      GO TO 4
    3 Z = 3.75 / X
      BI0 = (EXPF(X) / SQRTF(X)) * (.39894228 + Z * (.013285917 + Z *
     1      (.002253187 + Z * (-.001575649 + Z * (.009162808 + Z *
     2      (-.020577063 + Z * (.026355372 + Z * (-.016476329 + Z *
     3      .003923767)))))))
    4 RETURN
      END
*     LIST8
*     LABEL
*     SYMBOL TABLE
CBI1
      FUNCTION BI1 (X)
      IF (X - 3.75) 2, 2, 3
```

```
     2 Z = (X / 3.75)**2
       BI1 = (.5 + Z * (.87890594 + Z * (.51498869 + Z * (.15084934 +
      1      Z * (.02658733 + Z * (.00301532 + Z * .00032411))))))) * X
       GO TO 4
     3 Z = 3.75 / X
       BI1 = (EXPF(X) / SQRTF(X)) * (.39894228 + Z * (-.039880242 + Z *
      1      (-.003620183 + Z * (.001638014 + Z * (-.01031555 + Z *
      2      (.022829673 + Z * (-.028953121 + Z * (.017876535 - Z *
      3      .004200587)))))))))
     4 RETURN
       END
*      LIST8
*      LABEL
*      SYMBOL TABLE
CBK0
       FUNCTION BK0 (X)
       IF (X - 2.0) 2, 2, 3
     2 Z = (X / 2.0)**2
       SERIES = -.57721566 + Z * (.4227842 + Z * (.23069756 + Z *
      1         (.0348859 + Z * (.00262698 + Z * (.0001075 + Z *
      2         .0000074)))))
       BK0 = SERIES - LOGF(X / 2.0) * BI0(X)
       GO TO 4
     3 Z = 2.0 / X
       BK0 = (1.2533141 + Z * (-.07832358 + Z * (.02189568 + Z *
      1      (-.01062446 + Z * (.00587872 + Z * (-.0025154 + Z *
      2      .00053208)))))) / (SQRTF(X) * EXPF(X))
     4 RETURN
       END
*      LIST8
*      LABEL
*      SYMBOL TABLE
CBK1
       FUNCTION BK1 (X)
       IF (X - 2.0) 2, 2, 3
     2 Z = (X / 2.0)**2
       SERIES = 1.0 + Z * (.15443144 + Z * (-.67278579 + Z * (-.18156897
      1         + Z * (-.01919402 + Z * (-.00110404 - Z * .00004686)))))
       BK1 = SERIES / X + LOGF(X / 2.0) * BI1(X)
       GO TO 4
     3 Z = 2.0 / X
       BK1 = (1.2533141 + Z * (.23498619 + Z * (-.0365562   Z *
      1      (.01504268 + Z * (-.00780353 + Z * (.00325614 - Z *
      2      .00068245)))))) / (SQRTF(X) * EXPF(X))
     4 RETURN
       END
```

A.2.3 Sample Problem Treated with HEETR

```
*      DATA
000050000500010
4.95954    6.3196     8.63314    12.08232   14.01025   2.09405    2.73877
4.08302    6.21482    6.02223    0.09971                           0.00012
0.00020
                                                1.89093    1.4157     2.25252
0.61952    1.72336    3.04283    0.36910    0.92209    2.5515     4.66028
0.22214    0.55928    1.19568    3.45950    4.99393    0.34243    0.86211
1.84314    3.96243    9.01612    18.0
5.09747    6.10316    7.64974    9.67943    9.54225    3.11383    4.36451
6.15525    8.34681    7.46256    0.09707
                                                2.37824    1.54055    2.60086
0.37541    1.51716    2.91605    0.39792    0.73164    2.00747    3.80133
0.34311    0.68156    1.13754    2.60717    3.61584    0.03997    0.57194
1.58869    3.27094    5.92642    20.0
1.37       1.6        2.         2.48       2.97       1.37       1.6
2.         2.48       2.97       0.0263     0.0003     0.0004     0.0004
0.0007
                                                0.6917     0.305      1.0627
0.159      0.36       1.5696     0.095      0.083      0.331      2.0916
0.051      0.071      0.078      0.346      2.5653     0.042      0.023
0.021      0.042      0.404      27.0
3.88       4.73       4.86       5.08       5.58       3.88       4.73
4.86       5.08       5.58       0.02       0.035      0.058      0.115
0.193      1.21       1.29       1.31       1.27       1.22       3.09
2.79       2.62       2.53       2.52       0.661      0.11       1.454
0.337      0.201      1.857      0.507      0.421      0.343      2.409
0.475      0.52       0.611      0.437      3.396      0.560      0.809
0.681      0.849      0.771      235.0
3.9        4.63       4.87       5.01       5.59       3.9        4.63
4.87       5.01       5.59       0.010      0.022      0.057      0.129
0.139      0.609      0.581      0.43       0.024      0.         3.1
2.78       2.6        2.56       0.         0.774      0.135      1.483
0.425      0.257      2.476      0.64       0.551      0.739      3.893
0.6        0.678      0.865      0.595      4.921      0.707      1.058
0.303      0.369      0.530      238.0
3.6788     2.2313     1.3534     0.82085    0.49787
H2O   D2O   ALUM  U235  U238
000010001500001000050001200001000010000420002000100010
  DIAM.=0.25 IN., SPAC.=2.5 IN., ENRICH.=1.14 PER CENT
1.1042     0.004      0.996      0.         0.         0.
18.9       0.         0.         0.         0.0114     0.9886
18.9       0.         0.         0.                    0.9886
0.0005     0.         1.         0.         0.         0.
2.7        0.         0.         1.         0.         0.
000020000200002000020000400005000010000100001000010000100001000010  010000100001
00001
0.0794     0.1587     0.2381     0.3175     0.3329     0.4040     0.5080
0.762      1.016      1.270      1.524      1.778      2.032      2.286
2.54
0.05967    0.18152    0.30950    0.44931


1.         0.         3.3270     2.43       1.37
```

HEETR CODE COMPUTES EVENTS IN CYLINDRICAL CELLS FROM ESCAPE AND TRANSMISSION PROBABILITIES

PROBLEM NUMBER2C002

DIAM.=0.25 IN., SPAC.=2.5 IN., ENRICH.=1.14 PER CENT

SOURCE SUPPLIED FOR EACH REGION IS RELATIVE NUMBER OF NEUTRONS PRODUCED BY FISSIONS OCCURRING IN GROUP NG+1.

TRANSMISSICN AND ESCAPE PROBABILITIES ARE COMPUTED FROM TRANSPORT CROSS SECTIONS.

THE CELL APPROXIMATICN IS MADE WITH ZERO CURRENT AT THE CELL BOUNDARY.

		WEIGHT FRACTION OF				
TYPE NO.	DENSITY(G/CC)	H2O	D2O	ALUM	U235	U238
1	1.10420	.004000	.996000	0.	0.	0.
2	18.90000	0.	0.	0.	.011400	.988600
3	18.90000	0.	0.	0.	0.	.988600
4	.00050	0.	1.000000	0.	0.	0.
5	2.70000	0.	0.	1.000000	0.	0.

THERMAL VALUE OF NU=2.430 TEMPERATURE OF FISSION SPECTRUM MAXWELLIAN=1.370

PRINTOUT OF AVERAGED CONSTANTS

GROUP	EL(MEV)	SPECTRUM	FLUX	SIGMA-T	SIGMA-TR	SIGMA-C	SIGMA-F	NU*SIGMA-F	NU
1	3.679E 00	.14659	1.4496E-01	.1686	.1061	.00309	.00113	.00350	3.0998
2	2.231E 00	.20703	2.2242E-01	.2019	.1468	.00004	.00103	.00287	2.7803
3	1.353E 00	.22383	2.1495E-01	.2511	.2038	.00011	.00087	.00227	2.6007
4	8.208E-01	.17596	1.9891E-01	.3158	.2733	.00024	.00007	.00018	2.5485
5	4.979E-01	.11346	2.1877E-01	.3145	.2473	.00019	.00002	.00005	2.5200

SIGMA-IJ (TRANSFER TO GROUP I FROM GROUP J), ARRANGED AS 11, 21, 22, 31, 32, 33,...,(NG+1)(NG)

.0767	.0489	.0854	.0127	.0486	.0976	.0138	.0241	.0647	.1285	.0119
.0227	.0374	.0834	.1238	.0026	.0199	.0504	.1036	.1905		

PARAMETERS AVERAGED OVER SPACE AND ENERGY

SIGMA-T= .25492 SIGMA-TR= .20029 1/(TRMFP)= .18020 SIGMA-C= .000571 SIGMA-F= .000600 NU= 2.8039
NU*SIGMA-F= .001682 SIGMA-REMOVAL= .077930 TAU (TRMFP/(3*SIGMA-(C+F+R-NU*F)))= 23.893
FRACTION OF SOURCE NEUTRONS ARISING FROM THERMAL FISSIONS= .981483
RATIO OF FAST TO THERMAL FISSIONS= .01635
OVERALL RATIO OF U-238 TO U-235 FISSIONS= .01564

SYMMETRY CLASS, REGION	1, 1	1, 2	1, 3	1, 4
U-238/U-235 FISSIONS	.01949	.01806	.01612	.01382

DISADVANTAGE FACTORS AND VOLUME FRACTIONS

CLASS 1 NO.= 1 REGN 1 TYPE 2 RADIUS= .0794 VOL FRACT= .00057 THRML FISS SRCE= .05967 LAST ITER= .05967

GROUP	1	2	3	4	5
DISADVNTG FCTR	5.01564	4.77603	5.42884	5.12156	3.61768

CLASS 1 NO.= 1 REGN 2 TYPE 2 RADIUS= .1587 VOL FRACT= .00171 THRML FISS SRCE= .18152 LAST ITER= .18152

GROUP	1	2	3	4	5
DISADVNTG FCTR	4.71580	4.49822	5.10565	4.82447	3.42812

CLASS 1 NO.= 1 REGN 3 TYPE 2 RADIUS= .2381 VOL FRACT= .00285 THRML FISS SRCE= .30950 LAST ITER= .30950

GROUP	1	2	3	4	5
DISADVNTG FCTR	4.29694	4.10788	4.65281	4.40879	3.16279

CLASS 1 NO.= 1 REGN 4 TYPE 2 RADIUS= .3175 VOL FRACT= .00399 THRML FISS SRCE= .44931 LAST ITER= .44931

GROUP	1	2	3	4	5
DISADVNTG FCTR	3.81639	3.65879	4.13092	3.93078	2.85751

CLASS 1 NO.= 1 REGN 5 TYPE 4 RADIUS= .3329 VOL FRACT= .00090 THRML FISS SRCE=0. LAST ITER=0.

GROUP	1	2	3	4	5
DISADVNTG FCTR	3.31423	3.13469	3.54304	3.39169	2.51156

CLASS 1 NO.= 1 REGN 6 TYPE 5 RADIUS= .4040 VOL FRACT= .00473 THRML FISS SRCE=0. LAST ITER=0.

GROUP	1	2	3	4	5
DISADVNTG FCTR	2.67893	2.61135	2.93288	2.85490	2.18878

CLASS 1 NO.= 1 REGN 7 TYPE 1 RADIUS= .5080 VOL FRACT= .00857 THRML FISS SRCE=0. LAST ITER=0.

GROUP	1	2	3	4	5

```
    DISADVNTG FCTR    2.02447   2.19535   2.42739   2.38955   1.91298

CLASS 1  NC.= 1   REGN  8   TYPE 1   RADIUS=   .7620   VOL FRACT= .02914   THRML FISS SRCE=0.        LAST ITER=0.
         GROUP          1         2         3         4         5
    DISADVNTG FCTR    1.66693   1.65739   1.80269   1.80199   1.53635

CLASS 1  NC.= 1   REGN  9   TYPE 1   RADIUS=  1.0160   VOL FRACT= .04080   THRML FISS SRCE=0.        LAST ITER=0.
         GROUP          1         2         3         4         5
    DISADVNTG FCTR    1.35446   1.35538   1.43714   1.44559   1.30668

CLASS 1  NC.= 1   REGN 10   TYPE 1   RADIUS=  1.2700   VOL FRACT= .05246   THRML FISS SRCE=0.        LAST ITER=0.
         GROUP          1         2         3         4         5
    DISADVNTG FCTR    1.17888   1.18272   1.22664   1.23627   1.16823

CLASS 1  NC.= 1   REGN 11   TYPE 1   RADIUS=  1.5240   VOL FRACT= .06411   THRML FISS SRCE=0.        LAST ITER=0.
         GROUP          1         2         3         4         5
    DISADVNTG FCTR    1.06838   1.07266   1.09147   1.09968   1.07584

CLASS 1  NC.= 1   REGN 12   TYPE 1   RADIUS=  1.7780   VOL FRACT= .07577   THRML FISS SRCE=0.        LAST ITER=0.
         GROUP          1         2         3         4         5
    DISADVNTG FCTR     .99443    .99816    .99940   1.00540   1.01082

CLASS 1  NC.= 1   REGN 13   TYPE 1   RADIUS=  2.0320   VOL FRACT= .08743   THRML FISS SRCE=0.        LAST ITER=0.
         GROUP          1         2         3         4         5
    DISADVNTG FCTR     .94332    .94615    .93476    .93845    .96389

CLASS 1  NC.= 1   REGN 14   TYPE 1   RADIUS=  2.2860   VOL FRACT= .09939   THRML FISS SRCE=0.        LAST ITER=0.
         GROUP          1         2         3         4         5
    DISADVNTG FCTR     .91764    .91995    .88897    .89056    .92984

CLASS 1  NC.= 1   REGN 15   TYPE 1   RADIUS=  2.5400   VOL FRACT= .11074   THRML FISS SRCE=0.        LAST ITER=0.
         GROUP          1         2         3         4         5
    DISADVNTG FCTR     .88298    .88395    .85693    .85672    .91550

CLASS 1  NC.= 1   REGN 16   TYPE 1   RADIUS=  3.3270   VOL FRACT= .41714   THRML FISS SRCE=0.        LAST ITER=0.
         GROUP          1         2         3         4         5
    DISADVNTG FCTR     .83233    .83573    .81230    .81412    .86575
```

.15CC00E 02 .547701E-03 .547701E- 3 .141416E-03

REACTION RATE RATIO MATRIX

	PU(NF)	NP(NF)	IN(NN)	DU(NF)	NI(NP)	TH(NF)	ZN(NP)	S(NP)	P(NP)	AL(NP)	SI(NP)	FE(NP)	AL(NA)	IN(N2)	MG(NP)	RH(NN)
PU(NF)	1.00	.85	7.50	4.10	1 .47	17.57	37.45	18.50	41.88	281.35	96.60	874.681059.07		512.29	524.78	2.58
NP(NF)	1.18	1.00	8.87	4.85	13.38	20.79	44.29	21.88	49.54	332.78	114.261034.591252.69			605.95	620.73	3.05
IN(NN)	.13	.11	1.00	.55	1.40	2.34	4.99	2.47	5.59	37.52	12.88	116.65	141.24	68.32	69.99	.34
DU(NF)	.24	.21	1.83	1.00	2.55	4.28	9.13	4.51	10.21	68.56	23.54	213.16	258.09	124.84	127.89	.63
NI(NP)	.10	.08	.72	.39	1.00	1.68	3.58	1.77	4.00	26.88	9.23	83.58	101.20	48.95	50.15	.25
TH(NF)	.06	.05	.43	.23	.60	1.00	2.13	1.05	2.38	16.01	5.50	49.77	60.27	29.15	29.86	.15
ZN(NP)	.03	.02	.20	.11	.28	.47	1.00	.49	1.12	7.51	2.58	23.36	28.28	13.68	14.01	.07
S(NP)	.05	.05	.41	.22	.57	.95	2.02	1.00	2.26	15.21	5.22	47.29	57.26	27.70	28.37	.14
P(NP)	.02	.02	.18	.10	.25	.42	.89	.44	1.00	6.72	2.31	20.88	25.29	12.23	12.53	.06
AL(NP)	.00	.00	.03	.01	.04	.06	.13	.07	.15	1.00	.34	3.11	3.76	1.82	1.87	.01
SI(NP)	.01	.01	.08	.04	.11	.18	.39	.19	.43	2.91	1.00	9.06	10.96	5.30	5.43	.03
FE(NP)	.00	.00	.01	.00	.01	.02	.04	.02	.05	.32	.11	1.00	1.21	.59	.60	.00
AL(NA)	.00	.00	.01	.00	.01	.02	.04	.02	.04	.27	.09	.83	1.00	.48	.50	.00
IN(N2)	.00	.00	.01	.01	.02	.03	.07	.04	.08	.55	.19	1.71	2.07	1.00	1.02	.01
MG(NP)	.00	.00	.01	.01	.02	.03	.07	.04	.08	.54	.18	1.67	2.02	.98	1.00	.00
RH(NN)	.39	.33	2.91	1.59	4.06	6.82	14.53	7.18	16.25	109.18	37.49	339.43	410.98	198.80	203.65	1.00

GROUP ACTIVATION PERCENTAGES

REACTION	1	2	3	4	5
PU(NF)	.182674E 00	.254335E 00	.230301E 00	.220960E 00	.111731E 00
NP(NF)	.167502E 00	.257540E 00	.238874E 00	.210328E 00	.125756E 00
IN(NN)	.194261E 00	.427091E 00	.256564E 00	.977389E-01	.243453E-01
DU(NF)	.303475E 00	.379195E 00	.279770E 00	.356574E-01	.190323E-02
NI(NP)	.615215E 00	.338794E 00	.459911E-01	.000000E 00	.000000E 00
TH(NF)	.346115E 00	.384737E 00	.256423E 00	.127253E-01	.000000E 00
ZN(NP)	.725763E 00	.229931E 00	.405172E-01	.379631E-02	.000000E 00
S(NP)	.641383E 00	.352009E 00	.660758E-02	.000000E 00	.000000E 00
P(NP)	.548107E 00	.420072E 00	.318210E-01	.000000E 00	.000000E 00
AL(NP)	.944499E 00	.555056E-01	.000000E 00	.000000E 00	.000000E 00
SI(NP)	.100000E 01	.000000E 00	.000000E 00	.000000E 00	.000000E 00
FE(NP)	.100000E 01	.000000E 00	.000000E 00	.000000E 00	.000000E 00
AL(NA)	.100000E 01	.000000E 00	.000000E 00	.000000E 00	.000000E 00
IN(N2)	.100000E 01	.000000E 00	.000000E 00	.000000E 00	.000000E 00
MG(NP)	.100000E 01	.000000E 00	.000000E 00	.000000E 00	.000000E 00
RH(NN)	.196671E 00	.289705E 00	.266939E 00	.186413E 00	.603022E-01

A.3 RATIO, Activation Ratio Calculation

The RATIO code uses the results of the HEETR code and differential cross section data to compute differential energy spectra, a matrix of the ratios of the threshold reactions involving fast neutrons, and the percentage of the total of the reaction rates, resulting from interactions with neutrons in each energy group. These results make it possible to compare the differential energy spectra characteristic of different lattices and of different regions within the same lattice. The results of the RATIO calculations also permit the determination of theoretical intracellular distributions of the activations of the threshold reactions which can then be compared with experimental results.

A.3.1 RATIO Input Data

The input data are given below in the order required for use with the code. The names of the variables for each FORMAT statement are given, followed by the required format in parentheses, and then by a brief description of the variables.

MAXU, MAX (2I4)

MAXU is the number of reactions for which calculations are to be done.

MAX is the number of energy mesh points (spaced 0.25 Mev apart) to be used in the numerical integration of the reaction rates. In the present work, the value of MAX was 60.

NMIN(I), I=1, MAXU (18I4)

NMIN(I) is the value of the lowest energy mesh point for which there is a non-zero value of the cross section for the reaction denoted by I . The use of NMIN(I) avoids the necessity for reading in large numbers of zeros for the values of the cross sections at energies below the threshold energies.

LABEL(I), I=1, MAXU (12A6)

LABEL(I) is a label composed of a total of no more than 6 spaces of numbers and letters that can be used to identify each of the reaction rates.

SIG(I, J), J=NMIN(I), MAX, I=1, MAXU (8E9.4)

SIG(I, J) is the value of the cross section for the reaction denoted by I at the energy corresponding to the mesh point denoted by J. A new card is started each time I advances (i. e., for each different reaction).

ID(I), I=1, 12 (12A6)

ID(I) is an identification statement used to label the results. ID(I) will be printed as the first line of the set of output data for the problem.

EL(J), J=1, 5 (6E12.6)

EL(J) is the value of the lower energy limit for the energy group denoted by J (J = 1 for the highest energy group). In the present work, the values of EL(J) corresponded to those given in Table 4.2.

FL(J), J=1, 5 (6E12.6)

FL(J) is the magnitude of the integral flux in the energy group denoted by J. In the present work, the values used for FL(J) were those listed under the heading, "FLUX," in the HEETR results.

T, NFG, MORE, IFS (E12.6, 6I4)

T is the temperature of the Maxwellian distribution of the fission neutrons. The discussion in section A.2.1 of T in the input data for the HEETR code is applicable here.

NFG is the number of energy mesh points contained in the highest energy group. In the present work, the value of MAX was 60 and the value of EL(1) was 3.7 Mev, so that NFG was 46.

MORE is a control character for a series of calculations with one batch of input data. If MORE is zero, the program will terminate at the end of the calculations for the first problem. If MORE is positive, at the end of the calculations for the first problem, the program will read in data for calculations for a new problem, beginning with ID(I); i. e., the same cross section data will be used in all the succeeding problems. If MORE is negative, at the end of the calculations for the first problem, the program will read in a value for FMLT1, which is discussed below, and repeat the calculations with no other changes in the input data.

IFS is a control character for calculations involving a fission neutron spectrum. If IFS is non-zero, the values of FL(J) do not enter into the calculations. The energy spectrum of the fast flux and the corresponding ratios of the reaction rates will be consistent with the spectrum of fission neutrons.

If MORE is negative:

FMLT1 (6E12.6)

FMLT1 is a multiplying factor used to change the value of the fast flux at the mesh point corresponding to an energy of 0.25 Mev. The lower limit of the lowest energy group used in the HEETR calculations was about 0.5 Mev. The spectrum must be extrapolated to lower energies because some of the reactions have thresholds below 0.5 Mev. The RATIO code is written so that normally the magnitude of the flux at 0.25 Mev will be the same as the value at 0.5 Mev. The use of FMLT1 makes it possible to make calculations for other values of the flux at 0.25 Mev. None of the results for spectra of interest in the present work were significantly affected by changes in the value of the fast flux at 0.25 Mev. For example, making the assumption that the magnitude of the fast flux at 0.25 Mev was twice the value at 0.5 Mev gave reaction rate ratios that differed by less than 1% from those obtained by making the assumption that the magnitude of the fast flux at 0.25 Mev was zero. These results are not surprising because even for those reactions having the lowest thresholds, the values of the cross sections at 0.25 Mev are small.

A.3.2 Fortran Listing of RATIO

A Fortran listing of the RATIO code is given below.

```
*      LIST8
*      LABEL
*      SYMBOL TABLE
C RATIO
       DIMENSION SIG(20,60),EL(10),FL(10),FLD(60),SPRM(60),RR(20),RRR(20,
      120),NMIN(20),LABEL(20),ID(12),R1(20),R2(20),R3(20),R4(20),R5(20),
      2RT(20),SPRX(60)
  500 FORMAT (6E12.6)
  501 FORMAT (12A6)
  502 FORMAT (8E9.4)
  503 FORMAT (2I4)
  504 FORMAT (18I4)
  505 FORMAT (E12.6,6I4)
  506 FORMAT(29H GROUP ACTIVATION PERCENTAGES ,/9H REACTION ,5X,2H 1,10X
      1,2H 2,10X,2H 3,10X,2H 4,10X,2H 5 )
  507 FORMAT(2X,A6,6E12.6)
  510 FORMAT (66H ENERGY(MEV)  DIFF. FLUX FISSION FLUX SPRM. FISSION DEN
      1SITY SPRM.    )
  520 FORMAT (28H0REACTION RATE RATIO MATRIX //)
  530 FORMAT (7X,18(1X,A6))
  540 FORMAT (1X,A6,18(F7.2))
  550 FORMAT (1H1,12A6)
  560 FORMAT (2E12.6,E16.6,E21.6)
C  IFS IS FISSION SPECTRUM CASE CONTROL, F.S. IF NON-ZERO
C  I1 IS CONTROL FOR FLUX AT 0.25 MEV, =0.5 MEV FLUX IF ZERO
C                IF NOT, READ IN FMLT1
C  I2 IS CONTROL FOR GRP. PERCENTAGE OF ACT. CALC., CALCULATED IF ZERO
       READ INPUT TAPE 4,503,MAXU,MAX
       READ INPUT TAPE 4,504,(NMIN(I),I=1,MAXU)
       READ INPUT TAPE 4,501,(LABEL(I),I=1,MAXU)
       DO 5 I=1,MAXU
       N=NMIN(I)
     5 READ INPUT TAPE 4,502,(SIG(I,J),J=N,MAX)
       DO 20 I=1,MAXU
       N=NMIN(I)
       NN=N-1
       IF(N-1) 300,20,12
    12 DO 15 J=1,NN
    15 SIG(I,J)=0.0
    20 CONTINUE
    10 READ INPUT TAPE 4,501,(ID(I),I=1,12)
       WRITE OUTPUT TAPE 2,550,(ID(I),I=1,12)
       READ INPUT TAPE 4,500,(EL(J),J=1,5)
       READ INPUT TAPE 4,500,(FL(J),J=1,5)
       READ INPUT TAPE 4,505,T,NFG,MORE,IFS
       DO 40 J=2,5
    40 FL(J)=FL(J)/FL(1)
       FL(1)=1.0
       DO 117 I=1,60
       KI=61-I
       IF(I-1) 115,115,116
   115 SM=FNSPM(15.25,T)
       SPRM(60)=FNSPM(15.0,T)-SM
       GO TO 117
   116 SM=SM+SPRM(KI+1)
```

```
      EI=15.0-0.25*FLOATF(I-1)
      SPRM(KI)=FNSPM(EI,T)-SM
  117 CONTINUE
      AVG=0.0
      KI=61-NFG
      DO 120 K=KI,60
      I=61-K
      EI=15.0-0.25*FLOATF(I-1)
  120 AVG=AVG+SPRM(K)*SQRTF(EI)
      AVG=AVG/FLOATF(60-KI+1)
      RAT=FL(1)/((15.0-EL(1))*AVG)
      DO 125 K=KI,60
      I=61-K
      EI=15.0-0.25*FLOATF(I-1)
  125 FLD(K)=SPRM(K)*RAT*SQRTF(EI)
      DO 122 K=1,60
      I=61-K
      EI=15.0-0.25*FLOATF(I-1)
      SPRX(K)=SPRM(K)*RAT*SQRTF(EI)
  122 SPRM(K)=SPRM(K)*RAT
      IF(IFS) 200,130,200
  130 DO 135 K=1,3
  135 FLD(K)=FL(5)/(EL(4)-EL(5))
      DO 140 K=4,5
  140 FLD(K)=FL(4)/(EL(3)-EL(4))
      DO 145 K=6,8
  145 FLD(K)=FL(3)/(EL(2)-EL(3))
      DO 150 K=9,14
  150 FLD(K)=FL(2)/(EL(1)-EL(2))
      GO TO 200
  170 READ INPUT TAPE 4,500,FMLT1
      FLD(1)=FLD(1)*FMLT1
  200 WRITE OUTPUT TAPE 2,510
      DO 210 K=1,60
      E=0.25*FLOATF(K)
  210 WRITE OUTPUT TAPE 2,560,E,FLD(K),SPRX(K),SPRM(K)
      DO 250 J=1,MAXU
      RR(J)=(FLD(1)*SIG(J,1)+FLD(60)*SIG(J,60))/2.0
      DO 250 K=2,59
  250 RR(J)=RR(J)+FLD(K)*SIG(J,K)
      DO 270 J=1,MAXU
      DO 270 K=1,MAXU
  270 RRR(J,K)=RR(J)/RR(K)
      WRITE OUTPUT TAPE 2,520
      WRITE OUTPUT TAPE 2,530,(LABEL(I),I=1,MAXU)
      DO 280 J=1,MAXU
  280 WRITE OUTPUT TAPE 2,540,LABEL(J),(RRR(J,K),K=1,MAXU)
  282 WRITE OUTPUT TAPE 2,506
      DO 288 J=1,MAXU
      R5(J)=FLD(2)*SIG(J,2)+FLD(3)*SIG(J,3)
      R4(J)=FLD(4)*SIG(J,4)+FLD(5)*SIG(J,5)
      R3(J)=FLD(6)*SIG(J,6)+FLD(7)*SIG(J,7)+FLD(8)*SIG(J,8)
      R2(J)=0.0
```

```
      DO 283 K=9,14
  283 R2(J)=R2(J)+FLD(K)*SIG(J,K)
      R1(J)=0.0
      DO 284 K=15,60
  284 R1(J)=R1(J)+FLD(K)*SIG(J,K)
      RT(J)=R1(J)+R2(J)+R3(J)+R4(J)+R5(J)
      R1(J)=R1(J)/RT(J)
      R2(J)=R2(J)/RT(J)
      R3(J)=R3(J)/RT(J)
      R4(J)=R4(J)/RT(J)
      R5(J)=R5(J)/RT(J)
  288 WRITE OUTPUT TAPE 2,507,LABEL(J),R1(J),R2(J),R3(J),R4(J),R5(J)
  290 IF(MORE) 170,300,10
  300 CALL EXIT
      END
*     LIST8
*     LABEL
*     SYMBOL TABLE
CFNSPM
      FUNCTION FNSPM(E,T)
C     FRACTION OF FISSION NEUTRONS ABOVE E CALCULATED FROM
C     N(E)=A*SQRTF(E)*EXPF(-E/T) WHERE T IS TEMPERATURE OF MAXWELLIAN
      X=E/T
      SX=SQRTF(X)
      IF(SX-3.0) 1,1,11
    1 ANS=1.0
      S=0.0
      D=1.0
    2 S=S+1.0
      D=D*S
      TM=((-1.0)**S)*(SX**(2.0*S))/(D*(2.0*S+1.0))
      ANS=ANS+TM
      TEST=ABSF(TM/ANS)
      IF(TEST-0.000001) 5,2,2
    5 ANS=ANS*2.0*SX/1.7724539
    6 FNSPM=1.0+1.1283792*SX*EXPF(-X)-ANS
      RETURN
   11 ANS=1.0-1.0/(2.0*(SX**2))+3.0/(4.0*(SX**4))-15.0/(8.0*(SX**6))+105
     1.0/(16.0*(SX**8))-945.0/(32.*(SX**10))+10395./(64.*(SX**12))-
     2 135135./(128.*(SX**14))+2027025./(256.*(SX**16))
      EX=-(SX**2)
      ANS=1.0-EXPF(EX)*ANS/(SX*1.7724539)
      GO TO 6
      END
```

A.3.3 Sample Problem Treated with Ratio

```
*     DATA
0016006015.0
0001000100020003000400050005000600060011001600180024003 8  240001
PU(NF)NP(NF)IN(NN)DU(NF)NI(NP)TH(NF)ZN(NP) S(NP) P(NP)AL(NP)SI(NP)FE(NP)
AL(NA)IN(N2)MG(NP)RH(NN)
80.       300.      900.      1520.     1520.     1520.     1520.     1520.
1520.     1520.     1520.     1520.     1520.     1520.     1520.     1520.
1520.     1520.     1520.     1520.     1520.     1530.     1540.     1550.
1620.     1790.     1910.     1975.     2000.     2010.     2020.     2025.
2043.     2060.     2080.     2100.     2120.     2140.     2160.     2180.
2200.     2220.     2240.     2260.     2280.     2300.     2320.     2340.
2360.     2380.     2400.     2420.     2445.     2470.     2490.     2510.
2530.     2550.     2575.     2600.
.5571E 02.3000E 03.1300E 04.1660E 04.1768E 04.1840E 04.1873E 04.1890E 04
.1890E 04.1880E 04.1845E 04.1810E 04.1775E 04.1740E 04.1690E 04.1640E 04
.1610E 04.1580E 04.1555E 04.1540E 04.1545E 04.1570E 04.1635E 04.1760E 04
.1885E 04.1996E 04.2087E 04.2177E 04.2268E 04.2359E 04.2449E 04.2540E 04
.2598E 04.2585E 04.2553E 04.2520E 04.2495E 04.2470E 04.2455E 04.2440E 04
.2435E 04.2430E 04.2425E 04.2420E 04.2422E 04.2425E 04.2427E 04.2430E 04
.2435E 04.2440E 04.2445E 04.2450E 04.2459E 04.2469E 04.2478E 04.2507E 04
.2540E 04.2573E 04.2607E 04.2640E 04
10.       25.       65.       115.      175.      230.      275.      315.
355.      370.      350.      335.      325.      310.      30 .      290.
280.      265.      250.      230.      220.      207.      195.      182.
170.      157.      145.      132.      120.      107.      95.       82.
70.       57.       45.       32.       20.       7.        1.        0.
0.        0.        0.        0.        0.        0.        0.        0.
0.        0.        0.        0.        0.        0.        0.        0.
0.        0.        0.
5.        10.       110.      355.      450.      550.      56 .      565.
552.      540.      550.      559.      561.      565.      566.      567.
568.      570.      570.      575.      597.      620.      71 .      820.
910.      965.      1015.     1040.     1050.     1060.     1060.     1060.
1050.     1040.     1030.     1020.     1015.     1010.     1013.     1015.
1017.     1020.     1020.     1020.     1020.     1020.     1025.     1030.
1040.     1050.     1070.     1090.     1115.     1140.     1180.     1220.
1245.     1270.
.         .         .2384E-06.3133E 02.5601E 02.9409E 02.1327E 03.1714E 03
.2100E 03.2557E 03.3013E 03.3553E 03.4100E 03.4550E 03.5  0E 03.5300E 03
.5600E 03.5824E 03.6044E 03.6133E 03.6222E 03.6311E 03.6400E 03.6437E 03
.6475E 03.6512E 03.6550E 03.6556E 03.6562E 03.6568E 03.6517E 03.6439E 03
.6361E 03.6284E 03.6206E 03.6128E 03.6050E 03.5919E 03.5787E 03.5656E 03
.5525E 03.5394E 03.5262E 03.5131E 03.5000E 03.4812E 03.4625E 03.4437E 03
.4250E 03.4062E 03.3875E 03.3687E 03.3500E 03.3312E 03.3125E 03.2937E 03
.2643E 03
10.       75.       100.      115.      120.      125.      13 .      135.
138.      140.      140.      140.      140.      140.      14 .      140.
140.      140.      140.      140.      175.      250.      315.      335.
335.      335.      330.      325.      320.      315.      31 .      305.
300.      300.      298.      295.      290.      282.      278.      275.
275.      275.      278.      280.      285.      293.      30 .      310.
322.      337.      352.      368.      383.      398.      413.      426.
1.4       3.2       6.3       12.       18.       24.       32.       40.
49.       58.       68.       80.       93.       112.      13 .      150.
168.      188.      208.      228.      246.      265.      283.      302.
```

```
319.     333.     344.     360.     375.     387.     401.     412.
424.     435.     445.     453.     458.     465.     468.     470.
468.     465.     460.     450.     440.     427.     414.     400.
385.     370.     352.     335.     317.     300.     285.     270.
0.1      2.       5.       25.      60.      95.      125.     170.
210.     255.     290.     300.     305.     310.     315.     320.
325.     327.     330.     333.     336.     338.     34 .     342.
345.     347.     349.     350.     350.     350.     35 .     350.
350.     350.     350.     350.     347.     345.     342.     340.
337.     334.     331.     326.     318.     311.     303.     292.
281.     264.     250.     236.     223.     211.     20 .
0.1      5.       10.      20.      36.      65.      75.      80.
85.      88.      90.      95.      105.     120.     128.     132.
136.     138.     140.     140.     140.     140.     14 .     140.
140.     140.     140.     140.     140.     140.     14 .     140.
140.     140.     140.     140.     139.     136.     133.     130.
127.     124.3    121.     118.     114.     110.7    107.     102.4
98.      93.      88.      82.      76.      69.      60.
0.1      1.       2.       4.       5.       6.       9.       13.
16.      22.      27.      38.      45.      48.      52.      53.
54.      55.      59.      70.      75.      80.      83.      86.
90.      92.      95.      97.      99.      100.     101.     102.
102.     103.     103.     103.     103.     102.     102.     101.
100.     99.      97.      95.      93.      90.      88.      85.
81.      78.
3.       6.       8.       10.      18.      25.      50.      75.
105.     150.     250.     300.     325.     350.     375.     390.
400.     400.     400.     400.     400.     400.     40 .     400.
400.     399.     397.     395.     393.     391.     389.     388.
385.     383.     380.     381.     383.     386.     39 .     385.
380.     370.     360.     348.     335.
0.1      0.9      1.5      2.7      5.       8.5      12.      15.5
19.      22.7     26.5     30.      33.5     36.8     40.      44.
48.      52.      56.      59.      62.      66.      70.      74.
78.      81.5     85.      89.5     94.      97.      10 .     103.
106.     109.     112.     114.     116.     114.5    113.     110.
107.     103.5    100.
.4449E 01.5430E 01.6412E 01.1086E 02.1577E 02.2069E 02.2560E 02.3521E 02
.4482E 02.4594E 02.5838E 02.6699E 02.7179E 02.7659E 02.8140E 02.8620E 02
.9100E 02.9433E 02.9767E 02.1010E 03.1043E 03.1077E 03.1110E 03.1124E 03
.1139E 03.1153E 03.1167E 03.1181E 03.1196E 03.1210E 03.1224E 03.1230E 03
.1218E 03.1187E 03.1157E 03.1126E 03.1085E 03
32.      110.     230.     370.     490.     615.     74 .     860.
960.     1060.    1140.    1210.    1270.    1320.    1370.    1412.
1450.    1485.    1560.    1528.    1548.    1563.    1575.
.2471E 01.6933E 01.2164E 02.4447E 02.3835E 02.4501E 02.5220E 02.9490E 02
.1161E 03.1206E 03.1243E 03.1264E 03.1271E 03.1279E 03.1286E 03.1324E 03
.1485E 03.1605E 03.1630E 03.1630E 03.1630E 03.1636E 03.1665E 03.1694E 03
.1753E 03.1820E 03.1887E 03.1953E 03.2020E 03.2045E 03.2 50E 03.2010E 03
.1945E 03.1879E 03.1813E 03.1747E 03.1681E 03
75.      130.     220.     440.     550.     625.     685.     730.
760.     775.     780.     795.     800.     800.     78 .     770.
775.     790.     800.     810.     825.     830.     775.     700.
```

3

670. 670. 695. 710. 720. 720. 72 . 720.
715. 710. 705. 700. 690. 680. 67 . 660.
650. 640. 630. 620. 610. 600. 59 . 580.
570. 560. 550. 540. 530. 520. 51 . 500.
490. 480. 470. 460.
0.25 IN. DIAM., 2.5 IN. SPACING, FUEL CENTER
3.6788 2.2313 1.3534 0.82085 0.49787
0.15166 0.22162 0.24342 0.21251 0.1651
1.37 00460010

0.25 IN. DIAM., 2.5 IN. SPACING, FUEL CENTER

ENERGY(MEV)	DIFF. FLUX	FISSION FLUX SPRM.	FISSION DENSITY SPRM.
.250000E 00	.337055E 01	.523046E 00	.104609E 01
.500000E 00	.337055E 01	.799772E 00	.113105E 01
.750000E 00	.337055E 01	.967312E 00	.111696E 01
.100000E 01	.263116E 01	.105613E 01	.105613E 01
.125000E 01	.263116E 01	.108818E 01	.973302E 00
.150000E 01	.182827E 01	.108007E 01	.881877E 00
.175000E 01	.182827E 01	.104435E 01	.789453E 00
.200000E 01	.182827E 01	.990462E 00	.700362E 00
.225000E 01	.100953E 01	.925487E 00	.616991E 00
.250000E 01	.100953E 01	.854620E 00	.540509E 00
.275000E 01	.100953E 01	.781637E 00	.471345E 00
.300000E 01	.100953E 01	.709225E 00	.409471E 00
.325000E 01	.100953E 01	.639223E 00	.354577E 00
.350000E 01	.100953E 01	.572837E 00	.306194E 00
.375000E 01	.510805E 00	.510805E 00	.263779E 00
.400000E 01	.453542E 00	.453542E 00	.226771E 00
.425000E 01	.401162E 00	.401162E 00	.194592E 00
.450000E 01	.353634E 00	.353634E 00	.166705E 00
.475000E 01	.310802E 00	.310802E 00	.142606E 00
.500000E 01	.272430E 00	.272430E 00	.121834E 00
.525000E 01	.238206E 00	.238206E 00	.103962E 00
.550000E 01	.207805E 00	.207805E 00	.886083E-01
.575000E 01	.180933E 00	.180933E 00	.754542E-01
.600000E 01	.157247E 00	.157247E 00	.641960E-01
.625000E 01	.136429E 00	.136429E 00	.545718E-01
.650000E 01	.118157E 00	.118157E 00	.463451E-01
.675000E 01	.102200E 00	.102200E 00	.393369E-01
.700000E 01	.883132E-01	.883132E-01	.333792E-01
.725000E 01	.761773E-01	.761773E-01	.282915E-01
.750000E 01	.655917E-01	.655917E-01	.239507E-01
.775000E 01	.565296E-01	.565296E-01	.203060E-01
.800000E 01	.486193E-01	.486193E-01	.171895E-01
.825000E 01	.417214E-01	.417214E-01	.145255E-01
.850000E 01	.358019E-01	.358019E-01	.122800E-01
.875000E 01	.307841E-01	.307841E-01	.104069E-01
.900000E 01	.262573E-01	.262573E-01	.875244E-02
.925000E 01	.225575E-01	.225575E-01	.741685E-02
.950000E 01	.193277E-01	.193277E-01	.627075E-02
.975000E 01	.166539E-01	.166539E-01	.533351E-02
.100000E 02	.137184E-01	.137184E-01	.433813E-02
.102500E 02	.123902E-01	.123902E-01	.387004E-02
.105000E 02	.104895E-01	.104895E-01	.323712E-02
.107500E 02	.908767E-02	.908767E-02	.277171E-02
.110000E 02	.765106E-02	.765106E-02	.230688E-02
.112500E 02	.537556E-02	.537556E-02	.160268E-02
.115000E 02	.658344E-02	.658344E-02	.194135E-02
.117500E 02	.446699E-02	.446699E-02	.130316E-02
.120000E 02	.490510E-02	.490510E-02	.141598E-02
.122500E 02	.114202E-02	.114202E-02	.326293E-03
.125000E 02	.283469E-02	.283469E-02	.801772E-03
.127500E 02	.240933E-02	.240933E-02	.674748E-03
.130000E 02	.204679E-02	.204679E-02	.567678E-03
.132500E 02	.173741E-02	.173741E-02	.477303E-03
.135000E 02	.147489E-02	.147489E-02	.401414E-03
.137500E 02	.125226E-02	.125226E-02	.337710E-03
.140000E 02	.106149E-02	.106149E-02	.283695E-03
.142500E 02	.900708E-03	.900708E-03	.238603E-03
.145000E 02	.763539E-03	.763539E-03	.200515E-03
.147500E 02	.646657E-03	.646657E-03	.168375E-03

1.
1.
1.

Appendix B

SOME REMARKS CONCERNING THE SINGLE COLLISION TRANSPORT KERNEL

The single collision transport kernel expresses the neutron first collision density at a point r, resulting from a cylindrical shell source of infinite length and of radius r'. The kernel has been tabulated by Weinberg and Wigner (W1) and also derived from the point kernel by Cady (C1):

$$T_c(r, r') = \frac{\Sigma}{2\pi} \int_1^\infty K_o(\Sigma r y)\, I_o(\Sigma r' y)\, dy\,, \quad r > r'\,, \tag{B.1}$$

$$T_c(r, r') = \frac{\Sigma}{2\pi} \int_1^\infty K_o(\Sigma r' y)\, I_o(\Sigma r y)\, dy\,, \quad r < r'\,. \tag{B.2}$$

This kernel is the theoretical basis for the UNCOL code and has therefore been considered in some detail in this work. The kernel closely resembles the cylindrical shell diffusion kernel (W1):

$$D_c(r, r') = \frac{1}{2\pi D} K_o(kr)\, I_o(kr')\,, \quad r > r'\,, \tag{B.3}$$

$$D_c(r, r') = \frac{1}{2\pi D} K_o(kr')\, I_o(kr)\,, \quad r < r'\,. \tag{B.4}$$

Some additional remarks concerning this kernel are presented here because T_c and the integral of D_c are related to a wide class of integrals involving products of Bessel functions.

An integral somewhat similar to T_c can be integrated analytically:

$$I = \int_1^\infty K_o(\Sigma r y)\, I_o(\Sigma r' y)\, y\, dy\,, \quad r > r'\,, \tag{B.5}$$

$$I = \frac{1}{(\Sigma r)^2 - (\Sigma r')^2} \left[\Sigma r K_1(\Sigma r) I_o(\Sigma r') + \Sigma r' K_o(\Sigma r) I_1(\Sigma r') \right]. \tag{B.5a}$$

The integral in T_c, on the other hand, apparently cannot be expressed in closed form.

It is clear from the derivation of T_c that the dummy variable, y, is a function of the axial variable, z, of the cylinder (the kernel assumes the source is not a function of z). It might be expected that, since fast neutrons are attenuated exponentially as they leave the source, the relative values of the kernel at two points – say, r_1 and r_2 – should not be strong functions of the z dependence of the cylindrical source, especially for large values of z. These factors suggest that Eq. B.5a might provide a reasonable approximation to T_c. Calculations made with Eq. B.5a indicate that it is, in fact, generally a very poor approximation to Eq. B.1, even for the purpose of determining relative values of T_c for different values of r. Equation B.5a predicts an excessive relative attenuation for increasing r. This apparently means that small values of r are more highly favored by a z dependence of the source that increases in both the positive and negative directions.

The present situation occurs often with integrals of Bessel functions in that equations of the type Eq. B.1 frequently appear in practice, while only related types like Eq. B.5 have analytic solutions (M1, W2). Approximations like the one considered above must be regarded with caution.

Another method of solution of Eq. B.1 is the use of series for each of the two Bessel functions. Both I_o and K_o have convergent power series which are often useful for small values of the arguments, and both have asymptotic series for use with large values of the argument. The difficulty with this method arises in the region where the argument(s) increase to values of approximately five (5.0). The power series converge very slowly, requiring an excessive number of terms, while the asymptotic series are not yet sufficiently accurate, regardless of the number of terms used. Furthermore, the asymptotic series involve the use of exponentials, so that cases arise involving the products of exponentials and polynomials. Then the solution again results in an asymptotic series which may not converge rapidly enough.

A third alternative for the solution of Eq. B.1 involves the use of polynomial approximations. Polynomials have been obtained which approximate I_o and K_o to seven significant figures and which do not involve an excessive number of terms (A1). Here again, however, exponential terms are included and the approximations change as the arguments

increase. The term-by-term integrations produce asymptotic series and convergence may present a problem. Consider, for example, the general case. For small arguments, let:

$$I_o(\Sigma ry) \simeq P_{IS}(\Sigma ry) = \text{polynomial in } \Sigma ry = u_1 ,$$

$$K_o(\Sigma r'y) \simeq P_{KS}(\Sigma r'y) = \text{polynomial in } \Sigma r'y = u_2 ;$$

for large arguments, let:

$$I_o(\Sigma ry) \simeq e^{\Sigma ry} \, P_{IL}(\Sigma ry) = u_3 ,$$

$$K_o(\Sigma r'y) \simeq e^{-\Sigma r'y} \, P_{KL}(\Sigma r'y) = u_4 .$$

[Note that the ranges (of the argument) of applicability for the use of the small (or large) argument approximation are generally different for I_o and K_o.]

Then,

$$V = \int_1^{\infty} I_o(\Sigma ry) \, K_o(\Sigma r'y) \, dy , \tag{B.6}$$

$$V = \int_1^{\epsilon_1} u_1 u_2 \, dy + \int_{\epsilon_1}^{\epsilon_2} u_1 u_4 \, dy + \int_{\epsilon_2}^{\epsilon_3} u_3 u_4 \, dy , \tag{B.6a}$$

where ϵ_1 and ϵ_2 are selected so that valid approximations are used throughout as y increases, and ϵ_3 is chosen sufficiently large to approximate accurately the original integral.

The last two integrals involve products of exponentials and polynomials. They can be integrated by parts to give series solutions in two different ways (the exponential terms can be either integrated or differentiated). In general, only one method converges adequately, and the proper choice again depends upon the magnitude of the argument. Since one method cannot be used at ϵ_1 and the other at ϵ_2 for example, in the second integral, it is necessary again to break up the integrals as follows:

$$V = \int_1^{\epsilon_1} u_1 u_2 \, dy + \int_{\epsilon_1}^{\epsilon'_1} u_1 u_4 \, dy + \int_{\epsilon'_1}^{\epsilon_2} u_1 u_4 \, dy$$

$$+ \int_{\epsilon_2}^{\epsilon'_2} u_3 u_4 \, dy + \int_{\epsilon'_2}^{\epsilon_3} u_3 u_4 \, dy . \qquad \text{(B.7)}$$

The choices of ϵ'_1 and ϵ'_2 must be such that both methods of integration by parts converge adequately. It is a formidable task to construct a generalized selection criterion for use with a wide range of arguments. A rather extensive effort failed to produce a selection criterion that was adequate for the cases considered.

Still another alternative for a computer solution of Eq. B.1 is numerical integration. This method can be satisfactory provided the final result does not require still another integral (as in the present work). The infinite limit often requires large numbers of mesh points for accurate numerical integration. Since, in a double numerical integration, each point requires a number of mesh points equal to the product of the number of mesh points used for each individual integration, the amount of computer time required can be considerable.

Appendix C

A SIMPLE METHOD FOR ANALYSIS OF COMPLEX GAMMA SPECTRA

A problem quite frequently met by experimenters is that of accurately measuring the gamma activity of a particular nuclide in the presence of extraneous gamma activity. At least two methods have been used to treat this problem: treating the data obtained from integral counting by exponential least-squares methods, and the use of semiconductors such as lithium drift detectors which are capable of such high energy resolution that the activities of different gamma rays are easily separated. A third method is developed here. This method is probably not new, but does not appear to be discussed in the literature.

In the exponential least-squares method, a series of counts is made over a period of time. The time period must be comparable either with the half-life of the nuclide of interest or else with that of all extraneous gamma activities. Provided that the half-lives are sufficiently different, and that the desired activity is a sufficiently large fraction of the total count rate, the results can be analyzed by iterative least-squares methods to give the desired gamma activity. This method is particularly useful if multichannel analyzing equipment is not available. A good example of the method is the computer code, FRANTIC (R4).

The advent of lithium-drifted germanium diode detectors has brought about many innovations in gamma counting because of the greatly improved energy resolution attainable. Usually, the photopeak of the gamma energy of interest is so well defined that noise from all other sources can be accurately subtracted, or "stripped out." On the other hand, the efficiency of such devices is usually low, at least at the present time, as compared with that of scintillation detectors. Thus, while lithium-drifted germanium detectors are ideal for highly active sources with complicated gamma spectra, they may not be suitable when the low count rate is limiting.

To illustrate the third method, consider a typical scintillation counter-multichannel analyzer output for two gamma energies as in Fig. C.1.

Then,

$$C_1(t) = A_1(t) + fA_2(t)\,, \tag{C.1}$$

where:

$C_1(t)$ = total count rate under photopeak number 1,

$A_1(t)$ = photopeak activity of gammas with energy E_1,

$A_2(t)$ = photopeak activity of gammas with energy E_2,

f = constant relating $C_1(t)$, $A_1(t)$, and $A_2(t)$.

This equality merely states that the total count rate under photopeak number 1 is the sum of the photopeak activity from gammas of energy E_1 and some Compton effect counts resulting from gammas of the higher energy E_2. The constant f is the ratio of the Compton effect count rate between E_1^L and E_1^U to the photopeak count rate (E_2^L to E_2^U) for gammas with energy E_2.

In addition, we have:

$$A_1(t_2) = A_1(t_1)\, e^{-(t_2-t_1)/\tau_1}\,, \tag{C.2}$$

$$A_2(t_2) = A_2(t_1)\, e^{-(t_2-t_1)/\tau_2}\,. \tag{C.3}$$

Furthermore, provided that no gammas are counted with energies greater than E_2 which have a separate half-life,

$$A_2(t) = C_2(t)\,, \tag{C.4}$$

where,

$C_2(t)$ = total count rate under photopeak number 2.

Now, $C_1(t)$ and $C_2(t)$ can be measured and τ_1 and τ_2 are known. If the foil of interest is counted at two different times, we can construct two equations like Eq. C.1 which have only two unknowns, A_1 and f.* If the

*Equation C.3 is not required in the determination of f. It can, however, be used to check the assumption that all the higher energy gammas have the same half-life.

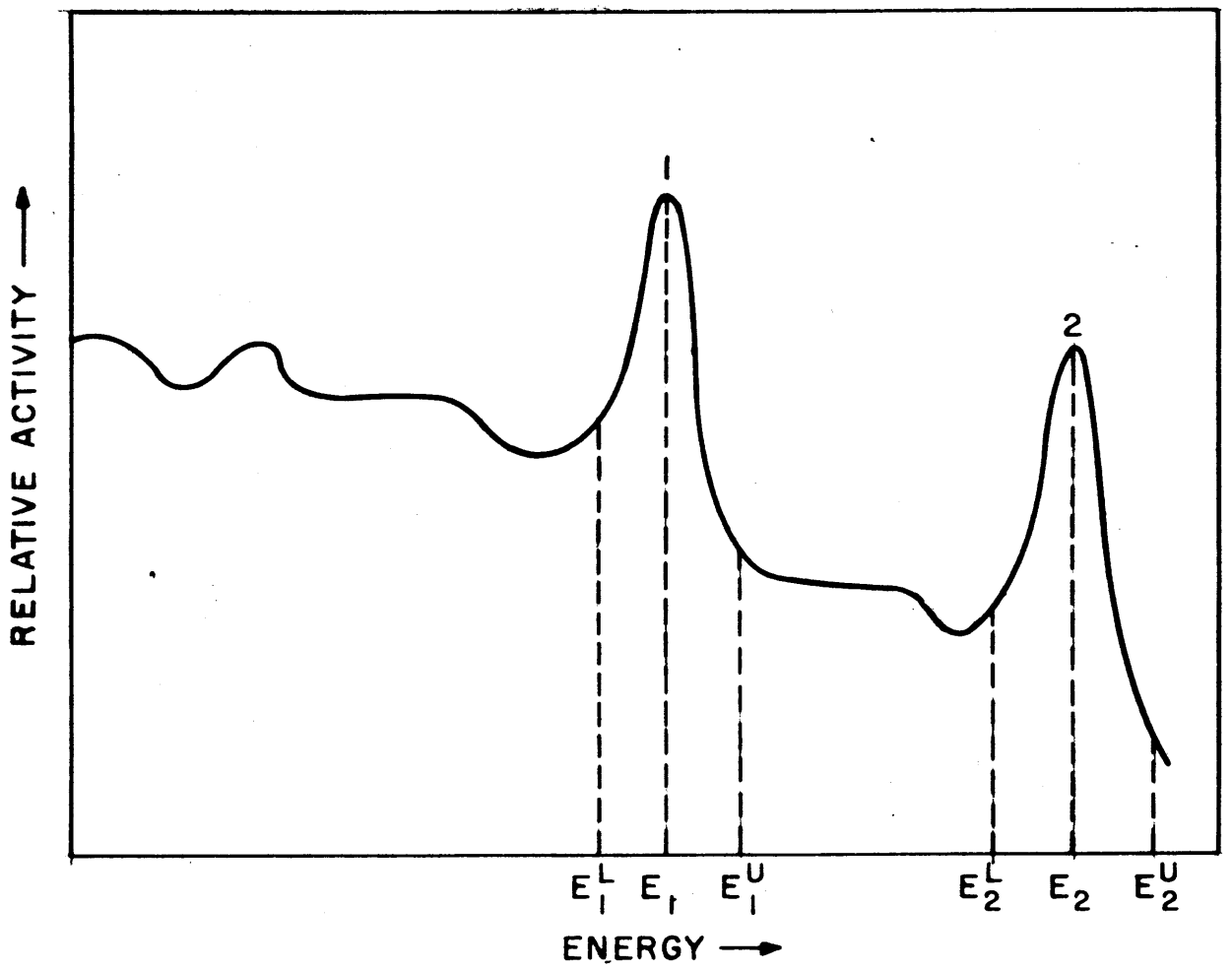

FIG. C.1 TYPICAL SCINTILLATION COUNTER GAMMA SPECTRUM WITH TWO PHOTOPEAKS

foil is counted more than twice, a redundant set of equations can be obtained. Values of f can then be averaged over several determinations and an estimate of the accuracy obtained. Furthermore, the value of f depends only on the counting setup; once it has been determined, it can be used to correct the counts of all the other foils counted with the same technique.* Thus, if a large number of foils must be counted and time is at a premium (because of a short half-life, for example), only one foil need be counted repeatedly.

This method is not limited to gamma spectra involving only two decay schemes. The extension to the general case is straightforward. With terminology similar to that of Eqs. C.1 - C.4:

$$C_1(t) = A_1(t) + f_2^1 A_2(t) + f_3^1 A_3(t) + \ldots f_n^1 A_n(t) ,$$

$$C_2(t) = A_2(t) + f_3^2 A_3(t) + f_4^2 A_4(t) + \ldots f_n^2 A_n(t) ,$$

$$C_n(t) = A_n(t) ,$$

and,

$$A_1(t_n) = A_1(t_1)\, e^{-(t_n - t_1)/\tau_1} ,$$

$$A_2(t_n) = A_2(t_1)\, e^{-(t_n - t_1)/\tau_2} ,$$

$$A_n(t_n) = A_n(t_1)\, e^{-(t_n - t_1)/\tau_n} .$$

Finally, this method can be expected to be more accurate generally than the exponential least-squares method, since more information is used to reduce the experimental uncertainty.

---

*Such a calibration is valid even when there are present many gamma rays having energies greater than the one of interest, provided only that all of the higher energy gammas have the same half-life. In this case, the calibration can be performed with any convenient higher photopeak, and f will in some cases exceed unity.

Appendix D

EFFECTS OF CROSS SECTION VARIATIONS ON RESULTS OF UNCOL CALCULATIONS FOR LATTICES

The UNCOL calculations for which results were reported in section 4.1.1 used values of removal cross sections of 0.093 cm^{-1} for heavy water and 0.100 cm^{-1} for uranium. Some examples of UNCOL calculations using other values of the removal cross sections are given here to show the sensitivity of the UNCOL results to such changes.

The results of UNCOL calculations of the spatial distribution of the fast flux within the lattice cell for lattices of 0.25-inch-diameter rods and 0.75-inch-diameter rods are given in Figs. D.1 and D.2, respectively. The spacing in both cases is 2.50 inches. Results are shown for four combinations of cross-section values in addition to those mentioned above. Both the fuel and moderator cross-section values were alternately varied, and the results normalized to the cell edge to be consistent with the results of section 4.1.1. These calculations show that the normalized values of the fast flux within the fuel rod increase when the moderator cross section is increased or when the fuel cross section is decreased. These results can be qualitatively explained in physical terms. For points within the fuel rod, the major source for fast neutrons is the rod, itself. Thus, for these points, the magnitude of the fast flux is affected more by the changes in the value of the fuel cross section than by changes in the value of the moderator cross section. The moderator region, on the other hand, contains no sources of fast neutrons.* Since all the neutrons reaching points in this region must pass through the moderator, the moderator cross section is more important here than the fuel cross section.

---

*The moderator region is a source of neutrons from the $H^2(\gamma, n)H^1$ reaction, but these are not significant compared to the fuel sources of neutrons except when the assembly is in a shutdown condition, or for calculations of problems in kinetic behavior.

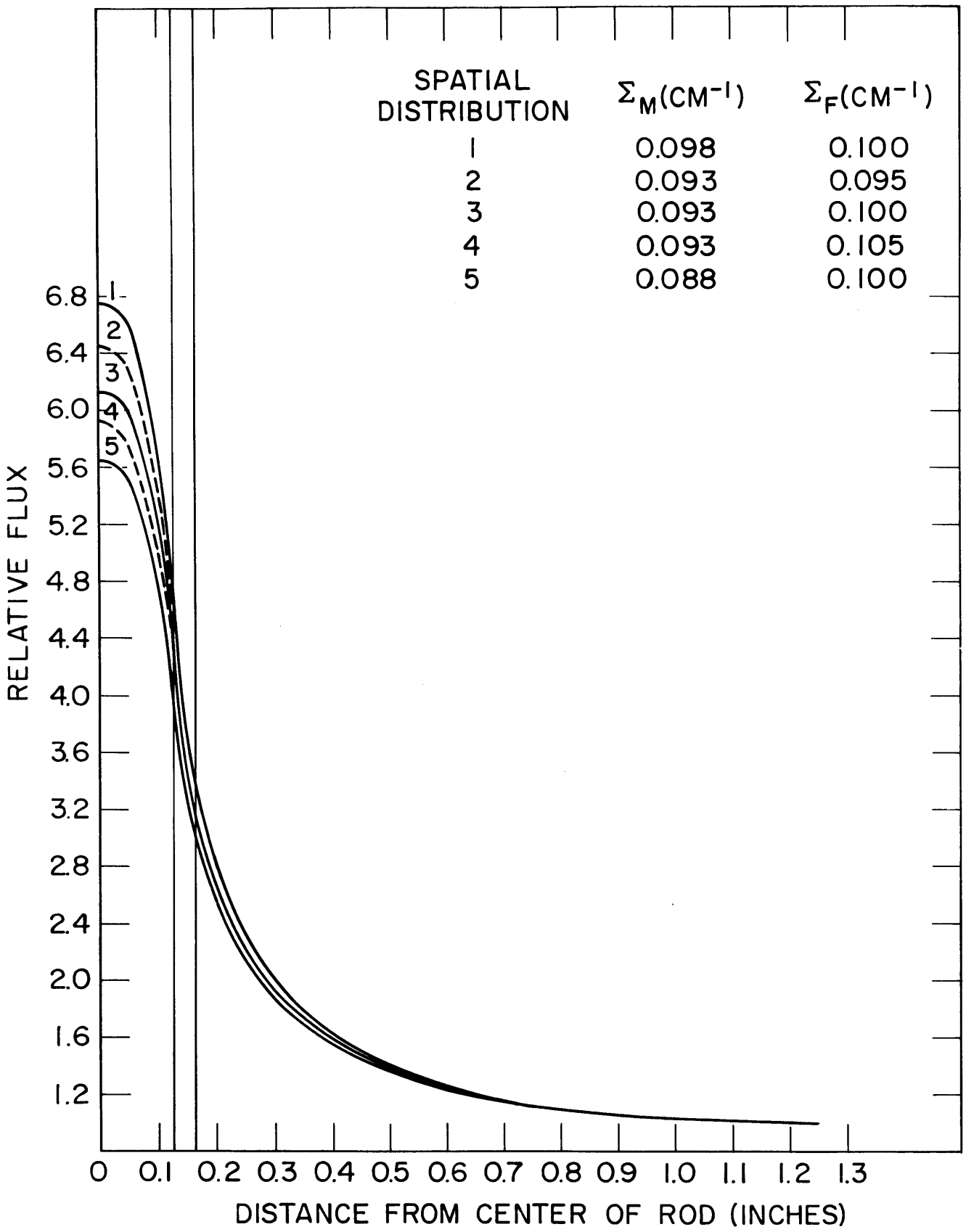

FIG. D.1 EFFECTS OF CROSS SECTION VARIATIONS ON UNCOL RESULTS FOR LATTICES OF 0.25 INCH DIAMETER RODS ON 2.50 INCH SPACINGS

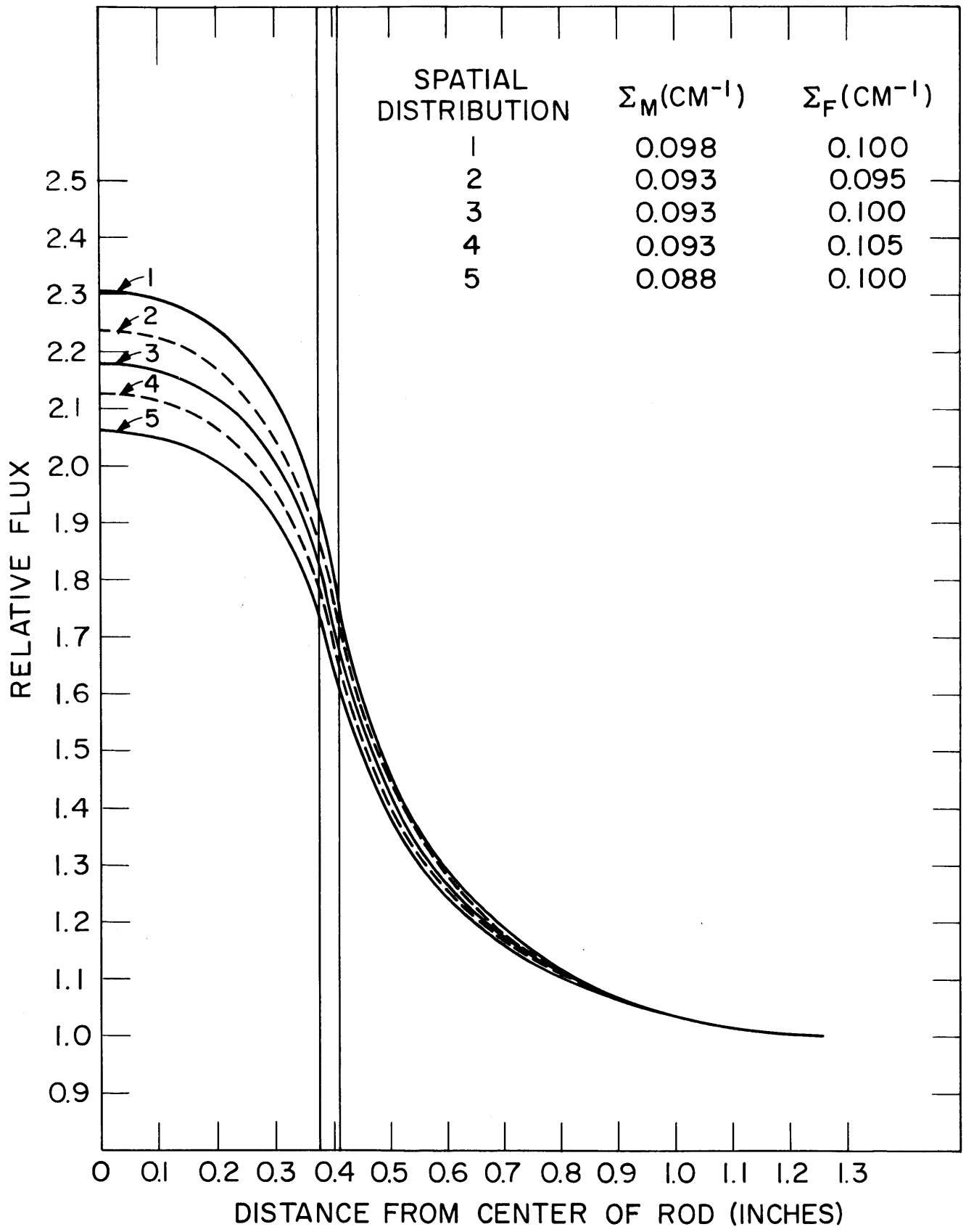

FIG. D.2 EFFECTS OF CROSS SECTION VARIATIONS ON UNCOL RESULTS FOR LATTICES OF 0.75 INCH DIAMETER RODS ON 2.50 INCH SPACINGS

The spatial distributions are more sensitive to changes in the values of the moderator cross section than to changes in the values of the fuel cross section. This effect is a result of the greater volume of D_2O than fuel in these lattices. The moderator to fuel volume ratios are 108.6 and 11.0 for the lattice of 0.25-inch rods and the lattice of 0.75-inch rods, respectively. For tighter spaced lattices, such as those characteristic of water-moderated assemblies, the effect of changes in the value of the fuel cross section should be increased.

As comparisons of the distributions show, the UNCOL results are quite sensitive to small changes in values of either the fuel or moderator cross sections. In view of the good agreement between experiment and UNCOL results with $\Sigma_M = 0.093\ cm^{-1}$ and $\Sigma_F = 0.100\ cm^{-1}$, these values can be considered experimental determinations of the group removal cross sections for a fast neutron energy group with a lower boundary of approximately 1 Mev. Estimates of the uncertainties in the cross sections so determined are $0.003\ cm^{-1}$ for the heavy water removal cross section and $0.005\ cm^{-1}$ for the slightly enriched uranium removal cross section. The values of these estimates are based on comparisons between the results displayed in Figs. D.1 and D.2 and the experimental results.

Appendix E

SUMMARY OF MITR LATTICE PROJECT LITERATURE

The work of the MITR Heavy Water Lattice Project is described in the reports and papers listed below. The list covers the period from September 1961 to August 1965.

1. Heavy Water Lattice Project Annual Report, NYO-9658, September 30, 1961.
2. Heavy Water Lattice Project Annual Report, NYO-10, 208 (MITNE-26), September 30, 1962.
3. Heavy Water Lattice Project Annual Report, NYO-10, 212 (MITNE-46), September 30, 1963.
4. Heavy Water Lattice Project Annual Report, MIT-2344-3 (MITNE-60), September 30, 1963.
5. Weitzberg, A., and T. J. Thompson, Coincidence Technique for U^{238} Activation Measurements, Trans. Am. Nucl. Soc., 3, 456 (December 1960).
6. Madell, J. T., T. J. Thompson, A. E. Profio, and I. Kaplan, Spatial Distribution of the Neutron Flux on the Surface of a Graphite-Lined Cavity, NYO-9657 (MITNE-18), April, 1962.
7. Weitzberg, A., I. Kaplan, and T. J. Thompson, Measurements of Neutron Capture in U^{238} in Lattices of Uranium Rods in Heavy Water, NYO-9659 (MITNE-11), January 8, 1962.
8. Palmedo, P. F., I. Kaplan, and T. J. Thompson, Measurements of the Material Bucklings of Lattices of Natural Uranium Rods in D_2O, NYO-9660 (MITNE-13), January 20, 1962.
9. Wolberg, J. R., T. J. Thompson, and I. Kaplan, A Study of the Fast Fission Effect in Lattices of Uranium Rods in Heavy Water, NYO-9661 (MITNE-15), February 21, 1962.

10. Peak, J., I. Kaplan, and T. J. Thompson, Theory and Use of Small Subcritical Assemblies for the Measurement of Reactor Parameters, NYO-10, 204 (MITNE-16), April 9, 1962.

11. Hansen, K. F., Multigroup Diffusion Methods, NYO-10, 206, April 1962.

12. Brown, P. S., I. Kaplan, A. E. Profio, and T. J. Thompson, Measurements of the Spatial and Spectral Distribution of Thermal Neutrons in Natural Uranium, Heavy Water Lattices, Brookhaven Conference on Neutron Thermalization, April 30 - May 2, 1962.

13. Madell, J. T., T. J. Thompson, I. Kaplan, and A. E. Profio, Calculation of the Flux Distribution in a Cavity Assembly, Trans. Amer. Nuclear Soc. 5 (June 1962), p. 85.

14. Weitzberg, A., J. R. Wolberg, T. J. Thompson, A. E. Profio, and I. Kaplan, Measurements of U^{238} Capture and Fast Fission in Natural Uranium, Heavy Water Lattices, Trans. Amer. Nuclear Soc. 5 (June 1962), p. 86.

15. Brown, P. S., P. F. Palmedo, T. J. Thompson, A. E. Profio, and I. Kaplan, Measurements of Microscopic and Macroscopic Flus Distributions in Natural Uranium, Heavy Water Lattices, Trans. Amer. Nuclear Soc. 5 (June 1962), p. 87.

16. Brown, P. S., T. J. Thompson, I. Kaplan, and A. E. Profio, Measurements of the Spatial and Energy Distribution of Thermal Neutrons in Uranium, Heavy Water Lattices, NYO-10, 205 (MITNE-17), August 20, 1962.

17. Kaplan, I., Measurements of Reactor Parameters in Subcritical and Critical Assemblies: A Review, NYO-10, 207 (MITNE-25), August 15, 1962.

18. Brown, P. S., I. Kaplan, A. E. Profio, and T. J. Thompson, Measurements of the Spatial and Spectral Distribution of Thermal Neutrons in Natural Uranium, Heavy Water Lattices, BNL-719, Vol. 2, 305-17, 1962.

19. Malaviya, B. K. and A. E. Profio, Measurements of the Diffusion Parameters of Heavy Water by the Pulsed-Neutron Technique, Trans. Am. Nucl. Soc., 6, 58 (June 1963).

20. Kaplan, I., D. D. Lanning, A. E. Profio, and T. J. Thompson, M. I. T. Exponential Lattice Studies, NYO-10, 209 (MITNE-35), presented at the IAEA Symposium on Exponential and Critical Experiments, Amsterdam, September 2 - 6, 1963.

21. Wolberg, J. R., T. J. Thompson, and I. Kaplan, Measurement of the Ratio of Fissions in U^{238} to Fissions in U^{235} Using 1.60-Mev Gamma Rays of the Fission Product La^{140}, NYO-10, 210 (MITNE-36), presented at the IAEA Symposium on Exponential and Critical Experiments, Amsterdam, September 2 - 6, 1963.

22. Kim, H., Measurement of the Material Buckling of a Lattice of Enriched Uranium Rods in Heavy Water, M. S. Thesis, M. I. T., June 1963 (Thesis Supervisor: T. J. Thompson).

23. Harrington, J., Measurement of the Material Buckling of a Lattice of Slightly Enriched Uranium Rods in Heavy Water, M. S. Thesis, M. I. T., July 1963 (Thesis Supervisor: T. J. Thompson).

24. Simms, R., I. Kaplan, T. J. Thompson, and D. D. Lanning, Analytical and Experimental Investigations of the Behavior of Thermal Neutrons in Lattices of Uranium Metal Rods in Heavy Water, NYO-10, 211 (MITNE-33), October 1963.

25. Malaviya, B. K., T. J. Thompson, and I. Kaplan, Measurement of the Linear Extrapolation Distance of Black Cylinders in Exponential Experiments, Trans. Am. Nuclear Soc., 6, 240 (1963).

26. Malaviya, B. K., I. Kaplan, D. D. Lanning, A. E. Profio, and T. J. Thompson, Studies of Reactivity and Related Parameters in Subcritical Lattices, MIT-2344-1 (MITNE-49), May 1964.

27. Simms, R., I. Kaplan, T. J. Thompson, and D. D. Lanning, The Failure of the Cell Cylindricalization Approximation in Closely Packed Uranium, Heavy Water Lattices, Trans. Am. Nucl. Soc., 7, 9 (June 1964).

28. Bliss, H., Measurement of the Fast Fission Effect in Heavy Water, Partially Enriched Uranium Lattices, M.S. Thesis, Nuclear Engineering Department, M.I.T (June 1964).

29. Malaviya, B. K., I. Kaplan, D. D. Lanning, and T. J. Thompson, Measurement of Lattice Parameters by Means of the Pulsed Neutron Technique. (Paper presented at the Winter A.N.S. Meeting, November 30 - December 3, 1964 at San Francisco.)

30. D'Ardenne, W. H., T. J. Thompson, D. D. Lanning, and I. Kaplan, Studies of Epithermal Neutrons in Uranium, Heavy Water Lattices, MIT-2344-2 (MITNE-53), 1964.

31. Papay, L. T., Fast Neutron Fission Effect for Single, Slightly Enriched Uranium Rods in Air and Heavy Water, S.M. Thesis, Nuclear Engineering Department, M.I.T., June 1965.

32. Goebel, D. M., Return Coefficient Measurements for the M.I.T. Enriched Uranium-D_2O Lattice, S.M. Thesis, Nuclear Engineering Department, M.I.T., May 1965.

Appendix F

NOMENCLATURE

A_i	saturated specific activation for reaction i (disintegrations/sec-gm)
C_1	coefficient of second-order term in S(r)
$D_c(r, r')$	diffusion kernel for cylindrical shell sources
d	distance (in., cm)
E_L	lower bound of neutron energy group (Mev)
F^{25}, F^{28}	fission rate for U^{235}, U^{238} (fissions/unit time)
G	factor defined by Eqs. 4.9 and 4.13
I	integral defined by Eq. B.5
I_n	modified Bessel function of the first kind, of order n
J_n	Bessel function of order n
k	constant used in Eq. 4.6
K_n	modified Bessel function of the second kind, of order n
ℓ_o	average chord length of fuel rod (cm)
N	atom density (atoms/gm)
P_{IS}, P_{KS}	polynomial approximations to I_o, K_o for small arguments
P_{IL}, P_{KL}	polynomials involved in approximations to I_o, K_o for large arguments
P_R	expressions involving Bessel functions given by Eqs. 3.16 and 3.17
r	distance (in., cm)

R_G average horizontal distance between MITR graphite facilities and core tank (in., cm)

R_{28} U^{238}-cadmium ratio for neutron capture

$S(r)$ relative fission source distribution for UNCOL calculations

$\overline{T}_c(r,r')$ single collision transport kernel for cylindrical shell sources

$T_c(r,r')$ uncollided flux transport kernel for cylindrical shell sources

$T_R(r)$ uncollided flux transport kernel for cylinder source

u_1, u_2 polynomial approximations to I_o, K_o for small arguments

u_3, u_4 approximations to I_o, K_o for large arguments

V integral defined by Eq. B.6

V_M/V_F moderator-to-fuel volume ratio

Nomenclature (Greek)

β numerical factor used in one-group theory

δ_{25} cadmium ratio for U^{235} fission

δ_{28} ratio of U^{238} fission rate to U^{235} fission rate

ν^{25}, ν^{28} neutrons produced per fission for U^{235}, U^{238}

$\Sigma(r)$ effective removal cross section for UNCOL calculations (cm^{-1})

$\Sigma_F, \Sigma_M, \Sigma_G$ effective removal cross section for UNCOL calculations for fuel, moderator, graphite (cm^{-1})

$\sigma_F(E)$ microscopic fission cross section for U^{238} (cm^2)

Φ integrated fast flux above E_L

$\phi(E)$ differential neutron spectrum

$\phi_F(r)$ fast flux spatial distribution

$\overline{\phi}_F$ average fast flux in fuel

$\overline{\phi}_M$ average fast flux in moderator

$\phi_{TH}(r)$	thermal flux spatial distribution
$\phi_i(E)$	spectrum of once-collided neutrons in uranium
$\phi_{ii}(E)$	spectrum of twice-collided neutrons in uranium
$\chi(E)$	fission neutron spectrum

Appendix G

REFERENCES

A1 Abramowitz, M. and I. A. Stegun, editors, Handbook of Mathematical Functions, p. 378, National Bureau of Standards, USGPO, Washington, D.C. (1964).

A2 Allard, E., "Monte Carlo Study of the Fast Fission Factor," S.M. Thesis, Nuclear Engineering Department, M.I.T. (August 1962).

A3 Aten, A.H.W., et al., "Remarks on the Use of Threshold Detectors," Neutron Dosimetry, Vol. 1, p. 399, IAEA, Vienna (1963).

A4 Reactor Physics Constants, ANL-5800, 2nd Edition (July 1963).

A5 ANL - RPCC Newsletters No. 1, June 1961 and No. 10, April 1963.

B1 Brolley, J., et al., "Neutron Multiplication in a Mass of Uranium Metal," CF-1627 (1944).

B2 Bliss, N. E., "Measurement of the Fast Fission Effect in Heavy Water, Partially Enriched Uranium Lattices," S. M. Thesis, Nuclear Engineering Department, M.I.T. (June 1964).

B3 Binder, D., "Techniques for Using the Np^{237} Fission Reaction as a Detector for Fast Neutrons in a Reactor," Rev. Sci. Instr., 31, No. 8, p. 902 (August 1960).

B4 Bresesti, M., et al., "Fast Neutron Measurements by Threshold Detectors in ISPRA-1 (CP-5 Type) and Avagadro RS-1 (Swimming Pool) Reactors," Neutron Dosimetry, Vol. 1, p. 27, IAEA, Vienna (1963).

B5 Bliss, H. E. and G. A. Price, "A Measurement of the Fast Disadvantage Factor in a Light Water Moderated, Slightly Enriched Uranium Lattice," paper presented at ANS Meeting, Gatlinburg, Tennessee (June 1965).

C1 Cady, K. B., "Neutron Transport in Cylindrical Rods," Ph.D. Thesis, Nuclear Engineering Department, M.I.T. (September 1962).

C2 Castle, H., H. W. Ibser, G. Sacher, and A. M. Weinberg, "The Effect of Fast Fission on k," Chicago Met. Lab., CP-644 (May 1943).

C3 Carlvik, I. and B. Pershagen, "The Fast Fission Effect in a Cylindrical Fuel Element," AEF-70 (1956).

C4 Chezem, C. G., "A Uranium-Metal Exponential Experiment," Nuclear Sci. Eng., 8, 652 (1960).

C5 Campan, J. L., P. P. Calvzon, and C. P. Zaleski, IAEA Seminar on the Physics of Fast and Intermediate Reactors, Paper SM-18/29, Vienna, August 3 - 11, 1961.

C6 Chernick, J., H. C. Honeck, P. Michael, S. O. Moore, and G. Srikantiah, "The Correlation of Integral Experiments and High Energy Cross Sections," Nucl. Sci. Eng., 13, 205-214 (1962).

C7 Carter, M. D., A. J. Perks, and L. G. Sanders, "The Measurement of U-238:U-235 Fission Ratios," AERE-R3205 (1960).

C8 Campbell, C. G. and M. D. Carter, "The Experimental Determination of Conversion Factors and Fast Fission Factors," AERE-R/R-2397 (1958).

C9 Clark, H. K., "Calculation of High Energy Events in Thermal Reactors," DP-609 (September 1961).

C10 Clark, H. K., "Calculation of High Energy Events in Thermal Reactors, II. A Computer Code - HEETR," DP-928 (November 1964).

D1 Dannels, R. A. and H. Honeck, "A Fast Effect Monte Carlo Code for the IBM 7090," WCAP-2685 (1965).

D2 D'Ardenne, W. H., T. J. Thompson, D. D. Lanning, and I. Kaplan, "Studies of Epithermal Neutrons in Uranium, Heavy Water Lattices," MIT-2344-2 (MITNE-53), (1964).

D3 Dierckx, R., "In-Pile Fast Neutron Spectrum Measurements by Threshold Detectors," Neutron Dosimetry, Vol. 1, p. 325, IAEA, Vienna (1963).

D4 Delattre, P., "Les Méthodes de Détermination des Spectres de Neutrons Rapides à l'Aide de Détecteurs à Seuil," Saclay Report CEA-1979 (1961).

D5 Dietrich, D. W. and J. Thomas, "Fast Neutron Spectra by Threshold Detector Activation," RIS Report, SM-18/6 (1961).

D6 Driscoll, M., Private communication, October 22, 1965.

E1 Erdick, E., "The Experimental Determination of the Fast Fission Factor in Light Water-Moderated, Slightly Enriched Uranium Rod Lattices," BNL Internal Report (March 11, 1960).

E2 Evans, R. D., The Atomic Nucleus, McGraw-Hill, New York (1955).

F1 Fleishman, M. R. and H. Soodak, "Methods and Cross Sections for Calculating the Fast Effect," Nuclear Sci. Eng. 7, 217-227 (1960).

F2 Futch, A. H., Jr., "Fast Fission Effect in Lattices of Natural Uranium and Heavy Water," Nuclear Sci. Eng. 5, 61 (1959).

G1 Gueron, H., M.I.T. unpublished memo (1956).

G2 Grader, R. J., "Measuring Neutron Spectra with Threshold Detectors," UCRL-6089 (1960).

G3 Grundl, J. and A. Usner, "Spectral Comparison with High Energy Activation Detectors," Nuclear Sci. Eng. 8, p. 598 (1960).

H1 Hill, D. L., "Fast Effect in Three Lattices," CF-1548 (1944).

H2 Hellens, R. L. and H. C. Honeck, "A Summary and Preliminary Analysis of the BNL Slightly Enriched Uranium, Water Moderated Lattice Measurements," IAEA Technical Report Series No. 12, 27, Vienna (1962).

H3 "Heavy Water Lattice Research Project Annual Report," NYO-9658 (September 1961).

H4 Hartmann, S. R., "A Method for Determining Neutron Flux Spectra from Activation Measurements," WADC-TR-57-375 (1957).

H5 Hurst, G. S., et al., "Techniques of Measuring Neutron Spectra with Threshold Detectors – Tissue Dose Determination," Rev. Sci. Instr. 27, No. 3, p. 153 (March 1956).

H6 Hildebrand, F. B., Introduction to Numerical Analysis, McGraw-Hill New York (1956)

H7 Honeck, H. C., "THERMOS, A Thermalization Transport Theory Code for Reactor Lattice Calculations," BNL-3826 (1961).

H8 Honeck, H. C. and J. L. Crandell, "The Physics of Heavy Water Lattices," BNL-8253 (June 1964).

H9 "Heavy Water Lattice Project Annual Report," MIT-2344-3 (September 1964).

H10 Harrington, J., Private communication, August 1965.

J1 Joanou, G. D. and J. S. Duder, "GAM-1, A Consistent P1 Multigroup Code for the Calculation of Fast Neutron Spectra and Multigroup Constants," GA-1850 (1958).

J2 Jones, G. A. and P. Garvey, unpublished, reported in Ref. (T5).

K1 Kranz, A. Z., "Measurements of Thermal Utilization, Resonance Escape Probability and Fast Fission Factor of Water Moderated, Slightly Enriched Uranium Lattices," WAPD-134 (1955).

K2 Kranz, A. Z. and G. G. Smith, "A Second Report on Measurements of f, p, and ϵ of Water Moderated, Slightly Enriched Uranium Lattices," WAPD-151 (1956).

K3 Kouts, H., G. Price, K. Downes, R. Sher, and V. Walsh, "Exponential Experiments with Slightly Enriched Uranium Rods in Ordinary Water," PICG 5, 183 (1955).

K4 Kouts, H. and R. Sher, "Experimental Studies of Slightly Enriched Uranium, Water Moderated Lattices," BNL-486 (T-111), (1957).

K5 Kaplan, I. and J. Chernick, "Uranium Graphite Lattices – The Brookhaven Reactor," PICG 5, 295 (1955).

K6 Klein, D., A. Z. Kranz, et al., "Measurements of Thermal Utilization, Resonance Escape Probability, and Fast Effects in Water-Moderated, Slightly Enriched Uranium and Uranium Oxide Lattices," Nucl. Sci. Eng. 3, 403-427 (1958).

K7 Klein, D., private communication to G. A. Price and R. L. Hellens, published in Ref. (P4).

L1 Lamberieux, J., "Dosimetrie et Spectrometrie des Neutrons Rapides par Radioactivation," Neutron Dosimetry, Vol. II, p. 157, IAEA, Vienna (1963).

L2 Lanning, W. D. and K. W. Brown, "Calculated and Measured Neutron Energy Spectral Distributions Using the Threshold Detector Technique," WAPD-T-1380 (1961).

M1 McLachlan, N. W., Bessel Functions for Engineers, Oxford Press, London (1955).

M2 Marshall, H. and L. Szilard, CP-316 (November 1941).

M3 Murley, T. M., "A Calculational Model for Fast Reactors," Sc. D. Thesis, Nuclear Engineering Department, M. I. T. (July 1965).

M4 Morgan, D. T. and E. A. Mason, "The Irradiation of Santowax OMP in the M. I. T. In-Pile Loop," IDO 11, 104 (MITNE-21), (May 1962).

M5 Mellish, C. E., J. A. Payne, and R. L. Otlet, "Flux and Cross Section Measurements with Fast Fission Neutrons in BEPO and DIDO," Harwell Report, AERE-I/R 2630 (1958).

M6 Martin, W. H. and D. M. Clare, "Determination of Fast-Neutron Dose by Nickel Activation," Nucl. Sci. Eng. 18, 468-473 (1964).

M7 Mayman, S., "Fuel Burnup in the MITR," S. M. Thesis, Nuclear Engineering Department, M. I. T. (June 1964).

N1 Nyland, O., "Measurements of the Fast Fission Factor in UO_2-Elements," AE-40 (1961).

O1 Olson, H. Schmidt, M. I. T. unpublished memo (1964).

O2 O'Shea, D. M., H. H. Hummel, W. B. Loewenstein, and D. Okrent, "Twenty-Six-Group Cross Sections," Trans. Amer. Nucl. Soc. 7, 2 (November 1964).

O3 Okrent, D., private communication to H. K. Clark, 1965.

P1 Price, G. A., "Fast Effect Measurements," BNL-1690 (1956).

P2 Price, G. A., et al., "Single Rod Fast Effects and Related Measurements," BNL-616 (T-185), (1960).

P3 Pershagen, B., G. Anderson, and I. Carlvik, "Calculation of Lattice Parameters for Uranium Rod Clusters in Heavy Water and Correlation with Experiments," PICG 12, 341 (1958).

P4 Price, G. A. and R. L. Hellens, "Lattice Studies in Light Water Moderated Systems," to be published in the Proceedings of the International Conference at Geneva, 1964.

P5 Price, G. A., private communication to L. Clark, September 15, 1965.

P6 Papay, L. T., "Fast Neutron Fission Effect for Single, Slightly Enriched Uranium Rods in Air and Heavy Water," S. M. Thesis, Nuclear Engineering Department, M. I. T. (June 1965).

R1 Rydin, R. A., N. C. Rasmussen, and G. L. Brownell, "Fast Neutron Spectroscopy and Dosimetry of the MIT Reactor Medical Therapy Facility Beam," AFCRL-64-404 (MITNE-47), (May 1964).

R2 Roy, J. C., R. W. Durham, A. G. Fowler, and J. J. Hawton, "Measurement of Fission Neutron Fluxes and Spectra with Threshold Detectors," AECL-1994 (May 1964).

R3 Roy, J. C. and Mrs. D. Wuschke, "Fast Neutron Reactions and Fast Neutron Flux in the NRX Reactor," Chalk River Report CRC-852 (1959).

R4 Rogers, P. C., "FRANTIC Program for Analysis of Exponential Growth and Decay Curves," M. I. T. Laboratory for Nuclear Science Technical Report No. 76 (1962).

S1 Spinrad, B. I., "Fast Effect in Lattice Reactors," Nuclear Sci. Eng. 1, 455 (1956).

S2 Snell, A. H., J. Brolley, J. Levinger, and R. Wilkinson, "Studies on a Five-Ton Metal Pile," Chicago Met. Lab. Report CF-589 (1943).

S3 Sefchovich, E., "Neutron Dose Rate in the MIT Reactor," S.M. Thesis, Nuclear Engineering Department, M.I.T. (January 1962).

S4 Sawyer, C. D. and E. A. Mason, "The Effects of Reactor Irradiation on Santowax OMP at 610°F and 750°F," IDO-11,107 (MITNE-39), (1963).

S5 Spangler, P., "Fusion Reactor Blanket Experiment," Sc.D. Thesis, Nuclear Engineering Department, M.I.T. (February 1965).

S6 Simms, R., I. Kaplan, T. J. Thompson, and D. D. Lanning, "Analytical and Experimental Investigations of the Behavior of Thermal Neutrons in Lattices of Uranium Metal Rods in Heavy Water," NYO-10,211 (MITNE-33), (October 1963).

S7 Sher, Rudolph and J. Leroy, "The value of ν for Fission Spectrum Induced and Spontaneous Fission of U-238," J. Nuclear Energy, Pt. A. Reactor Sci. 12, 101-7 (1960).

S8 Stassis, C. and D. Gournelos, "Influence of Photoneutrons in the Material Buckling of a D_2O Moderated Lattice," 22.42 Class Report, Nuclear Engineering Department, M.I.T. (May 1963).

T1 Timmins, T. H. and E. A. Mason, "Interpretation of Radiolysis of Terphenyls - Apparent Kinetics and Fast Neutron Effect," paper submitted for ANS Meeting, November 1965.

T2 Trice, J. B., "Two Neutron Energy Measurements in the Bulk Shielding Facility Using Radioactivants," AECD-3716 (1953).

T3 Trice, J. B., "A Series of Thermal, Epithermal, and Fast Neutron Measurements in the MTR," CF-55-10-140, ORNL (1955).

T4 Trice, J. B., "Fast Neutron Flux Measurements in E-25 of the Brookhaven Graphite Reactor," CF-55-7-130 (1955).

T5 Trebilcock, R. J., "Fast Flux Measurements in Zero-Energy Reactors," Neutron Dosimetry, Vol. 1, IAEA, Vienna (1963).

T6 Thompson, T. J., 1958 Geneva Conference, "The MIT Research Reactor," P/417, 10, 375 (1958).

T7 Timmins, T. H., private communication, October 22, 1965.

U1 Untermeyer, S., "Fission Rate Measurements in the Experimental Breeder Reactor (CP-4)," ANL-5070 (1953).

U2 Uthe, P. M., "Attainment of Neutron Flux Spectra from Foil Activations," WADC-TR-57-3, GNE-9 (1957).

V1 Vogt, E. W. and W. G. Cross, published in Ref. (R2).

W1 Weinberg, A. M. and E. P. Wigner, The Physical Theory of Neutron Chain Reactors, Univ. of Chicago Press (1958).

W2 Watson, G. N., The Theory of Bessel Functions, 2nd Ed., Cambridge Univ. Press, London (1958).

W3 Windsor, H. H. and E. Erdik, "Single-Rod Fast-Fission Effects in Low Enrichment Uranium Rods," Trans. Amer. Nucl. Soc. 3, 2 (1960).

W4 Wolberg, J. R., T. J. Thompson, and I. Kaplan, "A Study of the Fast Fission Effect in Lattices of Uranium Rods in Heavy Water," NYO-9661 (MITNE-15), (February 1962).

W5 Watson, G. N., op. cit., p. 133.

Y1 Yiftah, S., D. Okrent, and P. A. Moldauer, Fast Reactor Cross Sections, Pergamon Press, New York (1960).